

THE MICROHARDNESS OF OPAQUE MINERALS

VOL. I

THESIS

Submitted by

B.B. YOUNG, B.Sc., A.R.S.M.

Degree of Doctor of Philosophy

in the

Faculty of Science

UNIVERSITY OF LONDON

April, 1961

Department of Mining Geology,
Imperial College,
London.

CONTENTSVOL. I.

	Page No.
<u>Abstracts</u>	1
<u>Acknowledgements</u>	4
<u>Introduction</u>	5
<u>Chapter I. THEORY OF HARDNESS</u>	9
A. General	9
B. Nature of the bonding forces	10
C. Hardness in relation to polishing	14
D. Assessement of hardness	16
E. Microhardness testing instruments	22
<u>Chapter II. EXPERIMENTAL PROCEDURE</u>	25
A. Methods of mounting sections	25
B. Relative merits of the mounting media used	30
C. Grinding and polishing techniques	32
D. Orientation of sections	36
E. Measurement of microhardness	44
F. Routine procedure	42
G. Accuracy and reproducibility of results	45

	Page No.
<u>Chapter III. VARIATION OF MICROHARDNESS WITH LOAD</u>	53
A. Variation of microhardness values with load	53
(a) General	53
(b) Results	60
(c) Discussion of the results	69
(d) Conclusions	77
B. The relation between load and grain size	78
(a) General	78
(b) Discussion	80
C. Variation of the deformation characteristics with load	88
<u>Chapter IV. VARIATION OF MICROHARDNESS WITH ORIENTATION</u>	90
A. General	90
B. Microhardness values determined from randomly oriented sections	91
C. The relation, during indentation, between deformation processes and orientation	104
D. Microhardness values obtained on oriented sections of mineral	110
(a) General	110
(b) Discussion of the results	111
(i) Isometric minerals	111
(ii) Tetragonal minerals	130
(iii) Hexagonal mineral	139

	Page No.
(iv) Orthorhombic minerals	150
(v) Monoclinic minerals	163
(vi) Triclinic mineral	
E. Variation of microhardness on particular crystal faces	169
(a) General	169
(b) Theory	169
(c) Results and discussion	174
(i) Isometric minerals	174
(ii) Tetragonal minerals	181
(iii) Hexagonal minerals	183
(iv) Orthorhombic minerals	192
(v) Monoclinic minerals	207
(vi) Triclinic minerals	209
F. The variations of Knoop microhardness with reflectivity on particular crystal faces.	211
G. Variation of the diagonal lengths of Vickers indentation on rotation of the indenter on particular crystal faces	213
(a) Minerals whose crystals have been accurately oriented	214
(b) Minerals whose orientations were not precisely known	218
(c) General discussion	218

	Page No.
<u>Chapter V. THE SHAPE AND ASSOCIATED CHARACTERISTICS OF THE INDENTATIONS</u>	223
A. General	223
B. Variation in the shape of indentations	224
C. Variations in the dimensions of indentations	228
D. Associated deformation characteristics	229
E. Features of plastic deformation	230
F. Fracturing phenomena	231
G. Variations of the shape and deformation characteristics with orientation	235
H. Variations of the shape and deformation characteristics of indentations with mineral species	241
I. The relationship of indentation characteristics to atomic structure	254
 <u>Chapter VI. VARIATION OF MICROHARDNESS WITH CHANGES OF CHEMICAL COMPOSITION</u>	 267
A. Introduction	267
B. Microhardness variations in chemically analysed isomorphous series	269
C. Microhardness differences between end members of isomorphous or isostructural series	284
D. Variations of microhardness with chemical composition between different mineral species	296

	Page No.
<u>Chapter VII. SYSTEMATIC MICROHARDNESS DATA</u>	311
A. Accuracy and reproducibility of the results	311
B. Comparison of the microhardness values with established Mohs and Talmage hardness values	316
C. Comparison of Vickers microhardness and reflectivity results	331
D. Comparison of other physical properties of minerals with microhardness values	341
E. The relationship between microhardness, paragenetic sequence, and temperature of formation	345
F. Crystallochemical factors controlling microhardness	351
<u>Chapter VIII. MINERALOGICAL APPLICATIONS OF MICROHARDNESS TESTING TECHNIQUES</u>	359
<u>Chapter IX. GENERAL CONCLUSIONS</u>	364
<u>References</u>	378
<u>Appendix A. Photographs of Indentation Characteristics</u>	387
<u>Appendix B.</u>	413

VOL. II

	Page No.
<u>Introduction</u>	417
<u>Mineral Authentication</u>	419
<u>Abbreviations</u>	420
<u>References</u>	422
<u>RESULTS</u>	423

List of Tables

		Page No
I-IV	A-X Distance and hardness	12
V	Effect of mounting method on microhardness values	31
VI	Microhardness values on and off stage	39
VII	Effect of number of measurements on the probable error of the microhardness	52
VIII	Relationship of orientation to the microhardness and logarithmic index - Galena (Vickers indenter)	55
IX	Relationship of orientation to the microhardness and logarithmic index - Galena (Knoop indenter)	56
X	Relationship of orientation to the microhardness and logarithmic index - Sphalerite (Vickers and Knoop) indenters)	57
XI	Relationship of orientation to the microhardness and logarithmic index - other minerals	58, 59
XII	Probable errors of the mean microhardness values and logarithmic indices	62
XIII	Variation of microhardness with load on oriented sections of 10 minerals	70
XIV-XV	Effect of error in measurement of the diagonal length on the microhardness	72
XVI	Optimum load dependent upon the hardness of the minerals	79
XVII	Minimum Grain sizes	81 - 86
XVIII	Systematic Microhardness Data	92 - 99

	Page No.	
XIX	Variation of the microhardness anisotropism of minerals with crystal system	102
XX	Comparison of indentation and scratch microhardness values on the (100), (110) and (111) faces of galena	113
XXI	Oriented microhardness values obtained on some members of the spinel minerals	124
XXII	Oriented microhardness values obtained on Gold, Copper and Cuprite	125
XXIII	Oriented microhardness values	126 - 129
XXIV	The variation of microhardness and reflectivity values with orientation	133 - 138
XXV	Comparison of the microhardness values obtained by Bowie and Taylor (1958) and the present writer, on oriented sections of pyrrhotite	144
XXVI	A comparison of reflectivity and microhardness differences on the basal (0001) and prism (1010) faces of six hexagonal minerals	147
XXVII	% Knoop microhardness anisotropism on six hexagonal minerals	188
XXVIII	Comparison of Knoop microhardness maxima and minima with reflectivity maxima and minima - Hexagonal	204
XXIX	Comparison of Knoop microhardness and reflectivity maxima and minima - Tetragonal and Monoclinic	205
XXX	Comparison of Knoop microhardness and reflectivity maxima and minima - Orthorhombic	206
XXXI	The relationship of the elongation of indentations to movement planes	221 - 222

	Page No.	
XXXII	Examples of minerals showing different indentation types	225
XXXIII	Examples of minerals whose indentations show different degrees of "anisotropism"	226
XXXIV	Translation data deduced from the present studeies	262 - 264
XXXV	Deformation characteristics of the main mineral groups	265 - 266
XXXVI	Microhardness mean values for 10 analysed sphalerites	270
XXXVII	Microhardness values obtained on 10 analysed huebnerite-ferberites	275
XXXVIII	Microhardness values obtained on 7 analysed columbite-tantalites	277
XXXIX	Microhardness values - Native elements	298
XL	Microhardness values - Sulphides, selenides and tellurides	299 - 300
XLI	Microhardness values - Arsenides, antimonides, sulpharsenides and sulphantimonides	301
XLII	Microhardness values - Sulphosalts	302
XLIII	Microhardness values - Oxides, Hydroxides	303 - 304
XLIV	Microhardness values - Carbonates, phosphates	305
XLV	Ionic and atomic radii - After Evans (1939)	306
XLVI	Tetrahedral atomic radii - After Pauling and Huggins (1934)	307
XLVII	Variation in microhardness with chemical composition in some cobalt-bearing analogues of pentlandite	308
XLVIII	Comparison of calculated and actual hardness values for niccolite and breithauptite (After Povarennykh, 1959)	308

		Page No.
XLIX	The variation of microhardness with chemical composition in some copper iron sulphides	309
L	The variation of microhardness with chemical composition in some lead sulpho-salt minerals.	309
LI	The relationship between crystal system and microhardness in minerals having the compositions - ZnS and FeS ₂	310
LII	Vickers and Knoop microhardness values for the standard Mohs scale minerals	318
LIII	A comparison of Vickers mean microhardness data	319
LIV	Microhardness values obtained on the standard Mohs scale minerals - After Povarennykh (1959)	322
LV	Microhardness values extrapolated from Mohs and/or Talmage values	325 - 328
LVI	Microhardness values extrapolated from polishing hardness data	329 - 330
LVII	The relationship between bonding and the physical properties of minerals	344
LVIII	The relationship between structure, bonding, valency, microhardness and paragenetic sequence of sulphides	347
LIX	Relationship between temperatures of formation of minerals and their hardness values	349 - 350
LX	A comparison of calculated and measured microhardness values	356.

ABSTRACT

Knoop and Vickers microhardness values have been determined at different loads for over 200 mineral species. The microhardness data have been applied to a system of mineral identification, and some of the more theoretical problems associated with mineral hardness have been investigated. Although the minerals studied exhibited considerable variation in microhardness, the determination of the microhardness and reflectivity ranges and their mean values was found to be diagnostic for most of the minerals studied. Methods of mounting polished sections were investigated, and microhardness values of softer minerals have been shown to be appreciably affected by the stresses involved in thermoplastic methods. Cold-setting plastic mounting media were used in the present studies. The microhardness values were found to be strongly dependent upon the load applied during testing, and upon the physical anisotropy of the minerals, and a theory, based on the relative importances of rupture during indentation and subsequent elastic recovery, has been put forward to explain this phenomenon. Detailed studies have been carried out on over 50 oriented mineral species to investigate the extent of

their microhardness anisotrobism. The results indicate that the microhardness and deformation properties can be correlated with the orientation of the glide, twin and cleavage planes of the minerals, with respect to the indentation direction. A special study of the indentation features has shown that observation of the indentation shape and elongation and glide and fracture patterns can be usefully employed in systematic mineral identification based on microhardness and reflectivity determinations. Correlation of oriented indentation characteristics with oriented microhardness values has yielded new translation data for certain minerals. Indentation properties are considered as an indication of the bond type predominating in the mineral structure; covalent bonding producing brittleness, and metallic bonding giving rise to plastic deformation. Considerable microhardness variations have been found in analysed members of some isomorphous series, and these have been attributed to differences in lattice structures brought about by changes of chemical composition. The microhardness differences found between members of several isostructural series have been correlated with corresponding differences in their interatomic distances. Comparison of microhardness values with other physical properties reveals a fundamental interdependence between the physical properties of minerals and their crystal chemistry. The investigation shows that whilst a remarkable

parabolic relationship exists between Mohs scale values and Vickers values for the standard minerals, published Talmage and Mohs values for the opaque minerals are inaccurate. Other factors affecting the hardness of minerals have been reviewed, and a formula proposed for the calculation of mineral hardness from crystallochemical data.

ACKNOWLEDGEMENTS

I would like to express my sincere thanks for help and advice given to me by the following persons: Dr. P.G. Embrey, of the Department of Mineralogy, British Museum of Natural History, Mr. K. Taylor of the Atomic Energy Division of the Geological Survey of Great Britain, and Miss J. Harvey of the Mining Geology Department, Imperial College, for the loan of, and donation of, mineral specimens; Dr. J.R. Butler, Mr. A. Smith and Miss R.G. Thomas of the Geochemistry Department, Imperial College, for chemical analyses; Mrs. V. Hill, for the preparation of polished sections, Mr. J.A. Gee, for the preparation of photographs; Mr. R. Curtis for the preparation of X-ray powder photographs; and Miss N.J. Bowen for typing the thesis.

In particular I would like to record my thanks to Mr. I.M. Gray, working on the reflection characteristics of ore minerals, and to Dr. A.P. Millman, who supervised the work, for their continued help and encouragement.

Finally, the generous financial assistance from the Imperial College during the period 1958 to 1960 is gratefully acknowledged.

INTRODUCTION

The assessment of hardness, as an aid to mineral identification, has almost certainly been in use for many hundreds of years. Agricola in 1529 in his book "Bermannus" mentions how galena could be distinguished from native bismuth on differences of hardness. The first quantitative scale of hardness was that proposed by Mohs in 1824, and this system is still used in present day mineragraphic techniques. With the development of the polarising microscope in the 20th century, new methods for determining the hardness of minerals were evolved. These methods were, however, rather empirical being still based on scratching techniques. It was not until 1936 that indentation hardness techniques, well known in the metallurgical field, were adapted so that they could be used in mineralogical research work. This technique has been considerably improved with the passing of time and several workers have indicated that indentation microhardness testing may be successfully used in mineral identification.

During the past two and a half years, the writer, in conjunction with Mr. I.M. Gray, has been engaged upon a programme of determining the microhardness and reflection characteristics of about 200 fully authenticated

ore minerals. This work was carried out in the Mining Geology Department of the Royal School of Mines, London, under the supervision of Dr. A.P. Millman. The present thesis embodies the results of investigations into the microhardness of opaque minerals carried out by the writer.

The purposes of the research work were fourfold; firstly, to establish a reliable set of microhardness values and indentation characteristics for as many ore minerals as possible; secondly, to explore the applications and limitations of the technique in the identification of unknown minerals in polished sections; thirdly, to correlate the information collected with other properties of the mineral such as atomic structure and bonding; and fourthly, to attempt to solve some of the more theoretical problems associated with micro-indentation hardness testing and ore mineralogy.

Microhardness determinations were carried out on over 200 different mineral species, and more detailed investigations were carried out on oriented sections of about 50 ore minerals. Two types of indenters were used in this work, the Knoop and the Vickers. A special study was made of the deformation characteristics of the Vickers indentation. Particular attention was paid to the shape and dimensions of the impressions and to the type and amount of attendant

fracturing and/or trans^{su}formation twinning or gliding.

The methods of mounting and polishing ore minerals were investigated and the effects of these processes upon the microhardness were examined. A new set of microhardness values were made for the softer minerals at different loads i.e. 15 g. - 100 g. in an attempt to reduce the minimum grain size of a mineral for testing. A serious drawback to mineral identification techniques incorporating microhardness testing is the large overlap of the microhardness values. However, by studying as many different species of the minerals, and by making at least 10 impressions, each of which were made in a grain of differing orientation, fairly complete ranges of values have been obtained. In this way the ranges themselves have been shown to be of diagnostic value. Similarly it has been shown that the indentation characteristics of minerals may be used as an aid to mineral identification.

Variation of microhardness values with changes in chemical composition were examined for the following isomorphous series; Fe poor - Fe rich sphalerite, hübnerite-ferberite, and the columbite-tantalite series. In addition several other isomorphous series were examined.

Research has been directed towards answering some of the following problems associated with the microhardness testing

of minerals; the causes of the variation of the microhardness with load, the nature and mechanism of the deformation of minerals during indentation; the relationship between the scales of scratch hardness and indentation microhardness; the factors affecting the microhardness of minerals; general problems associated with the classification of the ore minerals.

CHAPTER I

THEORY OF HARDNESS

General

Hardness has been given many definitions but it is impossible to define it in precise terms because of the number of different physical properties which it embraces. The best general definition is probably that given by Ashby (1951): "Hardness is a measure of the resistance to permanent deformation or damage". Actual values of hardness depend on the method of testing employed, and it is often difficult to correlate the results from one method with those of another, unless conditions of testing are similar. For example, the results obtained from a scratching technique diverge from those of an indenting method. Hardness measurements are thus dependent on the combination of physical properties that have been brought into play during the testing of the material.

Deformation in minerals may be plastic, elastic or both. Hence properties such as elastic limit, yield point,

tensile and compressional strength, brittleness and cohesion are all related to hardness. Practically no data on such physical properties are available for minerals, apart from the native metals. It is therefore more convenient to discuss hardness in relation to the atomic structure of minerals, upon which these other physical properties are fundamentally dependent.

The strength of a crystal is dependent on the nature and strength of the bonding between atoms or ions, and hardness will be determined by the strength of the weakest bonding. Microhardness indentation measurements will be dependent on certain characteristics of the minerals, which are an expression of the crystal structure. Deformation of minerals during indentation will be controlled by the attitude of glide planes, translation twin planes and cleavages to the indenting direction. Easy gliding or twinning will result in permanent deformation and low hardness values. Considerable anisotropy of microhardness values is therefore to be expected in minerals. Different shapes of indenters will cause variations in amount of deformation and hence differing results for hardness values.

Nature of bonding forces

Evans (1939) lists four types of interatomic bonding

forces and gives an account of the relationship of hardness to bond strength. These four types of bonding are as follows:

(a) The ionic bond

The ionic bond arises from the electrostatic attraction between oppositely charged ions, as for example in halite Na Cl. Strength of bonding is related to two factors, (a) the distance between the ions and (b) the valency charges of the anions and cations. Goldsmidt (1928) and Ephraim (1931) showed the relationship between the A-X distance, i.e. the distance between cation and anion, and Mohs' hardness for the structurally similar oxide series BeO, MgO, CaO, SrO, and BaO (Table I), the hardness decreasing with increasing A-X distance. Evans shows the same trend, as the result of substitution of the anion by one of greater ionic radius, on the hardness in the series CaO, CaS, CaSe and CaTe (Table II). Tables III and IV, also after Evens, show that increasing valency of the ions causes an increase in hardness in the series NaF, MgO, ScN, TiC, LiCl and SrO; LiBr and MgSe. Similar results have been obtained by Povarennykh (1957). In this manner it should be possible to predict the hardness of ionic minerals of simple structure.

TABLE I	BeO	NgO	CaO	SrO	BaO
A-X distance	1.65	2.10	2.40	2.57	2.77
Hardness	9.0	6.5	4.5	3.5	3.3

TABLE II	CaO	CaS	CaSe	CaTe
A-X Distance	2.40	2.84	2.96	3.17
Hardness	4.5	4.0	3.2	2.9

TABLE III	+	++	+++	++++
	NaF	MgO	ScN	TlC
A-X Distance	2.31	2.10	2.23	2.23
Hardness	3.2	6.5	7-8	8-9

TABLE IV	+	++	+	++
	LiCl	SrO	LiBr	MgSe
A-X Distance	2.57	2.57	2.75	2.75
Hardness	3.0	3.5	2.5	3.5

(b) The homopolar bond

The homopolar bond arises from the mutual sharing of electrons between atoms. Diamond, C, exhibits this type of bonding. Figure 1 shows the atomic configuration. Each carbon atom is surrounded by four others arranged at the corners of a tetrahedron. Sphalerite, ZnS, has a similar structure (Figure 2).

The strength of the bonding is related to the "characteristic bond length"; the shorter the bond length, the greater the strength. In addition, the strength of the crystal is dependent upon the perfection or completeness of the bonding. Thus diamond, having a fully chemical and satisfied type of bonding, is extremely hard. Sphalerite, by contrast, is relatively soft, due to a large bond length, $Zn = 1.31$ and $S = 1.04$, ($C = 0.77$), and a chemical dissimilarity, even though the structure is identical.

(c) The metallic bond

The metallic bond arises from the attraction between atoms of chemically identical or similar elements, the strength of the bonding being dependent on the metallic radii of the elements concerned. It is generally a

Fig. 1.

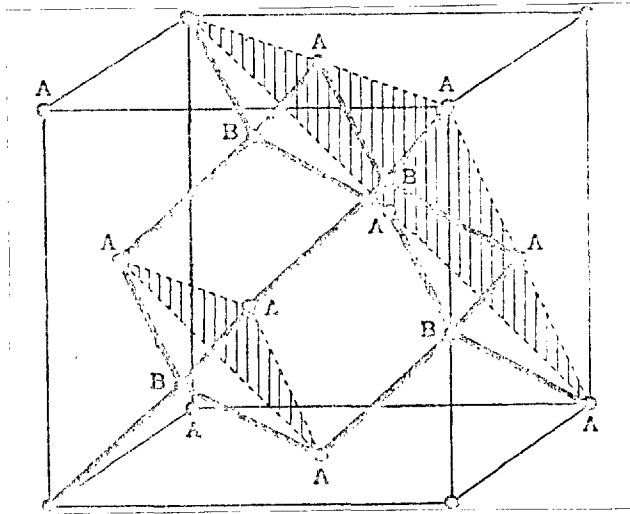
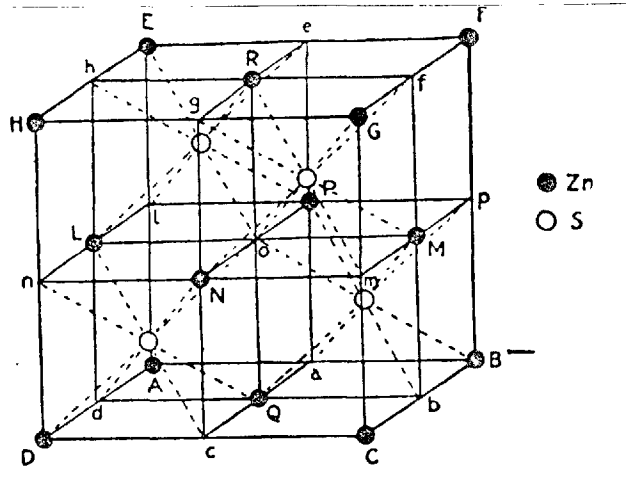


Fig. 2.



weak bond resulting in compounds of low hardness, such as gold, silver and copper.

(d) The Van der Vaal's bond

The Van der Vaal's bond arises from the attraction between atoms and molecules. It is generally a very weak force and results in compounds of low hardness such as graphite and molybdenite.

Hardness in relation to polishing

When certain materials, particularly metals, are polished, the polished surface is "work-hardened" i.e., the surface has been deformed by the polishing technique and made harder. Beilby (1921) postulated the theory that such hardening was due to the formation of an amorphous layer of material that flowed over the surface, bridging chasms and filling up irregularities producing a thin non-crystalline veneer over the surface of the section. This theory has been rejected by Samuels (1952) in favour of the theory of recrystallisation of the polished surface during polishing.

Such work-hardening can be quite considerable. Gogoberidze and Kopatski (1950) found that the microhardness

of halite was raised by 35% from the normal by polishing. Mitsche and Onitsch (1948) found considerable differences in microhardness values between results obtained on natural crystal faces and polished crystal faces of minerals.

The depth of the deformation is dependent on the material being polished and the method of polishing used. Softer minerals deform more easily than hard ones, so that the amount of work-hardening decreases with increasing hardness. Values for the thickness of the deformed layer have been given by several authors for different materials; for example, Bulian and Fahrenhorst (1944) found that the layer was 400 microns deep for magnesium and Buckle (1954) gives values of 30 - 80 microns for copper and silver, and 2 - 5 microns for hardened steel.

Work hardening has been shown to be due to heavy abrasion in the initial stages of grinding and improved techniques embodying finer abrasives have been found to reduce the deformation considerably, Samuels (1954). Stanton (1957) developed the technique described by Samuels for the polishing of ore minerals and found that such a method of polishing rendered what was considered to be optically isotropic pyrite, anisotropic.

From this brief resume it can be appreciated that the technique of polishing is of paramount importance in the

preparation of polished sections for microhardness testing. This subject is discussed more fully in Chapter II.

Assessment of hardness

There are basically two methods of measuring hardness; (a) comparative and (b) absolute.

(a) Comparative

These methods depend upon the comparison of the hardness of one mineral relative to another. Two methods are at present being used in economic mineralogy.

(i) The Mohs' scale of hardness

(ii) The comparative polishing hardness.

(i) Mohs' scale of hardness

Mohs (1824) postulated his now famous scale of hardness for minerals. The scale is given below:

1. Talc
2. Gypsum
3. Calcite
4. Fluorite
5. Apatite
6. Orthoclase
7. Quartz
8. Topaz

9. Corundum
10. Diamond

Each mineral is harder than the one numerically below it in the scale and can only be scratched by one above it. Using these ten minerals as standards, any other mineral can be classified according to a Mohs' scale of hardness number. For example, cobaltite, $H = 5.5$, will scratch apatite, $H = 5$, but will be scratched by orthoclase, $H = 6$. Such a method, admittedly crude, is still extremely useful for hand specimen mineral identification, but it is not sufficiently discriminating to detect subtle differences in hardness, such as between tetrahedrite and tennannite. In addition, such a method cannot be applied to ~~one~~ microscopy.

(ii) Polishing hardness

This method was first described by Van der Veen (1925) for the determination of "resistance to polish". Under normal polishing conditions some relief is produced on the polished section, hard minerals tending to be raised above the normal level of the section whilst soft minerals are reduced to a level slightly below the normal. When two minerals are found adjacent to one another in a polished

section it is possible to determine which is the harder of the two using the test described by Van der Veen;

"When the tube of the microscope is raised a bright line of light is seen to move from the hard towards the soft mineral; when the tube is lowered the reverse takes place".

It is thus possible to compile a list of relative polishing hardness values similar to Mohs' scale. This method is quite useful in ore-microscopy in helping to identify unknown mineral grains providing that the mineral grain is in contact with other known minerals. It does not give any absolute values and can only give results relative to those minerals in the polished section. Uytendogaardt (1951) uses such a method in preference to Mohs or Talmage values.

(b) Absolute methods

In these methods an actual numerical value can be assigned to the hardness of the material being tested. Several methods of testing exist (Mott 1956 p.2) but only the following methods have been used extensively in mineralogy

(i) Sclerometric Methods

Mohs' method of scratch testing was developed on a

more scientific basis in an instrument designed by Martens (1890). A loaded indenter is kept on the surface of the specimen, whilst the stage below is moved in a direction parallel to the cutting edge of the indenter. The size of the scratch produced is noted. No values were given for different materials and hence the method was still comparative.

This apparatus was further modified by Poschl (1909) and Bierbaum (1920) and in 1925 Talmage (1925) developed the technique to produce numerical values for different ore minerals. Talmage preferred to give minerals letters rather than numbers, soft minerals being A,B and C and hard ones, F and G. Short (1940) lists the Talmage hardness values for all the ore minerals but these results are not reliable. Uytendogaardt noted many anomalies in the values listed by Short. This method is slow - one measurement takes 15 minutes and is cumbersome to use.

(ii) Indentation methods

In these methods an indenter, usually made of a hard material, is pressed into the surface of the material being tested, under a given load. The size of the

resultant indentation is measured and the hardness expressed as the ratio of the load to the surface area of the impression multiplied by a known factor dependent on the shape of the indenter.

Thus

$$H = K \cdot \frac{L}{A}$$

where H = Hardness

K = Constant

L = Load applied

A = The area of the impression produced.

In the Brinell test, Meyer (1908), a steel ball is used as the indenter and loads up to 3000 Kg. are used. In microhardness indentation testing a specially cut diamond indenter is used and loads do not exceed 5000 g.

Two types of indenters were used in the present work, the Vickers and the Knoop. Several other types of indenters have been used by other authors. Berkovich (1950) used a triangular pyramid indenter and Grodzinski (1952), a "double-cone" indenter.

The Vickers indenter

The Vickers indenter consists of a square-based pyramid, the included angle between opposite faces being

136°00'. Hence the shape of a perfect impression is that of a square.

From the previous definition,

$$\begin{aligned} H_V &= \frac{L_V}{\frac{1}{2}d_V^2 \sin \frac{1}{2} (136^\circ)} \\ &= \frac{2L_V \sin 68^\circ}{d_V^2} \\ &= \frac{1.8544 L_V}{d_V^2} \end{aligned}$$

where H_V = Vickers microhardness number

d_V = Mean diagonal length

L_V = Load applied

The Vickers indenter has been used extensively in the mineralogical field:- Siebel (1943), Mitsche and Onitsch (1948), Taylor (1949), Tertsch (1950(a), 1950(b)), Nakhla (1956), Henriques (1957), Bowie and Taylor (1957, 1958), Shazly and Saleeb (1959), and Mookherjee and Sahu (1960)

The Knoop indenter

The knoop indenter consists of a pyramid elongated such that the angles between the long and short edges are 172°30'

and 130°00' respectively. A perfect impression has the shape of a parallelogram for which one diagonal is approximately seven times the length of the other.

$$\begin{aligned} H_K &= \frac{L_K}{\frac{1}{2} \cot \frac{1}{2}(172^\circ 30') \tan \frac{1}{2}(130^\circ) d_K^2} \\ &= \frac{L_K}{\frac{1}{2} \tan 3^\circ 45' \tan 65^\circ d_K^2} \\ &= \frac{L_K}{0.07028 d_K^2} \end{aligned}$$

where H_K = Knoop microhardness number

L_K = Load applied

d_K = Length of the long diagonal

The following authors have used the Knoop indenter in mineralogical work; Robertson and Van Meter (1951) and Winchell (1945).

Microhardness testing instruments

For routine ore-microscopy it is most convenient to have the surface of the polished ^{sections} under continuous visual observation for control purposes, and this is a serious drawback in the "inverted" type of instrument.

Secondly it is important to be able to view the section under polarized light. Many different types of hardness testers are marketed and the following have been used in mineralogical research.

(a) Durimet hardness tester.

This is an "upright" instrument where the polished surface is uppermost, and is manufactured by E. Leitz Ltd., Wetzlar, Germany. The present study has been made using this equipment which is described in detail later in the text. Nakhla(1956), Henriques (1957) and Mookherjee and Sahu (1960) used this machine together with a Vickers indenter.

(b) G.K.N. tester

This tester is manufactured by Hall Telephone Accessories Ltd., and can be fitted to any normal ore microscope. Like the Durimet, it is an "upright" tester. It has been used by Bowie and Taylor (1957, 1958) together with a Vickers indenter.

(c) The Tukon tester

This instrument is manufactured by the Wilson Instrument

Company of America and the Kentron tester is a modification of this equipment. It has been used in conjunction with a Knoob indenter by Winchell (1945) and Robertson and Van Meter (1951).

(d) The Zeiss-Hanemann tester

This is an "inverted" instrument similar to the C.T.S. tester. It has been used by Mitsche and Onitsch (1951) with a Vickers indenter.

(e) The C.T.S. tester

The instrument is similar in principle to the Zeiss-Hanemann tester being of the "inverted" type. It has been used by Taylor (1949) with a Vickers indenter.

CHAPTER II

EXPERIMENTAL PROCEDURE

A. Methods of Mounting Sections

In microhardness testing, it is essential that the mounting medium of the material being tested is rigid. If the mount is not rigid then anomalous low hardness values result. For example, if a polished section mounted on plasticene is tested under normal conditions, an extremely small impression is formed due to the "give" or deformation of the plasticene when compressed under loading. Several different types of mounting media have been used in the present work, ranging from dental plaster to cold-setting plastic. Each medium used is considered to be rigid under the stress conditions existing during low-load hardness testing.

Plastic "ice-cube" containers were used as moulds for dental plaster, cold-setting plastic and the low-melting-point alloy. The resultant mounts were not larger than 2 cm. x 3 cm. x 4 cm. For the purposes of description, the types of mounts can be divided into two groups;

- a. Those which are used with previously polished specimens of minerals and

b. Those which are used prior to the polishing of the mineral specimens.

a. Mounts used with previously polished specimens

i. Dental Plaster

Approximately equal amounts of powder and water are mixed up together in a single plastic mould so that a paste of a fairly stiff consistency results. The polished section, its polished surface uppermost, is slowly pressed into the paste so that the base of the section is deeply embedded in the mixture. By gently tilting the section, the polished surface is roughly levelled and is fixed in this position using pieces of plasticene. The plaster sets hard in about 30 minutes.

Mineral specimens mounted in this medium include cleavage fragments of wolframite and sphalerite, and also a crystal of native sulphur which could not be mounted in cold-setting plastic.

ii. Low Melting Point Alloy

The alloy used in the work is known as "Cerrolow 117" and is manufactured by Mining and Chemical Products Ltd., London. It is composed dominantly of bismuth and has a melting point of 47°C i.e. it can be melted in warm water.

A 500 cc. beaker half filled with air-free water (air-free to reduce the formation of dross) is warmed on a tripod and gauze using a bunsen burner until the temperature of the water rises to about 50°C. Alloy is then added and the water further heated until the temperature of the water reaches about 80°C.

Water is used as a means of preventing the alloy from becoming overheated during the melting process and also to insulate the metal from the air. The molten metal and the water are quickly poured into a plastic mould and the excess water is removed from the mould. Using metal tongs the mineral specimen with its polished surface uppermost, is lowered gently into position using pieces of plasticene. By carefully tilting the specimen the polished surface is levelled as accurately as possible. The alloy is then allowed to cool and solidify (15 minutes) and the plasticene is removed. To release the specimen from the mount, the mount and specimen are immersed in a beaker filled with hot water until the alloy melts.

Such a medium has enabled work to be done on different crystal faces of the same galena crystal. This method would be useful in the study of other minerals with well defined crystals for detailed orientation work.

It has also been used for mounting specimens too small to be securely gripped in the rotating sub-stage.

b. Mounts used with unpolished specimens

Three types of mounting media have been used.

- (i) Bakelite
- (ii) Clear Thermoplastic
- (iii) Clear cold-setting plastic

Prior to mounting, the mineral specimen is flattened and ground roughly to shape on a diamond-impregnated wheel.

(i) Bakelite

The bakelite used was supplied by Bakelite Ltd., London and is known as "Bakelite Moulding Material No. X386/21". The mounting press was supplied by Nash & Thompson Ltd., Surrey.

The polished section is placed face downwards in the bottom of the press and bakelite powder added. Both are then slowly heated and compressed until the bakelite powder liquifies. A maximum temperature of 170°C is attained and the pressure is not allowed to exceed 3,500 lbs/sq. in. The mount is cooled slowly and then removed ready for polishing. One mount can be made in 20 minutes.

This method of mounting was rejected for routine work on minerals because of the high temperatures and pressures involved. However microhardness measurements were made on over 100 already existing polished sections mounted in bakelite.

(ii) Clear Thermoplastic

Clear thermoplastic mounts are made in exactly the same way as bakelite mounts except that the process takes a longer time, about one hour. No new mounts were made in view of the high temperatures and pressures involved and only 13 polished sections already mounted in this medium were used for microhardness determinations. The thermoplastic compound used was supplied by Griffin and George Ltd., London.

(iii) Cold-setting plastic

Several different types of cold-setting plastics were tried and "Ceemar", supplied by Cromwell and Co. Ltd., Bishop Stortford, was found to be the most suitable. The method described below was established as the standard procedure for mounting all new mineral specimens.

The ground section is placed face downwards in the bottom of the mould. 100 cc. of "Embedding Resin" are thoroughly mixed with 8 cc. of "Hardener" and 10 drops of "Accelerator" and added. If incorrect proportions of the ingredients are used heating and cracking of the mount occurs. The resultant liquid is poured into the plastic mould and allowed to set. This takes about 24 hours. Normally 15 - 20 mounts are made at one time, and larger proportions of the liquids are made up. Using the ice-cube container trays, a large number of mounts can be made at one mixing. The two chief advantages of such

a system are that no high temperatures and pressures are involved, and crystals can be accurately oriented in the plastic

Relative Merits of the Mounting Media used.

The ideal mounting medium should be rigid, able to take a good polish, removable from the mineral specimen, and not affect in any way the physical properties of the material mounted. None of the mounting media used can fulfill all of these conditions, but if sufficient material is available then the cold-setting plastic is usually versatile enough to deal with work on detailed orientation studies. When small and rare crystals are being dealt with, then the low-melting point alloy is the best medium for orientation studies. On theoretical considerations, thermoplastic mounts were not used for normal mounting. The effects of the high temperatures and pressures involved in the thermoplastic mounting on the properties of the mineral specimens were investigated. A small crystal of galena, polished on the octahedral face (111), was mounted in the low-melting-point alloy and ten Vickers indentations were made randomly over the polished surface. Orientation effects were eliminated by maintaining the north-south diagonals of the indenters parallel to one of the three cleavage traces. The same crystal was removed from the alloy

and mounted in clear thermoplastic in the same orientation, and repolished. Similar indentations were made using the same orientation control. An attempt was made to make the polishing processes as similar as possible. The results are given below in Table V.

TABLE V

Mounting Medium.	V.M.H. Range Kg/mm ²	V.M.H. Mean Kg/mm ²
Alloy	63 - 68	66.0
Clear Thermoplastic	95 - 125	109.0

The difference of over 40% in values for the means and for the ranges cannot be accounted for by normal statistical errors. Values for other galena specimens mounted on the octahedral face (111) in both dental plaster and alloy agree to within $\pm 3\%$ of the value obtained on the alloy mounted crystal. It might be accounted for by a difference in chemical composition of the galena, for example non stoichiometry of the crystal exposed by the repolishing. However,

the crystal was etched with dilute nitric acid and no zoning was observed.

It is also interesting to note that the range of values in the thermoplastically mounted case is much larger (30 V.M.H. units for the thermoplastic as opposed to 5 V.M.H. units for the alloy). From these values it would appear that high pressures and temperatures involved in thermoplastic mounting have affected in some way the microhardness values for the galena. This is probable because under conditions of high stress the mineral becomes deformed and "work-hardened". Cleavage and parting are accentuated, rendering the mineral more brittle and resulting in a larger scatter of the hardness values. If this supposition is correct, the amount of work-hardening or deformation will decrease with increasing hardness of the minerals. Thus for hard minerals the effect is probably negligible as any difference due to deformation will be less than the probable error of the results. However, it seems from these results that substantial differences may occur with soft minerals. This topic is discussed more fully in Chapter VII.

C. Grinding and Polishing Techniques

It has already been shown that materials can be considerably

deformed and "work hardened" by coarse abrasion. After reviewing the literature on ore polishing, a method described by Stanton (1957) was investigated, using a wax-abrasive lap and diamond impregnated carrier pastes on napless cloth.

Stanton divides the method into four parts:-

1. Preliminary abrasion using a ^csuccession of silicon carbide abrasions, starting at about 400 mesh. on a rotating gun metal lap; finishing with American Optical Company 303.5 and 305 grades on stationary glass plates.
2. Intermediate abrasion using a cast abrasive-wax lap. The lap is used stationary with 10 - 20 μ silicon carbide.
3. Polishing with diamond abrasives in carrier pastes using napless cloths, the diamond abrasives starting at 4 - 8 μ and finishing with 0 - 1 μ . The 4 - 8 μ stage is used on a rotating lap. (150 r.p.m.) and the final stage (0 - 1 μ) is done by hand.
4. Final polishing using napped cloths and a paste of fine magnesium oxide on a stationary lap.

Attempts were made to cast a wax-abrasive lap as described by Stanton but little success was achieved. In most cases the wax-abrasive lap cracked on cooling. This problem was overcome by pouring the molten wax-abrasive mixture on to a preheated lap and allowing the mixture to cool slowly. It was found that the wax abrasive surface was extremely uneven and

resulted in very rough abrasion. One reason for this was the segregation of abrasive from wax during the slow cooling. As this method was difficult to carry out successfully it was decided to use a modified form of the method described by Barringer (1953). This method is at present employed in the ore-polishing section of the Mining Geology Department at the Imperial College. This method is summarised below.

Grinding Stages.

1. Grinding on a copper plate using 500 mesh silicon carbide and water.
2. Grinding on a copper plate using 850 mesh silicon carbide and water.
3. Grinding on a glass plate with 850 mesh alumina and water.

Polishing Stages

1. Polishing on a linen covered lap rotating at 500 r.p.m. using 850 mesh alumina and water.
2. Polishing on a nylon sueded simplex covered lap at 300 r.p.m. using a $1/5$ diamond paste with a few drops of thin oil.
3. Final polishing on a nylon sueded simplex covered lap at 150 r.p.m. with $0/2$ diamond paste with a few drops of thin oil.

It can be seen that the two methods are very similar

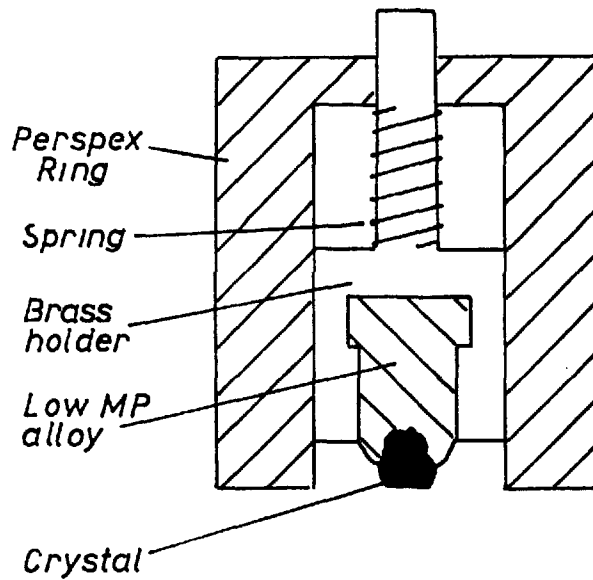
apart from the cast abrasive-wax lap stage. However, the grades of abrasives used in the early stage of Barringer's modified method are very fine and eliminate the need for the wax-abrasive lap stage. Stanton judges the quality of polish by the anisotropism of pyrite and other minerals, and by the lack of scratches produced by his technique. Gray (1961) finds that by this modified Barringer method a very high quality of polish is obtained. All the pyrite studied was found to be anisotropic, in addition to many other minerals formerly supposed to be optically isotropic.

For microhardness measurements it was found desirable to have a number of fine scratches left on the polished surface so the microscope could be accurately focussed.

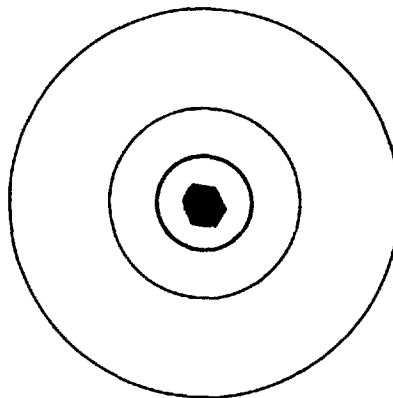
It was anticipated that some small rare crystals of minerals would be encountered in detailed orientation work and that this would present a special problem for the polishing of individual crystal faces. A special polishing holder was designed for such crystals (Figure 3). This apparatus consists of a thick cylindrical ring of perspex with a circular plate, also perspex, screwed to one end of the ring. A brass rod passes through a central hole in the plate and at its lower end its diameter is increased so that it fits and moves smoothly inside the perspex ring. A spring tends to push the brass rod downwards so that its lower end is made flush with the open

FIG. 3
POLISHING HOLDER FOR SMALL CRYSTALS

Natural size



SECTION



PLAN
"Worm's eye view"

end of the ring. Thus the rod is free to rotate and move up and down at the same time. The lower part of the brass rod is hollowed out to receive the low-melting point alloy.

To mount the crystal, the apparatus is inverted with the spring removed. The wide end of the brass rod is positioned about 1/16" below the surface of the ring. Molten alloy is then poured into the cavity until filled just to overflowing. The crystal, with the required face uppermost, is gently dropped into the alloy. A glass slide is placed over the open end of the ring so that the crystal face is aligned parallel with the end of the ring. Due to the high specific gravity of the alloy, nearly all crystals float and due to this buoyancy effect the crystal is pressed against the glass slide and maintained in this position until the alloy solidifies. When the alloy is cold the spring is replaced and the whole apparatus is then ready for polishing.

This method gives an orientation accuracy of $\pm 3^\circ$.

D. Orientation of Sections

(a) Accuracy of Orientation of Mineral Crystals

The accuracy of the mounted crystals depends to a large extent on the perfectness of the crystal faces. Smooth faces increase the accuracy of the work. Where possible actual

crystal faces are used, so that the particular face to be polished is laid face down on the bottom of the mould. With large crystals, particular directions can be cut and ground using a contact goniometer to check the accuracy. With these types of crystal faces, the accuracy is about $\pm 2^\circ$.

For very small crystals the accuracy of grinding is probably of the order of $\pm 5^\circ$.

(b) Orientation and Levelling of the Polished Section

For detailed orientation studies, it was necessary to have means of rotating the polished section in a horizontal plane, and to be able to level the surface of the polished section at right angles to the indenting direction. In addition, a means of securely gripping the section during the hardness determinations is necessary. A sub-stage, to fulfill these requirements, was designed to work in conjunction with the Durinet hardness tester (Figure 4).

The apparatus consists of three parts, a base plate, a triangular rotating upper plate and a top plate for supporting the polished section.

The base plate is circular in shape having a diameter of $3\frac{1}{2}$ " and is graduated every five degrees around its edge. It is marked every 10° from 0° - 360° in an anticlockwise sense.

FIG. 4

Sub-Stage Levelling Device



A triangular plate fits concentrically over a small central boss on the base plate so that it can rotate in the horizontal plane. It can be clamped in position by a central locking screw. At the apices of the triangular base are three foot screws, each of which has a full travel of approximately $\frac{1}{2}$ ". The top ends of the foot screws are cone-shaped to accomodate the top plate.

The top plate is also triangular in shape and rests on the foot screws. A clamping device, consisting of a shaped block of metal and a horizontal screw clamp, is fitted by means of screws to the top plate.

The whole apparatus is made of brass. No lubrication oil is used anywhere on the stage to prevent any "give" effects that may occur during indentation. A series of tests were carried out to see if there was any "give" in the stage during indentation. Three minerals, differing considerably in microhardness from one another, and mounted in different media, were tested both on and off the stage. In each case the orientation was kept constant. The results are given in Table VI. Microhardness values given are the means of ten hardness measurements.

TABLE VI

Mineral	Mounting Medium	Vickers mH. Kg/mm ²	
		On stage	Off stage
Galena ¹	C.Th.P	109	106
Wolframite ²	Bakelite	442	451
Pyrite ³	Dental Pl.	1250	1270

1. Galena. Locality-unknown. Orientation - octahedral face (111) N-S Diagonal parallel to a cleavage trace. Mounted in clear thermoplastic.
2. Wolframite. Locality - Castle-on-Dinas Mine, Cornwall. Orientation - unknown. N-S diagonal parallel to dominant cleavage trace. Mounted in bakelite.
3. Pyrite. Locality - unknown. Orientation - Octahedral face (111). N-S diagonal parallel to edge of crystal. Mounted in Dental plaster.

From these results it was concluded that there was no significant difference in the microhardness values for polished sections when mounted on the sub-stage. The small differences in the values of microhardness were attributed to local variations of hardness in the polished sections as they are well within the probable error of the results.

Routine Procedure for Levelling

(a) Vickers Microhardness Testing

The polished section is securely clamped on the top plate and a small circular bubble level placed on the polished surface. By adjusting the footscrews the bubble is brought to a central position and the level then removed.

(b) Knoop Microhardness Testing

Knoop testing requires a more accurate method for levelling the polished surface.

The surface is roughly levelled using the method described above for the Vickers microhardness work and the circular bubble level replaced by an elongated bubble level. A modification of the standard procedure for levelling a theodolite is used. The bubble level is turned on the surface of the section so that its axis is parallel to two foot screws and quickly levelled using those two foot screws. The level is then turned through 90° and levelled using the remaining foot screw. This procedure is repeated (usually twice) until the bubble is level in both directions. The bases of the bubble level are kept clean to avoid scratching of the polished surface.

(c) Orientation of Crystals in the Horizontal Plane

Orientations of the impressions relative to the position of crystallographic faces are fixed by setting the diagonals of the impression to some observable feature of the crystal, such as a cleavage trace, crystal edge, slip or twin plane etc. The indenters are fixed in the hardness tester so that the diagonals of a Vickers impression are always north-south (N-S) and east-west (E-W) and the long diagonal of a Knoop impression always east-west (E-W).

E. Measurement of Microhardness

The tester used is known as the "Durimet" and is manufactured by E. Leitz Ltd., Wetzlar. It is a standard bench-type instrument designed primarily for metallurgical work. A full description of the instrument is given in various operating manuals and also in a paper by Broschke (1952). Mott (1956) gives an excellent description (Figures 5,6) of the instrument:-

"The base (1) carries a table (2) and a column (3) on which is fixed the microscope (4) and the indenting mechanism (5). The indenter carrier is a double arm lever, the bearings of which consist of two steel points resting on two polished sintered carbide plates and is connected at one end to the lever and at the other to the housing. Any tendency for lateral movement as the indenter is brought into contact with the specimen is counteracted by steel wire springs, so that the indenter is flexibly positioned. The lever is actuated by a spring acting through a camshaft and an intermediate lever. The arm carrying the indenter is lifted by a Bowden cable (19) and at the same

FIG. 5

The Durimet Hardness Tester

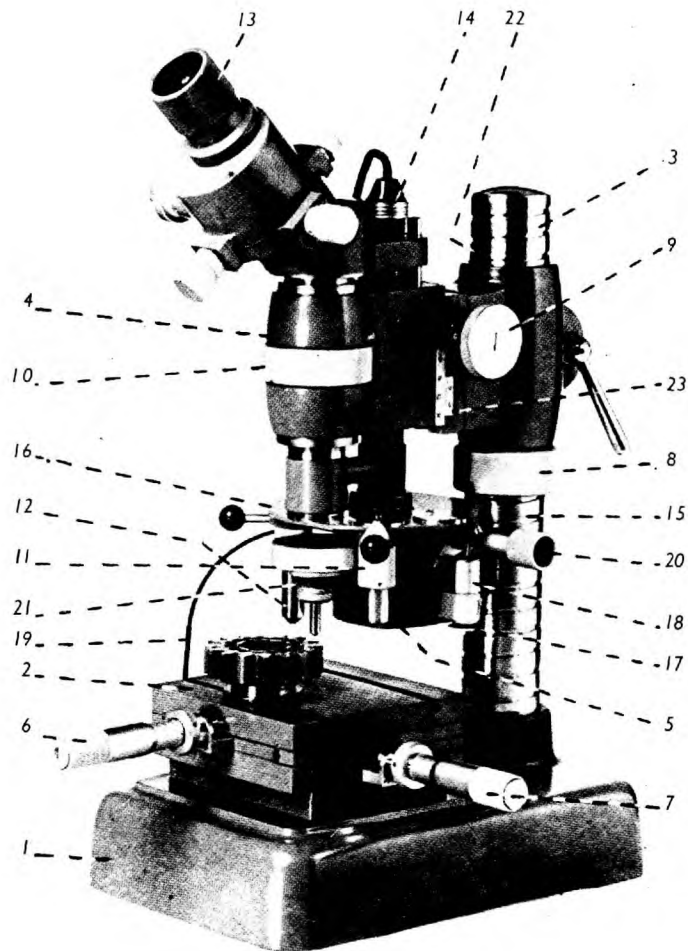


Figure 17. Durimet hardness tester

- | | | |
|-------------------------|----------------------------|-----------------------------------|
| 1—Base | 9—Rack and pinion movement | 17—Screw |
| 2—Table | 10—Fine adjustment | 18—Oil brake |
| 3—Column | 11, 12—Objectives | 19—Wire release |
| 4—Microscope | 13—Measuring eyepiece | 20—Knurled nut for winding up |
| 5—Indentation mechanism | 14—Illuminator | 21—Screw (for fixing the diamond) |
| 6, 7—Micrometer screws | 15—Flexible shaft | 22—Mark |
| 8—Knurled nut | 16—Changer | 23—Division |

FIG. 6

The Measurement of Indentations
Using the Durimet Tester

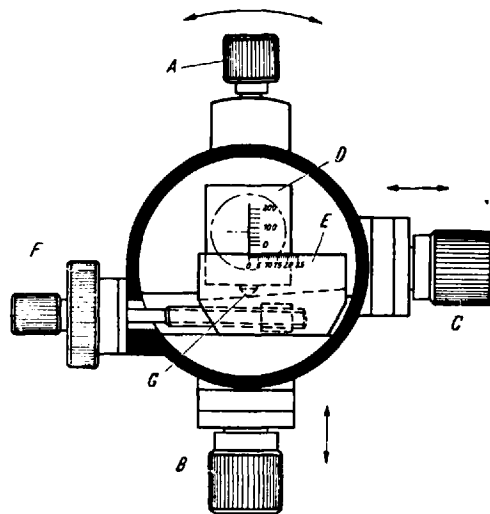


Diagram illustrating special eyepiece on Durimet tester¹¹²

- A—Screw for rotary movement*
- B and C—Screws for cross-slide*
- D and E—Graticules (centring mark and division)*
- F—Measuring screw*

time the spring is preloaded. When the spring is released the indenter approaches the specimen at a speed controlled by an oil brake. The spring pressure is automatically cut off when the full load is applied and the load is left on for 10 seconds before the indenter is withdrawn. The indentation is measured to an accuracy of $\pm 0.5 \mu$ by means of one of two objectives (11) and (12) which are mounted together with the indenter on a rotating head (16) and a special eyepiece shown in Figure 6. This consists of a rotating part which can be clamped by means of a screw (A), lateral movement on a cross slide being obtained by screws (B) and (C). Two graticules (D) and (E) are arranged in the image plane of the eyepiece and are moved independently over a wedge by a measuring screw (F). Loads of 15, 25, 50, 100, 200, 300 and 500 grammes can be applied and scratch hardness tests can be carried out by moving the table (2) with the micrometer. Screws (6) and (7) the movement of the table being on balls in cross-slides".

A green filter in the micrometer eyepiece was removed and no significant differences were found in the resolution of the optical system. The filter was fitted into an aluminium cap that could be placed over the eyepiece if necessary. A polaroid disc was placed into the optical system with its axis east-west, and another polaroid disc fitted into an aluminium cap that could be placed over the eyepiece. In this way the grain boundaries of some of the more strongly bi-reflectant minerals could be observed, but because of the limited strength of the light source pleochroism and anisotropism in weakly bi-reflectant minerals could not be detected.

F. Routine Procedure

The following procedure was made standard for all work in an attempt to obtain consistent results.

1. The light is switched on and the transformer scale set to 0.6 amps so that lighting conditions are constant.
2. The low power objective is swung into position and focussed on the levelled surface of the polished section.
3. The area required for indentation is selected by moving the table using the two micrometer screws.
4. The high-power objective is swung into position, focussed and the area required is positioned coincident with the cross-wires using the micrometer screws.
5. The indenter is swung into position and the Bowden cable released. After 30 seconds the indenter is withdrawn by turning the knurled knob (20) .
6. The lengths of the diagonals of the impression are accurately measured either twice or four times using the optical micrometer eyepiece.

The speed of indentation was fixed at 0.05 mm./sec. It was decided at the outset that Vickers and Knoop values should be determined for about 200 minerals. Orientation studies were to be carried out on minerals whose orientation could be accurately determined.

For unoriented mineral sections, it was decided that 10 impressions made where possible on differently oriented mineral grain, would give a reasonably complete range of the microhardness values. A balance had to be struck between

the number of impressions necessary to give a complete range and the time that could be spent on each mineral section. To obtain as complete a range as possible for any mineral it was decided to work on as many specimens from different localities as possible.

For oriented minerals sections, 10 impressions were made on any particular face usually rotating the crystal through 10° for each impression. With highly symmetrical minerals the rotation interval was reduced to 5° .

Whenever an impression was measured the shape of the sides was noted together with the amount and type of deformation i.e. cracking, the presence of dislocation planes (glide and twin planes and their orientation) and fracturing. The sizes of the smallest and largest impressions were noted and the mean impression size calculated. Using standard tables the mean and range of microhardness for a particular material is determined. In some cases, where testing extremely soft and extremely hard minerals, the hardness values had to be computed from the original formulae.

Two standard forms (Figures 7, 8) were drawn up and duplicated so that the data could be recorded concisely.

A number of precautions were taken to avoid anomalous values. These were as follows:

1. The minerals grain size (diameter) was not allowed to fall

FIGS. 7,8.

STANDARD FORMS

Index No. <u>R 1183</u>		Name. <u>Pyrrhotite (Bak). 3-11-24(C)</u>								
Crystal Syst.		Chem. Comp.								
Locality. <u>Probably Sudbury Mine Ontario, Canada</u>										
Type. Indenter. <u>VIX</u>										
State of Surface. - <u>Crystal / Cleavage / Polished.</u>										
Load.	<u>100 g</u>	Time.	<u>30 sec.</u>							
Speed. <u>0.05 mm/sec.</u>		"min.								
Orientation Surface. <u>Unknown</u>										
Orientation Indenter. <u>Unknown.</u>										
No.	1.	2.	3.	4.	5.	6.	7.	8.	Mean.	Description.
	N-S.	E-W.	N-S.	E-W.	N-S.	E-W.	N-S.	E-W.		
01	231	231	231	231					23 10	str side on face square
02	232	234	232	234					23 30	all cc faces not square
03	234	230	234	230					23 20	cv and str. sides less sq. if distorted
04	230	232	230	232					23 10	cc faces square on distor
05	230	234	230	234					23 20	str sides square on face.
06	237	239	237	239					23 80	all cc faces not square if sharp
07	238	234	238	234					23 60	not square if not flat str side
08	233	234	235	234					23 45	cv face from if distorted sq
09	234	236	234	236					23 30	cv str side if distorted
10	231	232	231	232					23 15	all cc faces square on face
11										
12										
13										
14										
15										
Totals.										

Further Notes.

1139


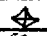

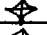
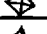
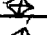
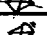
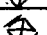
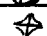

Mean. 23 30

Error.

Hardness Value. 342

Range = 231 - 238

VMH Range = 348 - 327

Index No. <u>R. 1183 (A)</u>		
Description of impression.	X-Co-ords	Y-Co-ords
01 	0248	7164
02 	7341	8764
03 	6731	4222
04 	9710	6313
05 	0012	0924
06 	0778	7128
07 	1375	3188
08 	5500	4009
09 	9663	3549
10 	0724	7351
11		
12		
13		
14		
15		

ADD. NOTES.

pol section 1139

below 3X the size (diagonal length) of the impression.

2. The impressions were made well away from crystal boundaries, crack, flows, twin planes and cleavage traces. When indenting small grains the impressions were kept as close to the centre as possible.

3. Impressions were kept more than 10 diameters apart from one another to prevent any mutual interference effects.

4. Any impression~~x~~ that developed excessive cracking and fracturing around its edges ~~were~~^{was} rejected for measuring purposes.

5. Any impression made whilst the instrument was subject to vibration was also rejected.

G. Accuracy and Reproducibility of Results.

(a) Instrumental Errors

Mot^t (1956) has described the various types of instrumental errors that can occur in microhardness testing.

- i. Deviation of loading from the nominal value.
- ii. Incorrect profile of the indenter
- iii Effect of tilt.
- iv Lateral movement of the indenter
- v Measurement of the impression.

i. Deviation of loading from the nominal value

As far as could be ascertained the instrument had no

loading errors due to defects in its manufacture. On a few occasions the instrument was subjected to vibration whilst indentation was taking place. Resultant impressions were anomalously large and not measured. They were often accompanied by an unusual amount of cracking. Such cases were rare and it was considered unnecessary to construct a "vibration-proof" table for the instrument.

The time of indentation was kept constant in all tests, at 12 seconds \pm 1 second. Mitsche and Onitsch (1951) give a series of values of the diagonal lengths for halite, galena fluorite, calcite and corundum on varying the times of indentation. They show a gradual increase in diagonal length with time. By standardising the time at 12 seconds such errors are eliminated.

ii. Incorrect profile of the indenter

The profiles of the Vickers and Knoop indenters were considered to be satisfactory but on receiving the instrument from the manufacturers it was found that the Knoop diamond had been inaccurately set in its mount so that impressions produced were pronouncedly asymmetric and gave anomalously low hardness readings. The diamond was remounted by Leitz so that a symmetrical impression was produced.

iii. Effect of tilt

The effect of tilt is discussed by Mott and he concludes

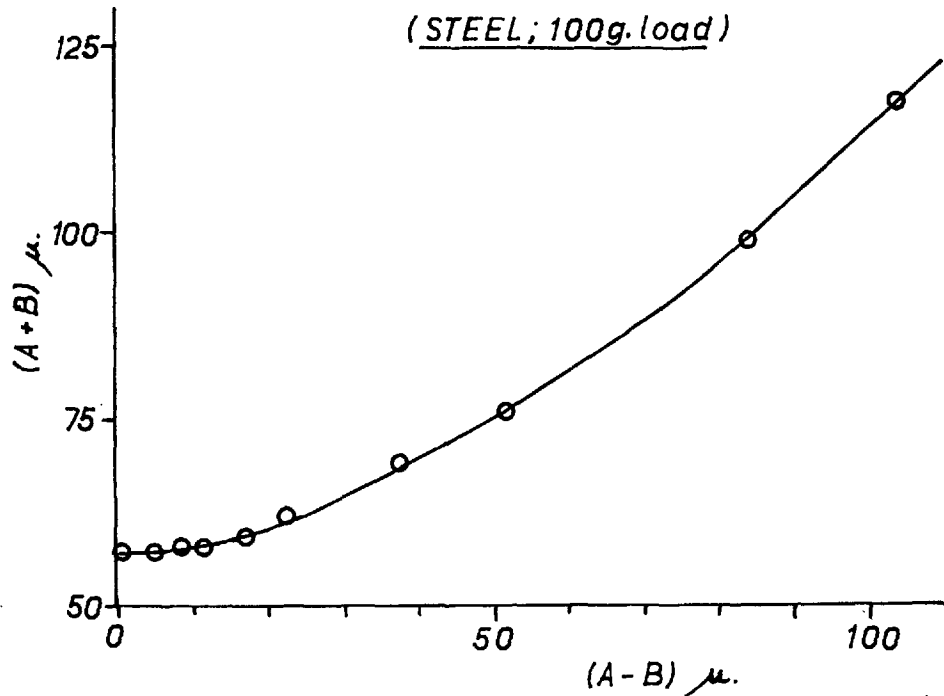
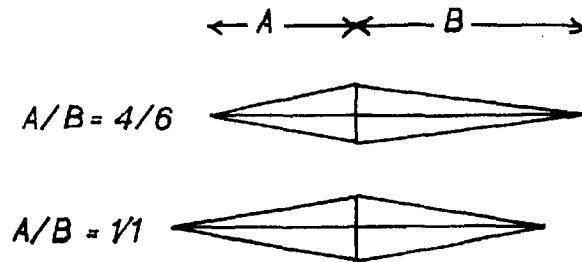
that for a Vickers indentation the mean hardness is a constant, whatever the tilt of the indented surface, provided that both diagonals of the indentations are measured. In detailed orientation work the effects of tilt had to be eliminated especially when studying the shape of the impressions and the relative lengths of the diagonals.

The effect of tilt on Knoop impressions is far more pronounced. Theoretically if the angle of tilt is $30^{\circ}45'$ then an impression of infinite length should be produced with a Knoop diamond. A series of tests were carried out on a standard steel block using a 200 g load. The block was tilted about a horizontal axis at right angles to the long diagonal of the Knoop indenter, and indentations made at varying angles of tilt. The lengths of the two halves of the impression, A and B, were measured separately. In Figure 9 A + B is plotted against A - B. From this graph it can be seen the maximum permissible ratio of A to B is 6:4. This means that the maximum amount of tilt is less than 1° .

It is particularly important to eliminate tilt effect in detailed orientation studies where it is necessary to rotate the polished surface through a horizontal angle of 90° . If tilt does exist in such tests, apparent microhardness anisotropism will result and this will either diminish, accentuate or confuse real mineral anisotropism.

Localised tilt often occurs on polished surfaces where

FIG. 9
EFFECT OF TILT ON THE LENGTH
OF KNOOP INDENTATIONS



excessive polishing relief has been produced. On some occasions using a Knoop indenter, it was found impossible to indent small soft grains of one mineral set in a matrix of a hard one. Under such conditions Knoop impressions were only made on large areas of such soft minerals. Hard minerals were indented towards the centres of the grains.

iv. Lateral movement of the indenter

One of the chief features of the design of the tester is to avoid any lateral movement of the indenter.

v. Measurement of the impression

If we take the formula for determination of hardness,

$$H = \frac{K L}{d^2}$$

where H = microhardness

K = constant

L = load

d = diagonal length.

then differentiating with respect to d

$$\begin{aligned} \frac{dH}{dd} &= - \frac{2KL}{d^2} \\ &= \frac{2H}{d} \end{aligned}$$

or $\frac{\Delta H}{H} = \frac{-2 \Delta d}{d}$

From this it can be seen that the error in hardness number for a given measurement of a diagonal is directly proportional to the hardness of the material.

For example, with hematite of V.M.H. = 1000, an error of 0.5μ in the measurement of a 13.5μ indentation diagonal at a load of 100 g., results in an error of 8%, whereas in the case of galena with V.M.H. = 75, an error of 0.5μ in the measurement of a 49.5μ indentation diagonal gives an error of 2%.

A series of tests were carried out to try to eliminate any personal error or bias in the measurement of impressions. 15 Vickers indentations were made on a test steel block at 100 g load and each diagonal length was measured 10 times. For any given diagonal length the average spread of the readings was about 0.5μ , but it was impossible to say whether the readings were assuming a log-normal distribution. A further set of 50 readings of 10 diagonal lengths were measured and histograms plotted. In all cases the histograms were symmetrical and on average 80% of the readings were within 0.05 of the arithmetic means. From this data it was concluded that the author had no particular tendency to measure too high or too low and that the measuring was reasonably consistent.

Other observers were then asked to measure the same

diagonal lengths independently and their results agreed in all cases to within 0.2% of the authors results. From these results it was concluded that for medium and large sized impression i.e. greater than 15 μ , two measurements of the diagonal lengths were sufficient, whilst with very small impressions i.e. less than 15 μ , four measurements of the diagonal lengths were necessary.

A number of points were brought out in these tests:

- 1.) The edges of the indentations should be focussed as sharply as possible each time a measurement is made and the measurement should be made quickly.
- 2.) The cross-hairs should be kept as fine as possible and frequently readjusted.
- 3.) The instrument and bench, other than the measuring eyepiece, should not be touched during the measuring of a diagonal length.
- 4.) The lighting should be kept constant (0.6 amps).
- 5.) Not more than two hours microscope work should be done without a break. It was found that after this period, readings took longer to make and were less accurate.

It should be stressed that in many minerals, fracturing occurred around the impressions and reduced the accuracy of measuring the diagonal length to about $\pm 0.5\mu$. It was also found difficult to obtain consistent measurements of diagonal lengths for minerals of low reflectivity.

(b) Errors dependent upon the nature of the material

Minerals in polished sections are seldom flawless, and these imperfections often lead to anomalous hardness results. Siebel (1943) considered that cavities and inclusions just below the surface indented affect the microhardness values. It has been noted that an increase in scatter of hardness values of galena may be brought about by the high pressures and temperature involved in thermoplastic mountings. Cracks and cleavages noticeably reduce microhardness results and result in uneven indentations. The values of microhardness for small inclusions of mineral are considerably lower than the standard values, and impressions are accompanied by extensive cracking.

Thus in order to obtain a representative value for the microhardness it is necessary to make a number of impressions and take a mean of these values. The precise number of impressions required will depend on the type of testing involved and on the nature of the minerals being tested.

Henriques (1957) discusses this problem in the determination of Vickers microhardness values on oriented sections of sphalerite crystals. In a statistical survey, he shows (Table VII) that error in microhardness values is considerably reduced by increasing the number of indentations. From this table it would appear that the optimum number of impressions

is 10. It is interesting to note that he considers that 70 - 95% of the spread in values for sphalerites is due to variations in the hardness of the mineral and only 10 - 25% is due to the measuring technique.

For unoriented minerals it was decided that 10 impressions at random orientations would give a reasonably complete spread of the values.

TABLE VII

Number of Measurements	Error of means of diagonal length in microns	Average error of means expressed in H.V.
1	0.403	4
2	0.285	3
3	0.233	2
5	0.180	2
10	0.128	1
15	0.104	1
20	0.090	1
25	0.081	1
50	0.057	1
100	0.040	1
200	0.029	1

After Henriques 1957.

CHAPTER III

VARIATION OF MICROHARDNESS WITH LOAD

A. Variation of the Microhardness Values with Load

a). General

It is now an established fact that microhardness values are dependent upon the load applied during indentation - Mott (1956). Many conflicting theories have been put forward to explain this phenomenon, particularly in the metallurgical field. Mott (1956) describes the opposing concepts of Onitsch and Grodzinski and concludes that more detailed and accurate results are needed before definite conclusions can be drawn. In the hope of throwing some light on this subject, from a mineralogical point of view, a series of tests were carried out on oriented sections of certain minerals. The indenting load was varied from 15 g. to 300 g. and the results plotted in graph form, (Figures 10 - 16). In addition, results have been obtained at varying loads on sections, mostly unoriented, of the remaining ore minerals. Details of these results are given in Volume II.

FIG. 10
VICKERS MICROHARDNESS / LOAD PLOT
FOR GALENA

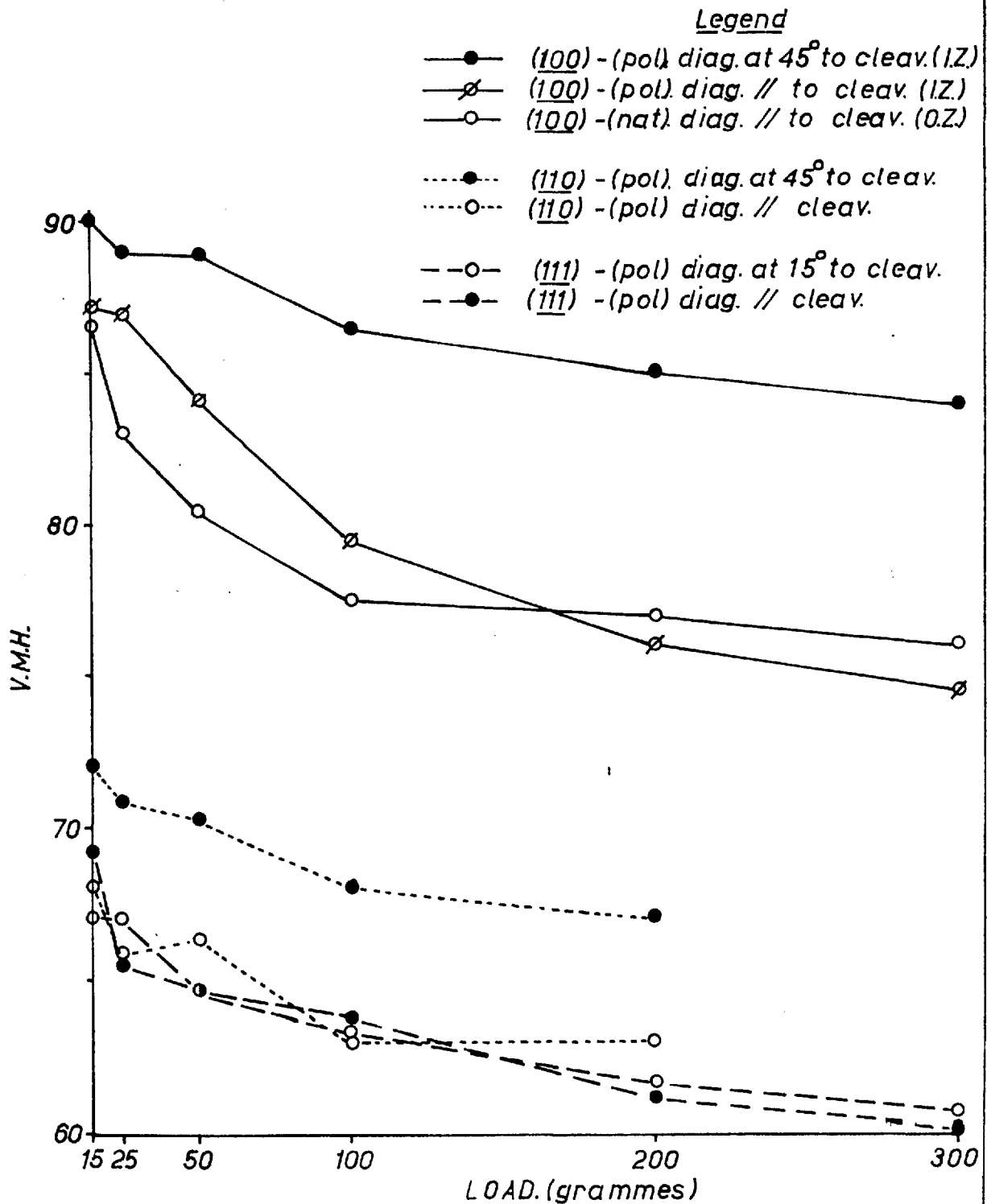


FIG.11
KNOOP MICROHARDNESS / LOAD
PLOT FOR GALENA

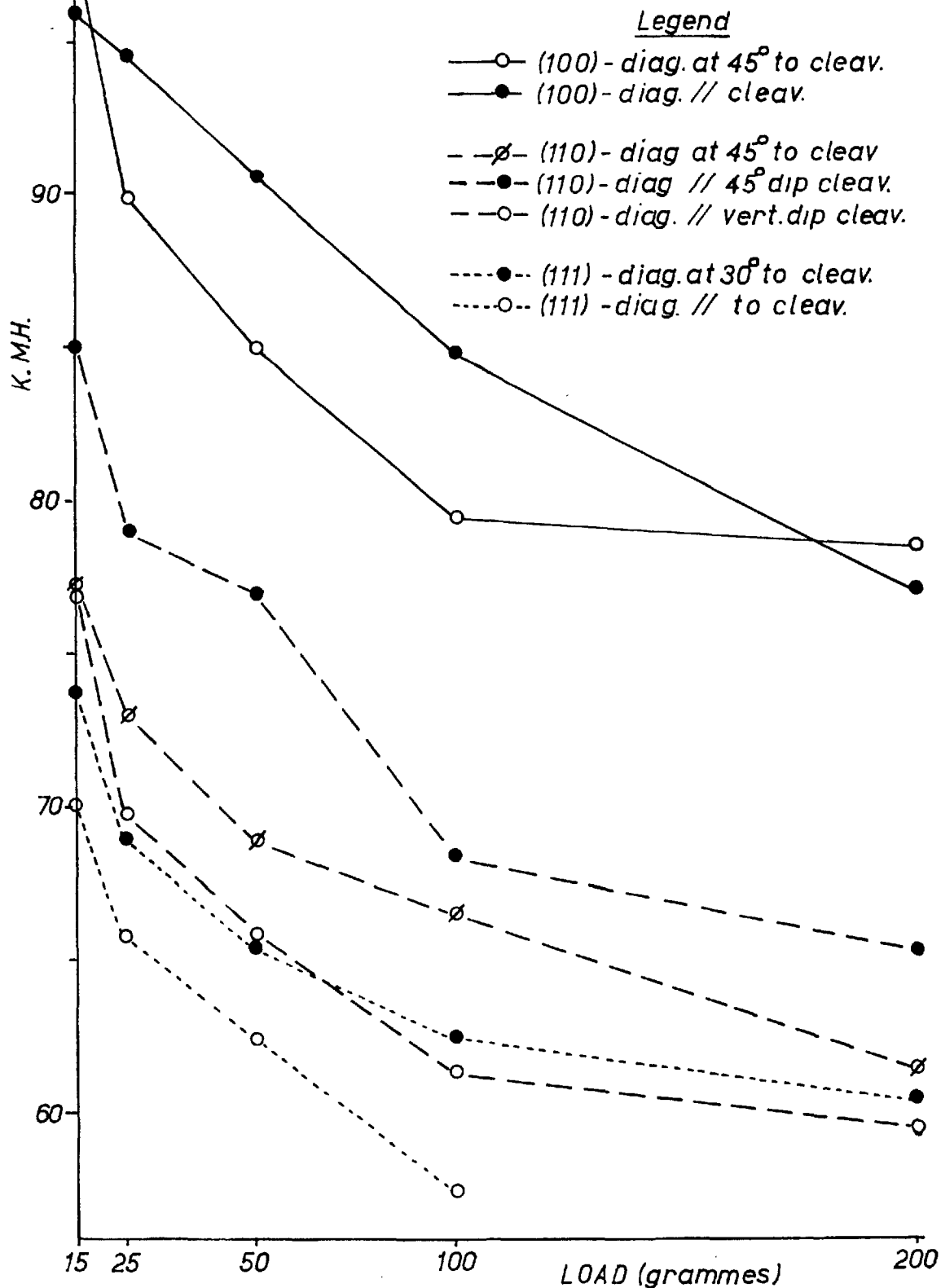


FIG. 12

MICROHARDNESS/LOAD PLOTS FOR
SPHALERITE

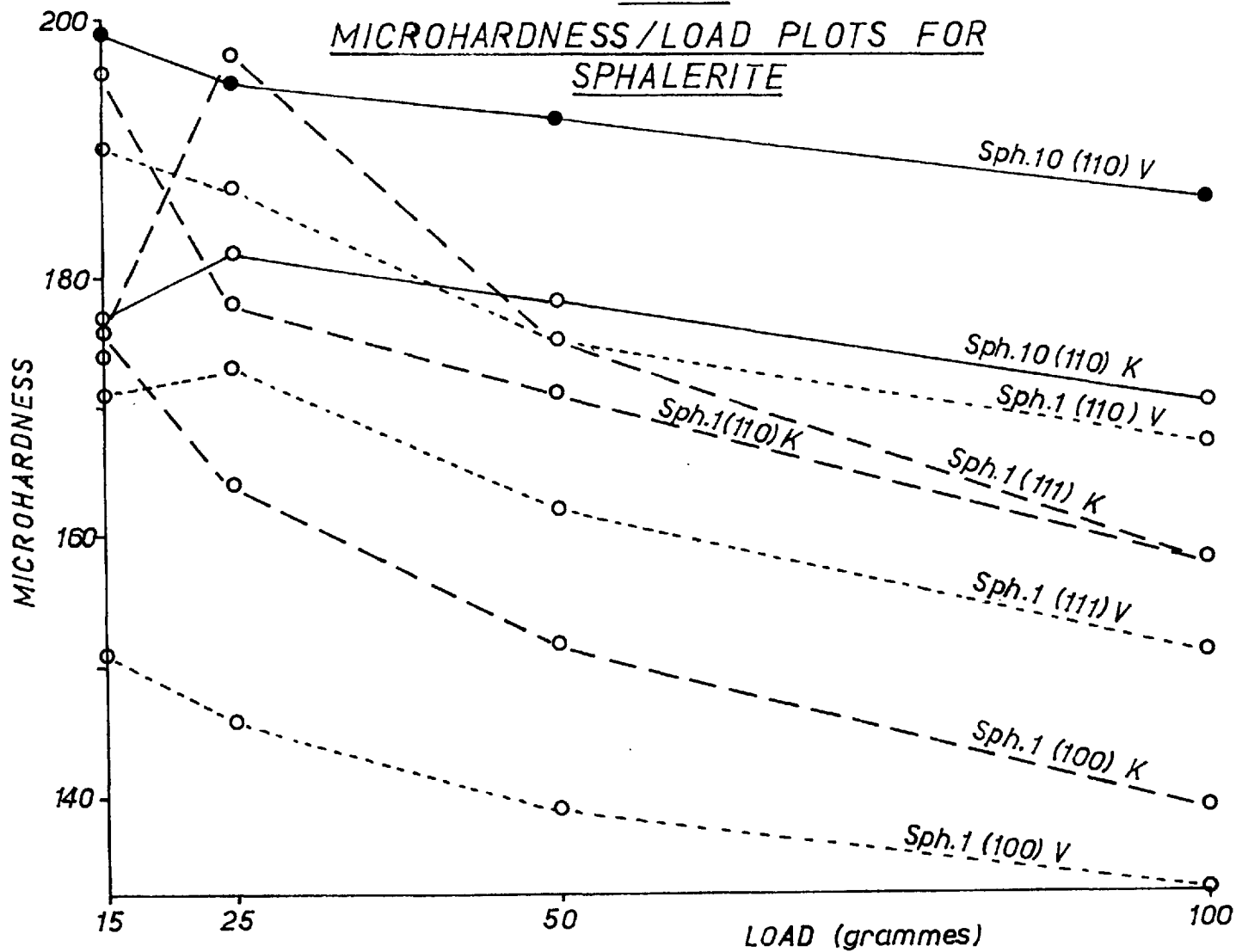


FIG. 13
MICROHARDNESS/LOAD
STIBNITE, BISMUTHINITE

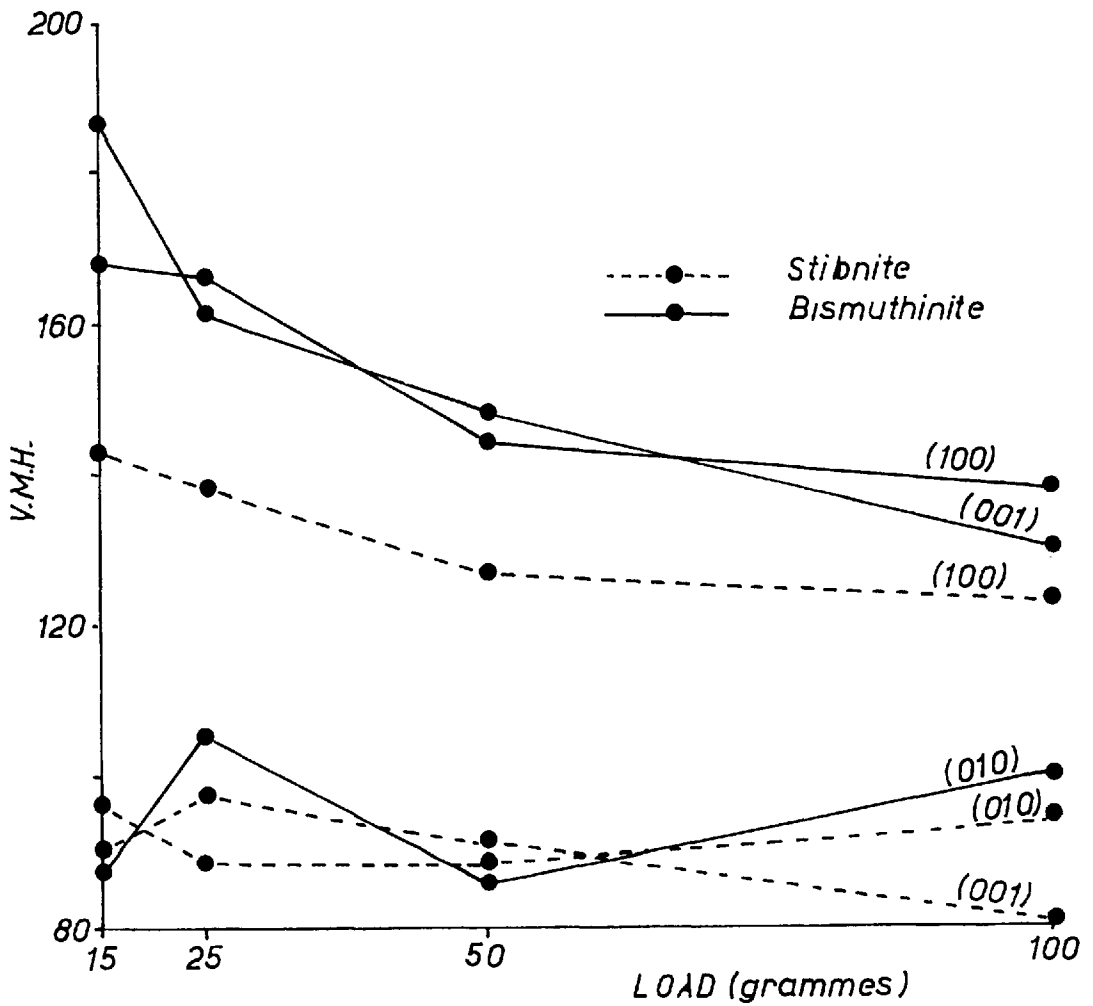


FIG.14
MICROHARDNESS/LOAD PLOTS

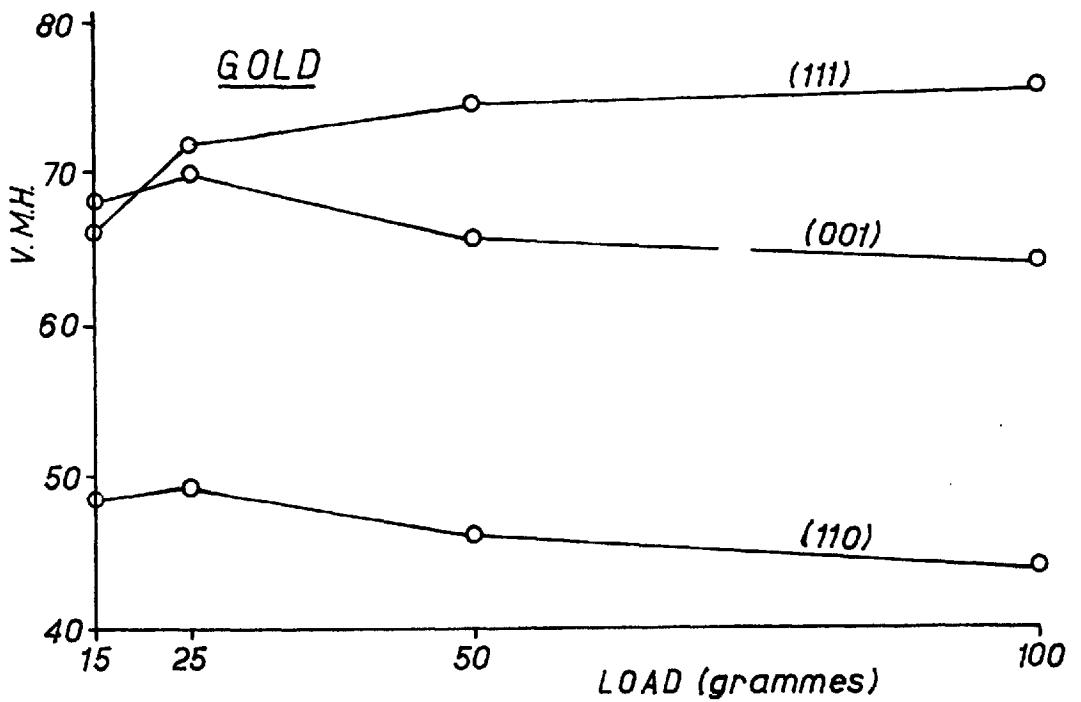
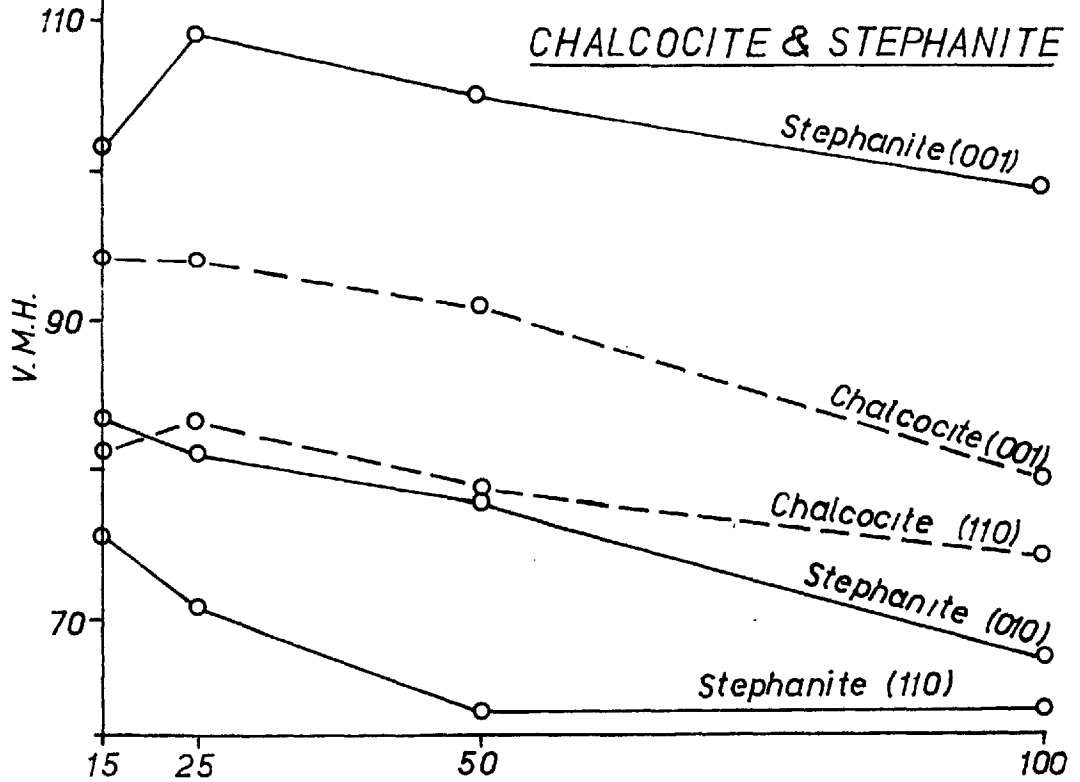
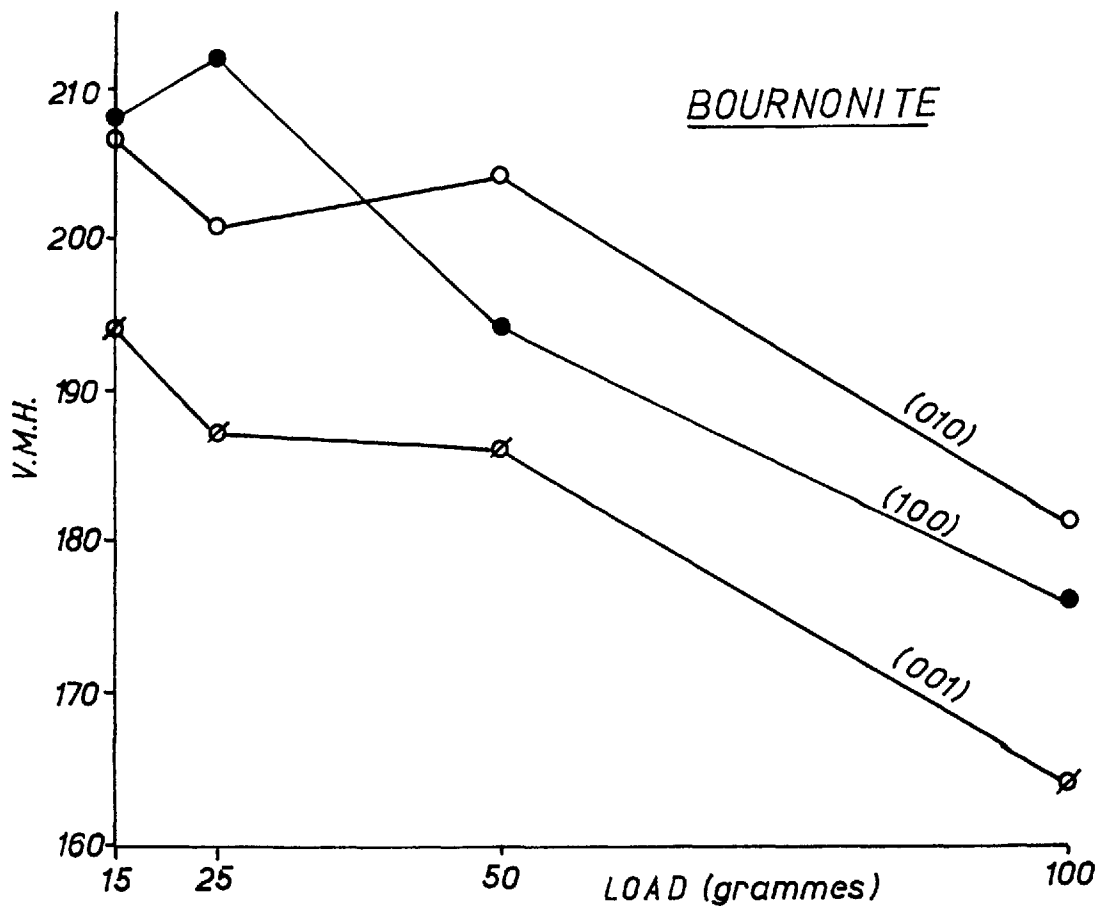
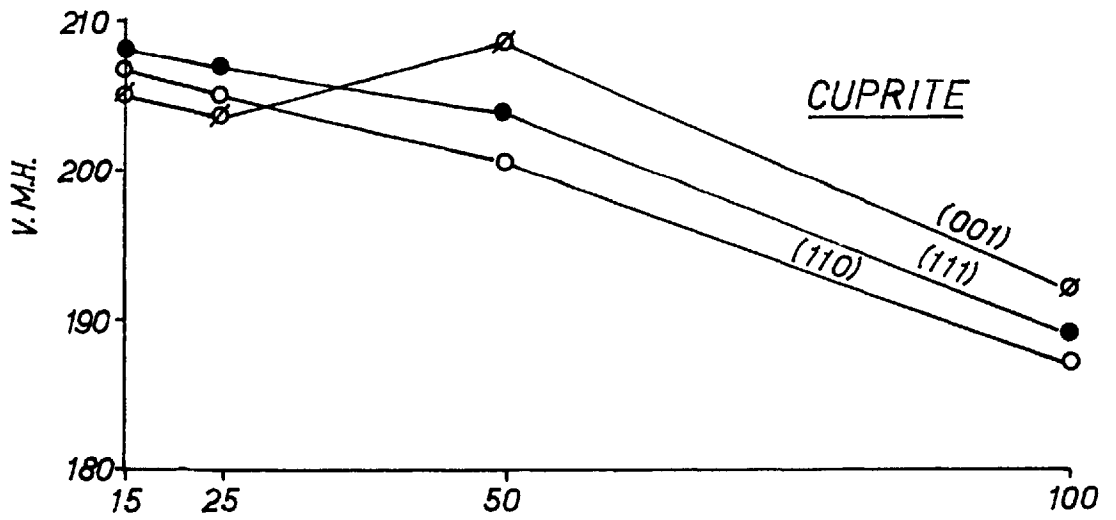
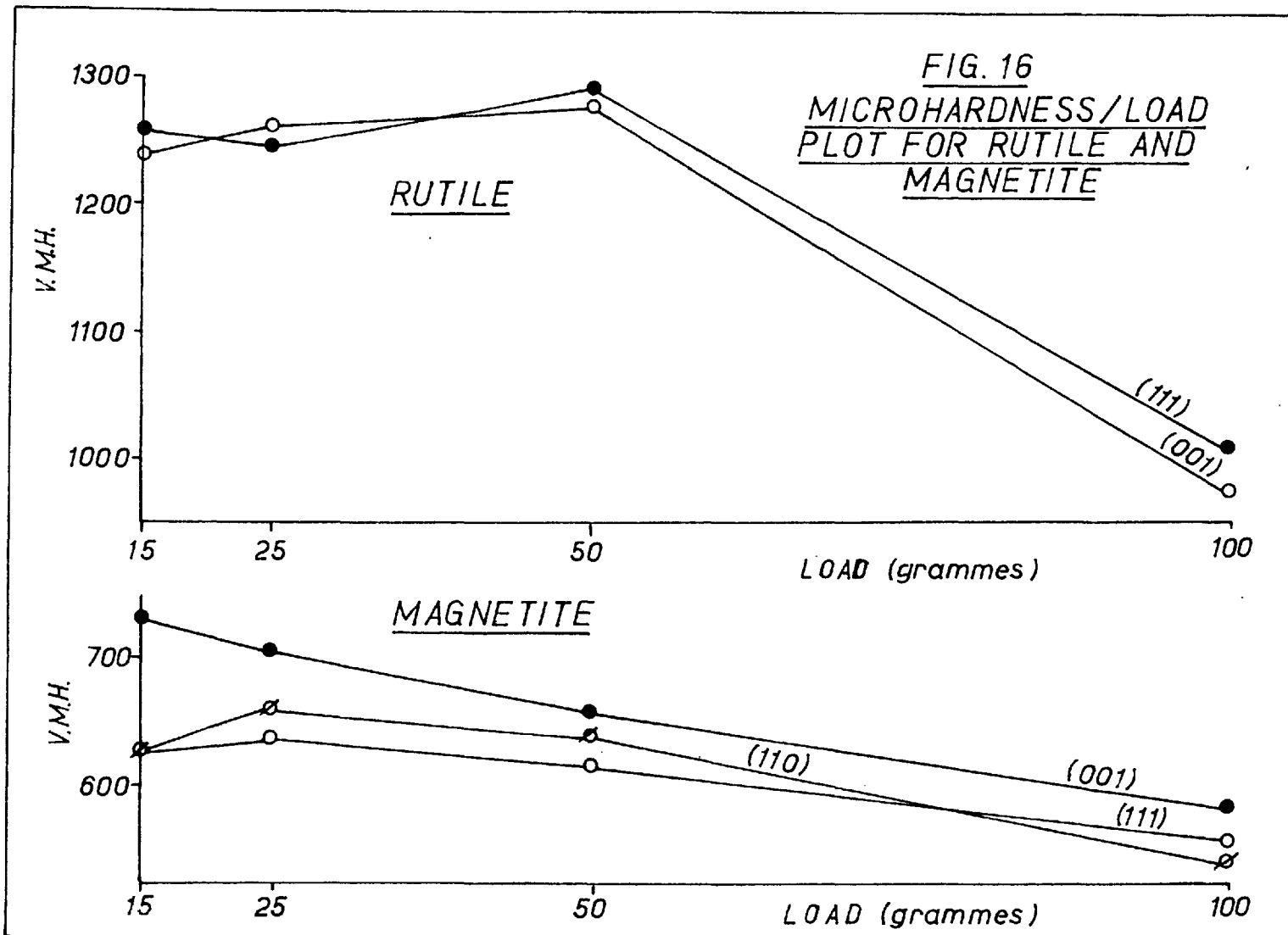


FIG. 15
MICROHARDNESS/LOAD PLOTS





Another method of expressing the variation of micro-hardness with load is by plotting "Meyer lines". Meyer (1908) found in Brinell hardness testing, using a spherical steel ball as the indenter, that for a given diameter of impression the following relationship was true:

$$L = ad^n$$

where,

L = load applied,

d = diameter of the impression,

and a and n are constants, for a given material.

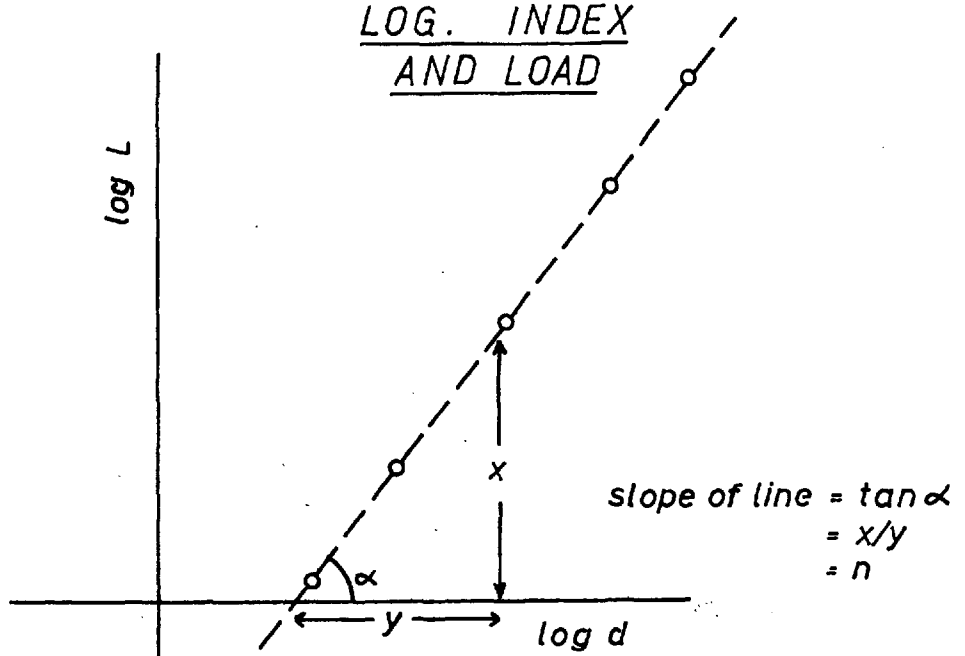
"n" was termed the "logarithmic index" and found to vary between 2.0 and 2.5 depending upon the condition of the surface tested. The value was found to be nearer to 2.5 for a fully softened state and nearer to 2.0 with increasing amount of cold-working applied to the material. Meyer considered that the value of "n" was representative of the capacity of work hardening of the material. It could be determined experimentally by plotting log L against log d, and measuring the slope of the line, since

$$\text{Log } L = \log a + n \log d \quad (\text{Fig. 17})$$

This test is known as the "Meyer Line Analysis".

Nakhla (1956) published a series of Vickers micro-hardness values for loads ranging from 25 g. to 300 g.,

FIG. 17
THE RELATIONSHIP BETWEEN
LOG. INDEX
AND LOAD



$$L = ad^n$$
$$\log L = \log a + n \log d$$

TABLE VIII

GALENA (VICKERS INDENTER)

Relationship of orientation to the microhardness and the logarithmic index.

Orientation of Surface	MH. (100 g) Kg/mm ²	"n"
Cube (100) Polished face ¹ . Diags. at 45° to cleav. traces.	86.4	1.98
Cube (100) Polished face ¹ . Diags // cleav. traces	79.5	1.91
Cube (100) Crystal face ¹ . Diags. at 45° to cleav. traces	77.6	1.89
Cube (100) Polished face ² . Diags. // cleav. traces	69.1	1.92
Cube (100) Crystal face ² . Diags. // cleav. traces	69.1	1.92
Rhombdodecahedral (110) Diags. at 45° to cleav. traces	68.4	1.94
Rhombdodecahedral (110) Diags. // to cleav. traces	62.9	1.96
Octahedral (111) Diags. to cleav. traces	63.5	1.92
Octahedral (111) Diags. at 15° to cleav. traces	63.1	1.92

TABLE IX

GALENA (KNOOP INDENTER)

Relationship of orientation to the microhardness and the logarithmic index.

Orientation of Surface	MH. (100g) Kg/mm ²	"n"
Cube 100 Diags. at 45° to cleav.trace	79.5	1.80
Cube 100 Diags. // cleav. traces.	84.9	1.84
Rhombdodecahedral (110) Diags. at 45° to cleav. traces	66.4	1.82
Rhombdodecahedral (110) Diags. // to cleav. traces of 45° dipping cleavages.	68.3	1.78
Rhombdodecahedral (110) Diags. // to cleav. traces of vertically dipping cleavages.	61.3	1.79
Octahedral (111) Diags. at 30° to cleav. traces.	62.4	1.80
Octahedral (111) Diags. cleav. traces	62.5	1.80

TABLE X

SPHLARERITE (VICKERS AND KNOOP INDENTERS)

Relationship of orientation to the microhardness and the logarithmic index.

Orientation of Surface		MH. (100g) Kg/mm ²	"n"
<u>VICKERS</u>			
Sph. 10.	(110)	186	1.92
Sph. 1.	(110)	167	1.91
Sph. 1.	(111)	151	1.86
Sph. 1.	(100)	133	1.87
<u>KNOOP</u>			
Sph. 10.	(110)	170	2.05
Sph. 1.	(110)	158	1.91
Sph. 1.	(111)	158	1.85
Sph. 1.	(100)	139	1.77

N.B.

Sph. 1. contains 0.08% Fe.
Sph. 10. contains 10.70% Fe.

For Vickers and Knoop values, the (E-W) diagonals were maintained parallel to prominent cleavage traces, for all orientations.

TABLE XI

(VICKERS INDENTER)

Relationship of orientation to the microhardness and the logarithmic index.

Mineral and Orientation	V.M.H. (100g) Kg/mm ²	"n"
Gold.	(001)	63.8
	(111)	75.7
	(110)	43.7
Chalcocite	(110)	74.3
	(001)	79.3
Stibnite	(001)	80.3
	(010)	94.3
	(100)	123
Bismuthimite	(001)	130.0
	(110)	101.0
	(100)	138.
Stephanite	(001)	98.5
	(110)	61.9
	(010)	67.0
Bournonite	(001)	164
	(010)	181
	(100)	176

TABLE XI Contd.

Mineral and Orientation		V.M.H. (100g) Kg/mm ²	"n"
Cunrite	(001)	192	1.96
	(111)	189	1.94
	(110)	187	1.92
Rutile	(001)	983	1.80
	(111)	1015	1.80
Magnetite	(001)	590	1.80
	(110)	546	1.84
	(111)	563	1.90

N.B.

The indenter was rotated through 90° on each crystal face for the above minerals. After each impression has been measured, the crystal face was rotated horizontally through 10°, and a subsequent impression made.

obtained on polished sections of about 50 ore minerals. These results were examined with a view to plotting Meyer line analyses but they were found to be inconsistent. No mention was made of the orientation of the minerals, except

in one case, or of the number of measurements taken. Consequently these results were considered unsuitable for the determination of "n" values.

In the present work, logarithmic indices were determined for oriented sections of the following minerals; galena, sphalerite, stibrite, bismuthinite, gold, stephanite, chalcocite, bournonite, cuprite, rutile and magnetite. Values for the logarithmic indices of these minerals may be found in Tables VIII, IX, X and XI.

(b) Results.

(i) Accuracy

Before discussing the results it is first necessary to assess the accuracy of the values obtained. Each value of microhardness is given in Tables VIII, IX, X and XI and Figs. 10 - 16, and is the mean obtained from the measurement of ten impressions. The probable error of the means for these results were calculated from the following formula;

$$E = 0.6745 \sqrt{\frac{d^2}{n(n-1)}}$$

where

E = probable error of the mean

d^2 = sum of the squares of the deviations
of the individual measurements from the
mean

n = number of measurements taken.

Table XII gives the ranges of probable errors of the mean values of microhardness obtained from the oriented sections of the minerals listed. Probable errors of the logarithmic indices were calculated in a similar manner.

On randomly oriented sections of minerals, no probable errors have been assigned to the mean values of microhardness. A mean~~x~~ is the average value obtained from ten impressions made in grains of different orientations. Thus, in anisotropic minerals, the probable error of the mean would depend largely on the randomness of the orientation of the mineral grains indented.

It should be stressed that in all microhardness determinations it is often only a measure of the self-consistency of the results and does not take into account any introduced biased errors caused by inadequacies of the human eye. This is particularly important when testing at low loads where relatively small errors in the measurement of the size of an impression results in large errors in microhardness values.

TABLE XII

Probable Errors of Mean Microhardness Values and Logarithmic Indices

Mineral	Max. Prob. Error in "n" \pm	Range of Probable error expressed in M.H. units \pm
Galena	0.01	0.2 - 1.0
Sphalerite	0.02	1 - 3
Gold	0.02	1 - 2
Chalcocite	0.02	1 - 2
Stibnite	0.05	3 - 7
Bismuthinite	0.05	3 - 7
Stephanite	0.03	3 - 7
Bournonite	0.03	1 - 3
Cunrite	0.01	0.5 - 1.0
Rutile	0.02	10 - 15
Magnetite	0.01	5 - 7

cleavage traces (100), and when the long diagonal is at 45° to the cleavage traces, (110). Such differences indicate different mechanisms of deformation of the galena during

The probable errors of the logarithmic indices are dependent upon the accuracy of means of the microhardness values. "n" is determined by drawing the best fitting line through a number of points, normally four, but five in the case of galena, and measuring the slope of the line. Thus the error is dependent upon the deviation of the points from the "best line". Where the points are close to the best line a small probable error, about ± 0.01 , will result. On strongly anisotropic mineral face, as for example on the (010) face of stibnite, the probable error may be as large as ± 0.5 .

(ii) Results obtained on oriented sections of minerals

Galena

In all the results, microhardness values increase with decreasing load, whatever the orientation. The Knoop values show a greater range of microhardness than the corresponding results for the Vickers indenter. This is reflected in the difference in values for "n"; 1.78 - 1.82 for the Knoop indenter, and 1.89 - 1.98 for the Vickers indenter. It is interesting to note the difference in profiles between the Knoop values on the cube face (100), when the long diagonal is parallel to the

indentation for these two positions. Minor irregularities in the other profiles are probably due to measuring errors. The probable error of "n" for this mineral is very small, less than ± 0.01 . There appears to be no correlation of the logarithmic index with orientation. According to Mott, the effect of polishing or cold-working is such as to increase the logarithmic index of the materials. The present results on a natural and polished cube face of galena indicate if anything the reverse in the case. No explanation can be given for these anomalies.

Sphalerite

In most cases an increase in microhardness results from a decrease in the load. The profiles of both the Knoop and Vickers are similar, the Knoop tending to be slightly steeper, giving rise in two cases to lower values for the logarithmic index. Whereas an increase in microhardness occurs for all orientations of both sphalerite from 100 g. to 50 g., and from 50 g. to 25 g., a marked variation occurs from 25 g. to 15 g. Of the eight profiles plotted, five show an increase of hardness from 25 g. to 15 g. whilst three show a decrease. There appears to be no significant differences in the profiles obtained from different orientations of sphalerite or from differences

in chemical composition. The large variations in microhardness for the octahedral face (111) of sphalerite L. may be accounted for by differences in chemical composition, as this particular polished section of sphalerite showed colour zoning. The high value of "n", 2.05, for the (110) section of sphalerite 10. (Knoop indenter) may be accounted for by anomalous microhardness values at 15 g.

Stibnite - Bismuthinite

On the (100) and (001) an increase in hardness is associated with a decrease in load. The profiles for the (010) faces are very irregular, showing no particular trend. These irregularities correspond with large probable errors of the means for the (010) faces, being considerably larger than for the other two faces. These irregularities are reflected in the large difference between the values for "n" on the (010) faces. The slopes of the profiles for the (100) and (001) faces of bismuthinite are steeper, i.e. resulting in a lower "n" value, for bismuthinite than for the corresponding stibnite profiles.

Gold.

The profiles for the (001) and (110) faces are similar, the microhardness increasing slightly with

decreasing load, down to 25 g. Below this load the microhardness decreases but such a change is small and within the probable error of the means of the microhardness values. The profile for the (111) face shows an increase in microhardness with increasing load resulting in a logarithmic index value greater than 2.0. This increase is greater than the probable errors of the means and is therefore significant.

A possible explanation of this anomalous increase of microhardness with increasing load may be sought in theory of "work hardening" of metals during deformation. However, it is difficult to understand why this process should operate only when the crystal is oriented parallel to the (111) plane. Further work on oriented sections of metals of the same structure, (cubic close packed), i.e., copper, silver, iron and platinum would provide interesting comparisons.

Stephanite

On all faces an increase in microhardness occurs on reducing the load from 100 g. to 25 g. From 25 g. to 15 g., the (001) and (010) faces show decreases in microhardness whilst the (110) face shows an increase. Such anomalies are probably not significant as the probable

error for stephanite can be as large as 7 V.M.H. units. A high hardness on the (001) corresponds with a high value for "n".

Chalcocite

Both faces, the (001) and (110) show slight increases in microhardness with decrease in load.

Bournonite

For all three faces an increase in microhardness occurs on decreasing the load from 100 g. to 50 g. From 50 g. to 25 g., the (001) and (100) faces show increases in microhardness whilst the (010) shows a corresponding decrease. From 25 g. to 15 g., the (001) and (010) faces show increases in microhardness whilst the (100) shows a corresponding decrease. Bournonite is an extremely brittle mineral exhibiting pronounced cracking around impressions even at 15 g. loads. The probable errors of the means are fairly high and anomalous results can therefore be expected. The mineral shows surprisingly little variation in the logarithmic index with orientation.

Cuprite

On the (111) and (110) faces, a consistent increase

in microhardness occurs with decrease in load. The (001) face, whilst showing a general increase in microhardness with decrease in load, shows a maximum microhardness at 50 g. load. Such a variation cannot be completely accounted by probable errors in the mean values. The logarithmic index values are very similar and correspond to similar small differences in the microhardness results.

Rutile

The (001) and (111) faces exhibit similar microhardness/load profiles. Large increases of microhardness occur on decreasing the load from 100 g. to 50 g., but from 50 g. to 15 g., the microhardness values remain practically constant. As in cuprite, these unusual profiles cannot be fully accounted for by probable errors in the means. Logarithmic indices are similar for both faces and are very low -1.80.

Magnetite

The (001) face shows a steady increase in microhardness with decreasing load. Both graphs for the (111) and (110) faces show similar profiles i.e. increasing microhardness from 100 g. to 25 g. and decreasing microhardness from 25 g. to 15 g. Once again, the shapes of the graphs cannot be fully accounted by probable errors in the means. The

variation in the logarithmic index with orientation is not coupled with any corresponding microhardness differences.

(iii) Results obtained on randomly oriented sections of minerals

As it was anticipated that the logarithmic index of a mineral could be dependent upon orientation, no detailed work was carried out on unoriented minerals. In an attempt to reduce the minimum grain size, microhardness values for some minerals were determined at two, and in some cases three, different loads. In such determinations attempts were made to indent grains in as many different directions as possible to obtain the fullest possible range. Over 100 minerals were tested in this manner and over 95% of the results showed that a decrease in load gave rise to an increase in microhardness.

Discussion of the results

In general the results show that for most minerals an increase in microhardness results from a decrease in the load. Unoriented studies show that this trend is true for over 95% of the minerals tested. The type of variation of microhardness with load for the oriented minerals is given in Table XIII. In the load range 25 g. to 15 g., 28% of the

TABLE XIII

Variation of Microhardness with Load on Oriented Sections
of 10 Minerals

Load Range	Increase of M.H.	Decrease of M.H.	Total
15 - 25 g.	36	14	50
25 - 50 g.	45	5	50
50 - 100 g.	47	3	50

microhardness values decrease with decrease in load.

From 50 g. to 25 g., only 10% of the values decrease with decrease in load and 100 g. to 50 g. only 6% of the values show a decrease.

Let us consider the possible causes of a variation in microhardness values with load. Firstly, the microhardness may in fact depend upon the load either increasing or decreasing with the load. Secondly, the microhardness may be independent of the load. Thirdly, instrumental

and human errors may introduce errors which would lead to either an increase or a decrease of microhardness with the load.

Let us assume that a certain mineral x has a microhardness of 100 V.M.H. units which in theory is independent of the load. Let us also assume that the observer measures an impression 0.5 microns smaller than the actual size. Table XIV shows the error expressed in microhardness units that would occur for different loads. The maximum error, at 15 g., is only 6 V.M.H. units. Similarly it can be seen that if the observer measures an impression 0.5 micron too large, then a similar error will be introduced. In this way an apparent increase or decrease in microhardness will result on varying the load.

If, however, we take another mineral y with V.M.H. = 1000, then the change in microhardness with load (Table XV) for an error of 0.5 micron, is considerable. The change, 150 V.M.H. units, is of the same order of difference as was found for rutile.

It has been stated previously that the author measured the impressions to within 0.2 microns of several other independent observers. Hence the error that is likely to be present in the results is less than 50% of the values given in Tables XIV and XV. Thus the variations in

TABLE XIV

Effect of Error in Measurement of the Diagonal Length on the Microhardness

Mineral x, V.M.H. = 100

Load	Correct diagonal length	Measured diagonal length	Apparent V.M.H.
15	16.7	16.2	106
25	21.5	21.0	105
50	30.4	29.9	104
100	43.0	42.5	103
200	60.9	60.4	102

TABLE XV

Effect of Error in Measurement of the Diagonal Length on the Microhardness.

Mineral y, V.M.H. = 1000.

Load	Correct diagonal length	Measured diagonal length	Apparent V.M.H.
15	5.3	5.8	1208
25	6.8	7.3	1168
50	9.6	10.1	1120
100	13.6	14.1	1051
200	19.3	19.8	1050

microhardness on galena cannot be attributed to errors in measurement. In harder minerals such as cuprite, magnetite and rutile the errors in measuring the impressions are comparable with the differences observed, and it is interesting to note the irregular profiles of some of the graphs of these minerals in Figs. 15 and 16. It is significant that variation in microhardness at lower loads in Table XIII become less well defined. This may well be a reflection of introduced measuring errors.

Robertson and Van Meter (1951) found an increase in Knoop microhardness with decrease in load for many ore minerals. Their explanation is as follows; "The eye does not resolve the end points of the impression perfectly, and a micron loss in small lengths would be larger percentage wise than in greater length". They also found that a compensating flat increase to the diagonal lengths, as recommended by the U.S. Bureau of Standards, did not fit for all minerals.

Mott (1956) explains the variation as follows:

"The most reasonable basis on which results can be explained is that the deformation mechanism operating on a small localised volume of material is different to that of a more extended deformation".

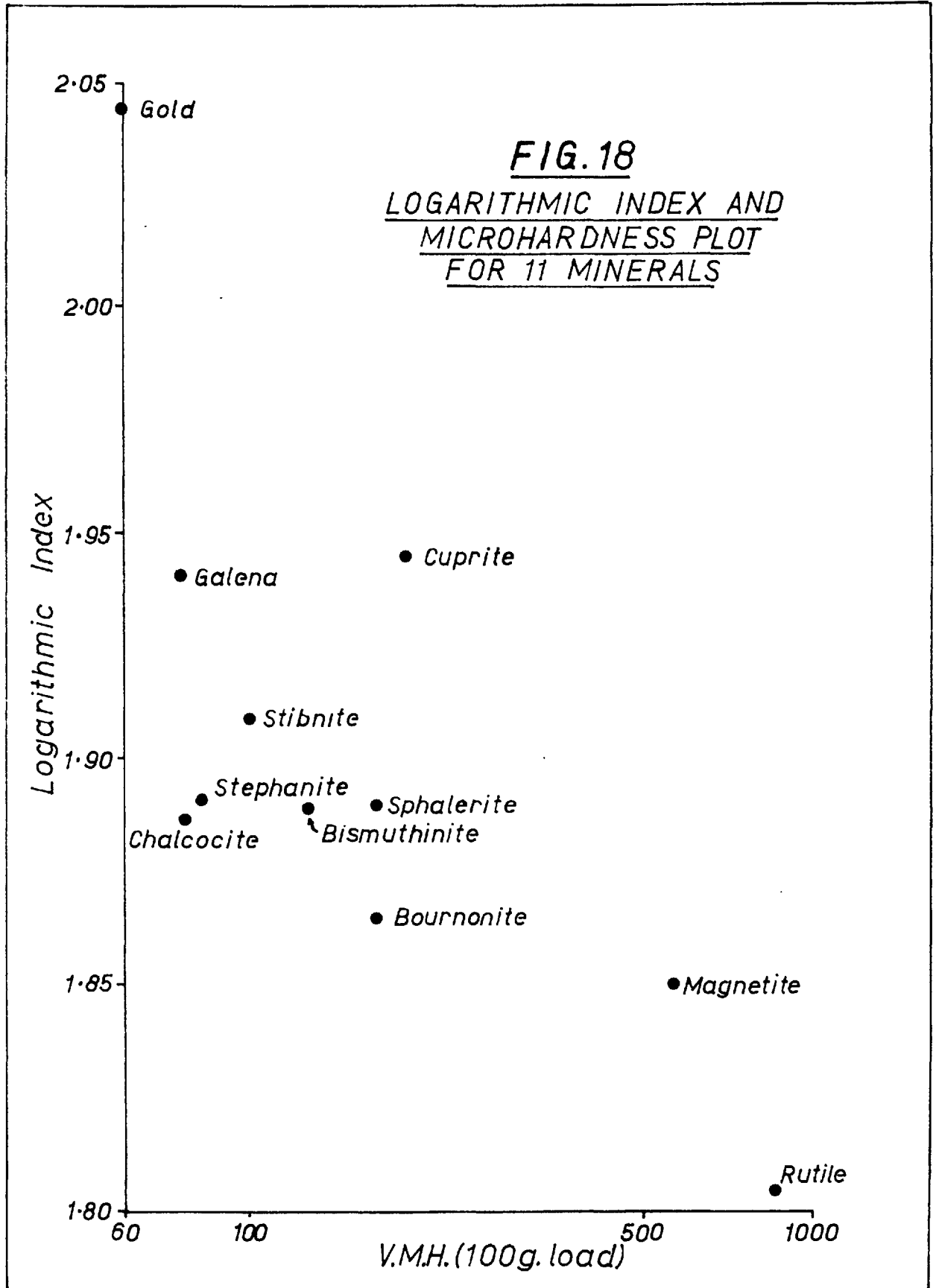
Various other authors have put forward theories for

variation in microhardness with load based on many different factors. A prominent explanation put forward by Schulze(1954) and others, is that elastic recovery causes a contraction in the diagonal length, the contraction being independent of the size of the impression. Experimental work, however, is not conclusive and other authors (Grodzinski(1952) Winton 1956), have shown the recovery is proportional to the size of the impression.

Most authors agree that soft materials have high logarithmic indices, and hard materials low logarithmic indices. In the present study it has been noted that a similar relation holds. In Fig. 18 the mean logarithmic has been plotted against the mean **Vickers** microhardness value for the oriented minerals tested. These results agree with results of Onitsch (1953), and Mott (1956) plotting data determined by Fitzer (1952).

It has been noted that deformation of the soft minerals is essentially plastic, indentations exhibiting straight or complex curving sides. Hard minerals usually exhibit concave sides indentation accompanied by slight fracturing. Thus most minerals deform by a combination of elastic and plastic deformation. In soft minerals plastic deformation is dominant with minor elastic recovery. In harder minerals some plastic deformation occurs but strong elastic recovery takes place

FIG. 18
LOGARITHMIC INDEX AND
MICROHARDNESS PLOT
FOR 11 MINERALS



after the indenter has been removed.

In searching for a solution of the load/hardness variation problem the following evidence must be borne in mind.

1. Soft minerals, particularly the metals, appear to deform perfectly by plastic processes. Some elastic recovery takes place.
2. Harder minerals, appear to deform at first plastically but this process of deformation is superseded by rupture of the crystal structure. Fracturing is increased on increasing the load.
3. Fracturing can be reduced to zero on decreasing the load.

The following theory is tentatively put forward in an attempt to explain the phenomenon.

To obtain permanent (non-elastic) deformation a certain threshold stress has to be exceeded. For soft materials the threshold value is extremely small; for harder materials the value is higher. (Brown (1952) shows that for metals the initial slip requires a lower shearing stress than after some deformation has taken place. According to these facts microhardness for metals should increase with increasing load. This does not agree with published data or with the present

work). Thus deformation in soft materials is dominantly plastic with relatively minor elastic recovery. Since gliding in soft materials is easy no rupture of the atomic structure should occur. Thus elastic recovery should be proportional to the size (or diameter) of indentations made in soft materials. Rupture of the structure would prevent proportional elastic recovery to take place.

With harder minerals, elastic recovery relative to plastic deformation, becomes increasingly important. In addition fracturing around indentations is more prevalent in harder minerals than in softer ones, but the amount may be decreased on decreasing the load. As the load is decreased the threshold stress value is approached and the amount of elastic recovery increases relative to the amount of plastic deformation. For soft minerals the threshold value is so low that in normal testing it is always exceeded. Rupturing of the structure occurs in nearly all the harder minerals and thus the elastic recovery is not proportional to the diameters of the indentations.

These two factors, (a) the increasing importance of the elastic recovery relative to the plastic deformation on decreasing the load for harder minerals and (b) the independence of the amount of elastic recovery on the diameters of indentation for harder minerals, are considered to be

main causes of the dependence of the hardness on the load.

This theory is in general agreement with the suggestions of Onitisch and Mott that the mechanism of deformation during indentation on small areas is different from that on larger areas.

(d) Conclusions

The unoriented work on over 100 minerals together with the bulk of the oriented studies shows that microhardness values increase with decrease of load. A real increase in microhardness has been detected for some of the softer minerals with one or two exceptions. The data for harder minerals is not so well defined and measuring errors may have aggravated the uncertainty of the results. Definite correlations can now be made between the logarithmic index and the orientation for gold and stibnite-bismuthmite. Although the relationship between orientation, microhardness values and logarithmic indices for most minerals is complex, a general theory has been evolved to explain the load - microhardness variation.

B. The relationship between load and grain size.

(a) General

Microhardness measurements are particularly useful in the identification of small grains of minerals in polished sections. Grain size is particularly important as there is a minimum grain size on which measurements can be accurately and reliably produced. The smaller the grains that can be tested, the greater the scope of the work.

Bowie and Taylor (1958) using a G.K.N. hardness tester considered that the minimum grain size for all minerals was 0.05 mm. (50 microns) at 30 g. load, and 0.10 mm. (50 microns) at 100 g. load. The lowest ratio, (D_g/D_i), minimum grain size (D_g) to indentation size (D_i) given was approximately 2/1. Microhardness values for all the minerals were given for 100 g. load. It has been shown in the previous section that microhardness values are dependent on the load applied. Thus microhardness values made say at 30 g. will not be the same as those made at 100 g. Hence it would be incorrect to assume that the values listed by Bowie and Taylor would be valid at lower loads. For this reason it was decided to subdivide the minerals according to hardness into four separate groups. The softest group were indented at 15 g.

load and the hardest at 100 g. load. (Table XVI shows the hardness limits for the load groupings of the minerals for Vickers and Knoop indentors). Minimum hardness for each mineral species was noted and from this value the minimum grain size was determined, see Table XVI.

TABLE XVI

Indenter	Load g.	Range of Vickers Microhardness of Minerals Kg/mm ²
Vickers	15	0 - 60
	25	60 - 120
	50	120 - 600
	100	> 600
Knoop	15	0 - 120
	50	120 - 1000
	100	> 1000

For the present work it was decided that the minimum ratio (Dg/Di) should be 3/1.

Hence,

$$\text{M.G.S.} = 3 \times d_{\text{max}}$$

where

M.G.S. = Minimum grain size for a particular load

d_{max} = Mean diagonal length of the impression giving the lowest hardness.

Table XVII gives minimum grain sizes for loads of 15 g., 25 g., 50 g., and 100 g.

It was decided to vary the load for Knoop microhardness studies (Table XVI) so that the diagonal lengths for softer mineral did not become unmanageably large.

(b) Discussion

In discussing the relationship between grain size and optimum load the following facts must be borne in mind.

1. The size of the impression is dependent upon the hardness of the mineral. For a given load, the softer the mineral the larger the impression.
2. The size of the impression is dependent upon the load; for a given hardness, the larger the load, the larger the impression.

TABLE XVII
MINIMUM GRAIN SIZE (μ)

Mineral	LOAD			
	15g.	25g.	50g.	1000g.
Acanthite	113	--	--	292
Aeschynite	--	--	--	51
Aikinite	--	--	65	101
Alabandite	--	--	73	111
Allanite	--	--	--	51
Altaite	88	--	--	222
Amalgam	81	--	--	187
Anatase	--	--	36	54
Andorite	--	--	67	100
Anglesite	--	59	--	126
Ankerite	--	--	49	69
Antimony	58	79	--	162
Apatite	--	--	37	61
Argyrodite	--	--	74	110
Arsenic	--	78	--	144
Arsenopyrite	--	--	--	53
Awaruite	--	--	62	88
Axinite	--	--	--	40
Barite	--	--	72	117
Berthierite	--	50	79	124
Beryl	--	--	--	38
Bismuth	141	--	--	375
Bismuthinite	55	73	112	158
Bixbyite	--	--	--	44
Bornite	--	63	--	140
Boulangerite	--	57	84	121
Bournonite	38	49	69	114
Braggite	--	--	--	57
Brannerite	--	--	--	55
Braunite	--	--	28	62
Bravoite	--	--	--	39
Breithauptite	--	--	39	61
Bröggerite	--	--	50	83
Brookite	--	--	--	45
Calaverite	--	--	65	99
Calcite	--	58	--	127

TABLE XVII Contd.

MINIMUM GRAIN SIZE (μ)

Mineral	LOAD			
	15g.	25g.	50g.	100g.
Cassiterite	--	--	--	37
Cerussite	--	--	73	110
Chalcocite	59	76	--	160
Chalcophanite	--	69	89	153
Chalcopyrite	--	--	67	98
Chalcostibite	--	--	61	94
Chromite	--	--	--	37
Cinnabar	--	61	--	194
Clausthalite	73	94	--	191
Cleveite	--	--	57	86
Cobaltite	--	--	--	43
Cohenitë	--	--	--	40
Coloradoite	104	--	--	279
Columbite-Tantalite	--	--	--	54
Colusite	--	--	49	75
Cooperite	--	--	--	54
Copper	64	--	--	188
Coronadite	--	--	49	69
Corundum	--	--	--	28
Corynite	--	--	40	58
Cosalite	--	65	101	151
Covellite	59	74	--	190
Cryptomelane	--	--	38	57
Cubanite	--	--	65	106
Cuprite	37	47	66	98
Cylindrite	89	118	--	253
Davidite	--	--	--	50
Descloizite	--	--	47	71
Diaphorite	--	--	63	93
Digenite	59	79	--	161
Dolomite	--	--	42	69
Domeykite	--	--	59	92
Dyscrasite	--	--	77	105
Electrum	64	--	--	165
Emplectite	--	--	64	100
Enargite	--	--	71	95
Eskolaite	--	--	--	27

TABLE XVII Contd.

MINIMUM GRAIN SIZE (μ)

Mineral	LOAD			
	15g.	25g.	50g.	100g.
Eucairite	--	73	--	176
Eucryptite	--	--	--	56
Euxenite	--	--	--	56
Famatinite	--	--	51	74
Ferberite	--	--	45	70
Fergusonite	--	--	--	50
Ferrite	--	--	58	85
Fluorite	--	--	68	98
Formanite	--	--	--	47
Franckeite	93	--	--	354
Franklinite	--	--	--	49
Freibergite	--	--	84	76
Gahnite	--	--	--	33
Galena	63	81	117	166
Geocronite	--	57	79	113
Germanite	--	--	47	67
Gersdorffite	--	--	--	55
Goethite	--	--	38	57
Gold	72	--	--	208
Glaucodot	--	--	--	44
Graphite	213	--	--	615
Gratonite	--	--	74	105
Grossularite	--	--	--	40
Gypsum	79	--	--	235
Halite	119	150	--	320
Hauerite	--	--	40	60
Hausmannite	--	--	38	59
Hematite	--	--	--	46
Hessite	100	--	--	265
Hercynite	--	--	--	35
Hetaerolite	--	--	34	53
Hollandite	--	--	--	--
Huebnerite	--	--	50	79
Idaite	--	--	68	98
Ilmenite	--	--	--	51
Ilmenorutile	--	--	--	46
Ilvaite	--	--	--	49
Iridosmine	--	--	37	59
Jacobsite	--	--	--	45
Jalpaite	96	--	--	288

TABLE XVII Contd.

MINIMUM GRAIN SIZE (μ)

Mineral	LOAD			
	15g.	25g.	50g.	100g.
Jamesonite	54	86	--	159
Jordanite	--	--	70	97
Kermesite	84	108	--	226
Kobellite	--	61	--	126
Krennerite	--	60	82	127
Kyanite	--	--	--	58
Laurite	--	--	--	31
Lead	162	--	--	606
Lepidocrocite	--	--	49	107
Linnaeite	--	--	39	57
Livingstonite	--	76	--	151
Löllingite	--	--	36	68
Mangantantalite	--	--	52	71
Magnesite	--	--	48	67
Magnetite	21	27	39	59
Manganite	--	--	35	52
Marcasite	--	--	--	47
Maucherite	--	--	37	53
Meneghinite	--	57	82	122
Merumite	--	--	--	31
Metacinnabar	--	--	60	93
Miagyrite	--	70	91	138
Millerite	--	--	61	58
Molybdenite	135	--	--	615
Monazite	--	--	--	49
Nagyagite	79	94	--	208
Naumannite	90	--	--	233
Niccolite	--	--	48	70
Nigerite	--	--	--	34
Orpiment	82	--	--	277
Orthoclase	--	--	--	52
Osmiridium-Iridium	--	--	46	76
Pararammels-bergite	--	--	--	50
Patronite	--	--	--	65
Pearceite	--	54	76	109
Pentlandite	--	--	61	89
Perovskite	--	--	--	44
Petalite	--	--	--	133
Pitchblende	--	--	46	73
Platinum	--	--	61	98

TABLE XVII Contd.

MINIMUM GRAIN SIZE (μ)

Mineral	LOAD			
	15g.	25g.	50g.	100g.
Polybasite	--	57	82	114
Proustite	--	--	--	144
Pyragyrite	--	72	100	130
Pyrochlore	--	--	40	63
Pyrolusite	--	49	73	122
Pyromorphite	--	--	59	95
Pyrite	--	--	--	47
Pyrrhotite	--	--	53	85
Quartz	--	--	--	36
Rammelsbergite	--	--	--	51
Realgar	70	89	--	190
Renierite	--	--	51	75
Rhodochrosite	--	--	60	85
Rhodonite	--	--	39	56
Rutile	15	19	24	42
Safflorite	--	--	--	53
Samarskite	--	--	--	53
Scheelite	--	--	45	73
Schulzenite	54	72	--	204
Semseyite	--	57	85	124
Siderite	--	--	48	72
Siegenite	--	--	41	60
Silver	73	--	--	192
Skutterudite	--	--	--	56
Smithsonite	--	--	41	67
Sperrylite	--	--	--	42
Sphalerite	40	51	78	109
Sphene	--	--	--	48
Spinel	--	--	--	36
Stannite	--	46	65	111
Stephanite	64	92	123	193
Sternbergite	87	103	--	550
Stibarsenic	--	--	73	102
Stibiotantalite	--	--	44	62
Stibnite	61	76	109	168
Strüverite	--	--	--	40
Sulphur	118	--	--	238
Sylvanite	--	--	66	103
Talc	185	--	--	720
Teallite	59	76	--	233

TABLE XVII contd.
MINIMUM GRAIN SIZE (μ)

Mineral	LOAD			
	15g.	25g.	50g.	100g.
Tellurium	93	--	--	250
Tennantite	--	--	49	72
Tenorite	--	--	61	91
Tetradymite	81	--	--	247
Tetrahedrite	--	--	50	73
Thoreaulite	--	--	7	60
Thorianite	--	--	--	43
Tiemannite	102	--	--	253
Titanohematite	--	--	--	42
Topaz	--	--	--	34
Tourmaline	--	--	--	38
Trevorite	--	--	38	55
Ullmannite	--	--	40	58
Umangite	--	73	--	146
Vallereite	--	--	64	94
Violarite	--	--	51	84
Wittichenite	--	--	71	100
Wolframite	--	--	45	77
Wurtzite	--	--	73	108
Zincite	--	--	64	98
Zinkenite	--	49	76	100
Zircon	--	--	--	36

3. The hardness value for a given mineral is dependent on the load. In general, the lower the load, the higher the hardness and the smaller the impression.
4. The probable error in measuring a diagonal is **dependent** on the hardness of the mineral. The harder the mineral, the smaller the impression and the greater the probable error in the measurement of the hardness.
5. The amount of cracking around impressions increases with increasing load. Thus in brittle minerals increasing load results in increasing probable error in the measurement of hardness.

To obtain a satisfactory minimum grain size for minerals showing a range of hardness from 10 - 1800 V.M.H. units, a system as described is necessary. This method makes easier the identification of small grains of the soft minerals, for example, the native metals, simple sulphides, selenides and tellurides and some of the sulphosalts.

For example, in identifying suspected native bismuth using a Vickers diamond indenter, the minimum grain size is reduced by 220 microns, from 360 microns at 100 g. load to 140 microns at 15 g. load.

It may be argued that higher microhardness values at lower loads may be computed from the values at say 100 g. load. This problem was discussed by Robertson and Van Meter (1951) as described previously in the text. Whilst, in general, it is true that microhardness values are a function of the logarithmic index for the whole group of minerals, many exceptions exist. A large spread of values exists and this indicates that no single compensating factor could be confidently applied to all the values obtained at 100 g. load.

C. Variation of deformation characteristics with load

Deformation phenomena are fully dealt with in Chapter V and it is proposed only to discuss the effect of load on such phenomena.

As seems logical, the amount of fracturing around impressions decrease in load. Nakhla (1956) found that loads of over 100 g. on pyrite and rammelsbergite produced large shell-shaped cracks whilst at loads of 25 g. and 50 g. fine cracks only were produced.

In the present work, it was found that simple sulphides such as sphalerite, wurtzite and chalcopyrite no fracturing occurred at lower loads - 15 g. and 25 g. The sulphosalts,

seemed to fracture whatever the load, although the intensity lessened with decreasing load. For example, the "star - radial" pattern developed in tennantite at 15 g. load is often superseded by a "shell - fracture" pattern at 100 g. load. Minerals which do not fracture, but exhibit glide and twin planes around impressions usually show increasing amounts of these dislocations with increasing load. Examples of such minerals include antimony, arsenic and bismuth. At loads from 15 g. to 100 g. no obvious slip planes were observable on galena crystals, but at 200 g. slip planes are easily seen.

Small grains of minerals are adversely affected by indentations made at high loads. Even galena, which under normal conditions of testing deforms perfectly, develops cleavage fractures in small grains (less than 100 microns) at high loads.

CHAPTER IV

VARIATION OF MICROHARDNESS WITH ORIENTATION

A. General

Several authors have found considerable anisotropy of microhardness with orientation. Winchell (1945) found anisotropism of Knoop microhardness for beryl, talc, corundum, topaz and tetrahedrite. In the case of molybdenite, MoS_2 , Robertson and Van Meter (1951) correlated a 5:1 difference in ratio for Knoop microhardness values obtained on the basal (0001) face and on the prism (10 $\bar{1}$ 0) face. Arsenopyrite was found to exhibit a large range of Knoop microhardness, 633 - 1148, depending upon the orientation of the mineral. Kohn, Cotter and Potter (1955) correlated Knoop microhardness values with orientation on tungsten carbide (WC) crystals. Nakhla (1956) reported variations of Vickers microhardness on stibnite due to orientation effect. Henriques (1957) showed significant Vickers microhardness variations for different orientation of sphalerite: the (111) face was found to be hardest and the (100) the softest. Butkovich (1958) found anisotropy of microhardness in single ice crystals due to orientation

effects. Bowie and Taylor (1958) gave Vickers microhardness values for oriented sections of about 12 ore minerals.

Bloss, Shekarachi and Shell (1959) correlated Knoop microhardness values obtained on basal (001) sections of natural and synthetic micas with orientations.

One of the purposes of the present study was to increase the amount of data on oriented sections of economic minerals, and where possible to relate this data to the atomic structures of these minerals. In addition, microhardness measurements have been made to determine the range of microhardness exhibited by randomly oriented minerals. Investigations were carried out on oriented sections of about 50 minerals and on randomly oriented sections of over 150 minerals. Both Vickers and Knoop indenters were used.

B. Microhardness Values determined from randomly oriented minerals

Table XVIII lists the ranges of Knoop and Vickers microhardness values determined at 100 g. loads for all the minerals examined. In addition, the following data are also given: the percentage variation of the reflectivity (pers. comm., I. Gray), the percentage variation of the Vickers microhardness, the range of reflectivity values

TABLE XVIII

Mineral	Reflectivity (white light)	R. aniso %	V.M.H. Range	V.M.H. aniso %	K.M.H. Range
Acanthite	27.6	0	19.6-22.0	10.9	24.2-31.3
Aeschynite	14.8-15.6	0.8	661-720	8.2	615-726 ²
Aikinite	40.0-44.8	4.8	165-227	27.3	179-230 ²
Alabandite	22.7	0	137-186	26.3	161-186 ²
Allanite	9.7	0	646-1105	41.3	780-976 ²
Altaite	58.5-60.5	2.0	34.1-38.3	10.9	35.1-46.6 ⁴
Amalgam	85.1-93.0	8.9	48.2-80.5	77.5	46.6-85.4 ⁴
Anatase	20.0-21.1	1.1	576-623	7.5	634-908 ²
Andorite	33.3-37.5	4.2	170-192	11.4	154-170 ²
Anglesite	----	---	106-128	17.2	101-166 ²
Ankerite	----	---	353-490	27.9	338-468 ⁴
Antimony	67.2-70.2	3.0	64.3-69.9	8.0	59.7-11.6 ⁴
Apatite	----	---	454-606	25.1	423-638 ²
Argyrodite	23.9	0	138-162	14.8	132-174 ⁴
Arsenic	47.0	0	81.7-167	50.8	42.1-107 ²
Arsenopyrite	46.3-54.3	8.0	599-1206	50.2	678-1381 ²
Awaruite	68.0	0	220-253	13.1	232-322 ²
Axinite	----	---	1097-1187	7.5	975-1161 ¹
Barite	----	---	124-190	34.8	137-191 ²
Berthierite	35.2-40.3	5.1	110-213	48.3	146-232 ²
Beryl	----	---	1159-1764	34.2	1098-1500 ¹
Bismuth	65.0-71.0	6.0	10.5-14.3	26.5	10.7-16.8 ⁴
Bismuthinite	37.3-47.3	10.0	67.3-216	68.9	31.6-223 ²

TABLE XVIII contd.

Mineral	Reflectivity (white light)	R. aniso %	V.M.H. Range	V.M.H. aniso %	K.M.H. Range
Bixbyite	23.7	0	882-981	10.1	921-1138 ²
Bornite	28.3-30.5	2.2	85.6-98.0	12.6	105-121 ²
Boulangerite	37.7-38.7	1.0	116-210	44.7	126-169 ²
Bournonite	33.9-36.1	2.2	131-194	32.3	152-219 ²
Braggite	57.0-59.0	2.0	514-560	9.4	-----
Brannerite	16.6-17.4	0.8	572-693	17.5	580-676 ²
Braunite	19.0-19.1	0.1	441-1048	57.8	976-1120
Bravoite	45.5-47.6	2.1	1105-1343	17.8	807-1196 ²
Breithauptite	48.7-61.3	12.6	450-569	21.0	543-615 ²
Broggerite	17.5-19.0	1.5	242-835	71.1	306-976 ²
Brookite	21.5-21.9	0.4	841-960	12.4	991-1138 ²
Calaverite	63.0-66.5	3.5	172-228	24.5	127-281 ²
Calcite	----	--	133-174	9.4	133-174 ⁴
Cassiterite	11.5-13.7	2.2	1141-1478	22.8	1161-1389 ¹
Cerussite	----	--	140-254	44.8	136-249 ²
Chalcocite	26.2-30.7	4.5	59.6-85.4	18.5	57.4-103 ⁴
Chalcophanite	13.5-22.6	9.1	72.0-194	62.9	45.5-419 ²
Chalcopyrite	45.0-47.0	2.0	177-200	11.5	202-227 ²
Chalcostibite	34.0-42.0	8.0	193-266	27.4	179-309 ²
Chromite	11.4-12.7	1.3	1256-1332	5.7	1068-1580 ¹
Cinnabar	23.2-26.4	3.2	44.6-133	66.4	28.0-109 ²
Clausthalite	43.1-48.2	5.1	46.0-71.9	36.1	59.3-174
Cleveite	----	--	227-330	31.1	208-348 ²
Cobaltite	53.0-55.4	2.4	967-1367	29.3	917-1122
Cohenite	57.5-61.0	3.5	1081-1246	13.2	935-1224
Coloradoite	35.0-36.6	1.6	21.6-22.9	5.7	19.7-26.9 ⁴
Columbite-Tantalite	15.6-18.8	3.2	595-1056	43.9	615-901 ²
Colusite	31.7	0	296-376	21.3	297-356 ²

TABLE XVIII Contd.

Mineral	Reflectivity (white light)	R. aniso %o	V.M.H. Range	V.M.H. aniso %o	K.M.H. Range
Cooperite	39.5	0	592-634	6.9	-----
Copper	77.5-92.0	14.5	47.5-122	60.5	52.1-101 ⁴
Coronadite	25.3	0	359-542	15.3	351-561 ²
Corundum	-----	---	2097-2758	23.9	1751-2470 ¹
Corynite	48.2-49.6	1.4	498-545	8.6	500-615 ²
Cosalite	38.8-46.5	7.7	73.6-158	53.2	74.9-176 ²
Covellite	15.8-27.4	11.6	46.4-151	69.3	85.4-211 ⁴
Cryptomelane	-----	---	525-698	24.8	520-908 ²
Cubanite	43.5-44.3	0.8	150-264	43.2	163-282 ²
Cuprite	24.5-25.3	0.8	176-237	25.7	154-206 ²
Cylindrite	30.7-33.5	2.8	26.3-114	76.9	21.9-178 ⁴
Davidite	17.3	0	693-762	9.0	630-740 ²
Descloizite	16.0-17.4	1.4	333-392	15.4	351-382 ²
Diaphorite	34.2-3618	2.6	197-242	18.5	168-204 ²
Digenite	25.0	0	64.8-76.0	14.7	73.6-102 ⁴
Dolomite	-----	---	358-437	18.1	378-451 ²
Domeykite	55.0-56.0	1.0	201-238	15.5	236-262 ²
Dyscrasite	63.5-65.8	2.3	152-176	13.6	115-194 ²
Electrum	-----	---	61.9-106 ⁴	41.7	47.5-118 ⁴
Emplectite	30.0-36.8	6.8	169-217	22.1	198-258 ²
Enargite	25.5-29.0	3.5	188-370	49.2	155-401 ²
Eskolaitite	19.3-22.5	3.2	2239-3087	26.5	1881-2370 ¹
Eucairite	-----	---	54.2-93.6	42.0	78.8-111 ²
Eucryptite	-----	---	542-748	27.6	-----
Euxenite	13.5	0	530-767	30.9	568-690 ²
Famatinitite	28.8-32.4	3.6	309-339	8.8	261-396 ²
Ferberite	17.9-20.7	2.8	342-657	47.9	-----
Fergusonite	15.4	0	689-757	9.0	653-750 ²

TABLE XVIII Contd.

Mineral	Reflectivity (white light)	R. Aniso %o	V.M.H. Range	V.M.H. aniso %o	K.M.H. Range
Ferrite	61.5	0	233-288	19.1	276-322 ²
Fluorite	----	-	174-203	14.2	166-220 ²
Formanite	13.3	0	772-870	11.3	615-876 ²
Franckeite	33.3-36.0	2.7	13.3-68.6	81.1	21.4-151 ⁴
Franklinite	18.2-20.0	1.8	720-853	15.5	607-770 ²
Freibergite	30.7	0	292-322	9.3	223-298 ²
Gahnite	8.0	0	1491-1605	7.1	1224-1576 ²
Galena	42.0-44.4	2.4	61.2-84.0	27.2	35.0-91.9 ⁴
Geocronite	37.7-39.4	1.7	133-153	13.1	83.1-187 ²
Germanite	27.4	0	373-417	10.6	336-401 ²
Gersdorffite	48.1-55.1	7.0	569-907	37.3	740-908 ²
Goethite	16.2-17.5	1.3	527-551	43.5	597-901 ²
Gold	80.5-87.7	7.2	38.9-94.1	58.7	88.0-47.0 ⁴
Glaucodot	49.5-52.7	3.2	864-1277	32.3	717-1138
Graphite	-35.1	---	4.4-7.7	42.8	5.1-21.4 ⁴
Gratonite	40.2-40.7	0.5	153-195	23.2	150-190 ²
Grossularite	----	---	1081-1551	30.7	1110-1389 ¹
Gypsum	----	---	30.5-45.2	36.8	38.0-156 ⁴
Halite	----	---	16.0-18.2	12.0	13.4-18.8 ⁴
Haucrite	25.4	0	478-528	9.5	456-574 ²
Hausmannite	16.7-19.1	2.4	493-620	20.4	407-673 ²
Hematite	23.9-29.0	5.1	813-1039	25.2	846-1260 ¹
Hessite	37.2-37.6	0.4	23.9-37.2	35.8	24.0-40.1 ⁴
Hercynite	6.6-7.6	1.0	1378-1347	10.9	1283-1570 ¹
Metaerolite	16.7-18.3	1.6	609-817	24.8	537-1029 ²
Hollandite	----	---	274-792	71.2	-----
Huebnerite	15.1-17.5	1.6	274-403	32.0	315-456 ²
Idaite	34.0-36.2	2.2	176-202	12.9	190-214 ¹

TABLE XVIII Contd.

Mineral	Reflectivity (white light)	R. Aniso %	V.M.H. Range	V.M.H. aniso %	K.M.H. Range
Ilmenite	19.1-22.2	3.1	642-752	14.3	602-821 ²
Ilmenorutile	19.5-23.3	3.8	803-1018	21.1	630-1138 ²
Ilyite	6.4-10.7	4.3	703-772	8.9	653-750 ²
Iridosmine	57.5-62.0	4.5	483-734	34.2	403-1005 ²
Jacobsite	19.7	0	841-870	3.4	801-882 ²
Jalpaite	25.5-30.0	4.5	23.4-54.5	57.0	20.5-44.6 ⁴
Jamesonite	32.7-39.3	6.6	66.8-123	45.8	85.4-178 ⁴
Jordanite	36.7-39.7	3.0	181-198	3.5	153-191 ²
Kermesite	23.9-28.1	4.2	33.0-77.0	57.1	52.1-165 ⁴
Kobellite	38.7-42.8	4.1	106-160	33.8	115-145 ²
Krennerite	52.3-61.0	8.7	105-111	5.4	91.9-138 ²
Kyanite	-----	---	500-214 ⁴	76.9	359-232 ²
Laurite	42.7	0	1605-2167	25.9	1380-1881
Lead	-----	---	4.5-5.5	18.1	9.5-13.7 ⁴
Lepidocrocite	14.0-19.7	5.7	147-401	63.1	249-407 ²
Linnaeite	46.0-47.5	1.5	525-542	3.1	577-661 ²
Livingstonite	30.0-34.7	4.7	74.2-119	37.5	87.8-179 ²
Löllingite	50.4-54.0	3.6	368-1048	64.8	520-1129 ²
Manganantialite	14.7-17.9	3.2	335-627	46.5	309-1013
Magnesite	-----	---	373-512	27.1	454-657 ²
Magnetite	20.0-21.1	1.1	490-661	25.8	485-760 ²
Manganite	14.5-22.0	7.5	638-835	23.6	370-807 ¹
Marcasite	43.8-51.6	7.8	762-1367	44.2	1077-1470 ¹
Maucherite	56.3-56.6	0.3	602-635	5.2	615-812 ²
Meneghinite	34.7-38.5	3.8	113-155	27.1	118-182 ²
Merumite	-----	---	1782-2097	15.0	1267-1481 ¹
Metacinnabar	-----	---	194-304	25.6	172-215 ²
Miargyrite	28.2-38.2	10.0	88.0-121	27.2	104-127 ²

TABLE XVIII Contd.

Mineral	Reflectivity (white light)	R. aniso o/o	V.M.H. Range	V.M.H. aniso o/o	K.M.H. Range
Millerite	51.8-59.0	7.2	219-317	30.9	227-407 ²
Molybdenite	16.2-46.6	30.4	4.4-74.2	94.1	3.7-80.1 ⁴
Monazite	---	---	704-988	28.7	611-1138 ²
Nagyagite	37.4-40.2	2.8	38.9-110	64.2	46.2-163 ⁴
Naumannite	29.5-31.5	2.0	30.9-36.9	16.3	28.5-82.1 ⁴
Niccolite	55.4-59.0	3.6	348-533	34.6	322-528 ²
Rigerite	---	---	1478-1561	4.6	1268-1751 ¹
Orpiment	21.4-22.0	0.6	21.3-30.1	27.5	34.0-59.5 ⁴
Orthoclase	---	---	642-1470	32.0	423-717 ²
Osmiridium-Iridium	69.2-72.0	2.8	297-572	48.1	409-615 ²
Pararammelsbergite	57.0-64.1	7.1	673-824	18.3	740-908 ²
Patronite	19.5-22.3	2.8	401-592	32.1	456-775 ²
Pearceite	31.1-31.2	0.1	142-151	5.9	129-146 ²
Pentlandite	51.5	0	213-231	7.8	252-312 ²
Perovskite	16.5-16.8	0.3	900-995	9.5	834-1138 ²
Petalite	---	---	94.9-703	86.3	---
Pitchblende	14.0	0	314-483	35.0	322-534 ²
Platinum	67.0	0	176-433	59.3	239-317 ²
Polybasite	27.7-30.0	2.3	131-139	5.7	117-133 ²
Proustite	28.1-30.7	2.6	81.5-114	28.1	84.1-156 ²
Pyrochlore	---	---	420-703	40.1	490-634 ²
Pyrolusite	34.3-36.2	1.9	113-345	67.1	109-555 ²
Pyromorphite	---	---	186-262	29.0	168-261 ²
Pyrargyrite	24.2-26.9	2.7	106-130	20.0	84-156 ²
Pyrite	52.4-54.5	2.1	1378-1836	24.5	980-1635 ¹
Pyrrhotite	40.8-49.4	8.6	234-363	35.5	240-368 ²
Quartz	---	---	1266-1561	18.9	890-1307 ¹
Rammelsbergite	56.2-59.3	3.1	657-830	20.9	493-882 ²
Realgar	16.9-17.3	0.4	46.7-52.7	11.4	54.6-65.7 ⁴

TABLE XVIII Contd

Mineral	Reflectivity (white light)	R. Aniso %o	V.M.H. Range	V.M.H. aniso %o	K.M.H. Range
Renierite	30.7-34.5	3.8	305-425	28.2	323-355 ²
Rhodochrosite	----	----	232-245	5.3	204-323 ²
Rhodonite	----	----	548-681	19.5	615-895 ²
Rutile	20.7-25.2	4.5	866-1132	29.5	594-1138 ¹
Safflorite	50.5-53.6	3.1	606-988	38.5	716-1147 ¹
Samarskite	17.1	0	612-645	5.1	534-623 ²
Scheelite	10.7-11.0	0.3	315-464	31.4	274-463 ²
Schulzenite	16.2	0	40.4-149	73.2	42.8-174 ⁴
Semseyite	36.0-38.3	2.3	109-173	37.0	127-168 ²
Siderite	----	----	330-371	11.0	405-509 ²
Siegenite	52.7	0	471-579	18.7	454-634 ²
Silver	85.0-93.5	8.5	45.5-70.2	35.0	54.6-91.9 ⁴
Skutterudite	53.0-55.9	2.9	554-974	43.1	543-790 ²
Smithsonite	----	----	383-519	26.1	493-695 ²
Sperrylite	54.0-57.5	3.5	974-1226	19.7	960-1175 ¹
Sphalerite	16.1-18.6	2.5	142-235	39.5	135-186 ²
Sphene	----	----	752-853	11.8	717-976 ²
Spinel	----	----	1378-1505	8.4	1389-1510 ¹
Stannite	28.5-30.8	2.3	140-202	30.7	171-263 ²
Stephanite	26.6-32.0	5.4	45.1-107	57.8	37.0-120 ²
Sternbergite	32.0-40.0	8.0	5.3-72.0	92.3	27.9-105 ⁴
Stibarsenic	59.2	0	161-205	21.5	121-126 ²
Stibiotantalite	12.0-12.8	0.8	441-603	26.7	332-485 ²
Stibnite	30.7-42.5	11.8	59.2-129	53.8	30.8-166 ²
Struverite	18.7-20.5	1.8	1048-1123	6.6	846-1196 ¹
Sulphur	----	----	29.7-66.0	55.1	19.4-54.6 ⁴
Sylvanite	62.5-67.5	5.0	158-221	28.4	174-242 ²
Talc.	----	----	7.0-18.5 ⁴	60.4	3.8-7.4 ⁴

TABLE XVIII Contd.

Mineral	Reflectivity (white light)	D. Aniso %o	V.M.I. Range	V.M.H. aniso %o	K.M.I. Range
Teallite	39.7-45.2	5.5	30.9-82.5	62.4	77.7-120 ⁴
Tellurium	52.5-61.8	9.3	26.9-33.4	19.4	14.4-60.2 ⁴
Tennantite	27.9	0	333-383	13.1	317-368 ²
Tenorite	23.5-29.0	5.5	203-253	19.7	171-359 ²
Tetradymite	48.9-52.9	4.0	27.6-52.4	47.2	28.8-85.4 ⁴
Tetrahedrite	31.7	0	319-383	16.7	293-351 ²
Thoreaulite	17.6-20.6	3.0	473-874	45.9	480-969 ²
Thorianite	13.7	0	920-1235	25.6	834-1138 ²
Tiemannite	29.2	0	26.2-29.1	9.8	21.2-32.2 ⁴
Titanohematite	19.2-21.6	2.4	981-1056	7.1	890-1068 ¹
Topaz	---	---	1478-2012	26.6	1238-1815 ¹
Tourmaline	---	---	1187-1478	19.7	1011-1481 ¹
Trevorite	18.8	0	569-606	6.1	581-690 ²
Ullmannite	46.6-48.0	1.4	500-551	9.2	493-611 ²
Umangite	18.3-27.5	9.2	78.8-89.6	12.1	79.4-109 ²
Valleriite	43.7-47.3	3.6	189-257	26.4	256-284 ²
Violarite	50.7	0	241-373	35.4	284-388 ²
Wittichenite	33.3-36.2	2.9	170-206	17.5	177-196 ²
Wolframite	14.9-20.0	5.1	286-437	45.0	329-537 ²
wurtzite	17.7-18.2	0.5	146-264	44.6	133-284 ²
Zincite	12.2-12.6	0.4	174-309	43.8	111-345 ²
Zinkenite	37.0-40.4	3.4	168-201	16.4	169-189 ²
Zircon	---	---	1114-1505	25.9	1141-1443 ¹

(pers. comm., I. Gray) and the minimum grain size for Vicker indentations. The percentage variation of Vicker microhardness is derived by dividing the difference in values by the larger value.

Correlation of Reflectivity with Vickers Microhardness

Minerals exhibiting large differences in reflectivity (over 6.0% in some cases) also exhibit differences in Vickers microhardness values, of over 30%. Examples of such minerals include the following; covellite, sternbergite, molybdenite, stibnite, bismuthinite, pyrrhotite, marcasite, arsenopyrite, cosalite, chalcophanite and jamesonite. It is interesting to note that all these minerals are crystallographically, structurally and optically, strongly anisotropic. They usually exhibit prismatic or lath shaped crystals, frequently with a well developed cleavage.

Some isometric minerals show small ranges of microhardness, i.e. less than 10%. Examples of such minerals include the following; hauerite, linnaitite, mancherite, ulemannite, pentlandite, pearceite, polybasite, freibergite, gahnite, perovskite and chromite.

The bulk of the results, however show no apparent correlation of anisotropism of reflectivity with anisotropism

of microhardness. Some optically isotropic minerals are notably anisotropic in microhardness; for example, galena, clausthalite, sphalerite, ferrite and hessite. Similarly, some optically anisotropic minerals show small ranges of microhardness. All these results must be treated with caution as various factors may influence the percentage difference values. Perfection of polish may give rise to variations in reflectivity values as for example in gold, silver, copper, amalgam and galena - all isotropic minerals. It is realised that the ranges of microhardness values are incomplete. However, it is considered that ten impressions made on grains of differing orientation should give a reasonably complete range - probably 70 - 80% for most minerals. It can be seen from Table XVIII that if the percentage variations of the Knoop microhardness ranges had been taken, even greater microhardness anisotropy would have been revealed. Using such values, several other minerals could be included in the "anisotropic" group. Such minerals would include the following: umangite, tellurium, miargyrite, breithauptite and lepidocrocite. However, no percentage differences have been listed for the Knoop microhardness ranges, since different loads were used for different minerals.

When the more reliable Vickers values are plotted against one another (Fig. 19), it can be seen that in general

FIG. 19

THE RELATIONSHIP BETWEEN REFLECTIVITY
ANISOTROPISM AND MICROHARDNESS ANISOTROPISM

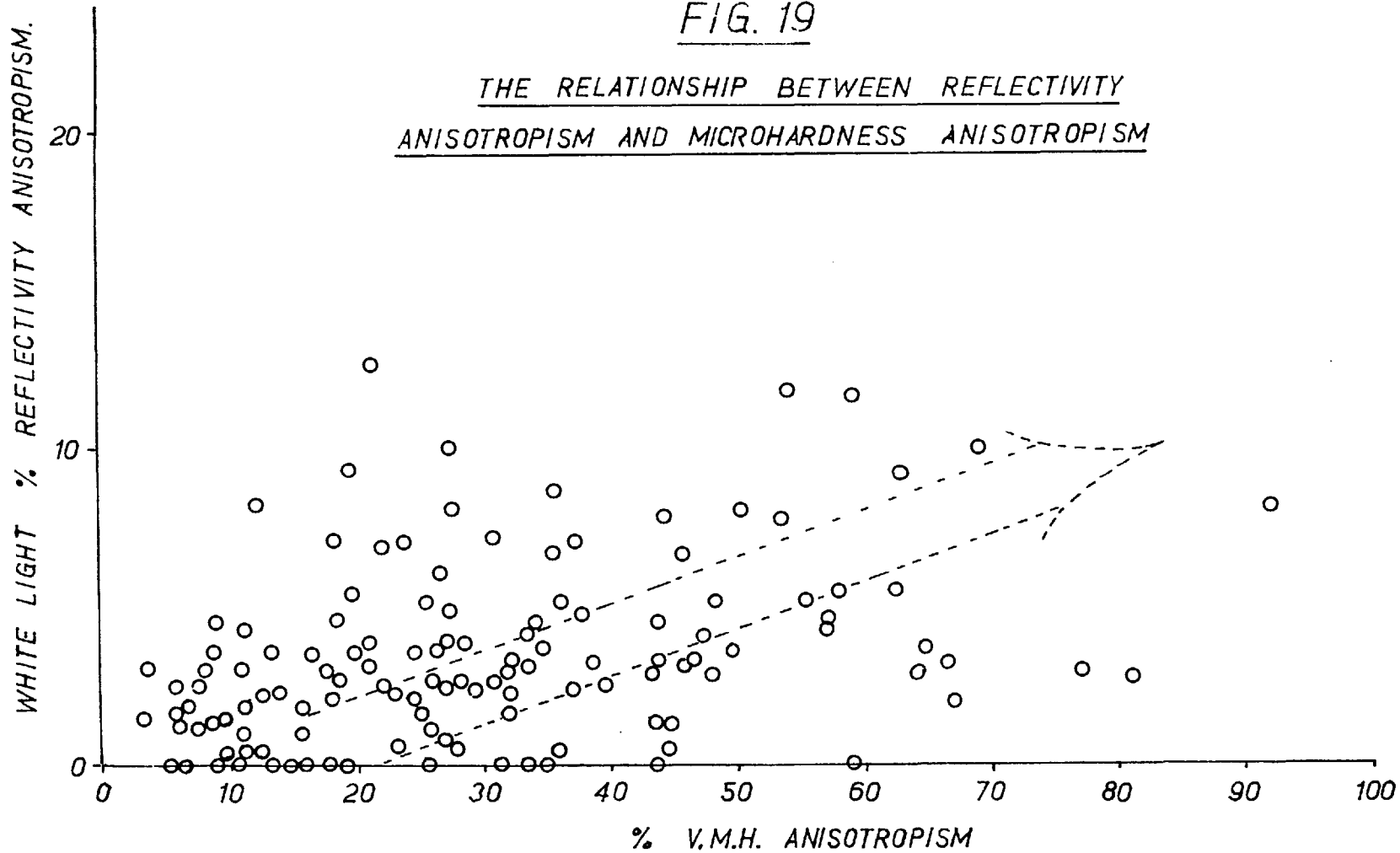


TABLE XIX

Variation of the Microhardness Anisotropism of Minerals with Crystal System.

Crystal System.	Average of % diffs. of M.H.	No of mineral species taken
Isometric	23.4	62
Tetragonal	31.9	17
Hexagonal	31.7	42
Orthorhombic	37.6	40
Monoclinic	32.8	28
Triclinic	28.9	4

terms the percentage differences of reflectivity increases with increasing percentage difference of microhardness. The large spread indicates that individually there are many minerals which show exceptions to this trend. Although minerals showing weak optical anisotropism can have large ranges of microhardness, the converse is not true to the same extent. For most minerals, we may conclude that microhardness anisotropy and reflectivity anisotropy are not

necessarily sympathetically related. Both reflectivity and microhardness are fundamentally related to the atomic structures of the minerals. Whilst reflectivity is dependent upon such factors as the type and density of packing of the atoms, microhardness is mainly controlled by the strength of the weakest bonding of the structure. Hence it is not surprising that there are exceptions to the general rule. On the other hand, the fact that the average percentage microhardness difference for isometric minerals (Table XIX) is lower than the mean value for anisotropic minerals is significant. Anisotropism in atomic structure is likely to produce anisotropism of bond strength between atoms in the structure, resulting in microhardness anisotropism. It is unlikely that an anisotropic atomic structure will give small microhardness differences, but a few cases do occur, such as breithauptite, chalcostibite, niargyrite, tellurium and umangite. Such anomalously low microhardness ranges would disappear if equivalent Knoop values were plotted. Isometric minerals may have atomic structures which produce anisotropism of bond strength resulting in large microhardness variations. The strength of the microhardness anisotropism of an isometric mineral will depend upon the complexity and symmetry of the configuration of the atoms in the structure. Thus galena, having a relatively simple structure shows

greater hardness anisotropism than chromite having a more complex structure. Table XIX shows how the degree of anisotropism of microhardness in anisotropic minerals is directly related to the strength of anisotropism or symmetry of the atomic structure. Thus the minerals of the orthorhombic and monoclinic crystallographic systems show greater anisotropy of microhardness than minerals belonging to the tetragonal and hexagonal systems. The average value of 28.9% for the anisotropy of microhardness for the triclinic minerals is not significant, being the mean derived from only 4 values.

C. The relationship during indentation between deformation processes and orientation

In the following sections, Knoop and Vickers microhardness results obtained on oriented sections of minerals will be described and discussed in relation to atomic structure. No detailed theories have been put forward to explain the mechanism of indentation in minerals. It is therefore convenient at this point to outline possible mechanisms of deformation taking place during indentation. The following factors are of obvious importance:

- (a) the types and characteristics of movement mechanisms in crystals.

- (b) the orientation of these movement planes relative to the indentation direction.
- (c) the shape of the indenter.

(a) The types and characteristics of movement mechanisms in crystals

The following types of movement may occur in minerals during deformation.

- (i) translation slip
- (ii) translation twinning.
- (iii) movement along parting planes.
- (iv) movement along cleavage planes.
- (v) movement along fracture planes.

(i) Translation slip

Buergler (1928) has shown that movement occurs by the slipping of one portion of a crystal, relative to another, in crystallographic directions which are parallel to rows of consecutively like-charged atoms or ions in the lattice, (Fig. 20(a)). Movement in other directions along the slip plane would bring similarly charged atoms, at some stage, opposite one another and the resultant repulsion would cause cleavage (Figs. 20(a),(c)).

FIG. 20

Glide movements in ionic bonded crystals.

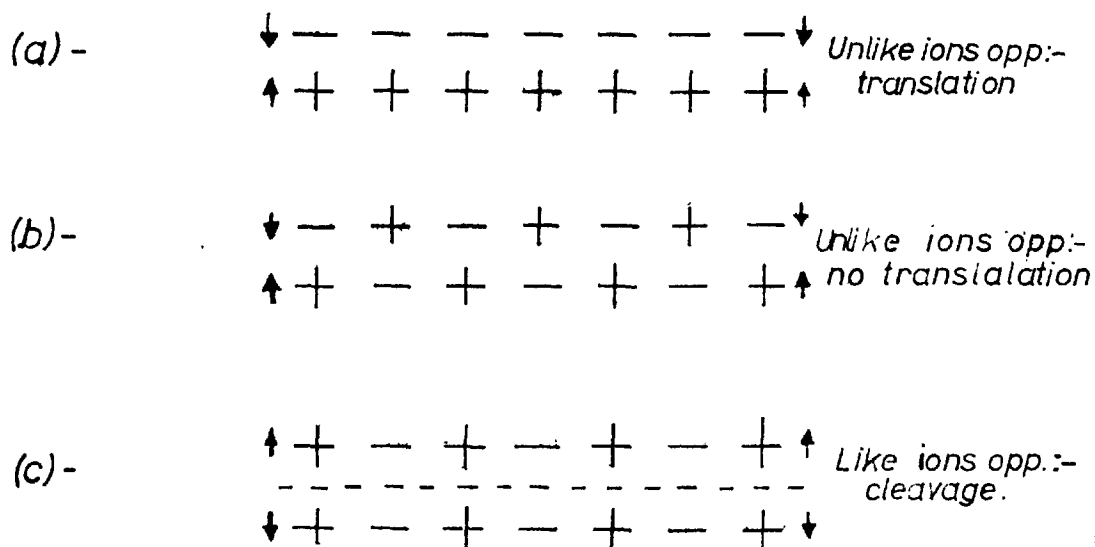
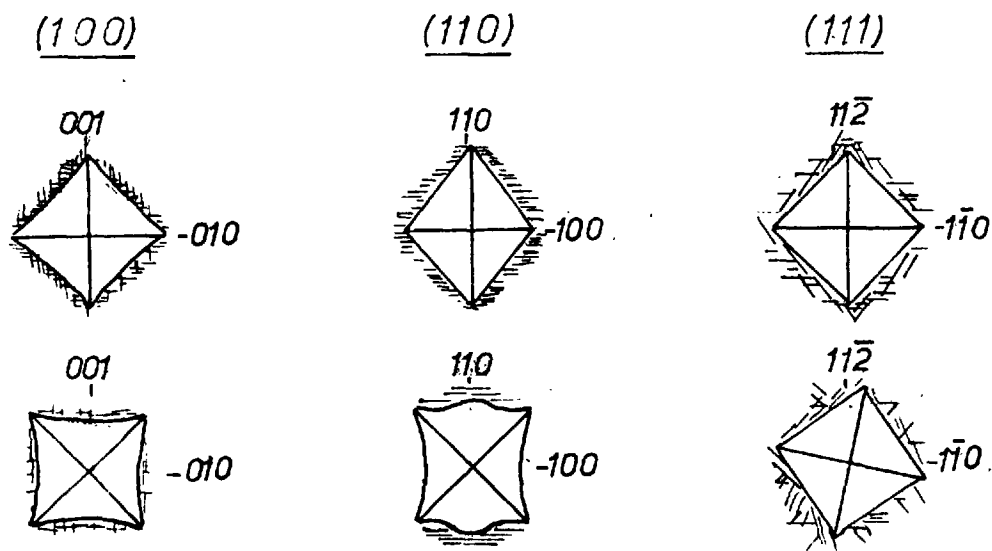


FIG. 21

Deformation characteristics of galena.



The glide planes and glide directions may thus be predicted from a knowledge of the atomic structure. Buerger (1928) summarized the principles upon which predictions can be made as follows:

"Translation may occur only in those crystallographic directions which are parallel to rows of consecutively like-charged ions in the lattice".

"Translation will occur along that family of planes containing a translation direction which has the greatest interplanar spacing".

Easy flowage occurs in many layer-lattice structures. Whilst the atoms within the layers are firmly bonded together, the force of attraction between the layers is slight. Movement occurs with great ease along the planes between layers.

Minerals having chain structures tend to deform along planes parallel to length of the chains. In stibnite, the bonding between different chains is weak and translation slip occurs along (010) planes in the (001) direction.

(ii) Translation twinning

Translation twinning occurs by the slipping of alternate layers past one another. Twinning involves a rotation of the crystal structure through 180° . Such processes have been shown by Buerger (1928) to take place during the deformation of sphalerite.

(iii) Movement along parting planes

In the mechanisms just described, the movements caused no actual rupturing of the structure, i.e. the deformation is entirely plastic. In many minerals no planes of easy glide exist and movement occurs along planes of weakness by fracturing. If the mineral exhibits no cleavage, deformation may take place along parting planes.

(iv) Movement along cleavage planes

Deformation in brittle minerals occurs by fracturing along cleavage planes. The more perfect the cleavage, the more easily movement can occur along the plane. In some minerals a cleavage plane is also a translation plane, as for example in stibnite. If the direction of movement is co-incident with the translation direction only minor fracturing will occur. Movement in a cleavage plane not co-incident with a translation plane results in cleavage fracture.

(v) Movement along fracture planes.

Minerals possessing no glide or cleavage planes deform by fracturing along irregular planes not related to the atomic structure.

(b) The orientation of the movement planes relative to the indentation direction

Buenger (1928) showed that a maximum shearing component for slip along a single plane occurs when the shearing forces are at 45° to the slip planes, and a minimum component occurs when the forces are perpendicular or at right angles to the slip plane. This theory was expanded to accommodate a crystal (galena) having three planes of movement at right angles to one another, the cube (100) planes. When the shearing forces are parallel and perpendicular to the slip planes i.e. at right angles to the (100) face, practically no movement takes place. If the slip planes are at angles to the shearing forces, movement will take place, the ease of movement being greater the nearer the slip planes approach to the 45° position.

Although the indenter faces make angles of more than 20° with the indenter, we may consider that for general purposes the shearing forces during indentation are dominantly vertical. Minor non-vertical frictional shear stresses may be set up due to contact between the indenter and the mineral but these stresses are in most cases insignificant. If a mineral possessing one perfect cleavage is oriented such that the cleavage planes are perpendicular to the indentation direction, then secondary frictional stresses will become important.

(c) The shape of the indenter

The Vickers indenter is a square-based pyramid, the angle between opposite faces being 136° . When the indenter is perpendicular to the surface, each face makes an angle of 22° with the surface. Thus the indentation of a mineral may be likened to that of a steeply faceted chisel being driven into a piece of wood. Material will be moved downwards and outwards from the first point of contact during the indentation process. Maximum movement in a truly isotropic medium will occur at the centres of the sides. Because of the high symmetry of the Vickers indenter, anisotropic effects on particular faces will be reduced and this renders it more useful than the Knoop indenter for determining differences of microhardness between different crystal faces of the same mineral. Indentation using a Vickers pyramid may be thought of as a pressure acting upon an approximately equidimensional area. Due to complex geometrical considerations, the interpretation of Vickers microhardness anisotropism with rotation of the indenter on particular crystal faces will be difficult. The problem becomes very complex when dealing with minerals exhibiting more than one glide plane.

The Knoop indenter is a pyramid elongated such that the angles between the long and the short edges are $172^{\circ} 20'$ and $130^{\circ} 00'$ respectively. Bloss, Shekarchi and Shell (1959)

have likened Knoop indentation to that of a wedge being pushed into the surface. Thibault and Nyquist (1947) have shown that maximum stress during the indentation of an isotropic medium is concentrated adjacent to the short diagonal. Thus maximum movement of material during Knoop indentation is also close to the short diagonal. Because of the lower symmetry of the Knoop indenter it is potentially more useful than the Vickers indenter in detecting microhardness anisotropy on particular crystal faces. Knoop indentation is best considered as a pressure acting vertically downwards upon an elongated area. If the area contains glide plane traces parallel to the elongation, low hardness should result since the pressure is acting upon relatively few glide planes. If the glide plane traces are at right angles to the elongation, higher hardness will result as the pressure is distributed over a greater number of glide planes. The difference of Knoop microhardness values on different crystal faces of the same mineral should be of the same order as those values obtained with a Vickers indenter.

D. Microhardness values obtained on oriented sections of minerals.

(a) General

For some of the minerals described later the translation planes and directions are already known. The microhardness

results for these minerals are discussed in relation to the known translation data. Minerals are grouped according to their crystallographic systems and the microhardness results together with reflectivity values where measured may be found in tables XXI, XXII, XXIII, XXIV and Figs. 10, 11, 12, 13, 14, 15 and 16. For convenience the results are discussed firstly in relation to microhardness variations on different crystal faces and secondly in relation to microhardness anisotropism on particular crystal faces.

(b) Discussion of the Results

(i) Isometric Minerals

Galena.

Buerger (1928) showed that plastic deformation in galena took place by gliding along (100) and (111) planes, the (100) plane being of much greater importance. The translation direction in the (100) planes was found to be perpendicular to the (1 $\bar{1}$ 0).

From Figs. 10, 11 it can be seen that the following relationship has been established:

$$H_{(100)} > H_{(110)} > H_{(111)}$$

Glide planes were observed around impressions made on all three faces. In every case they paralleled the cleavage trace directions. On the cube (100) face, two faint sets of glide plane traces were observed running parallel with cleavage traces i.e. at right angles to one another. The rhombododecahedral (110) face showed one prominent set of dislocations coursing parallel to 45° -dipping cleavage traces. A weaker set were observed parallel to the vertically dipping cleavage traces. The two sets of glide planes intersected at right angles. The octahedral (111) face gave three sets of dislocations intersecting one another at 60° , also paralleling the cleavage traces. Fig. 21 shows diagrammatically the relationship of the glide plane traces to the crystallographic directions in the minerals. The glide planes were made more distinct by light etching with a mixture of alcohol and dilute nitric acid in the ratio (1 : 3).

Table XX shows the close comparison of scratch hardness values obtained by Boiarskaia (1957) with the Knoop and Vickers values found in the present work. Not only do the values show the same order of hardness for the different faces but they also show the same relative difference between the faces. Such variations of hardness between the different faces are readily explained by applying the Buerger theory of the deformation of galena. Buerger showed that little

TABLE XX

Comparison of Indentation and Scratch Microhardness Values on the (100), (110) and (111) Faces of Galena.

Orientation	(100)	(110)	(111)
Knoop indentation values	85.0-	68.5-	62.5-
Kg/mm ² 100 g. load	79.5	61.5	57.5
Range and Mean	82.3	65.0	60.0
Ratio of Means	1.00	0.79	0.73
Vickers indentation values	86.5-	68.5-	63.5-
Kg/mm ² 100 g. load	69.0	63.0	63.0
Range and Mean	77.7	65.7	63.3
Ratio of Means	1.00	0.84	0.81
Scratch indentation values	38.5-	34.2-	32.7-
Kg/mm ² 5 g. load	28.6	24.1	22.1
Range and Mean [‡]	33.5	29.1	27.4
Ratio of Means.	1.00	0.87	0.82

[‡]After Boiarskaia (1957)

deformation would occur if pressure were applied perpendicular to the cube (100) face as the glide plane would be either perpendicular or parallel to the shearing stresses. Maximum shear stress should occur when all three glide planes make equal angles with the pressure direction i.e. when the pressure is perpendicular to the octahedral face (111).

The relationship of the glide plane to the indentation direction is shown in Fig. 22. On the cube (100) face (Fig. 22(a)) there is little tendency for movement along the (100) planes in the (110) directions. Deformation that does occur is presumably, from observed glide plane traces, either along (100) or (110) planes. The resistance to gliding results in the high hardness value for the cube face.

On the rhombicuboctahedral (110) face, (Fig. 22(b)), deformation occurs along two glide planes oriented at 45° to the indentation direction. Some movement would presumably take place along the (100) plane, as the translation direction is co-incident with the indentation direction. The lower hardness value for the (110) face, compared with the (100) face, is a reflection of easy glide along the two 45° -dipping (100) glide planes.

On the octahedral (111) face, (Fig. 22(c)), all three glide planes make angles of 35° with the indentation direction. Hence all three (100) planes are capable of easy glide although

FIG. 22

Orientation of (001) glide planes in galena
with respect to the (100), (110) and (111) faces.

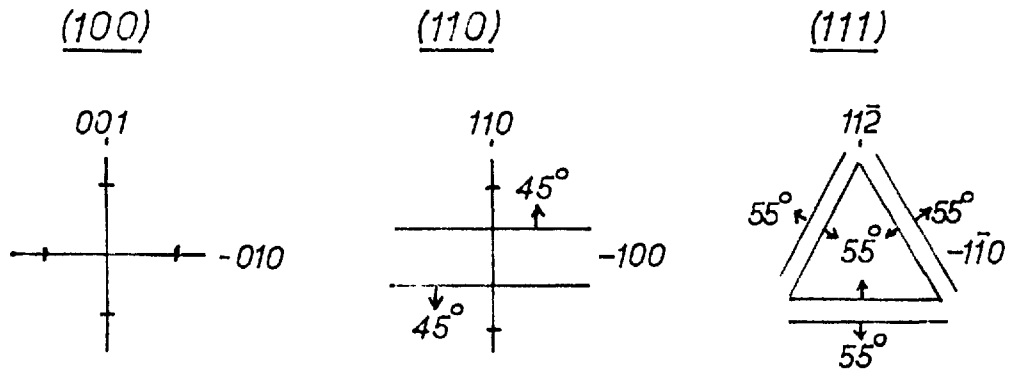
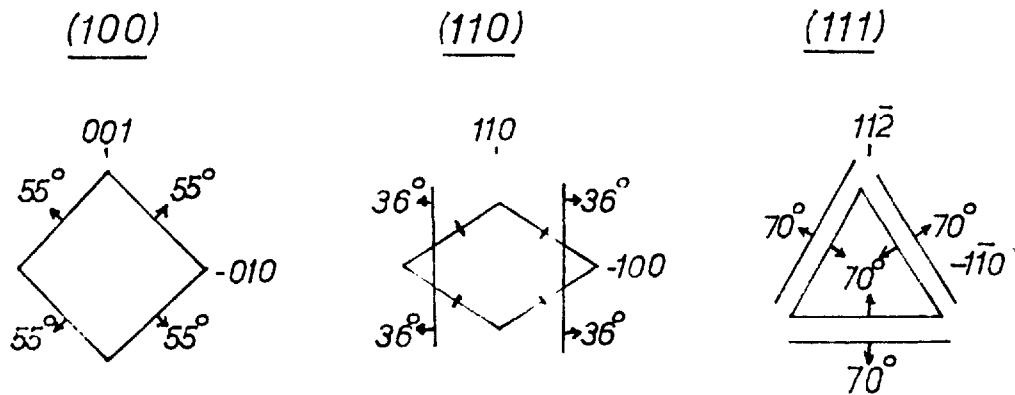


FIG. 23

Orientation of (111) movement planes in sphalerite
with respect to the (100), (110) and (111) faces.



the maximum shear stress cannot be applied to one of the glide planes. The combined effect of easy glide on three planes as compared with two on the rhombododecahedral face results in a slightly lower hardness value for the octahedral face, relative to the rhombododecahedral face hardness value.

Sphalerite

Buerger, (1928), showed that sphalerite deforms plastically by translation twinning along (111) planes in a direction perpendicular to (112). Henriques (1957) showed the Vickers microhardness of sphalerite depends upon two factors

- (a) the orientation of the surface indented and,
- (b) the amount of iron substituting for zinc in the crystal lattice.

The following formulae were derived to express the hardness values for the surface examined

$$HV_{(001)} = 165. + 16 \log C$$

$$HV_{(011)} = 187 + 18 \log C$$

$$HV_{(111)} = 193 + 19 \log C$$

where

HV = Vickers Microhardness

and C = Fe content of the sphalerite.

Fig. 12 shows the values obtained in the present work compared with the results obtained by Henriques. Both Vickers and Knoop indenters were used in the present work. Whilst in agreement with Henriques' work, the (100) face was found to be the softest face in all cases except one, there appeared to be practically no difference in microhardness between the (111) and (110) faces. In fact, most of the results indicate that the (110) face is slightly harder than the (111) face. The differences are, however, small, and well within the probable errors of the means. The relationship between the hardness on the different faces may be summarized as follows:

$$H_{(111)} \approx H_{(110)} > H_{(100)}$$

No dislocation planes were observed around impressions made on the different faces.

Assuming that sphalerite deforms by translation twinning along (111), and that no other mechanism of deformation would occur, it is possible to derive the theoretical hardness relationships between the faces. Fig. 23 shows the relationship of the indentation to the translation twin plane.

On the cube face (100) (Fig. 23(a)) there are four planes of possible translation twinning oriented at approximately 35° to the indentation. Easy movement can occur

along each of these planes and a low hardness value is to be expected. This is in accordance with the results of Henriques and the present work.

On the rhombododecahedral face (110) (Fig. 23(b)) there are four (111) planes which intersect the face. Two of these planes dip vertically and intersect one another at about 108° . The other two planes make angles of 54° with the indentation direction. Movement can take place easily therefore along only two planes. A hardness higher than that obtained on the (100) is to be expected and this is also in accordance with the results of Henriques and the present work.

On the octahedral face (111) (Fig. 23(c)), there are six (111) planes which make angles of 20° to the indentation direction. Movement can take place only relatively easily along all of the (111) planes. A hardness higher than that obtained on the (100) is to be expected and this is also in accordance with the results of Henriques, and the present work. It is impossible to state with confidence whether the octahedral face is harder than the rhombododecahedral face or not from theoretical considerations. It is significant however that Henriques' results are comparable to the results obtained by Winkler (1950) on the polishing hardness of diamond on the (100), (110) and (111) faces. Winkler also shows that the relative hardness of the faces may be derived theoretically

from the number of C - C bonds which bind the atoms for each unit surface, the ratio being (100) : (110) : (111) = 1.00 : 1.41 : 1.73. The errors of microhardness means in the present work are probably due to factors such as zoning i.e. variation of the iron content in the sphalerite and excessively coarse grinding in the initial stages of surface preparation.

The Spinel Minerals.

The spinels frequently exhibit a weak octahedral (111) parting. No translation data are known but twinning is reported, Palache et.al.(1944), to occur along (111) planes.

The microhardness results are summarized in Table XXI. As the probable errors of the mean values are only slightly less than the differences between the values, it would be incorrect to deduce significant microhardness differences between the different faces. Vickers and Knoop values for magnetite and franklinite indicate that the cube~~x~~ (100) face shows greater hardness than the (110) and (111) faces. The small differences in microhardness values with orientation on hercynite and hercynite-chromite are not significant, since measuring errors on minerals of such high hardness are of the same magnitude as the differences. The more detailed results obtained on magnetite (Fig. 16) indicates the following relationship:

$$H_{(100)} > H_{(110)} > H_{(111)}$$

No glide planes were observed around impressions on any of the minerals.

The microhardness values obtained on the (100), (110) and (111) faces of the spinel minerals vary in a similar manner to the results obtained on the same orientations of galena. This indicates that translation probably occurs along cube (100) planes in the spinel minerals.

Metals having the cubic close-packed structure

Translation gliding in metals having the cubic close-packed structure occurs along octahedral (111) planes in a direction perpendicular to (211). Two minerals of this group, gold and copper, were studied and the results are summarized in Table XXII and Fig. 14.

From Fig. 14 it can be seen that the microhardness of gold is strongly dependent upon the load. The type and amount of hardness variation varies from face to face so that at 15 g. load $H_{(100)} > H_{(111)}$ whilst at 100 g. load $H_{(111)} > H_{(100)}$. At 100 g. load the following relationship holds:

$$H_{(111)} > H_{(100)} > H_{(110)}$$

Knoop values at 50 g. load confirm this relationship.

Although no detailed load/microhardness studies have been carried out, it has been found that the microhardness of copper

is also strongly dependent upon the load. Vickers values at 100 g. load indicate the following relationship

$$H_{(111)} \gg H_{(110)} \approx H_{(100)}$$

Knoop values at 15 g. load indicate the following relationship

$$H_{(111)} \gg H_{(110)} > H_{(100)}$$

Octahedral (111) glide plane traces were observed around most impressions made in copper. Glide planes traces observed around impressions made in gold were much less distinct but appeared to parallel the (111) directions.

The results for gold and copper show only a limited agreement with one another. Several reasons for these discordant results may be put forward: inaccuracies in orientation of the crystal, resulting in uneven stress distributions during indentation; variations in chemical composition over the polished surface of the sections; inaccuracies in determining the microhardness values due to insufficient readings.

In general the results indicate the following relationship;

$$H_{(111)} > H_{(110)} \neq H_{(100)}$$

The relationship between the microhardness values on the (110) and (100) faces is indistinct. For gold, $H_{(100)} > H_{(110)}$,

but for copper $H_{(100)}$ or $= H_{(100)}$. Theoretically the relative hardnesses of the faces should approximately correspond to those obtained on sphalerite. The mode of deformation is however different. In sphalerite the deformation movement occurs by translation twinning in a direction perpendicular to (112), whilst in gold and copper the movement occurs by translation gliding in a direction perpendicular to (211). Ignoring the slightly conflicting differences between $H_{(100)}$ and $H_{(110)}$ for gold and silver, the results are concordant with the values obtained on sphalerite.

Cuprite

According to Palache et.al., (1944), cuprite shows an interrupted (111) cleavage and a less prominent (001) cleavage. No translation data are known for cuprite.

The differences of Vickers microhardness values obtained on the (100), (110) and (111) faces at 100 g. load are within the probable errors of the means and are therefore not significant. At 50 g. and 100 g. load (Fig. 15) the following relationship holds

$$HV_{(100)} > HV_{(111)} > HV_{(110)}$$

At 15 g. and 25 g. the following relationship holds

$$HV_{(111)} > HV_{(110)} > HV_{(100)}$$

Known values at 50 g. load also agree with the latter relationship.

Glide planes were observed around impressions made on the cube (100) face, the traces of which paralleled the octahedral cleavage traces. No glide planes were observed on the (110) and (111) faces.

On balance, the results indicate that the following relationship is probably valid:

$$H_{(111)} > H_{(110)} > H_{(100)}$$

There is some evidence of deformation along (111) planes. If the total deformation occurs along the (111) planes, then the latter relationship, by analogy with sphalerite, is theoretically to be expected. It is of interest to compare the results obtained from sphalerite with those of cuprite. Both minerals are isometric and have approximately the same microhardness. Sphalerite shows considerable anisotropy of microhardness with orientation, whereas the microhardness anisotropy of cuprite is small. The cause of the difference may be found in the differences between the atomic structures of the minerals. Sphalerite (Fe, Zn)S has a relatively simple symmetrical A-X type structure whereas cuprite, Cu_2O , has an asymmetric A_2X type structure. In cuprite the structure gives rise to a

relatively even bonding between atoms in all directions resulting in small differences of shear strength with orientation. The structure of sphalerite tends to produce an unevenness of bonding which gives rise to anisotropy of shear strength in different directions.

Fluorite and Pyrochlore

No translation data is known concerning either mineral. Fluorite exhibits a perfect octahedral (111) cleavage and pyrochlore a less perfect octahedral (111) parting.

Vickers and Knoop microhardness values in Table XXIII indicate the following relationship for both minerals:

$$H_{(111)} > H_{(100)}$$

No glide planes were observed around impressions made on either mineral.

If deformation during indentation takes place along the cleavage planes, i.e. planes of weakest bonding, then the above relationship is concordant with those found in sphalerite, gold, copper and cuprite.

Perovskite, Skutterudite and Sperrylite.

No translation data are known for these minerals. The minerals exhibit the following cleavages: perovskite - (001), perfect; Skutterudite - (001), (011) and (111) perfect; Sperrylite - (001), indistinct.

TABLE XXI

Oriented microhardness values obtained on some members of the spinel minerals.

Mineral	Orientation	V.M.H. Range and Mean (100g. load)	K.M.H. Range and Mean (100 g. load)
Magnetite	(100)	606 - 575 590	760 - 549 631
	(110)	566 - 530 546	695 - 587 619
	(111)	535 - 539 563	615 - 485 561
Franklinite	(100)	824 - 763 795	770 - 650 696
	(111)	752 - 720 734	703 - 607 650
Hercynite	(100)	1533 - 1478 1500	1560 - 1323 1413
	(110)	1547 - 1378 1450	1570 - 1283 1416
Chronite- Hercynite	(100)	1478 - 1366 1421	1530 - 1291 1406
	(110)	1491 - 1320 1417	1580 - 1068 1298
	(111)	1533 - 1378 1468	1389 - 1231 1287

TABLE XXII

Oriented microhardness values obtained on Gold, Copper and Cuprite.

Mineral	Orientation	V.M.H. Range and Mean (100 g. load)	K.M.H. Range and Mean (50 g. load)
Gold	(100)	69.4 - 57.1 63.8	69.8 - 56.2 63.0
	(110)	55.1 - 40.8 43.7	55.1 - 44.4 47.1
	(111)	94.1 - 66.0 75.7	96.2 - 67.8 78.2
Copper	(100)	54.0 - 47.5 49.9	71.9 - 52.1 [‡] 61.0
	(110)	52.8 - 47.5 49.6	85.4 - 56.0 [‡] 64.5
	(111)	92.0 - 61.0 80.1	101.0 - 73.2 [‡] 87.5
Cuprite	(100)	206 - 181 192	200 - 156 180
	(110)	190 - 185 187	199 - 154 181
	(111)	193 - 184 189	206 - 193 198

[‡]Values obtained at 15 g. load.

TABLE XXIII

Oriented Microhardness Values

ISOMETRIC

Mineral	Orientation	V.N.H. Range (100 g. load)	K.N.H. Range (100 g. load)
Fluorite	(100)	181 - 174	188 - 166 [#]
	(111)	203 - 174	220 - 182 [#]
Pyrochlore	(100)	642 - 420	549 - 490 [#]
	(111)	703 - 557	634 - 493 [#]
Perovskite	(100)	1131 - 1003	1102 - 834
	(111)	1131 - 988	1158 - 976
Fe-skutterudite	(100)	694 - 627	790 - 543 [#]
	(111)	665 - 599	765 - 645 [#]
Sperrylite	(100)	1277 - 960	1098 - 960
	(111)	1225 - 1048	1175 - 1039

TETRAGONAL

Pyrolusite	<u>l</u> c	345 - 268	555 - 241 [#]
	//c	193 - 113	432 - 109 [#]

[#]At 50 g. load.

TABLE XXIII Contd.

Oriented Microhardness Values

HEXAGONAL

Mineral	Orientation	V.M.H. Range (100 g. load)	K.M.H. Range (100 g. load)
Apatite	(0001)	606 - 454	638 - 498 [‡]
	(10 $\bar{1}$ 0)	596 - 426	634 - 423 [‡]
Beryl	(0001)	1760 - 1160	1430 - 1100
	(10 $\bar{1}$ 0)	1590 - 1402	1500 - 1360
Corundum	(0001)	2598 - 2097	2186 - 1751
	(10 $\bar{1}$ 0)	2758 - 2341	2470 - 2186
Eskolaite	(0001)	2861 - 2239	2276 - 2011
	(10 $\bar{1}$ 0)	3087 - 2478	2370 - 1881
Pyromorphite	(0001)	262 - 225	249 - 247 [‡]
	(10 $\bar{1}$ 0)	242 - 186	261 - 168 [‡]
Quartz	(0001)	1465 - 1266	1307 - 1039
	(10 $\bar{1}$ 0)	1561 - 1378	1231 - 890
Tourmaline	(0001)	1380 - 1190	1310 - 1100
	(10 $\bar{1}$ 0)	1480 - 1340	1480 - 1010

[‡]At 50 g. load.

TABLE XXIII
Oriented Microhardness Values

ORTHORHOMBIC

Mineral	Orientation	K.M.H. Range (100 g. load)	K.M.H. Range (100 g. load)
Stephanite	(001)	107 - 92.0	120 - 85.4 [✓]
	(110)	77.9 - 45.1	102 - 37.0 [✓]
	(010)	78.2 - 47.2	101 - 37.4 [✓]
Topaz	(001)	2010 - 1670	1740 - 1390
	(010)	1750 - 1480	1640 - 1380
	(100)	1820 - 1620	1810 - 1240

MONOCLINIC

Gypsum	(001)	47.5 - 30.5	156 - 38.0 [✓]
	(010)	48.2 - 34.8	69.3 - 38.0 [✓]
Monazite	(001)	988 - 734	1130 - 829
	(010)	888 - 772	1138 - 686
	(100)	946 - 704	1045 - 661
Orthoclase	(001)	933 - 642	655 - 531 [≠]
	(010)	913 - 642	717 - 423 [≠]
	(110)	882 - 681	717 - 463 [≠]

✓ At 15 g. load.

≠ At 50 g. load.

TABLE XXIII Contd.

Oriented Microhardness Values

TRICLINIC

Mineral	Orientation	V.M.H. Range (100 g. load)	K.M.H. Range (100 g. load)
Kyanite	(001)	1190 - 500	1640 - 400
	(010)	1730 - 1430	2320 - 1970
	(100)	2140 - 1100	1910 - 360

The differences in microhardness values between different faces, (Table XXIII), are sufficiently small to be within the probable errors of the mean values. Hence no significant correlation can be made between orientation and microhardness values.

(ii) Tetragonal Minerals

Rutile

Two translation twin planes are known to exist in rutile; the (011) and (092) planes (Palache et.al. (1944)). Rutile also exhibits a distinct (110) cleavage, a less distinct (100) cleavage and a poor (011) cleavage.

Results in Fig. 16 and Table XXIV show the following hardness relationship between the faces

$$H_{(001)} \approx H_{(111)} > H_{(110)}$$

Glide planes were observed around only one impression - made on the (111) face. No correlation could be established between these dislocation planes and the known planes of translation.

The differences between the microhardness values for the (001) and (111) faces are comparable to the probable errors of the means and hence no correlation can be made with orientation.

The relatively isotropic nature of rutile is surprising in view of the potential planes of twinning and gliding.

Pyrolusite

Pyrolusite exhibits a perfect (110) cleavage. No translation data are known for the mineral.

No precise orientations of pyrolusite were obtained. However, values in Table XXIII show that a section cut parallel to the c-axis is softer than one cut perpendicular to the c-axis.

Although some cleavage fractures were observed around impressions made on the section cut perpendicular to the c-axis no form of dislocations were observed around impressions made on the section cut parallel to the c-axis.

If deformation during indentation takes place along (110) cleavage planes, the above relationship is to be expected. During indentation on the (001) face there is no shearing stress acting on the (110) cleavage planes, whilst at the (100) and (010) faces the (110) planes are oriented at approximately 45° to the indentation direction. As some cleavage fractures were observed around impressions made on the section perpendicular to the c-axis and not on the section parallel to the c-axis, it may also be inferred that translation movement may occur in a direction parallel to the a-axis, i.e. perpendicular to $(\bar{1}\bar{1}0)$.

Cylindrite

The crystallography of this mineral is not known but it exhibits cylindrical structures which have a tetragonal symmetry. Cylindrite exhibits a cylindrical shell-like parting which runs parallel to the length of the structure.

Microhardness values in Table XXIV show that a section cut parallel to the length is softer than one cut perpendicular to the length.

Deformation during indentation has been observed to occur by gliding along the parting planes (photos 88,89).

The microhardness values are in accordance with theoretical expectations if deformation takes place by movement along the parting planes. During indentation of the "basal" section, there is no component acting along the parting planes. This results in a high hardness for the basal section. On the "prism" section, the amount of shearing component acting along the partings will depend upon the "depth of cut" of the section (Fig.21(A)). In Fig.21(A)(a) and 21(A)(b) high hardness will result as the shearing force is either parallel or perpendicular to the parting planes. Minimum hardness is approached when the parting planes approach the 45° position. This theory offers an explanation for the large range of microhardness values.

FIG. 21(A)
THE ATTITUDE OF THE CYLINDRICAL
CLEAVAGES TO THE INDENTING
DIRECTION ON PRISMATIC SECTIONS
OF CYLINDRITE

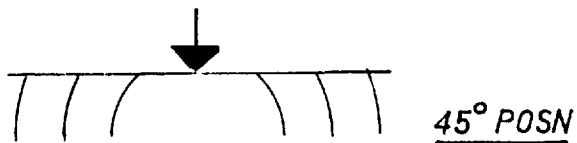
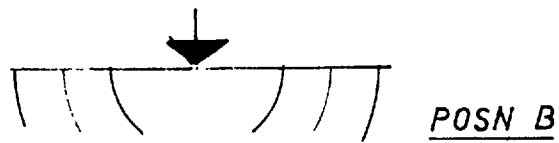
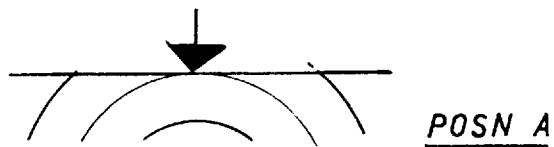


TABLE XXIV

The variation of microhardness and reflectivity values with orientation

TETRAHEDRAL

Mineral	Orientation	V.M.H. Values (100 g. load)	K.M.H. Values (diff. loads)	R% values (white light)
Cylindrite	(\parallel length)			
	diag. \perp length	58.1	152	30.7
	diag. \parallel length	58.1	22.0	32.7
	(\perp length)	114-74.5 95.1	178-94.6 135	33.5- 31.1
Rutile	(001)	1041-933 983	1138-1005 1078	21.6
	(111)	1056-974 1015	1138-941 1040	22.2-20.7 21.4

HEXAGONAL

Covellite	(0001)	128-93.6 110	163-127 142	17.7
	(10 $\bar{1}$ 0)			
	diag. \parallel c } diag. \parallel a ₁ a ₂ }	107-58.6 77.3	211 85.4	15.8 24.0
Monatite	(0001)	967-914 940	976-812 884	26.4
	(10 $\bar{1}$ 0)			
	diag. \parallel c } diag. \parallel a }	1018-920 963	1195 962	23.9 25.3

TABLE XXIV Contd.

HEXAGONAL

Mineral	Orientation	V.M.H. Values (100g. load)	K.M.H. Values (diff. loads)	R% values (white light)
Molybdenite	(0001)	74.2-33.0 45.3	23.6-17.0 20.5	46.6
	(10 $\bar{1}$ 0) diag. // c } diag. // a }	9.7-4.4 6.7	80.1 3.7	16.2 31.7
Pyrrangyröte	(0001)	108-100 104	177-95.0 107	31.5
	(10 $\bar{1}$ 0) diag. // a } diag. // c }	130-106 119	156 84.1	26.9 30.0
Pyrrhotite	(0001)	348-297 321	368-322 350	43.4
	(10 $\bar{1}$ 0) diag. // a } diag. // c }	259-234 245	311 240	46.3 49.4
Wurtzite	(0001)	264-245 254	284-279 281	18.2
	(10 $\bar{1}$ 0) diag. // a } diag. // c }	167-146 156	227 133	17.7 18.2

TABLE XXIV Contd.

ORTHORHOMBIC

Mineral	Orientation	W.N.H. Values (100g. load)	K.N.H. Values (diff. loads)	R _x Values (white light)
Bournonite	(001)	175-159 164	199-152	34.9-34.3 34.6
	(010) diag. // c } diag. // a }	194-163 180	219 179	36.1 35.0
	(100)	183-168 176	204-177 187	34.7-34.1 34.4
Chalcocite	(001)	85.4-65.5 79.3	94.0-84.0 90.0	29.1-28.5 28.8
	(110) diag. // c } diag. // a }	80.2-62.7 74.3	57 103	30.7 29.5
Enargite	(001) diag. // a } diag. // b }	407-376 391	363 363	28.1 26.8
	(010) diag. // a } diag. // c }	276-168 225	367 166	26.7 29.0
	(100) diag. // b } diag. // c }	303-234 260	363 145	25.5 23.7
Ilvaite	(001)	772-703 741	750-653 695	10.5
	(100) diag. // a } diag. // c }	743-703 728	669 882	6.4 10.7

TABLE XXIV Contd.

ORTHORHOMBIC

Mineral	Orientation	F.M.H. Values (100g. load)	K.H.H. Values (diff. loads)	R% Values (white light)
Manganite	(001)			
	diag. // a }	782-673	465	17.5
	diag. // b }	725	700	15.8
	(010)			
	diag. // a }	772-661	400	16.6
	diag. // c }	727	640	20.8
	(100)			
	diag. // b }	803-703	79P	14.5
	diag. // c }	741	700	22.0
Manganotantalite	(001)			
	diag. // a }	514-363	520	15.1
	diag. // b }	430	1013	16.1
	(100)			
	diag. // b }	488-370	962	15.7
	diag. // c }	431	309	16.4
	(010)			
	diag. // a }	373-335	543	...#
	diag. // c }	361	336	...#
Marcasite	(001)			
	diag. // a }	1256-797	1185-1093	44.0
	diag. // b }	1048	1135	49.6
	(010)			
	diag. // a }	1288-762	1321-1077	48.2
	diag. // c }	1088	1188	51.6
	(100)			
	diag. // b }	1250-1033	1120	48.0
	diag. // c }	1135	1470	43.8

[#]R_{max} and R_{min} are not concordant with crystallographic axes.

TABLE XXIV Contd.

ORTHORHOMBIC

Mineral	Orientation	V.M.H. Values (100g. load)	K.M.H. Values (diff. loads)	R% Values (white light)
Stibnite	(001)			
	diags. 45° axes	69.0	--	--
	diag. // b }	92-69	118	30.7
	diag. // a }	80	50	36.0
	(010)			
	diag. // c }	110-70	30	40.0
	diag. // a }	82	113	37.6
	(100)			
	diag. // c }	129-112	62	42.5
diag. // b }	120	145	34.5	
Bismuthinite	(001)			
	diags. 45° axes	67.0	--	--
	diag. // b }	216-67.0	170	38.5
	diag. // a }	120	32	44.1
	(010)			
	diag. // c }	95-60	75	47.3
	diag. // a }	75	60	45.7
	(100)			
	diag. // c }	160-120	108	47.0
diag. // b }	145	217	37.3	

TABLE XXIV Contd.

MONOCLINIC

Mineral	Orientation	W.M.H. Values (100 g. load)	K.H.H. Values (diff. loads)	R% Values (white light)
Arsenopyrite	(010)			
	diag. // a }	1206-1056	1080	52.0
	diag. // c }	1120	1345	50.3
	(100)			
	diag. // b }	933-772	678	48.0
	diag. // c }	849	1350	46.3
	(101)			
	diag. // b }	960-599	807	53.4
	diag. // c }	825	1345	
Hubnerite	(001)			
	diags. 45° axes	---	500	--
	diag. // a }	397-351	456	15.1
	diag. // b }	371	456	16.1
	(100)			
	diag. // b }	302-285	360	16.6
	diag. // c }	294	360	17.1
	(010)			
	diag. a	327-297 307	403-315 355	--# --#

*R_{max.} and R_{min.} not concordant with crystallographic axes.

(iii) Hexagonal Minerals

The hexagonal minerals studied may be conventionally subdivided into groups as follows:

- (a) those on which reflectivity measurements have been determined for the basal (0001) and prism (10 $\bar{1}$ 0) faces,
- (b) those on which no reflectivity measurements have been determined.

(a) Minerals on which microhardness and reflectivity values have been correlated

The following minerals are included in this group:

Covellite
Hematite
Molybdenite
Pyrargyrite
Pyrrhotite
Wurtzite

The translation characteristics and microhardness results for each mineral are discussed below, and this is followed by a discussion of the results of the whole group.

Covellite

Translation in covellite occurs along (0001) planes in a

direction perpendicular to $(10\bar{1}0)$, Ramdohr, (1951). It possesses a perfect basal (0001) cleavage.

The basal face (0001) shows a higher hardness than the prism $(10\bar{1}0)$ face - see Table XXIV.

On the basal face no well defined glide planes were observed but on the prism $(10\bar{1}0)$ section, marked slip planes parallel to the (0001) cleavage could be clearly seen, (photo 80).

The results are in agreement with theoretical expectations based on the assumption that deformation movement during indentation occurs along basal (0001) planes in a $(10\bar{1}0)$ direction. On the basal section (0001), the indentation direction is perpendicular to the plane of movement. The translation planes therefore take no component of the shearing forces and high hardness results. On the prism face $(10\bar{1}0)$, the indentation direction is co-incident with the translation direction. This movement occurs more easily in this direction resulting in lower hardness. Reflectivity values, (white light), are higher on the prism face $(10\bar{1}0)$ than on the basal face (0001).

Hematite

Translation in hematite is reported to occur along (0001) planes in a direction perpendicular to $(10\bar{1}0)$, Ramdohr, (1951).

Hematite exhibits no cleavage but sometimes shows partings parallel to (0001) and $(10\bar{1}0)$ due to twinning.

The differences of microhardness between the basal and the prism faces are relatively small, the prism face being slightly harder than the basal face, (Table XXIV).

No dislocations were observed around impressions made on either face.

The results are not in agreement with theoretical expectations based on the assumption that deformation occurs along (0001) planes in directions perpendicular to $(10\bar{1}0)$. It seems more likely that movement may occur along other planes such as the $(10\bar{1}0)$ planes by translation twinning. Pressure twinning in corundum, which is isostructural with hematite, deforms under pressure along (0001) and $(10\bar{1}0)$ planes - Palache et.al. (1944). If deformation during indentation does occur along both these planes, then the relative theoretical hardnesses of the faces can be assessed. On the basal face, six $(10\bar{1}1)$ planes would be oriented at approximately 45° to the indentation direction. On the prism face, two $(10\bar{1}1)$ planes would be oriented at about 45° to the indentation direction and the remaining four would form very small angles with the indentation direction. In addition some gliding would occur along the (0001) planes in the $(10\bar{1}0)$ directions. The basal face (0001) shows a higher reflectivity than the

prism face $(10\bar{1}0)$.

Molybdenite

Deformation in molybdenite occurs by translation along (0001) planes, (Palache et.al. (1944)), the translation direction is perpendicular to $(10\bar{1}0)$. Molybdenite exhibits a perfect basal cleavage.

Microhardness values in Table XXIV shows that the basal face (0001) is harder than the prism face.

Gliding along (0001) planes was observed around all impressions made on the $(10\bar{1}0)$ face.

The microhardness results, which are entirely analogous with those of covellite, are in agreement with theoretical expectations, based on the assumption that gliding takes place along (0001) planes. Reflectivity values for the basal face (0001) are higher than those obtained on the prism face.

Pyrrargyrite

Pyrrargyrite exhibits a perfect $(10\bar{1}1)$ cleavage and a less distinct $(01\bar{1}2)$ cleavage. Pressure twinning occurs along $(10\bar{1}4)$ planes, (Palache et.al. (1944)).

Microhardness values in Table XXIV indicate that the prism face $(10\bar{1}0)$ is slightly harder than the basal face (0001) .

No dislocations were observed around any of the impressions.

The results are in agreement with the theoretical assumption that deformation takes place by gliding along $(10\bar{1}4)$ planes. On the basal face, six $(10\bar{1}4)$ planes are oriented at about 75° to the indentation direction. On the prism face, two $(10\bar{1}4)$ planes make angles of about 15° to the indentation direction and the remaining four are oriented at very small angles to the indentation direction. The basal face (0001) shows a higher reflectivity than the prism face $(10\bar{1}0)$.

Pyrrhotite

Pyrrhotite exhibits a parting parallel to (0001) . Translation gliding is reported to occur along (0001) planes in a direction perpendicular to $(10\bar{1}0)$, (Ramlohr, 1951).

Microhardness values in Table XXIV indicate that the basal face is harder than the prism face.

No glide planes were observed around impressions made on either the prism or the basal faces.

The results are in agreement with theoretical expectations based on the assumption that gliding during deformation occurs along (0001) in a direction perpendicular to $(10\bar{1}0)$. It is

of interest to compare the present results with those obtained by Bowie and Taylor, (Table XXV).

TABLE XXV

Comparison of the microhardness values obtained by Bowie and Taylor (1958) and the present writer, on oriented sections of pyrrhotite.

	Bowie and Taylor		Young
Isotropic sections	318 - 280 303	(0001)	348 - 297 321
Anisotropic sections	259 - 230 248	(10 $\bar{1}$ 0)	259 - 234 244

The results for pyrrhotite show similar differences of microhardness with orientation compared with the values obtained on covellite and molybdenite. Reflectivity values on the prism face are higher than those on the basal face.

Wurtzite

Wurtzite exhibits a perfect (11 $\bar{2}$ 0) cleavage, and a parting parallel to (0001). No translation data are known for wurtzite.

Microhardness results in Table XXIV indicate that the basal face is considerably harder than the prism face.

Dislocations have been observed (Photo 262) running parallel to the traces of the $(11\bar{2}0)$ cleavage.

The results are in agreement with the theoretical expectations based on the assumption that movement during indentation occurs by gliding along either $(11\bar{2}0)$ or (0001) planes, or both. On the basal face (0001) , the (0001) plane is perpendicular to the indentation direction and the $(11\bar{2}0)$ cleavages are parallel to the indentation direction. As these are only minor shearing components on either of these planes, high hardness results. On the prism face $(10\bar{1}0)$, the basal plane cleavages (0001) are parallel to the indentation direction and therefore carry little shearing component. Two of the $(11\bar{2}0)$ cleavage planes are oriented at 60° to the indentation direction. The third $(11\bar{2}0)$ plane is perpendicular to the indentation and carries little shearing component. Deformation on the prism face is therefore slightly easier and results in lower hardness. Reflectivity on the basal face is slightly higher than on the prism face.

Discussion

The minerals may be sub-divided into two groups according to their mode of deformation. Covellite, molybdenite and pyrrhotite all deform by translation along (0001) planes in directions perpendicular to $(10\bar{1}0)$. The

basal sections for these minerals are considerably harder than the prism faces. Hematite, pyrrargyrite and wurtzite deform along planes other than the basal cleavage.

Pyrrargyrite and hematite, having pyramidal glide planes show greater hardness on the prism faces than on the basal faces. Wurtzite, having prismatic and basal glide planes, shows greater hardness on the basal face than on the prism face.

There appears to be a united correlation between the hardness and reflectivity values between the groups. Of the group - covellite, molybdenite, pyrrhotite, covellite (in white light) and pyrrhotite show an increase in reflectivity from the basal face to the prism face, and molybdenite exhibits the reverse relationship. Hematite, pyrrargyrite and wurtzite all show an increase in reflectivity from the prism face to the basal face. The relationships are summarised in Table XXVI.

TABLE XXVI

A comparison of reflectivity and microhardness differences on the basal (0001) and prism (10 $\bar{1}$ 0) face of six hexagonal minerals.

Mineral	Reflectivity (white heat) Basal to Prism	Microhardness Basal to Prism
Covellite	I	D
Pyrrhotite	I	D
Molybdenite	D	D
Wurtzite	D	D
Henatite	D	I
Pyrrargyrite	D	I

I = Increase D = Decrease.

(b) Minerals for which no reflectivity values are available

The following minerals are included in this group:

- Apatite
- Beryl
- Corundum
- Pyromorphite
- Quartz
- Tourmaline

Beryl, Quartz and Tourmaline

Microhardness values in Table XXIII indicate that there are no significant differences between the basal and the prism faces for these minerals.

Quartz shows no well defined cleavages. Beryl sometimes exhibits an imperfect (0001) cleavage and tourmaline has ill defined $(11\bar{2}0)$ and $(10\bar{1}1)$ cleavages. No translation data are known for any of the minerals and no glide planes were observed around impressions made in the minerals.

The results are in accordance with theoretical expectations. None of the minerals has any well defined structural weakness an expression of their complex silicate network type structure.

Pyromorphite and Apatite

Microhardness values in Table XVIII indicate that the basal faces are harder than the prism faces.

Apatite shows an imperfect (0001) cleavage, and a less perfect $(10\bar{1}0)$ cleavage. Pyromorphite exhibits weak $(10\bar{1}0)$ and $(10\bar{1}1)$ cleavages. No translation data are known about the minerals and no glide planes were observed around impressions.

The results are in accordance with theoretical

expectations if the assumption is made that deformation during indentation occurs along cleavage planes. For apatite, on the basal face, the cleavages (0001) and (10 $\bar{1}$ 0) are perpendicular and parallel to the indentation resulting in high hardness. On the prism face, the (0001) cleavage is parallel to the indentation direction but the (10 $\bar{1}$ 0) cleavages make angles of 30° with the indentation direction. The combined result: gives a lower hardness for the prism face than for the basal faces. For pyromorphite, on the basal face, the prismatic cleavage is perpendicular to the indentation direction but the (10 $\bar{1}$ 1) cleavages make angles with indentation direction. On the prism face, both the (10 $\bar{1}$ 0) and (10 $\bar{1}$ 1) cleavages make angles with the indentation direction. Thus the basal face is harder than the prism face.

Corundum

Microhardness values in Table XXIII indicate that the prism face is harder than the basal face.

Corundum exhibits a weak parting parallel to (0001). Pressure twinning is known to occur along (10 $\bar{1}$ 1) and (0001) planes. No glide planes were observed around impressions in corundum.

The results are in accordance with theoretical

expectations based on the assumption that gliding takes place along (0001) and $(10\bar{1}1)$ planes. On the basal face, the (0001) planes are perpendicular to the indentation direction. Six $(10\bar{1}1)$ planes form angles of approximately 60° with the indentation direction. On the prism face the (0001) planes are parallel to the indentation direction. Only two $(10\bar{1}1)$ planes form angles of approximately 30° with the indentation. The four remaining $(10\bar{1}1)$ planes form very small angles with the indentation direction. Thus the total shear component is greater on the (0001) face than on the $(10\bar{1}0)$ face and this results in the (0001) face being softer than the $(10\bar{1}0)$ face.

(iv) Orthorhombic Minerals

The following orthorhombic minerals were studied:

Bournonite

Chalcocite

Enargite

Manganite

Manganotantalite

Stephanite

Stibnite-Bismuthinite

Topaz.

Bournonite

Twin gliding in bournonite is reported to occur along (110) planes, Mügge (1920). Bournonite exhibits a perfect (010) cleavage, and less perfect cleavages parallel to (100) and (010), Palache et.al. (1944).

Microhardness values are given in Table XXIV. No glide planes were observed around the impressions. The differences of microhardness values are insufficiently large to be correlated with orientation of the glide planes. Movement can take place along the (110) twin glide planes and also along the (010) cleavages. It is therefore surprising to find bournonite relatively isotropic in microhardness.

Chalcocite

Pressure twinning in chalcocite is reported to occur along (201) and (131) planes, Mügge, (1920). Interpenetration twinning and cleavage occur most commonly along (110) planes.

Microhardness values in Table XXIV indicate that the basal face (001) is harder than the prism face (110). If deformation occurs by movement along (201) and (131) planes,

then the hardness of the basal and prism faces should be approximately the same. Strong parting planes were observed, photos 52, 53, around indentations made on both faces, but no glide planes were observed. These parting planes are probably due to a fine lamella intergrowth of digenite along (111) planes.

Oriented Knoop microhardness values obtained on the (110) face, Table XXIV, indicate a plane of weakness where traces are parallel to the c-axis. Detailed orientation studies of the diagonal lengths of indentations made on the (110) face, Fig. 56, also indicate that movement occurs along planes parallel to the c-axis.

Thus, the results of the present studies indicate that movement by translation twinning along (201) and (131) planes during indentation is not important. Rather they indicate that movement occurs along planes parallel to the c-axis, probably along (110) planes. This conclusion is substantiated by additional evidence given in Chapter V, based on the shape of Vickers indentations made on the (110) face, Fig. 56.

Enargite

No translation data are known concerning enargite.

According to Palache et.al. (1944) enargite possesses a perfect (110) cleavage, less perfect (010) and (100) cleavages, and an imperfect (001) cleavage.

Microhardness results in Table XXIV indicate the following relationship:

$$H_{(001)} > H_{(010)} \approx H_{(100)}$$

Numerous (110) cleavage fractures were observed around impressions made on all the faces, (photos 97 - 102).

The above relationship indicates that movement during indentation may take place by movement along cleavage planes, particularly the (110) cleavage planes. On the (100) and (010) faces, the (100), (010) and (001) cleavages are either parallel or perpendicular to the indentation directions. The (110) cleavages form angles of approximately 45° with the indentation direction. Maximum shearing component takes place along the (110) planes and low hardness for the (100) and (010) faces results. On the (001) face, the (100), (010) and (110) cleavages are parallel to the indentation direction, whilst the (001) cleavage is perpendicular to the direction. Since no shearing component can occur along any of the planes of movement, high hardness results.

Manganite

Translation gliding has been reported to occur along (010) planes in a direction perpendicular to (001), Mügge (1920). Manganite exhibits a perfect (010) cleavage and less perfect (110) and (001) cleavages.

Microhardness results in Table XXIV indicate the following relationship,

$$H_{(100)} > H_{(010)} \approx H_{(001)}$$

Cleavage fractures were observed around impressions on all faces.

The results are consistent with translation movement during indentation taking place along the (010) glide planes in a direction perpendicular to (001). Some movement may also occur along the (110) and (001) cleavage planes. On the (001) face, the (010) twin glide plane and the (110) cleavages are parallel to the indentation direction. The (001) cleavage is perpendicular to the indentation direction. Movement will occur relatively easily along the (010) glide plane as the translation and indentation directions are coincident. On the (010) face, the (010) glide plane and the (001) cleavage are respectively perpendicular and parallel to the indentation direction. The (110) cleavages form angles of approximately 45° with the indentation direction.

On the (100) face, the geometrical configuration is similar to that on the (010) face except that the (010) twin glide plane is parallel to instead of perpendicular to the indentation direction. The (001) face shows a low hardness because easy translation takes place along the (010) planes. High hardness values on the (100) face, relative to those obtained on the (010) face, are attributed to the difficulty of movement along the (010) planes, in directions perpendicular to (100). On the (010) face lower hardness is caused by easy lateral movement along the (010) planes in directions perpendicular to (001).

Mangantantalite

Translation gliding in Columbite-Tantalite is reported to occur along (100) planes in directions perpendicular to (001) and (010)., Mügge (1898). Columbite-tantalite exhibits a distinct (010) cleavage and a less distinct (100) cleavage.

Microhardness results in Table XXIV and indicate the following relationship

$$H(001) \approx H(100) > H(010)$$

Microhardness values obtained on oriented sections of various members of the columbite-tantalite series (Table XXXVIII) show the following relationship,

$$H(001) > H(100) \gg H(010)$$

The results are in agreement with theoretical expectations based on the assumption that translation gliding takes place along the (100) plane in the (010) plane, but not, as reported by Mügge, in the (001) plane. On the (001) face, the (100) twin plane and the (100) and (010) cleavages are parallel to the indentation. If, as Mügge has reported, slip occurs easily along the (100) glide plane then low hardness should result. However, the (100) face exhibits the highest hardness of the three faces. On the (010) face, the (100) glide and cleavage planes and the (010) cleavage planes are respectively parallel and perpendicular to the indentation direction. Mügge reports that translation occurs along the (010) direction in directions perpendicular to (100) which is coincident with the indentation direction. Low hardness for the (010) face is therefore concordant with this data. On the (100) face, the (010) cleavage planes and the (100) twin and glide planes are respectively parallel and perpendicular to the indentation direction. Deformation during indentation is presumably restricted to lateral movement along (100) glide planes in directions perpendicular to (010) together with slight movement along the (010) cleavage planes. Such limited movement would be in agreement with the intermediate - high hardness value for the (100) face. The high hardness value for the (100) face is not in accordance with

translation perpendicular to the (001) in the (100) glide planes. It is therefore considered, in the light of the present work, that translation does not occur easily in a direction perpendicular to (001).

Stephanite

No translation data has been reported concerning stephanite, but twinning along (110) planes is known to occur commonly. Stephanite also exhibits imperfect (010) and (021) cleavages, Palache, et.al. (1944).

Microhardness results in Fig. 14 and Table XXIV indicate the following relationship

$$H_{(001)} \gg H_{(110)} \approx H_{(010)}$$

Extensive gliding occurs around impressions made on the (110) and (010) faces, (photos 226, 227). On both faces the glide plane traces are parallel to the c-axis, suggesting that movement during indentation occurred along prismatic planes. No similar glide planes were observed around impressions made on the basal face.

Microhardness values and observed glide plane data indicate that deformation during indentation occurs by translation gliding along (110) planes. On the basal section (001), the prismatic glide planes would be parallel

to the indentation direction. No shearing component would occur along these planes and a high hardness value for the (001) face will result. On the (010) and (110) faces, some of the prismatic twin planes would make angles of 30° with the indentation direction. Considerable shearing component would occur along these planes and this would result in low hardness values.

Stibnite-Bismuthinite

Translation gliding in these minerals has been reported by Mügge (1898) to occur along (010) planes in a direction perpendicular to (001). Stibnite and bismuthinite both exhibit a perfect (010) cleavage, and less perfect (100) and (110) cleavages.

Microhardness values in Fig. 13 and Table XXIV indicate the following hardness relationship for stibnite and bismuthinite:

Stibnite:-

$$H_{(100)} > H_{(010)} \approx H_{(001)}$$

Bismuthinite:

$$H_{(100)} > H_{(001)} > H_{(010)}$$

In general, the microhardness values obtained on the (100), (010) and (001) faces of bismuthinite are equal

or higher than the corresponding values for stibnite. The greatest and least differences of microhardness values occurs for the (001) and (010) faces respectively.

No glide planes were observed around impressions made on any of the faces, but considerable cleavage fracturing occurred around impressions made on the (100) and (010) faces. On the (001) faces only minor (010) cleavage fracturing occurred (photos 25, 26, 231, 232). On the (100) faces considerable fracturing parallel to the (010) cleavage traces was observed, (photos 27, 28, 233, 234). A prominent cleavage fracture pattern, cleavage traces being parallel to the axis, was developed around all impressions made on the (010) faces, (photos 29, 30, 230, 235). The cleavage pattern is probably caused by a basal (001) parting since no known twin or cleavage planes can account for this phenomenon.

The microhardness results and observations of indentation characteristics indicate that gliding during indentation occurs along (010) planes in the directions perpendicular to (001). On the (001) faces the indentation and translation directions are coincident and the resultant easy gliding during indentation gives rise to low hardness values. The absence of prominent (010) cleavage fractures around impressions made on the (001) face is further evidence that the translation direction is perpendicular to (001). On the (100) faces,

the indentation and translation directions are perpendicular to one another. Translation perpendicular to (100) is difficult and high hardness values result. The resultant strong cleavage fracturing around impressions in accordance with the principle expressed by Buerger (1928), i.e. that movement in the glide plane in directions other than the translation direction results in instantaneous cleavage. On the (010) face, the indentation direction is perpendicular to the (010) translation plane. (001) cleavage fractures around impressions indicate that movement has occurred by rupture of the chain structures along preferred parting planes. Lateral movement along the (010) planes consequently becomes easier. The elongation of the indentations in the (001) direction indicates flowage along the (010) planes in directions perpendicular to (001). Hardness values for the (010) faces are therefore considerably lower than those obtained on the (100) faces.

Differences of microhardness between stibnite and bismuthinite may be accounted for by differences in the bonding strengths between atoms. Perfection of cleavage is a function of the strength of the atomic structure of a crystal. It is well known that stibnite possesses a more perfect cleavage than bismuthinite. If the metallic radii of

bismuth and antimony are compared, $Bi = 1.55$, $Sb = 1.45$, Evans (1939)[ⓧ], it can be appreciated that such a difference could well account for the difference of cleavability.

The structure of stibnite-bismuthinite is that of a chain elongated in the direction of the c-axis. An increase in covalent radii, caused by the substitution of Bi atoms for Sb atoms would increase the distance between Bi atoms and S atoms and therefore reduce the strength of the individual chain structures. However, the substitution of Bi atoms for Sb atoms would also decrease the strength of the repulsive forces between adjacent chains and would therefore increase the strength of the weakest bonding in the mineral. Hence deformation on the (001) and (100) faces of bismuthinite is slightly more difficult than on the corresponding faces of stibnite. This results in higher microhardness values for bismuthinite than for stibnite. On the (010) faces deformation is controlled by the ease of rupture of the chain molecules. This results in very similar hardness values for both minerals, stibnite, having the higher chain strength being slightly harder than bismuthinite. The irregular nature of the deformation on the (010) faces is reflected in the large scatter of the plot of load against hardness for the (010)

[ⓧ]No data on the covalent radii of Sb or Bi are available. It is assumed that the covalent radii will have approximately the same difference ratio as the metallic radii.

faces in Fig. 13.

The relationship of microhardness and solubility with orientation will be discussed later in the chapter.

Topaz

No translation data are known for topaz. It exhibits a perfect basal (001) cleavage, Winchell (1951).

The microhardness values in Table XXIII indicate the following relationship

$$H_{(001)} > H_{(100)} > H_{(010)}$$

No glide planes or cleavage fractures were observed around any of the impressions.

The results indicate that deformation during indentation takes place, to a limited extent, along (001) cleavage planes. On the (001) face, the indentation direction is perpendicular to the cleavage and high hardness results. On the (100) and (010) faces, the (001) cleavage is parallel to the indentation direction and some slip along the (001) cleavage planes occurs resulting in slightly lower hardness values. The slight difference in values on the (100) and (010) faces indicate that the direction of easiest slip is perpendicular to (010).

(v) Monoclinic Minerals

The following minerals were included in the present studies:

Arsenopyrite

Gypsum

Hubnerite

Monazite

Orthoclase

Arsenopyrite

No translation data are known concerning arsenopyrite. It exhibits a distinct (101) cleavage and a poor (010) cleavage, Palache, et.al. (1944).

Microhardness results in Table XXIV indicate the following relationship:

$$H_{(010)} > H_{(100)} \approx H_{(101)}$$

No glide planes or cleavage fractures were observed around impressions made on any of the faces tested.

The results indicate that movement during indentation may take place along the (101) cleavage traces. On the (100) face, the (101) cleavages form two sets of planes making angles of about 30° with the indentation direction. Similarly on the (101) face, the (101) cleavage planes form a set of planes

making angles of about 30° with the indentation direction. Thus relatively easy slip occurs along the (101) planes and low hardness values for the (100) and (101) result. On both faces, the (010) cleavage is parallel to the indentation direction. On the (010) face, the (010) and (101) cleavages are respectively perpendicular and parallel to the indentation direction. No shearing component can take place along these planes and high hardness results.

There appears to be no correlation between hardness and reflectivity results.

Gypsum

No translation data are available for gypsum. It exhibits a perfect (010) cleavage and imperfect cleavages parallel to (100) and $(\bar{1}11)$, Winchell (1951).

Microhardness values in Table XXIII indicate the following relationship:

$$H_{(010)} > H_{(001)}$$

The difference of hardness of the two faces is very small.

No glide planes were observed. On the (001) face, (010) cleavage fractures were strongly developed around impressions.

The results indicate that movement during indentation

occurs along (010) cleavage planes. Gypsum has a very weakly bonded chain type structure which gives the mineral its low hardness. This low strength of the basic unit of the structure reduces hardness anisotropy to a minimum. On the (001) and (010) faces, the cleavage planes are respectively parallel and perpendicular to the indentation direction. Whilst on the (010) face, the lattice of the mineral presents a facet of the structure which has to be ruptured before indentation can take place, the (001) face presents a structure where gliding is immediately possible. The difference of orientation results in a slightly higher hardness perpendicular to the cleavage than parallel to it. This is in agreement with the hardness data for other minerals possessing one perfect cleavage, for example, molybdenite and covellite.

Huebnerite

No translation data are known for the mineral.

Huebnerite exhibits a perfect (010) cleavage and partings parallel to (100) and (102).

The microhardness values in Table XXIV and the values in Fig. 65 for various members of the huebnerite-ferberite series indicate the following relationships:

$$H_{(001)} > H_{(010)} > H_{(100)}$$

No glide planes were observed. (010) cleavage fractures occurred around impressions made on the (001) and (100) faces.

The results indicate that movement during indentation takes place along (010) cleavage planes. Easiest translation takes place along the (100) direction. On the (100) and (001) faces, the indentation directions are parallel to the (010) cleavage planes. Higher hardness on the (001) face compared with hardness values obtained on the (100) face indicate the translation direction is (100). Translation perpendicular to this translation direction is difficult, as described in mangantantalite. On the (010) face, the (010) cleavages are perpendicular to the indentation direction. Indentation on the (010) face is inhibited the resistance of the structure to rupture. After rupture has occurred, lateral movement takes place along the (010) planes in a direction perpendicular to (100), resulting in hardness values intermediate between those obtained on the (100) and (001) faces.

There appears to be no correlation between hardness and reflectivity results.

Orthoclase and Monazite

Vickers and Knoop microhardness values shown no

significant variation with orientation. The ranges of values on the faces are more a measure of the irregular nature of the deformation during indentation. Orthoclase exhibits a perfect (001) cleavage and less perfect (010) and (110) cleavages; monazite exhibits partings parallel to (001), (010) and (100). The relative "isotropism of microhardness" of these minerals is probably a reflection of the complex network type structure of these minerals.

(vi) Triclinic Minerals

Kyanite

No translation data are available for kyanite. It exhibits a perfect (100) cleavage, a less perfect (010) cleavage and a basal parting (001).

Large ranges of microhardness for the individual faces, (Table XXIII), due to anisotropism with rotation of the indenter, cause considerable overlap of values.

No glide planes were observed but considerable cleavage fracturing occurred on all the faces.

From the results it may be concluded that the direction of easiest movement is perpendicular to (001). The mineral exhibits two good cleavages, (100) and (010), and as the (100)

cleavage is more perfect than the (010) cleavage, it seems reasonable to expect more movement to occur along the (100) planes. On the (001) face, these two cleavages are oriented parallel to the indentation direction. Translation along these planes in the (001) direction results in low hardness values.

The old greek name for kyanite is "disthene", which literally translated means "two strengths". Kyanite has come to be known, in the mineralogical field, as the classic example of a mineral showing hardness anisotropy.

Winchell (1951) gives the variation of scratch hardness for the (001), (010) and (100) faces as follows: on the (001) face, $H = 5.5$ parallel to the b-axis, and 6.5 parallel to the a-axis; on the (010) face, $H = 6$ parallel to the c-axis, and 7 parallel to the a-axis; on the (100) face, $H = 4-5$ parallel to the c-axis and $6 - 7$ parallel to the b-axis.

Knoop and Vickers values for the (010) face indicate that movement is difficult in the (010) direction. On the (100) face, the indentation direction is parallel to the (010) cleavage, but perpendicular to the (100) cleavage. Little movement can occur on the (100) planes and high hardness for the (100) face results.

E. Variation of Microhardness on Particular Crystal Faces

(a) General

The Knoop indenter was used in preference to the Vickers indenter for detailed studies on particular crystal faces because of its lower symmetry. However, some anisotropy has been observed using the Vickers indenter on those minerals showing strong Knoop microhardness anisotropism. Tables XXI - XXIV and Figs. 25 - 45 illustrate the variation of Vickers and Knoop microhardness on particular crystal faces.

In the following pages the results shown in Tables XXIII, XXIV and Figs. 25 - 45 are described and discussed in relation to the orientation of cleavage and glide plane and directions. No mention of known translation data is given except in cases where the mineral data has not been described in the previous section.

(b) Theory

No theories have been put forward relating the microhardness anisotropy with rotation of the indenter on particular crystal faces. It is therefore convenient at this point to discuss the theoretical microhardness variations that would be caused by differences of orientation of the glide and

cleavage planes and directions, different shapes of indenters, and variations in the direction of indentation.

In most of the minerals discussed later, there is usually one plane of weakness or of easy glide which is more strongly developed than the others. The following theory has been developed for Knoop and Vickers indenters used on minerals showing one preferred plane of weakness.

(i) Minerals with one preferred plane of weakness

(1) Indenter diagonals parallel and perpendicular to the traces of a vertically dipping plane of weakness

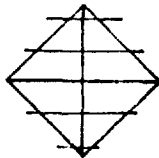
Fig. 24 shows that when the long diagonal of the Knoop indenter is parallel to the cleavage trace, Position A, the number of lines (cleavage traces) per unit area is less than when the long diagonal is at right angles to the cleavage traces, Position B. The "pressure" of the indentation in position A is concentrated on relatively few dislocation planes and deformation occurs easily resulting in low hardness values. In position B, the "pressure" is spread over a considerably greater number of dislocation planes and total deformation is less easy, resulting in higher hardness values. Due to the higher symmetry of the Vickers indenter, the Vickers hardness values will be identical for these positions.

FIG. 24

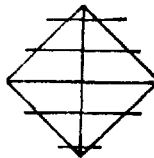
Variation of the No. of M.P.T.P.A.E.I.
with direction of indentation.

VICKERS.

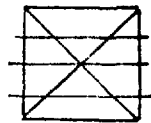
PosⁿA.



PosⁿB.



PosⁿC.



KNOOP.

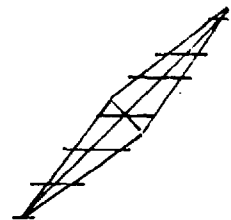
PosⁿA.



PosⁿB.



PosⁿC.



(2) Indenter diagonals at 45° to the traces of vertically dipping planes of weakness

From Fig. 24 it can be seen that for the Vickers indenter, a slightly greater number of planes per unit area are covered when the diagonals are parallel and perpendicular to the planes of weakness than when the indenter is in the 45° position, Position C. A lower hardness is therefore to be expected when the indenter is in the 45° position. For the Knoop indenter, a greater number of movement plane traces per unit area are covered in the 45° position, Position C, than when the long diagonal is parallel to the cleavage traces. This results in a higher hardness when the indenter is in the 45° position relative to the hardness value obtained when the indenter is in Position A.

(3) Indenter diagonals parallel, perpendicular and at 45° to the traces of inclined planes of movement

The same relative hardness values should result as those values given for the positions as described in sections (i) and (ii). Should other planes of potential movement exist then the theoretical hardness values would have to be modified to take into account movement along these planes.

(4) Indenter perpendicular to the plane of easiest glide or greatest weakness

Little or no movement can take place along the plane of greatest weakness and the indenter will tend to pick out differentially the other planes of weakness.

(ii) Minerals showing two preferred planes of weakness

(1) Indenter diagonals parallel and perpendicular and at 45° to two vertically dipping cleavages at right angles to one another.

An example of such an orientation configuration would be the basal section of a tetragonal mineral showing prominent (110) cleavages. The number of cleavage lines per unit area is greater when the diagonals of a Vickers indentation are parallel to the cleavage traces than when the diagonals are at 45° to the diagonal traces. Thus the Vickers microhardness is greater when the diagonals are parallel to the cleavage traces than in the 45° position. With the Knoop indenter, the number of cleavage lines per unit area is slightly greater in the 45° position than when the diagonals and cleavage traces are coincident. Thus the Knoop hardness in the 45° position is greater than when the diagonals are parallel with the cleavage traces.

- (2) Indenter diagonals parallel, perpendicular and at 45° to two inclined cleavages that are at right angles to one another

A similar example of such an orientation would be the front pinacoid face of the tetragonal mineral. The negative hardness results would vary in a similar manner to those discussed in section (a), (i), (ii) and (iii).

- (3) Minerals showing more than two cleavages.

On faces where three or more glide planes intersect the surface of the mineral, the mode of deformation will become so complex that no significant differences of Vickers microhardness will occur. The Knoop indenter will tend to pick out the small microhardness difference, low hardness values being coincident with cleavage traces.

It is realised that the above theory has taken no account of the effect of subsequent elastic recovery after indentation. As elastic recovery is also dependent upon orientation, a few apparently incongruous hardness values may be expected to occur in practice in contradiction to the theory outlined*.

* In the later text, for the sake of brevity the word "No of M.P.T.P.A.E.I." will be substituted for the phrase "Number of movement plane traces per unit area enclosed by an indentation".

(c) Results and Discussion

(i) Isometric Minerals

The following isometric minerals were examined for microhardness anisotropism on different crystallographic faces:

Copper	Perovskite
Cuprite	Pyrochlore
Fluorite	Skutterudite
Galena	Sperrylite
Gold	Sphalerite
Halite	Spinel Group

Cuprite

Fig. 25 shows the relationship between microhardness and orientation of the indenter on the cube face (100) of cuprite. It can be seen that the following relationship is shown by both Vickers and Knoop indenters:

$$H_{(100)} > H_{(100)}$$

No significant differences of microhardness were detected on the octahedral (111) and rhombododecahedral (110) faces.

It has already been noted that dislocations occur around indentations made on the cube face. The traces of the

FIG. 25- CUPRITE

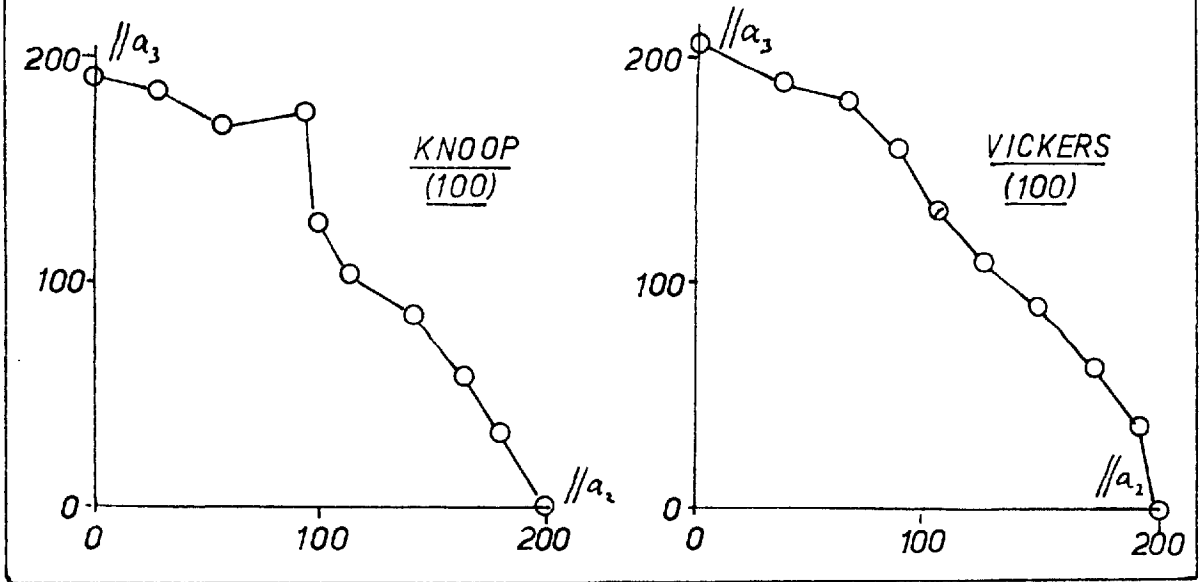


FIG. 26 FLUORITE

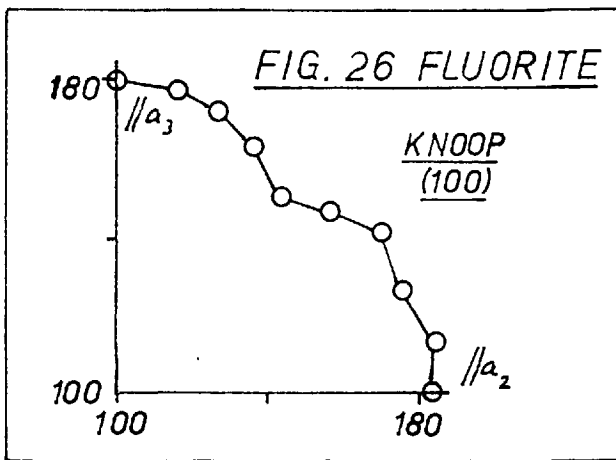
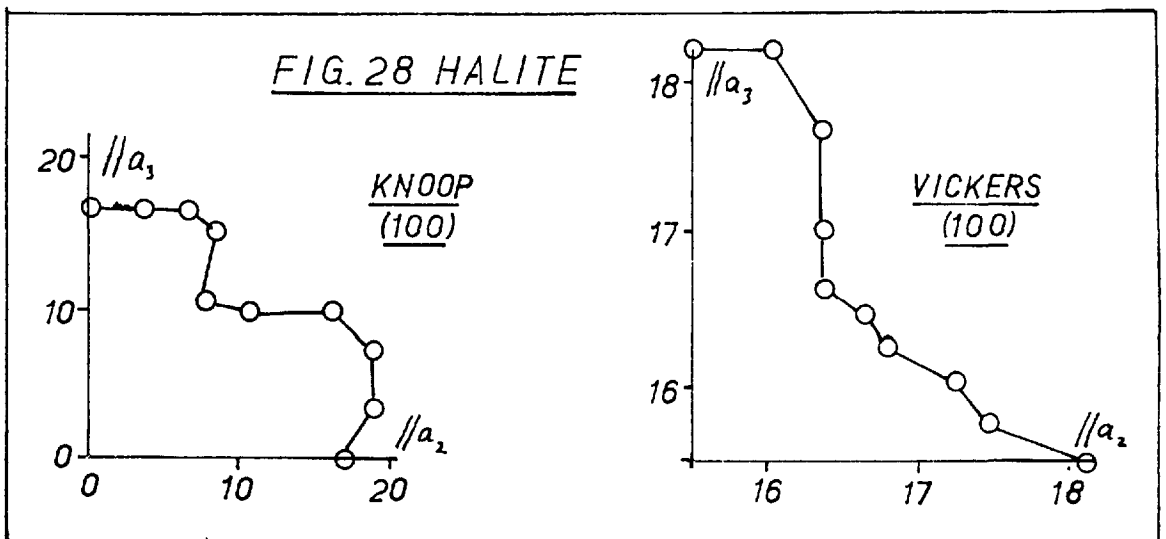


FIG. 28 HALITE



dislocations are parallel to the octahedral cleavage.

If movement is assumed to have occurred along these planes then Knoop results are in agreement with the proposed theory. The Vickers results however are contrary to expectations.

Fluorite

No significant variations of microhardness were found on the octahedral (111) face. On the cube face, Fig. 25, Knoop values indicated the following relationship:

$$H_{(100)} > H_{(110)}$$

These results are in accordance with results obtained on cuprite. As the mineral has an octahedral cleavage it is not unreasonable to expect movement during indentation to occur along these planes. If this assumption is correct, then the results are in agreement with expectations.

Galena

The following results are indicated from the results in Figs. 10, 11:

Cube face (100);

$$HK_{(100)} \neq HK_{(110)} \text{ (dependent upon the load)}$$

$$HV_{(110)} > HV_{(100)}$$

Rhombohedrahedral face (110);

$$HK_{(110)} > HK_{(at\ 45^\circ)} > HK_{(100)}$$

$$HV_{(at\ 45^\circ)} > HV_{(100)}$$

Octahedral face (111);

$$HK_{(11\bar{2})} > HK_{(\bar{1}10)}$$

$$HV_{(\bar{1}10)} \stackrel{H}{=} H_{(at\ 15^\circ\ to\ \bar{1}10)}$$

The following discussion is based on the assumption that galena deforms during indentation along (100) planes in directions perpendicular to (110), as described by Buerger(1923).

On the cube face (100), differences of Knoop microhardness results obtained when the indenter is in the (100) and (110) positions, appear to be dependent upon the load - (Fig. 11). Vickers microhardness results are not in accordance with the proposed theory. The number of cleavage traces (planes of movement) per unit area is greater in the (100) position than in the (110) position. Hence the theoretical hardness relationship should be as follows:

$$HV_{(100)} > HV_{(110)}$$

Such conflicting results are perhaps evidence of movement along other planes and in other directions, during indentation. Buerger (1928) shows that deformation can occur also along (110)

planes. As translation along (001) planes is difficult, the (001) planes are parallel or perpendicular to the indentation direction, it seems highly likely that deformation would occur by movement along (110) planes. If movement along these (110) planes does not occur then the No. of M.P.T.P.A.E.I. in the (110) position is greater than in the (100) position and is concordant with the Vickers microhardness values.

On the rhombdodecahedral face (110), the Vickers and Knoop results are in agreement with the proposed theory. In the (100) position, the No. of M.P.T.P.A.E.I. for both indenters is a minimum resulting in minimum hardness. In the 45° position Knoop and Vickers indentations contain a higher number of movement planes per unit area resulting in higher hardness than the (100) position. Knoop indentations in the (110) position contain a maximum No. of M.P.T.P.A.E.I. and give maximum Knoop microhardness.

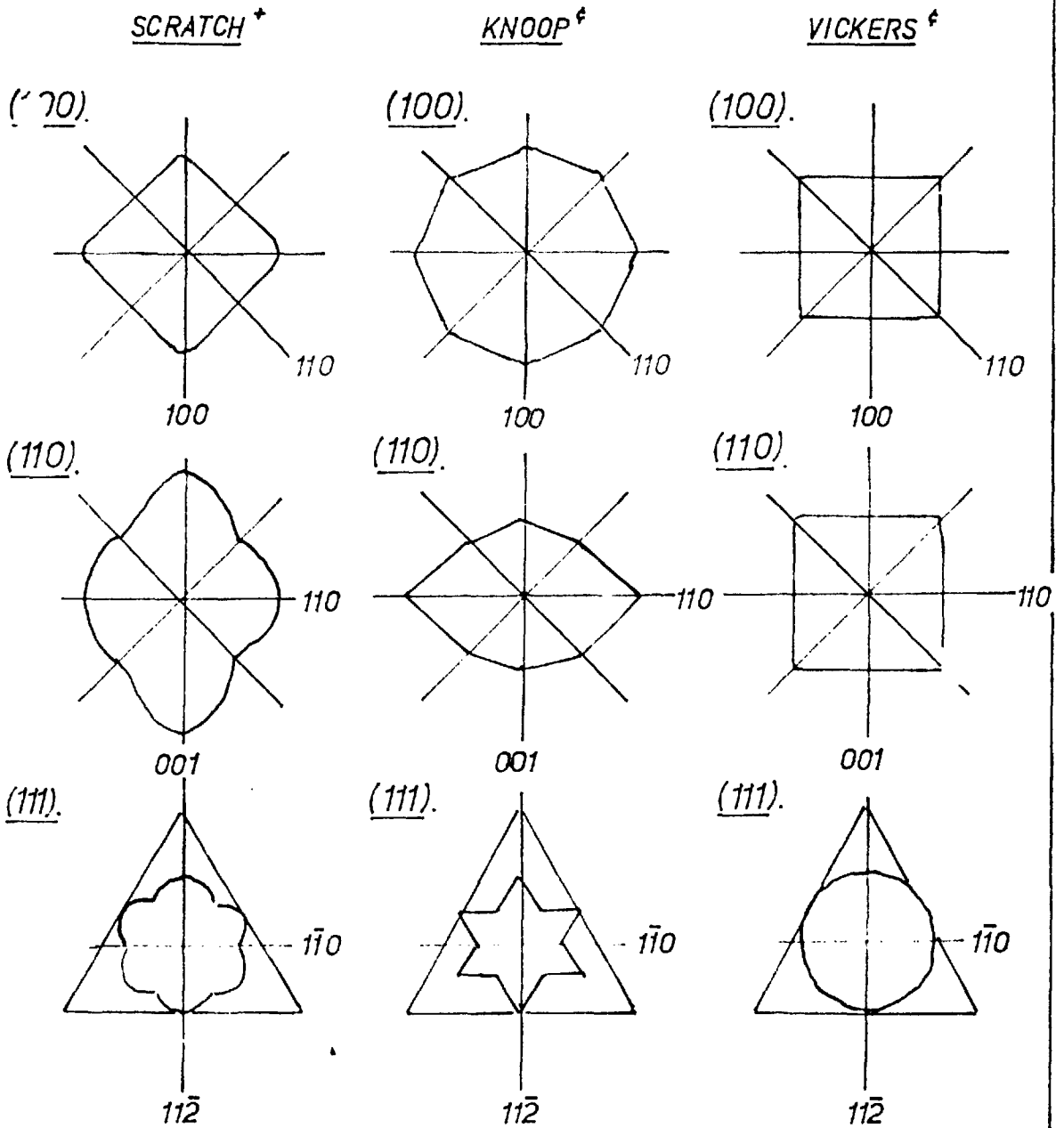
On the octahedral face (111), the Knoop results are in agreement with the proposed theory. In the $(\bar{1}10)$ position indentations contain fewer movement plane traces per unit area than in the $(11\bar{2})$ position resulting in a higher Knoop microhardness in the $(11\bar{2})$ position. Due probably to the higher symmetry of the Vickers indenter, no significant differences of Vickers microhardness were detected. This is in accordance with theoretical expectations, as the

No. of M.P.T.P.A.E.I. for the two positions are approximately the same.

In Fig. 27 the variation of Vickers, Knoop and Scratch microhardness values with orientation are compared, graphically, against one another. Differences between Vickers and Knoop values may be ascribed to the differences in symmetry of the indenters. Thus, on the (111) face, no significant variations in Vickers microhardness were discovered as compared with the six-fold microhardness anisotropy shown by Scratch and Knoop microhardness results. A comparison of indentation and Scratch hardness results shows that the positions of maximum and minimum are dependent upon the method of determination of microhardness. For example, on the rhombododecahedral face (110), the positions of maximum hardness for the Scratch, Vickers and Knoop techniques are respectively (001), at 45° to (001) and (110). The positions of maximum and minimum hardness on the (100 and (110) faces for indentation and scratch techniques are reversed. On the (111) face the positions of hardness maxima and minima for indentation and scratch techniques are coincident, minima positions corresponding to cleavage trace directions. Summarizing, the diagrams in Fig. show how the microhardness anisotropism of galena is dependent upon the individual characteristics of the method

FIG. 27

Microhardness anisotropism of galena
on the (100) (110) and (111) faces.



+ - Boiarskaia (1957).

‡ - Young

of testing.

Halite

Vickers and Knoop microhardness results, in Fig. 28, show the following relationship for the cube (100) face:

$$H_{(100)} > H_{(110)}$$

Halite exhibits a perfect cubic (100) cleavage. Deformation experiments by Buerger (1930), and Tertsch (1930), have shown that movement during deformation takes place along the following planes: (110) planes, in a direction perpendicular to $(1\bar{1}0)$; (001) planes, in a direction perpendicular to (110); and (111) planes.

As the atomic structure of halite is similar to that of galena, and has a similar (001) cleavage, it seems reasonable to expect that translation movement would occur most easily along (001) planes.

The results indicate that deformation takes place mainly along (110) and for (111) planes - in agreement with the work of Buerger and Tertsch. It should be pointed out that little movement is to be expected to take place along (001) planes as these planes are oriented parallel or perpendicular to the indentation directions. The high hardness parallel to (100) therefore implies that little movement takes place along the

45° dipping (110) planes, and consequently that most of the deformation movement occurs along (111) planes.

It is surprising to find this reversal of Knoop microhardness maxima and minima compared with similar results obtained on galena. However, it is of interest to note that Boiarskaia (1957), also found a corresponding reversal of scratch hardness anisotropism between halite and galena. This reversal of microhardness anisotropism indicates a different mode of deformation for halite.

Other isometric minerals tested.

Many other isometric minerals were examined for microhardness anisotropism of particular crystal faces. The following minerals were examined; the spinels, gold, copper, perovskite, skutterudite, sperrylite, pyrochlore and sphalerite. No significant microhardness anisotropy of particular faces was found on any of the above minerals. Considerable orientation work was carried out on sphalerite crystals of differing iron content but no significant variations of Knoop and Vickers microhardness were found with rotation of the indenters on the faces tested, i.e. the (100), (110) and (111) faces. These results are in agreement with those obtained by Henriques who found no significant Vickers microhardness

variations on the (100), (110) and (111) faces with rotation of the indenter.

(ii) Tetragonal Minerals

The following tetragonal minerals were examined for microhardness anisotropism on different crystallographic faces:

Anatase	Pyrolusite
Cassiterite	Rutile
Chalcopyrite	Scheelite
Cylindrite	

Cylindrite

As explained previously, this mineral has been included into the tetragonal group of minerals, because of the tetragonal symmetry that the cylindrite structures show.

The results in Table XXIV indicate the following relationships for the "basal" and "prism" faces:

On the basal face,

$$^{HK}_{\text{diag.} // \text{cleav. traces}} < ^{HK}_{\text{(diag. } \perp \text{ cleav. traces)}}$$

On the "prism" face

$$^{HK}_{\text{(diag. } \perp \text{ cleav. traces)}} > ^{HK}_{\text{diag.} // \text{cleav. traces}}$$

Reflectivity values indicate the reverse relationship for the prism faces. No significant Vickers microhardness variations were found on the "basal" and "prism" faces with rotation of the indenter, due probably to the higher symmetry of the Vickers indenter.

The above relationships are in accordance with the proposed theory on the assumption that movement takes place along the cylindrical partings during indentation. On the basal and prism faces, Knoop indentations whose long diagonals are parallel to the cleavage traces enclose more movement plane traces per unit area than those whose long diagonals are perpendicular to the cleavage.

Pyrolusite^{*}

The results in Table XXIII indicate the following relationship on the (001) and (100) faces:

On the (001) face;

$$HK_{(\text{diag. } \perp \text{ cleav. traces})} > HK_{(\text{diag. } // \text{ cleav. traces})}$$

On the (100) face;

$$HK_{(\text{diag. } \perp \text{ cleav. traces})} > HK_{(\text{diag. } // \text{ cleav. traces})}$$

Thus in both instances the microhardness variations are

^{*}The specimen of pyrolusite examined showed only one prismatic (110) cleavage instead of the normal two.

in accordance with the proposed theory, on the assumption that movement during indentation takes place along (110) cleavage planes. Minimum microhardness occurs when the long diagonals are parallel to the planes of movement and hence enclose a minimum number of movement plane traces per unit area.

No significant Vickers microhardness variations were found on the faces tested due probably to the higher symmetry of the Vickers indenter.

Other tetragonal minerals tested

Several other tetragonal minerals were examined for Vickers and Knoop microhardness anisotropism but no significant variations were found. They include the following; anatase, cassiterite, chalcopyrite, rutile and scheelite.

(iii) Hexagonal Minerals

The following minerals were examined for microhardness anisotropism for particular crystal faces:

Apatite	Molybdenite
Beryl	Pyrrhotite
Cinnabar	Pyromorphite
Corundum	Pyrrhotite
Covellite	Quartz

Descloizite	Tellurium
Eskolaite	Tourmaline
Hematite	Wurtzite

The minerals, for the purposes of discussion are divided into three main groups as follows:

- (1) Minerals exhibiting a basal cleavage or parting,
- (2) Minerals having structural weaknesses in planes other than the basal plane,
- (3) Minerals which exhibit no pronounced structural weaknesses.

(1) Minerals exhibiting a basal cleavage or parting

The following minerals are included in this group; corundum, covellite, eskolaite, hematite, molybdenite, pyrrhotite and wurtzite.

The results in Tables XXIII, XXIV and Figs. 29, 30 for these minerals indicate a much larger anisotropism of microhardness on the prism $(10\bar{1}0)$ faces than on the basal (0001) faces. Several minerals, for example wurtzite (Fig. 29) show practically no anisotropism of microhardness on the basal faces.

Knoop values on the prism faces of wurtzite and pyrrhotite

FIG. 29
WURTZITE

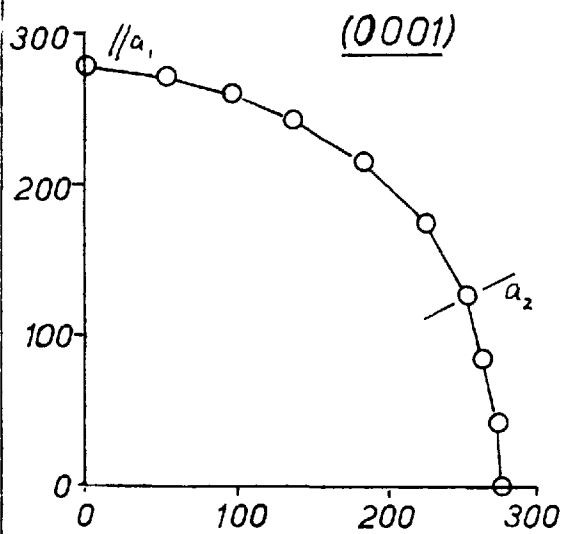
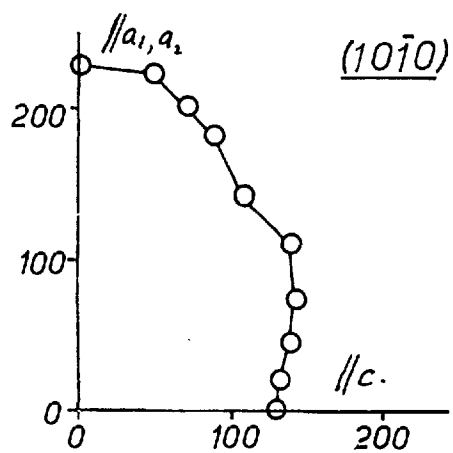
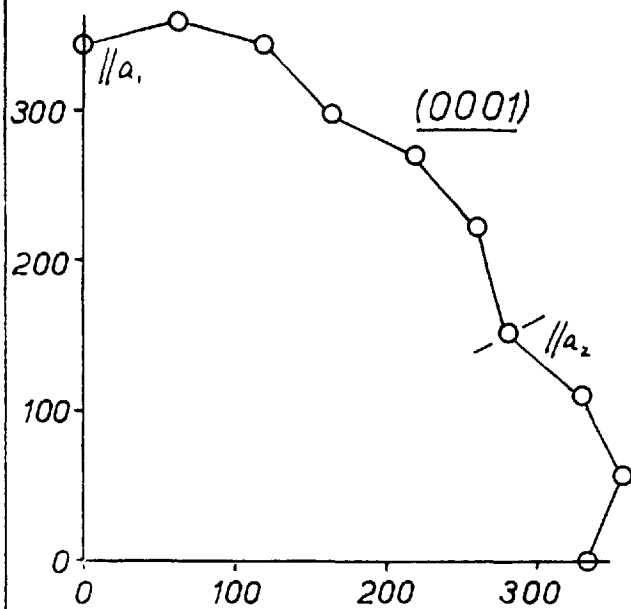
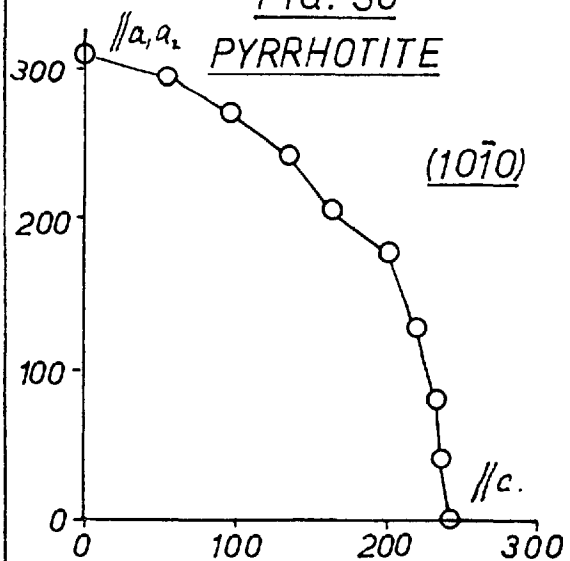


FIG. 30
PYRRHOTITE



show the reverse relationship:

$$HK_{(\text{long diag.} // \text{a-axes})} > HK_{(\text{long diag.} // \text{c-axis})}$$

These relationships indicate that deformation movement occurs more easily along prismatic planes, than along basal planes. Additional studies, the results of which are given in Chapter V, confirm these conclusions.

Knoop values obtained on the prism faces of hematite, molybdenite and covellite indicate the following relationships:

$$HK_{(\text{long diag.} // \text{c-axis})} > HK_{(\text{long diag.} // \text{a-axes})}$$

Corresponding results obtained on eskolaite and corundum were inconsistent and therefore not considered to be significant.

The results are in accordance with the proposed theory, on the assumption that deformation during indentation takes place most easily along the (0001) planes. When the long diagonal of a Knoop indenter is made parallel to the basal cleavage traces on a prismatic (10 $\bar{1}$ 0) face, a small number of movement plane traces per unit area is enclosed by an indentation resulting in low hardness. When the long diagonal is perpendicular to the cleavage traces, a large number of movement plane traces per unit area is enclosed and high hardness results. The percentage Knoop microhardness

anisotropism on the prism faces appears to be related to the strength of the cleavage or parting, (Table XXVII).

On the basal faces, the microhardness variations are small due probably to the "isotropic" nature of the structure. The indentation direction is perpendicular to the planes of movement and thus deformation occurs with equal difficulty whatever the orientation of the indenter. If movement during indentation can occur along secondary movement planes then slight anisotropism is to be expected. Thus pyrrhotite, Fig. 30, shows a twelve fold Knoop microhardness rosette on the basal face, the low values being coincident with the $(11\bar{2}0)$ cleavage traces and $(10\bar{1}2)$ twin plane traces. Such microhardness symmetry is in full agreement with the proposed theory.

Vickers microhardness results for minerals showing pronounced (0001) cleavages or partings i.e. covellite, molybdenite, pyrrhotite and wurtzite show similar but less well marked trends to the Knoop results. Prism sections show a greater range of microhardness than the basal sections. Corundum, eskolaite and hematite, minerals having prismatic and pyramidal glide, twin and cleavage planes in addition to (0001) basal partings, show approximately equal microhardness anisotropism on the basal and prism faces. Such relative equality of anisotropism is mainly due to two factors:-

(a) the complex nature of deformation movements during indentation and

(b) the high symmetry of the Vickers indenter.

The microhardness results in some ways parallel the reflectivity values obtained on the same minerals. For example, the basal sections, which give isotropic reflectivity values, exhibit relatively small microhardness variations. Prism sections show larger microhardness ranges which may be correlated to corresponding anisotropy of reflectivity results. The orientation of minima and maxima of reflectivity and Knoop microhardness values are in most minerals reversed, i.e. maximum reflectivity is coincident with minimum Knoop microhardness.

(2) Minerals having structural weaknesses in planes other than the basal plane

The following minerals are included in this group; cinnabar, pyrargyrite and tellurium.

Cinnabar

Cinnabar exhibits a perfect $(10\bar{1}0)$ cleavage. No translation data are available concerning the mineral.

Fig. 31 illustrates the variation of Knoop microhardness with rotation of the indenter on the $(10\bar{1}1)$ face.

FIG. 31
CINNABAR

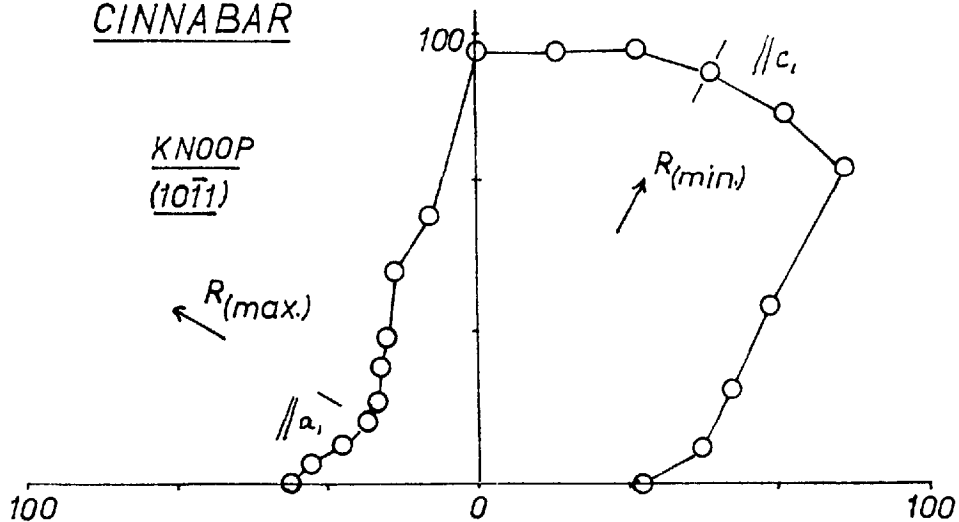


FIG. 32
PYRAGYRITE

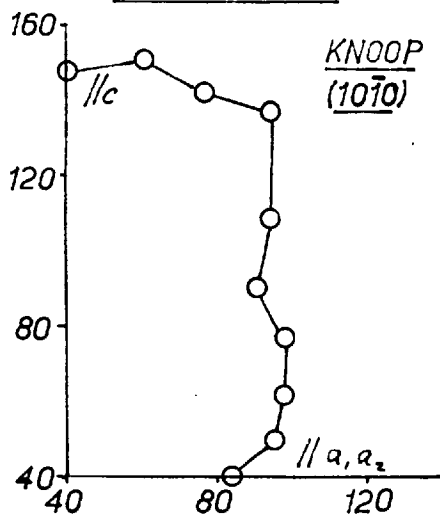


FIG. 33
TELLURIUM

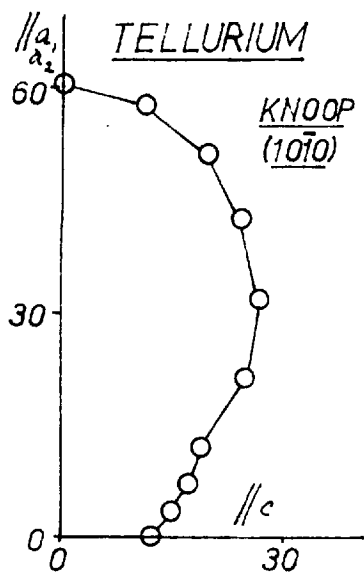


TABLE XXVII

Mineral	Type of cleavage or parting Palache et. al (1944)	% Knoop [^] Micro- hardness Aniso- tropism.
Molybdenite	Very perfect (0001) cleavage	96.5
Covellite	Highly perfect (0001) cleavage	59.0
Wurtzite	Perfect (11 $\bar{2}$ 0) cleavage; poor (0001) cleavage	41.3
Corundum	Parting (0001) sometimes distinct	29.1
Pyrrhotite	Parting (0001); less perfect (11 $\bar{2}$ 0)	22.8
Eskolaite	Weak parting (0001) [‡]	20.7
Hematite	Weak partings (0001) and (10 $\bar{1}$ 1)	20.0

[‡]After Kuovo and Vuorelainen (1958)

[^]The percentage of Knoop microhardness anisotropism is derived by dividing the maximum differences of Knoop microhardness values obtained on the (1010) face by the highest Knoop microhardness values obtained on the prism face.

On the $(10\bar{1}1)$ face the $(10\bar{1}0)$ cleavages form two sets of traces intersecting at a small angle, 40° , the cleavages dipping at about 65° . The third cleavage dips at a shallow angle and the traces bisect the acute angle between the other two cleavage traces.

Minima and maxima of reflectivity values correspond with minima and maxima of Knoop microhardness values and they are oriented at right angles to one another. Minimum Knoop microhardness occurs when the long diagonal of the indenter is parallel to the traces of the steeply dipping cleavages. The results are in accordance with the proposed theory on the assumption that movement during indentation takes place along $(10\bar{1}0)$ cleavages. When the direction of the long diagonal of the indenter bisects the traces of the steeply dipping $(10\bar{1}0)$ cleavages, the number of $(10\bar{1}0)$ plane traces per unit area enclosed by an indentation is a minimum, resulting in low hardness. When the diagonal is perpendicular to this position, a maximum number of $(10\bar{1}0)$ cleavage plane traces per unit area are enclosed by an indentation occurs resulting in maximum hardness. An unusual feature of the "rosette" of microhardness is the "squareness" of the shape of the graph. The large range of high microhardness is probably due to the fact that over this particular range of orientations of the indenter, the number of movement plane

traces per unit area enclosed by indentations, is approximately constant. Furthermore, when the long diagonal of the indenter is parallel to the position of maximum hardness, it is also parallel to the cleavage traces of the shallow dipping $(10\bar{1}0)$ cleavage and thus the maximum hardness is reduced.

No significant variations of Vickers microhardness with rotation of the indenter were observed.

Pyrargyrite

Fig. 32 shows the variation of Knoop microhardness with rotation of the indenter on the $(10\bar{1}0)$ face. The following relationships are indicated

$HK_{(max)}$ - long diag. // c-axis.

$HK_{(min.)}$ - long diag. // a-axes.

Corresponding reflectivity results show a reversal of maxima and minima values. The microhardness results indicate that movement during indentation takes place along $(10\bar{1}4)$ twin planes and/or $(10\bar{1}1)$ and $(01\bar{1}2)$ cleavage planes. When the long diagonal is parallel to the a-axes the number of movement planes, i.e. $(10\bar{1}4)$, $(10\bar{1}1)$ etc., per unit area enclosed by an indentation is a minimum, resulting in minimum microhardness values. When the indenter is at

right angles to this position, a maximum number of movement plane traces are enclosed by an impression and maximum microhardness results. No significant variations of Vickers microhardness were found on the $(10\bar{1}0)$ face.

Tellurium

Tellurium exhibits a perfect $(10\bar{1}0)$ cleavage and an imperfect (0001) cleavage, Palache, et.al. 1944. No translation data are available concerning tellurium.

Fig. 33 shows the variation of Knoop microhardness values with rotation of the indenter on the $(10\bar{1}0)$ faces. The following relationship is indicated;

$HK(\max)$ - long diag // a-axis

$HK(\min)$ - long diag. // c-axis.

These results are in accordance with theoretical expectations based on the assumption that deformation during indentation occurs mainly along $(10\bar{1}0)$ planes. This assumption is substantiated by the presence of $(10\bar{1}0)$ cleavage fractures around the impressions. Thus, when the long diagonal of the indenter is parallel to the c-axis and at the same time, parallel to the traces of the inclined $(10\bar{1}0)$ cleavage planes, a minimum No. of I.P.P.A.E.I. occurs and minimum hardness results. When the indenter is

perpendicular to this position, the number of movement plane traces enclosed is a maximum and maximum hardness results.

No significant variations of Vickers microhardness were detected on the $(10\bar{1}0)$ face.

(3) Minerals which exhibit no pronounced structural weakness

The following minerals are included in this group; apatite, beryl, descloizite, pyromorphite, quartz and tourmaline.

None of the above minerals display prominent cleavages or partings and no translation data are known concerning them. It is therefore not surprising to find that no significant variations of Knoop or Vickers microhardness with rotation of the indenters on particular faces were found. Thus the results are a reflection of the isotropic nature of the physical strength of these minerals.

(iv) Orthorh^{ho}ombic Minerals

The following minerals were examined for microhardness anisotropism on particular crystal faces.

Bismuthinite	Ilvaite
Bournonite	Manganite
Brookite	Mangantentalite

Chalcocite	Marcasite
Chalcostibite	Stephanite
Cubanite	Stibnite
Enargite	Topaz

Bismuthinite-Stibnite

Fig. 34 shows the Knoop and Vickers microhardness variations with rotation of the indenter for the (001), (010) and (100) faces of bismuthinite. In addition oriented Vickers and Knoop microhardness values together with corresponding reflectivity values are given in Table XXIV. Fig. 34 shows the relationship between Knoop microhardness values and reflectivity values obtained on the (001), (010) and (100) faces of stibnite.

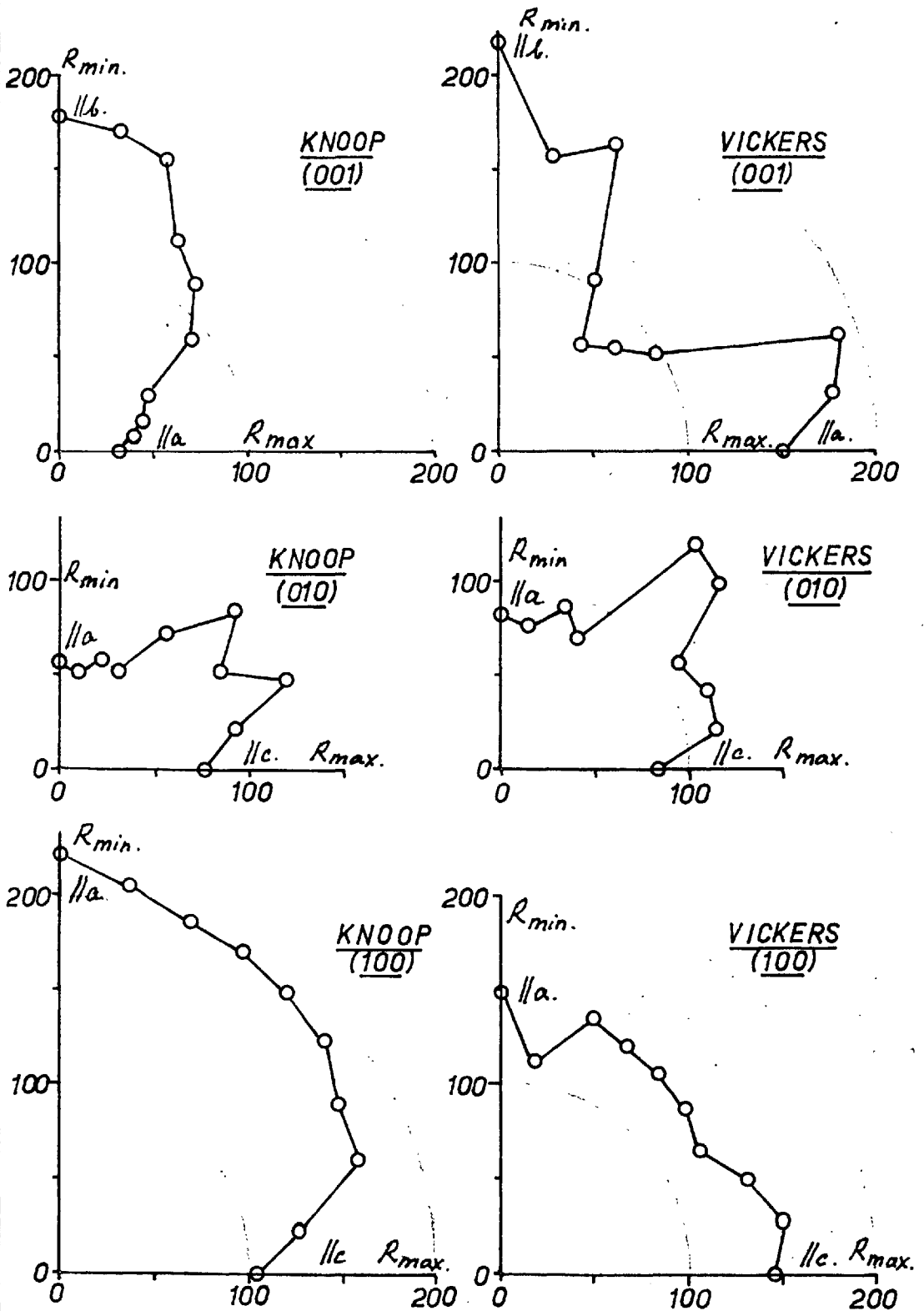
On the (001) faces, the following Knoop microhardness relationships are indicated:

$HK(\text{max.})$ when long diag. // b-axis

$HK(\text{min.})$ when long diag. // a-axis

These relationships indicate that easy movement during indentation takes place along (010) planes in the (001) direction. When the elongation is parallel to the b-axis the No. of M.P.T.P.A.E.I. is a maximum resulting in maximum microhardness. A minimum No. of M.P.T.P.A.E.I.

FIG. 34
BISMUTHINITE



occurs when the elongation is parallel to the a-axis resulting in minimum hardness.

On the (010) faces, Knoop microhardness values for stibnite and bismuthinite are in poor agreement. For both minerals, maximum Knoop microhardness occurs in the 45° position. In the orientations where the elongation of the indenter is parallel to the c and a axes, the results are in juxtaposition. This disparity of results may be explained as follows: Movement during indentation of the (010) face is initiated by rupture of the chain structures along (001) and (100)(?) partings and followed by lateral gliding along (010) planes in directions perpendicular to (001). As the (001) parting is more strongly developed in bismuthinite than in stibnite, a lower Knoop microhardness for the (010) section of bismuthinite is to be expected in the "a" axes direction. Some inherent weakness occurs parallel to the c-axis, either in (100) or (110) planes as cleavage fracture were observed around impressions whose traces parallel to c-axis. Thus, lower hardnesses parallel to the c and a axes, and maximum hardness values in the 45° position, are in accordance with the proposed theory assuming that movement takes place along (001) and (100)(?) partings. If movement were to take place along only one set of planes then the position of maximum microhardness

would not be at 45° to the axes.

On the (100) face, the following Knoop microhardness relationships are indicated;

HK(max.) when long diag. // b-axis

HK(min) when long diag. // c-axis.

The results are in accordance with theoretical expectations based on the assumption that movement occurs along the (010) planes. The No. of H.P.T.P.A.E.I. is a minimum when the elongation is parallel to the c-axis and a maximum at right angles to this position.

On the (001) and (100) faces, reflectivity maxima and minima are in reverse positions to the Knoop microhardness maxima and minima. On the (010) faces, the positions of maximum and minimum Knoop microhardness are not coincident with the positions of maxima and minima of reflectivity.

Vickers microhardness results show no significant variations on the (100) face. On the (001) and (010) faces, the following relationships are indicated;

On the (001) face,

H.V. (max.) - diags. // axes.

H.V. (min.) - diags. at 45° to axes.

On the (010) face,

H.V. (max.) - diags. at 45° to axes.

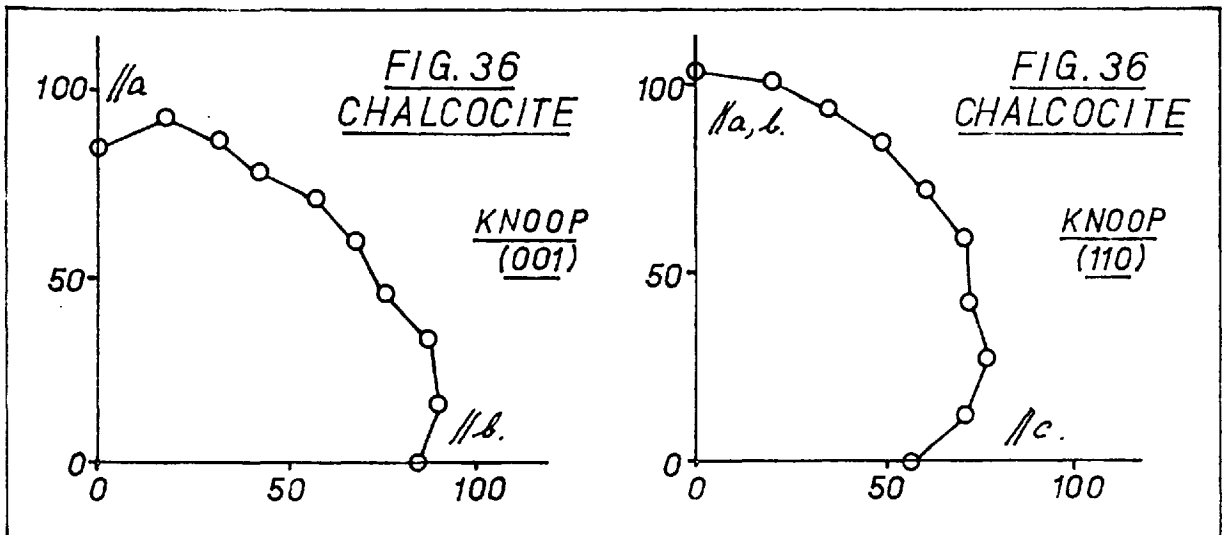
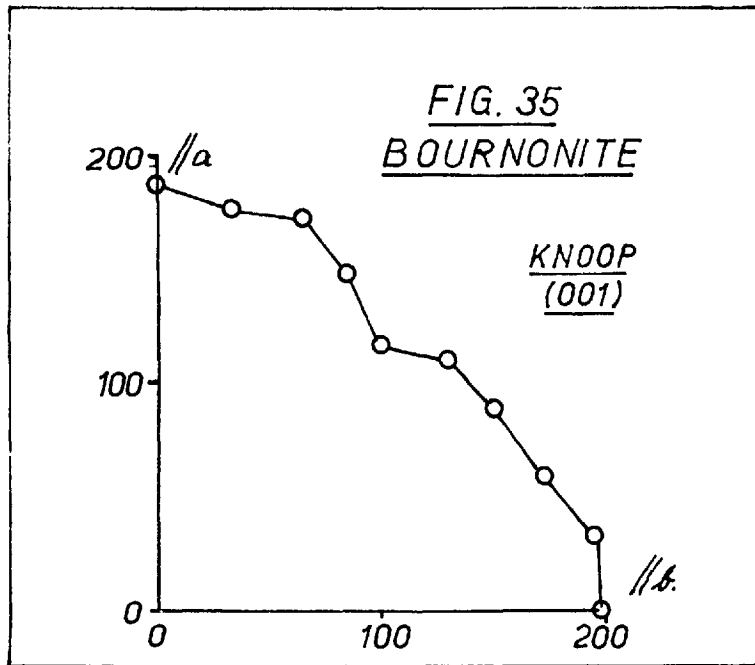
H.V. (min.) - diags. // axes.

The results on the (001) face are in accordance with theoretical expectations but the results on the (010) face are contrary to expectations. A greater No. of M.P.T.P.A. occurs when the diagonals are parallel to the axes than in the 45° position. Thus the relationship derived from the proposed theory is directly opposed to the actual result. No explanation for this contradiction can be given.

Bournonite

No significant variations of Knoop microhardness were found on the (100) and (010) faces.

Fig. 35 shows the slight variations of Knoop microhardness on the (001) face. Minimum microhardness occurs in the 45° position which is coincident with the traces of the (110) twin glide planes. A maximum microhardness occurs when the elongation of the indenter is parallel to the a and b axes. Thus, on the assumption that movement during indentation occurs along (110) twin glide planes, the results, are concordant with theoretical expectations i.e. the No. of M.P.T.P.A.E.I. is a minimum in the 45° position and a maximum parallel to the crystallographic axes.



Chalcocite

Fig. 36 shows the variations of Knoop microhardness on the (110) and (001) faces.

The variations of Knoop microhardness on the (001) face are small and within the probable error of the measurements. On the (110) face, however, the results indicate the following relationship;

$$HK_{(\text{long. diag.} // \text{a-axis})} < HK_{(\text{long diag.} // \text{a-axes})}$$

This relationship confirms the conclusion made earlier in this chapter i.e. that chalcocite deforms during indentation by movement along (110) planes. The lack of microhardness anisotropism of the basal face suggests that the movement direction is not perpendicular to (001). A more logical movement direction would be perpendicular to (1 $\bar{1}$ 0)

Cubanite

No precise orientations could be obtained on cubanite but Knoop microhardness values indicate the following relationship;

$HK_{(\text{max.})}$ - when long diag. // length of laths.

$HK_{(\text{min.})}$ - when long diag. \perp length of laths.

The mineral twins along (110) planes and shows partings parallel to (110) and (1 $\bar{3}$ 0) planes. Cubanite deforms along

(001) planes, (Ramdohr, 1951), and when associated with chalcopyrite, the intergrowth is usually oriented such that the (001) of cubanite lies parallel to the (111) of chalcopyrite, Buerger (1934). If deformation during indentation occurs along (001) planes, then, according to theoretical expectations, the following relationship should be found:

$$\text{HK} (\underline{1} \text{ to } (001)) > \text{HK} (// \text{ to } (001))$$

The actual results are therefore contrary to expectations based on the assumption of gliding along (001) planes. Fracture patterns around indentations (photo 82) indicate planes of movement perpendicular to the elongation of the laths. If the intergrowth orientation relationship is correct, i.e. (001) of cubanite // (111) of chalcopyrite, then the present results indicate that deformation during indentation takes place along (110) and/or (1 $\bar{3}$ 0) cleavages and/or (110) twin planes.

Enargite

Fig. 37 shows the variation of Knoop microhardness values with rotation of the indenter on the (001), (010) and (100) faces.

On the basal face, minimum microhardness occurs when the long diagonal is parallel to the (110) cleavage traces.

FIG. 37 ENARGITE

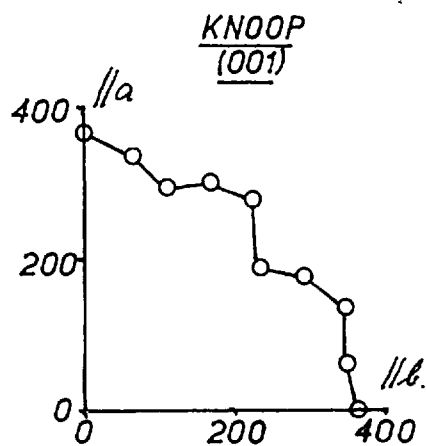
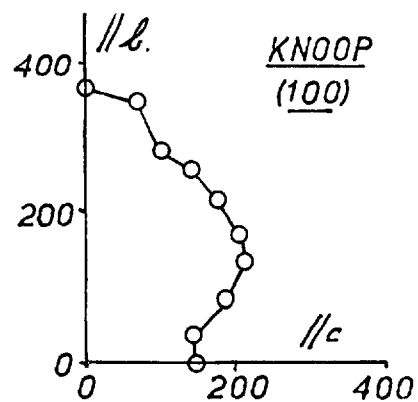
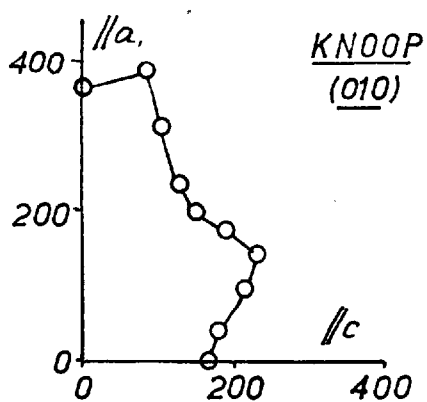
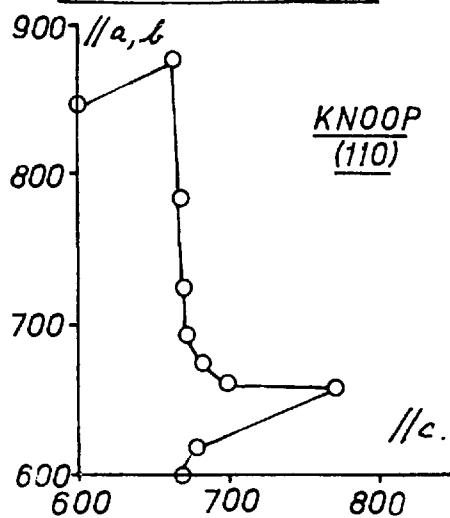


FIG. 38 ILVAITE



Microhardness maxima occur in two positions at angles of about 15° - 20° to the minima position and intermediate values occur when the elongation is parallel to the (100) and (010) cleavage traces. The above relationships are in accordance with theoretical expectations. Maximum hardness occurs where the No. of M.P.T.P.A.E.I. is a maximum and minimum hardness along the (110) cleavage trace direction where the No. of M.P.T.P.A.E.I. is a minimum. Intermediate values occur when the elongation is parallel to the a and b axes because movement is presumably more difficult along the less perfect (100) and (010) cleavages.

On the (010) and (100) faces, minimum microhardness occurs when the indenter elongation is parallel to the (110), (100) and (010) cleavage traces where No. of M.P.T.P.A.E.I. is a minimum. Maximum microhardness occurs when the indenter elongation is parallel to the a and b axes and No. of M.P.T.P.A.E.I. is a minimum.

Reflectivity maxima and minima for the (010) and (100) faces are in reciprocal positions to maxima and minima of Knoop microhardness.

Ilvaite

Ilvaite exhibits two distinct cleavages parallel to (010) and (001). No translation data are available

concerning the mineral.

On the (001) face, no significant variations of Knoop microhardness were found. On the prism face (110), Fig.38, the following relationship is indicated:

HK(max.) - long diag. \perp c-axis

HK(min.) - long diag. \parallel c-axis.

The results indicate that movement occurs more easily along (010) cleavage than along (001) cleavages. Reflectivity maxima and minima are in reciprocal positions to Knoop microhardness maxima and minima.

Manganite

Fig. 39 shows the variation of Knoop microhardness with rotation of the indenter on the (001), (010) and (100) faces.

The following relationships are indicated;

On the basal face,

HK(max.) - when long diag. \parallel b-axis.

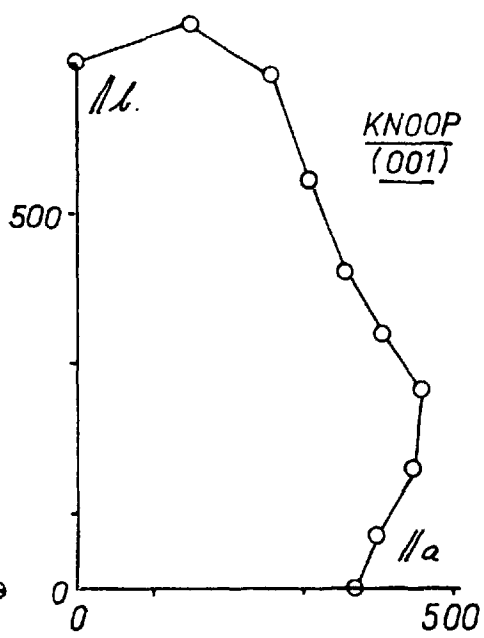
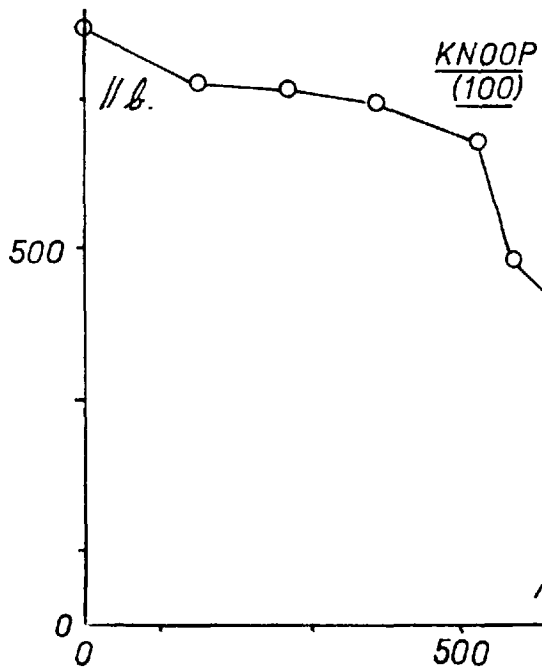
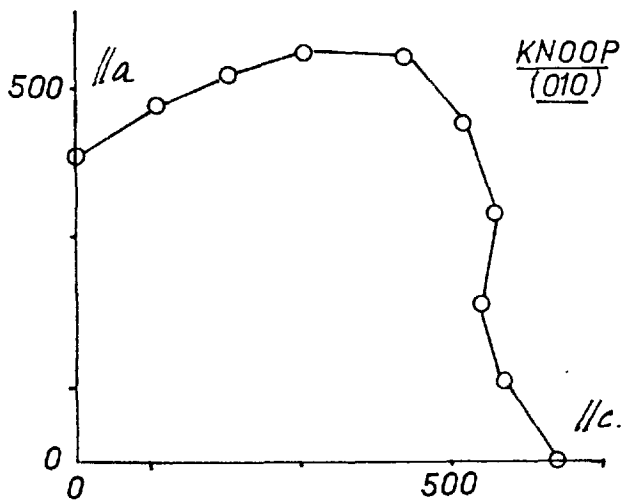
HK(min.) - when long diag. aprox. \parallel c-axis.

On the (010) face,

HK(max.) - when long diag. at 45° to a and c-axes.

HK(min.) - when long diag. \parallel a-axis.

FIG. 39 MANGANITE



On the (100) face,

HK(max.) - long diag. at 45° to b and c-axes.

HK(min.) - long diag. // c-axis.

The above relationship indicates that easy movement occurs along (010) planes in the (001) direction. On the basal face, the No. of M.P.T.P.A.E.I. is a maximum parallel to the b-axis, and a minimum parallel to the c-axis. On the (010) face, it would appear that movement occurs more easily along (001) cleavages than along (110) cleavages. The No. of M.P.T.P.A.E.I. is a maximum at 45° to the a and c-axes assuming that movement takes place along both (001) and (110) planes. On the (100) face, No. of M.P.T.P.A.E.I. is a minimum parallel to the c-axis and a maximum in the 45° position, assuming that movement takes place along (010) and (001) planes.

The results show how movement along (010) planes in the (100) direction is difficult but how along the known translation direction, perpendicular to (001), the movement is easy. In many ways the characteristics of the anisotropism of manganite are similar to those of stibnite-bismuthinite.

Reflectivity maxima and minima on the (001) face are in reciprocal positions to Knoop microhardness maxima and minima. On the (010) and (100) faces, the positions of maxima and minima of reflectivity and Knoop microhardness are not coincident.

Mangantantalite

Fig. 40 shows the variation of Knoop microhardness with rotation of the indenter on the (001), (010) and (100) faces. The following relationships are indicated;

On the (001) face,

HK(max.) when long diag. // b-axis

HK(min.) when long diag. // a-axis

On the (010) face,

HK(max.) when long diag. // a-axis

HK(min.) when long diag. // c-axis

On the (100) face,

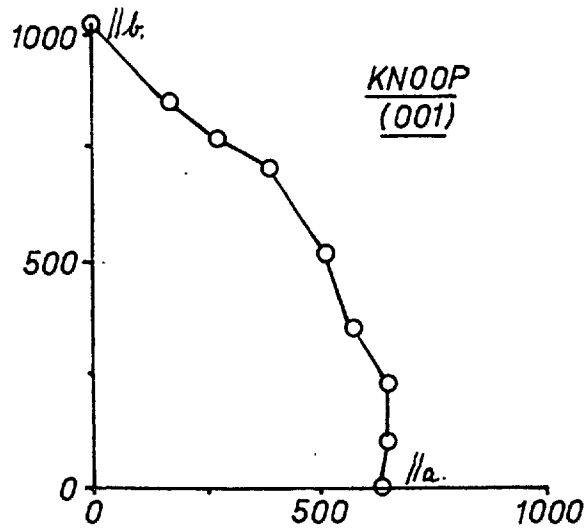
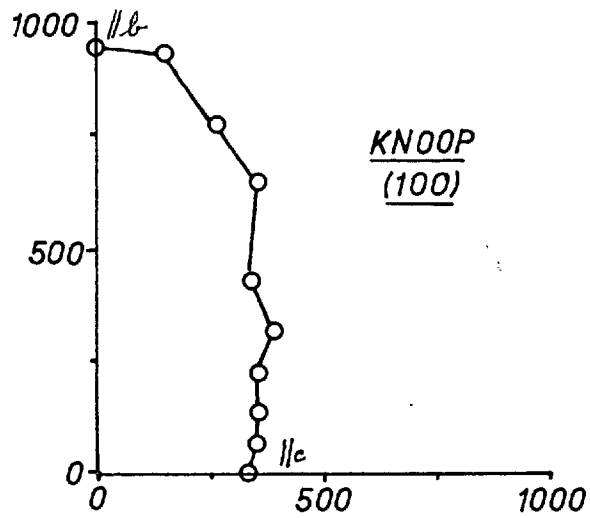
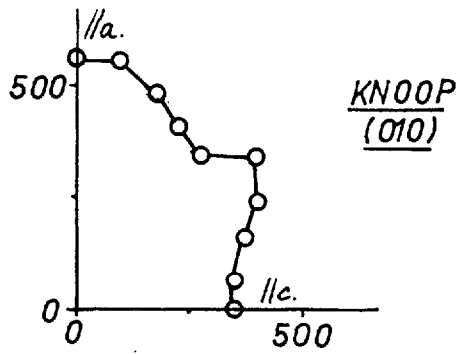
HK(max.) when long diag. // b-axis

HK(min.) when long diag. // c-axis.

On the assumption that the proposed theory is correct, the results conflict with existing translation data. Mügge (1920) reported that translation occurs along (100) planes in directions perpendicular to (001) and (010). The results indicate that movement along (100) planes is difficult in the (001) direction but easy in the (010) direction. Furthermore, easy movement along (010) cleavage planes in both the (001) and (100) directions is indicated by the results.

Reflectivity maxima and minima are coincident with Knoop microhardness maxima and minima for the (001) face but are reversed for the (100) face.

FIG.40
MANGANTANTALITE



Stephanite

Knoop microhardness variations on the (010) and (001) faces are inconsistent. Fig. 41 shows the variation of Knoop microhardness values with rotation of the indenter on the (110) face. The following relationships are indicated;

HK(max.) when long diag. // a and b-axes.

HK(min.) when long diag. // c-axis.

The results indicate that movement during indentation takes place along (110) twin planes i.e. the No. of M.P.T.P.A. E.I. is a minimum parallel to the c-axis and a maximum parallel to the a and b-axes.

Topaz

No significant variations of Knoop microhardness were found on the (001) and (010) faces of topaz.

Fig. 42 shows the variation of Knoop microhardness found on the (100) face. The following relationships are indicated;

HK(max.) when long diag. at 45° to the c and b-axes.

HK(min.) when long diag. // b-axis.

These results indicate that the easiest direction of movement in topaz is along (100) planes in a direction perpendicular to (001).

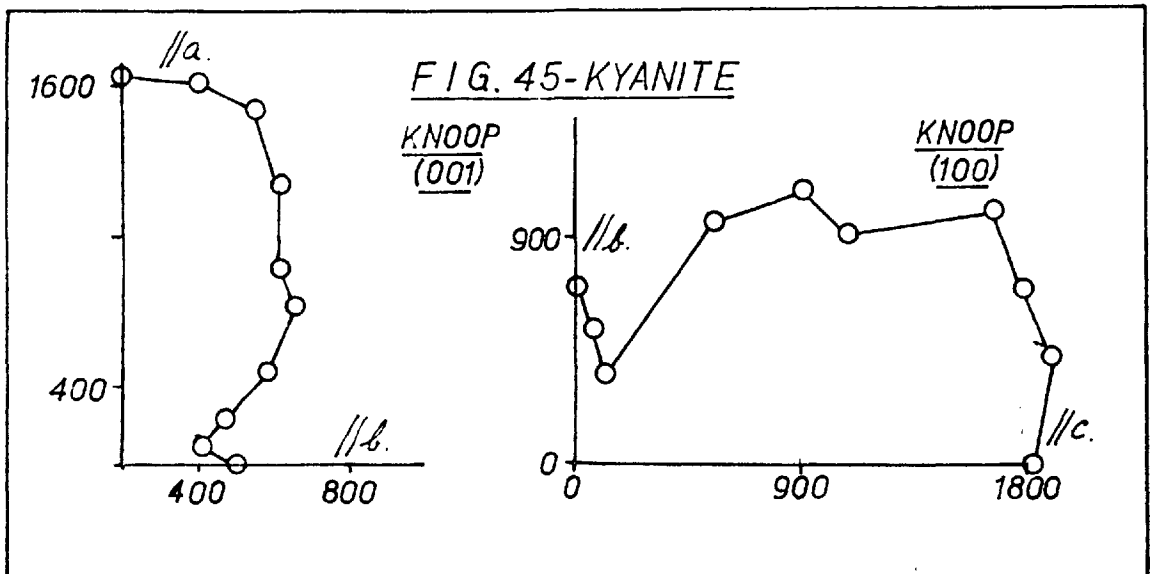
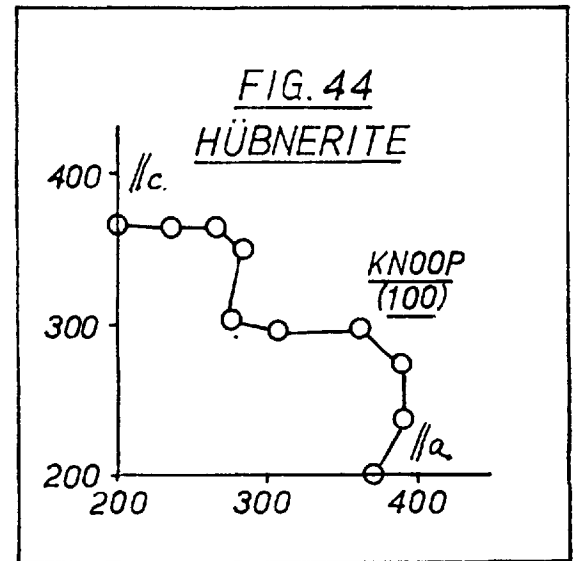
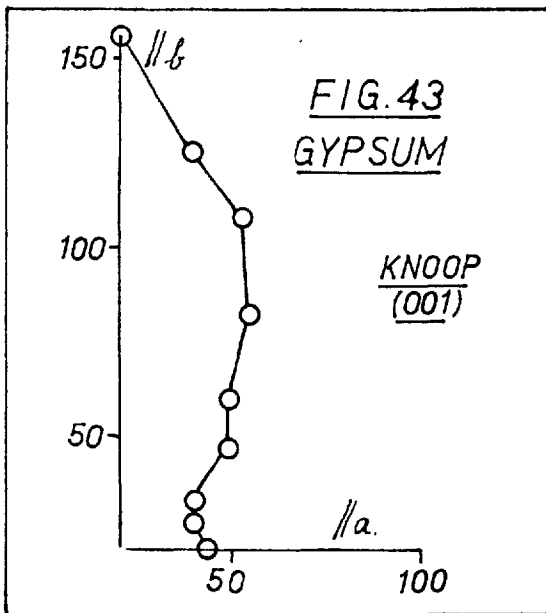
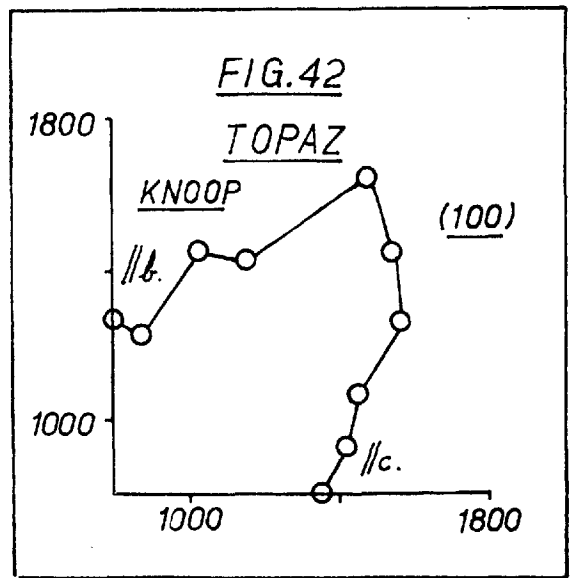
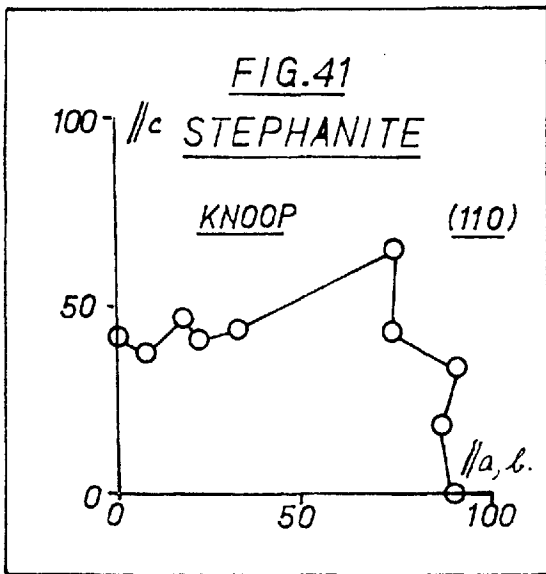


TABLE XXVIII

Comparison of Knoop microhardness maxima and minima with reflectivity maxima and minima

HEXAGONAL

Mineral	Orientation	Reflectivity value	K.M.H. Value
Covellite	(10 $\bar{1}$ 0)		
	//c	Min.	Max.
	//a	Max.	Min.
Hematite	(10 $\bar{1}$ 0)		
	//c	Min.	Max.
	//a	Max.	Min.
Molybdenite	(10 $\bar{1}$ 0)		
	//c	Min.	Max.
	//a	Max.	Min.
Pyrargyrite	(10 $\bar{1}$ 0)		
	//c	Min.	Max.
	//a	Max.	Min.
Pyrrhotite	(10 $\bar{1}$ 0)		
	//c	Max.	Min.
	//a	Min.	Max.
Wurtzite	(10 $\bar{1}$ 0)		
	//c	Max.	Min.
	//a	Min.	Max.

TABLE XXIX

Comparison of Knoop microhardness and reflectivity Maxima and Minima

TETRAGONAL AND MONOCLINIC

Mineral	Orientation	Reflectivity values	K.M.H. Values
Cylindrite	// length	Max.	M
	diag. // length	Min.	Min.
Arsenopyrite	diag. <u>l</u> length	Max.	Max.
	(010)	Max.	Min
	// a	Min.	Max.
	// c		
Huebnerite	(100)	Max.	Min.
	// b	Min.	Max.
	// c		
	(001)	Min.	Intermediate
	// a	Max.	Intermediate
	// b	Min.	Intermediate
	// c	Max.	Intermediate

TABLE XXX

Comparison of Knoop microhardness and reflectivity maxima and minima

Mineral	REFLECTIVITY VALUES						KNOOP MICROHARDNESS VALUES					
	(001)		(010)		(100)		(001)		(010)		(100)	
	//b	//a	//c	//a	//c	//b	//b	//a	//c	//a	//c	//b
Bismuthinite	N	X	X	N	X	N	X	N	X	N	N	X
Bournonite	-	-	X	N	-	-	-	-	X	N	-	-
Enargite	N	X	X	N	X	N	=	=	N	X	N	X
Ilvaite	-	-	-	-	X	N	-	-	-	-	X	N
Manganite	N	X	X	N	X	N	X	N	X	N	N	X
Mangantantalite	X	N	-	-	X	N	X	N	N	X	N	X
Marcasite	X	N	X	N	N	X	-	-	-	-	X	N
Stibnite	N	X	X	N	X	N	X	N	N	X	N	X
Chalcocite [⊠]	-	-	X	N	-	-	-	-	N	X	-	-

Key

X = Maximum
 N = Minima
 - = No values
 = = Values equal

⊠(110) face of chalcocite was tested.

Other Orthorhombic minerals

Detailed orientation studies were carried out on several other orthorhombic minerals but no significant anisotropism was detected. These minerals include the following; brookite, chalcostibite and marcasite.

(v) Monoclinic Minerals

The following monoclinic minerals were examined for anisotropism of Knoop microhardness on particular faces,

Arsenopyrite

Gypsum

Huebnerite

Arsenopyrite

The results in Table XXIV show the variation of Knoop microhardness on the (010), (100) and (101) faces with rotation of the indenter.

No translation data are available concerning arsenopyrite. Knoop microhardness values indicate that movement during indentation takes place along the (101) and (010) cleavage. For the (010) face, the No. of M.P.T.P.A.E.I. is a maximum parallel to the c-axis and a minimum parallel to the a-axis. On the (100) and (101) faces the No. of M.P.T.P.A.E.I. is a maximum parallel to the c-axis and a minimum parallel to the

c-axis and a minimum parallel to the b-axis and the (101) cleavage traces.

Reflectivity maxima and minima are in reciprocal positions to Knoop microhardness maxima and minima for the (010) and (100) faces.

Gypsum

No significant Knoop microhardness variations were found on the (010) face.

Fig. 43 shows the variation of Knoop microhardness with rotation of the indenter on the (001) face. Microhardness is a maximum when the elongation is perpendicular to the cleavage traces and a minimum when the elongation is parallel to the cleavage traces. Thus the plane of easiest slip in gypsum appears to be (010).

Huebnerite

No significant Knoop microhardness variations were found on the (010) and (100) faces. Fig. 44 shows the variation of Knoop microhardness with rotation of the indenter on the (001) face.

The following relationships are indicated;

HK(max.) when the long diag. at 45° to a and b-axes.

HK(min.) when long diag. // a-axis.

The results indicate that movement takes place most easily along (010) planes. For maximum hardness to occur in the 45° position, the No. of M.P.T.P.A.E.I. must also be a maximum in this position. This is only possible if movement during indentation occurs along (010) and (100) planes.

(vi) Triclinic Minerals

The following triclinic minerals were examined for microhardness anisotropy on particular crystal faces;

Axinite

Kyanite

Sphene

No significant variations were found on axinite or sphene.

Kyanite

No significant microhardness variations were found on the (010) face. Fig. 45 shows the Knoop microhardness variations with rotation of the indenter on the (001) and (100) faces.

On the (001) face, maximum and minimum Knoop microhardness are coincident with the traces of the (010) and (100) cleavages respectively. Minimum microhardness is parallel to the b-axis as the (100) cleavage is more perfect than the

(010) cleavage.

On the (100) face i.e. parallel to the best cleavage, maximum microhardness occurs parallel to the (010) cleavage and minimum microhardness at about 20° to the b-axis or (001) parting traces.

Although it appears possible to explain the variations on the (001) face by correlating the orientation of the indenter to the direction and strength of the cleavages, it is not possible to explain the variation on the (100) face in a similar manner. Also no explanation can be given for the apparent "isotropism" of microhardness on the (010) face.

It is interesting to note that scratch and Knoop microhardness maxima and minima, on the (001) and (100) faces, are at right angles to one another. This "reverse" relationship is comparable with the one found between scratch microhardness values and Knoop microhardness values found on oriented sections of galena.

F. The Variation of Knoop Microhardness with Reflectivity on Particular Crystal Faces

During the detailed microhardness/orientation investigations on particular crystal faces it was noticed that in many cases Knoop microhardness maxima and minima directions were in reciprocal positions to reflectivity maxima and minima[‡]. Tables XXVIII, XXIX and XXX give comparisons of Knoop microhardness and reflectivity maxima and minima for particular crystal faces of minerals ranging in crystallography from tetragonal to monoclinic.

Tables XXVIII - XXX show that of the 29 crystal faces analysed in this manner, 21 showed reversal of microhardness and reflectivity maxima and minima, 5 showed concordant maxima and minima, and 3 showed indefinite relationships. Thus over 70% of the faces examined were found to exhibit this reverse microhardness/reflectivity relationship. An explanation of this relationship is given as follows.

Gray (1961), shows that tightness of packing of the atoms in a mineral controls its reflectivity value; a high reflectivity results from a "loosely bonded" structure, e.g. a metallic type of bonding; low reflectivity results from strong bonding e.g. covalent bonding. It is shown in Chapter VII

[‡]All the reflectivity values quoted are for white light, (tungsten filament at critical temperature of 3050°K). The photoelectric cell used was a Mullard O.R.P. 11 cadmium sulphide photo conductive cell. For all measurements, the axis of the polarizer was maintained east-west.

how the strength of the structure of a mineral is related to its microhardness; in a loose "metallic" type of bonding, low hardness results whilst a covalently bonded mineral has a high hardness. By analogy, the reverse microhardness/reflectivity relationships, on particular faces, may be considered in the same light. Both maximum reflectivity and minimum microhardness are compatible with a structural weakness or plane of loose bonding of the atomic configuration. Conversely, the position of minimum reflectivity and maximum microhardness would be coincident with a direction or zone of the atomic structure having great strength.

The exceptions to the rule indicate that this explanation is over simplified. In some cases microhardness and reflectivity values are probably influenced by other features in addition to the strength of the structure of the mineral.

G. Variation of the Diagonal Lengths of Vickers Indentations on Rotation of the Indenter on Particular Crystal Faces.

For impressions made using a Vickers indenter, the microhardness is calculated from the mean value of the two diagonal lengths. In many cases, where a mineral has strong physical anisotropism, the measured anisotropism of microhardness is considerably diminished by averaging the lengths of the two diagonals. For example, on rotation of the indenter on a crystal face of such an anisotropic mineral, one diagonal may increase in length as the other correspondingly decreases. The resultant microhardness values may remain constant. In some minerals, for example galena, the anisotropism may be so great that variations in Vickers microhardness are still apparent.

The manner in which the diagonal lengths vary with rotation has been investigated for some of the more anisotropic minerals. Results are shown in Figs. 46-53 and Table XXXI and the variations are discussed below. For convenience, the minerals studied have been divided into two groups;

- (a) Minerals whose crystals have been accurately oriented
- (b) Minerals whose orientations are not precisely known.

(a) Minerals whose crystals have been accurately oriented

The following minerals were studied;

Galena

Pyrrhotite

Wurtzite

Chalcocite

Enargite

Manganite

Stibnite-Bismuthinite

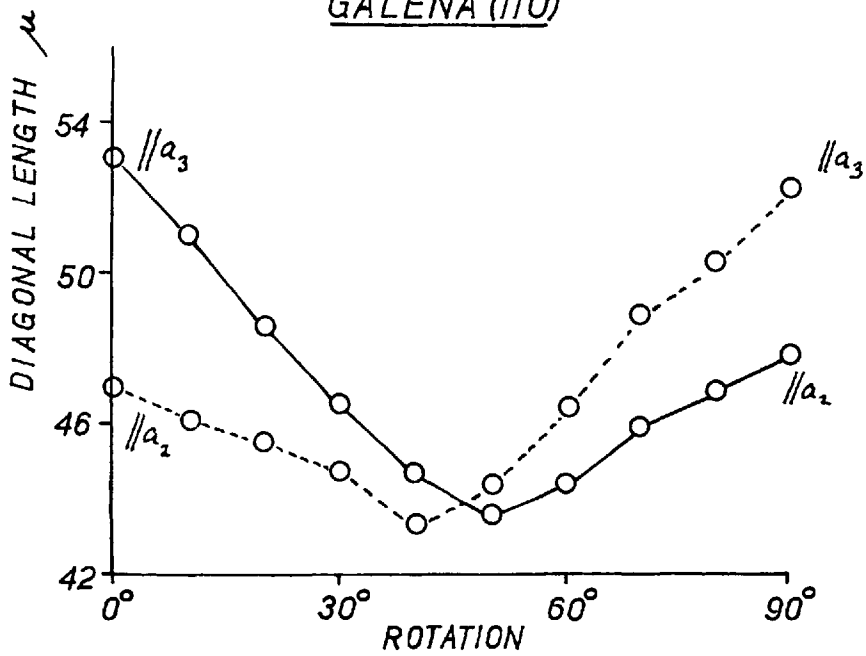
Galena

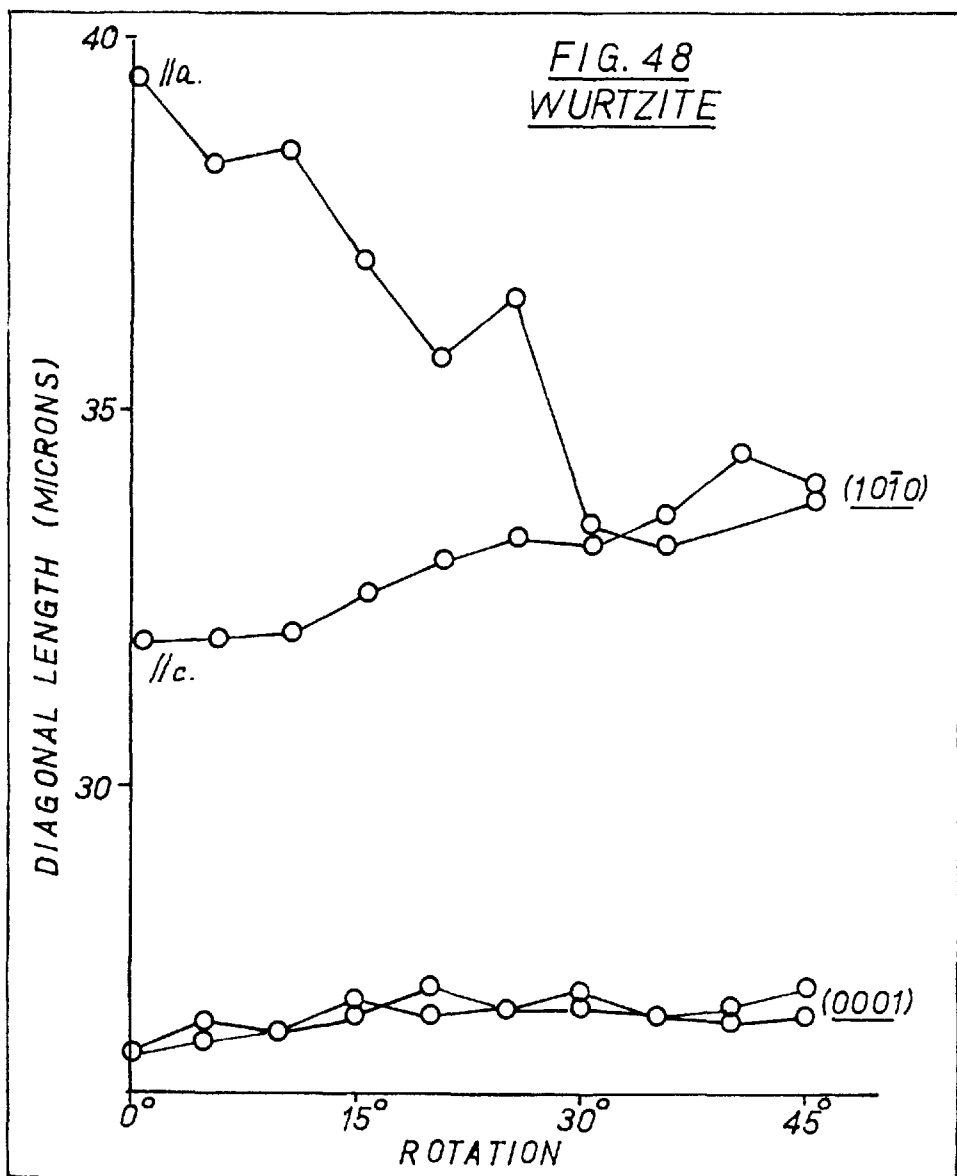
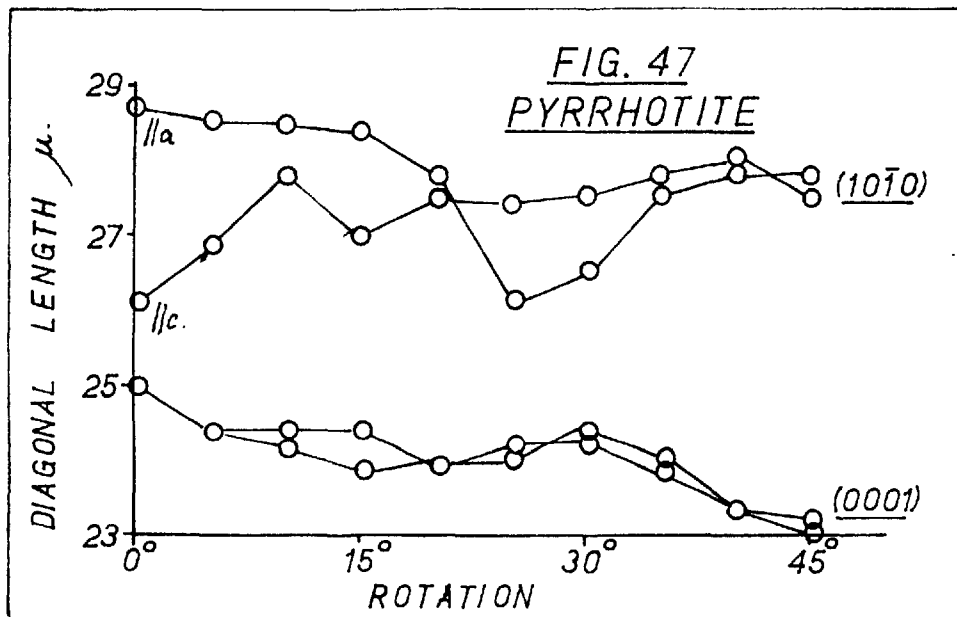
No significant differences in diagonal lengths were found with rotation of the Vickers indenter on the (100) and (111) faces. On the (110) face, the differences of diagonal lengths is a maximum, Fig. 46, when the diagonals are parallel to the cleavage traces and approaches zero when the indenter is in the 45° position. In the position of maximum difference of diagonal lengths, the long diagonal is parallel to the traces of the vertically dipping cleavages i.e. parallel to the a_1 and a_3 axes. The change of diagonals length is accompanied by variations in the shape of the indentations.

Pyrrhotite and Wurtzite

Figs. 47 and 48 illustrate the isotropic nature of the

FIG. 46
GALENA (110)

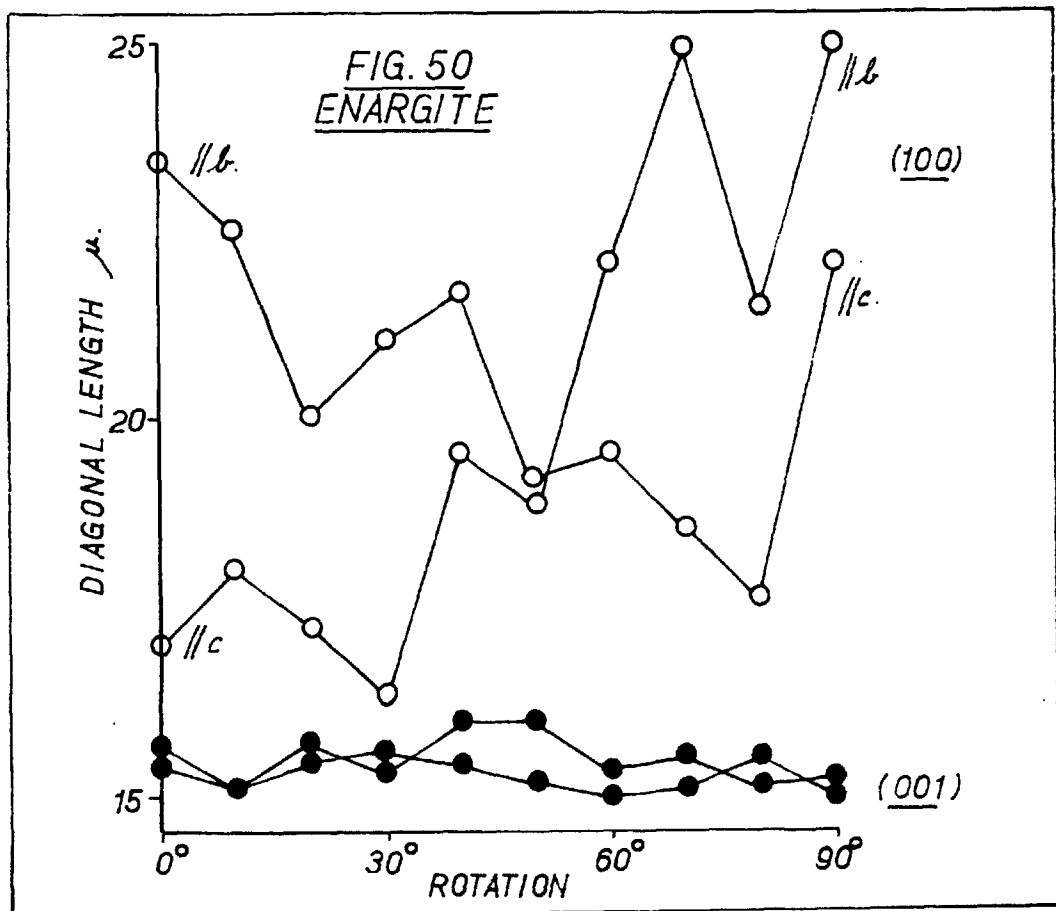
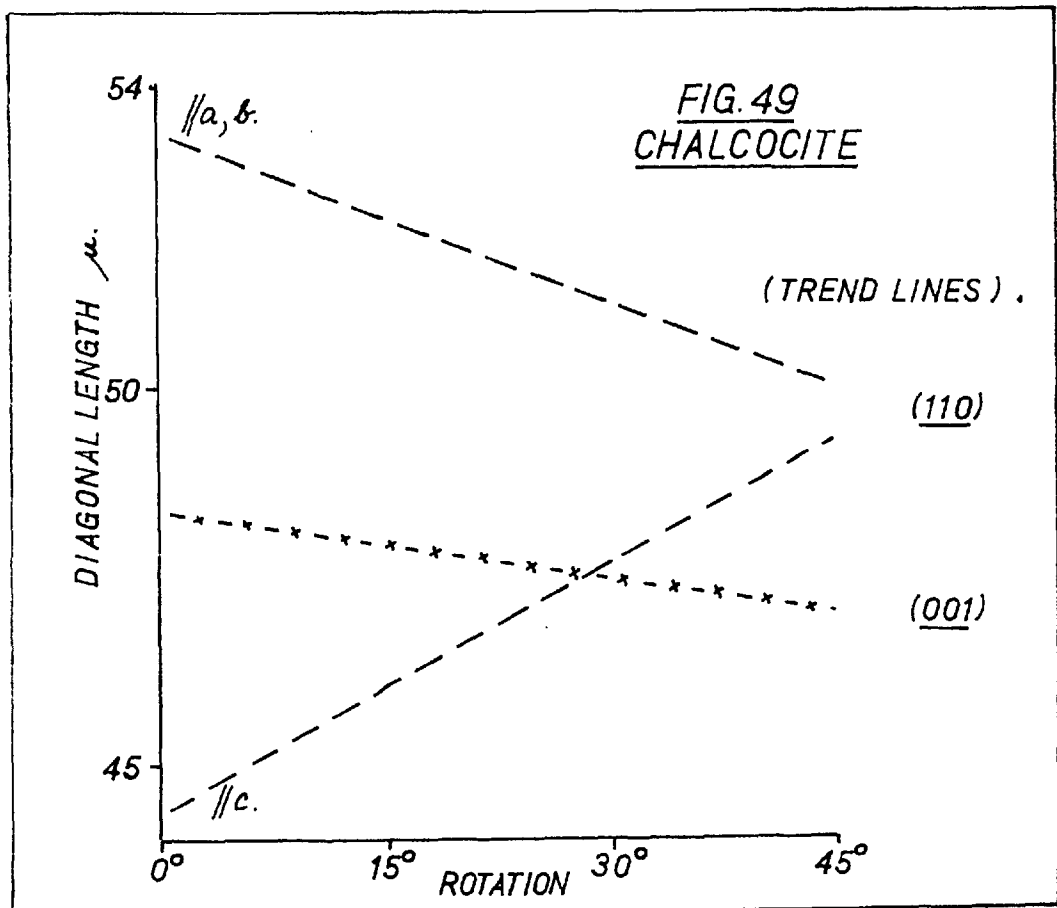




basal (0001) faces relative to the anisotropism of the prism (10 $\bar{1}$ 0) faces. In both minerals, the difference in diagonal lengths on the prism faces is a maximum where the diagonals are parallel to the c and a-axes and approaches zero at the 45° position. In the position of maximum difference of diagonal lengths, the long diagonal is parallel to the a-axis. It is interesting to compare these results with corresponding Knoop microhardness results, Figs. 29,30. The difference in the Vickers microhardness "anisotropism" between wurtzite and pyrrhotite compares favourably with corresponding Knoop microhardness variations. The profiles of the graphs for the N-S diagonal lengths of impressions made on the prism faces for wurtzite and pyrrhotite are quite distinct. On wurtzite the length decreases sharply but evenly from 0° to 30°, but from 30° to 45° the length decreases very slowly with rotation. On pyrrhotite, the decrease of length with rotation is even and small.

Chalcocite

Fig. 49 shows the diagonal length variations for the (001) and (110) faces. On the basal (001) face, the variation is small and inconsistent and compares closely with Knoop microhardness variations, Fig. 36. On the prism (110) face, the difference is a maximum when the diagonals are



parallel to the crystallographic axes and approaches zero at the 45° position. In the position of maximum difference of diagonal lengths, the long diagonal is parallel to the a-axis.

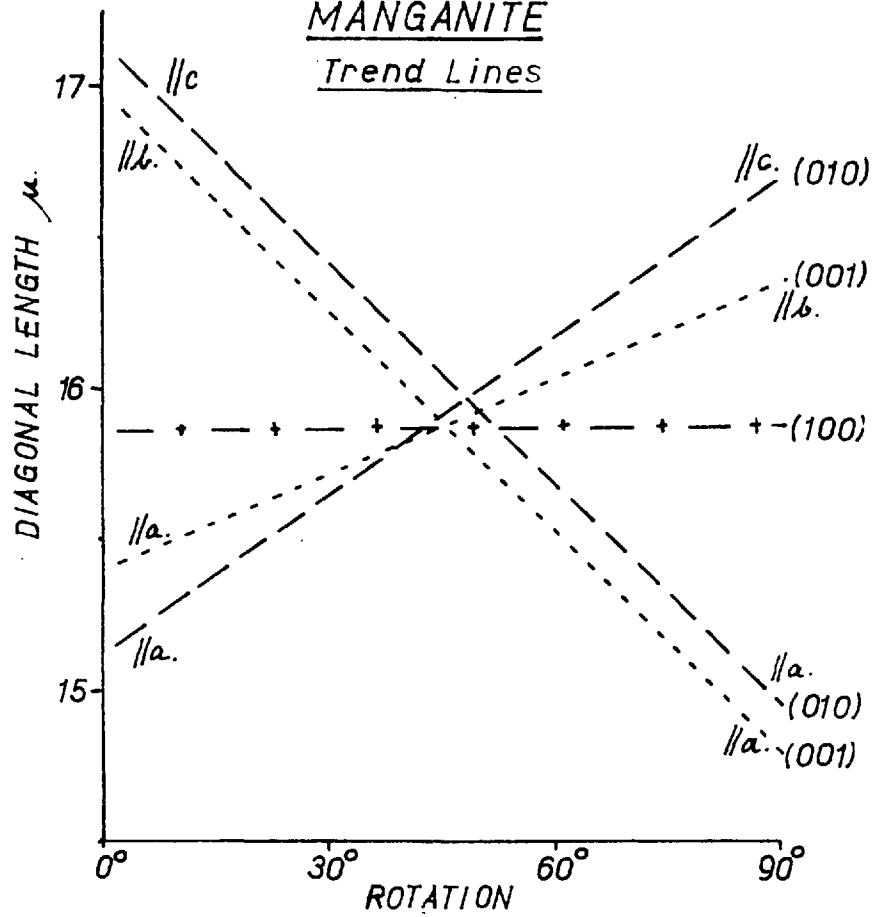
Enargite

Fig. 50 shows the diagonal length variations for the (001) and (010) faces. The (001) face shows little variation in values but the difference is a maximum in the 45° position where the diagonals are approximately parallel to the (110) cleavage traces. On the (010) face, the difference is a maximum where the diagonals are parallel to the crystallographic axes and approaches zero at the 45° position. In the position of maximum difference of diagonal lengths, the long diagonal is parallel to the a-axis.

Manganite

On plotting the actual diagonal lengths against rotation for the (001), (010) and (100) faces of manganite a very confused picture results. Fig. 51 shows a plot of the trend lines for these faces. Graphs for the (001) and (100) faces show no significant variations with orientation. On the (010) face, a maximum difference of diagonal lengths occurs when the diagonals are parallel to the axes and a minimum

FIG. 51
MANGANITE
Trend Lines



difference in the 45° position. In the position of maximum difference of diagonal lengths, the long diagonal is parallel to the c-axis.

Stibnite and Bismuthinite

Figs. 52,53 show the variation of diagonal lengths with rotation for the (001), (010) and (100) faces. No significant differences in diagonal lengths were found on the (100) faces.

On the (010) face the difference in diagonal lengths is a maximum when the diagonals are parallel to the axes and approaches zero at the 45° position. In the position of maximum difference of diagonal lengths, the long diagonal is parallel to the c-axis. On the (001) face, the difference in diagonal lengths is a maximum parallel to the a and b-axes, the long diagonal being parallel to the b-axis, and approaches zero at the 45° position.

The rate of change of diagonal length with rotation is not constant. On both the (010) and (001) faces, the rate of change is small with the diagonals at about 30° to the crystallographic axes, but increases rapidly as the 45° position is approached.

FIG. 52
BISMUTHINITE

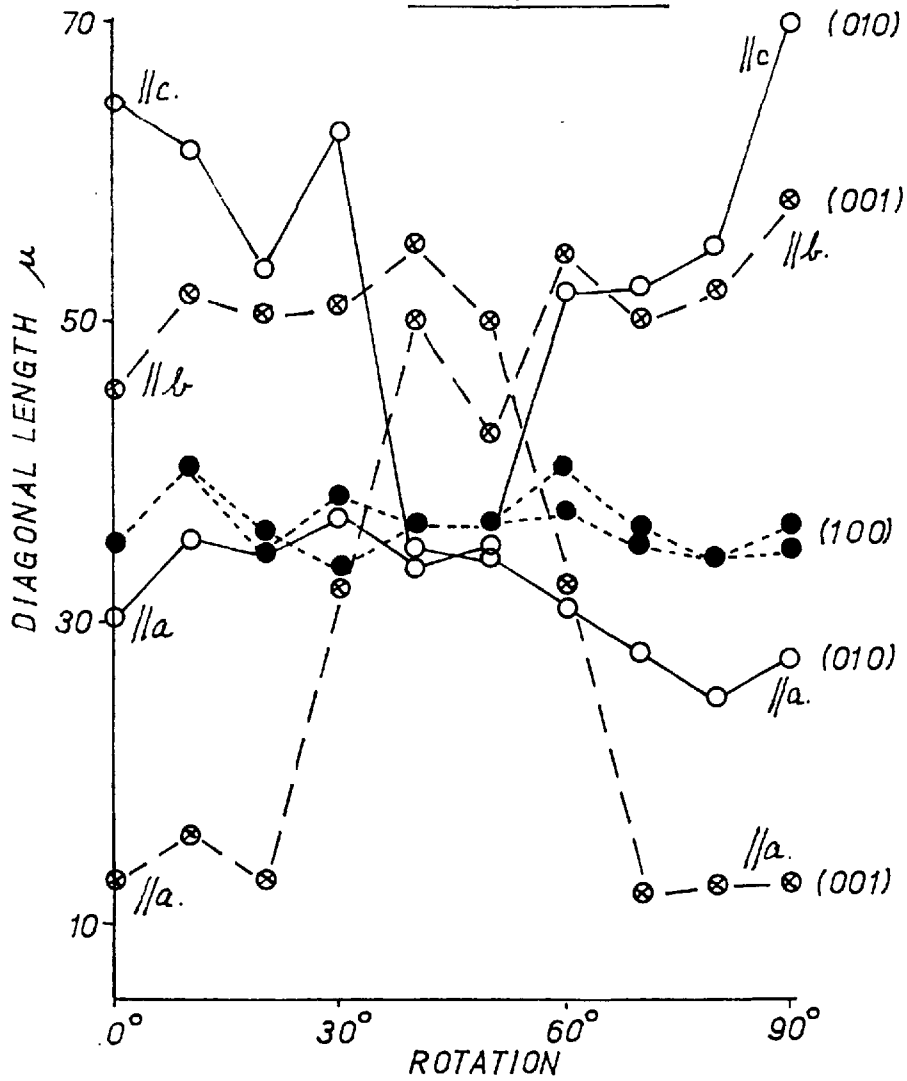
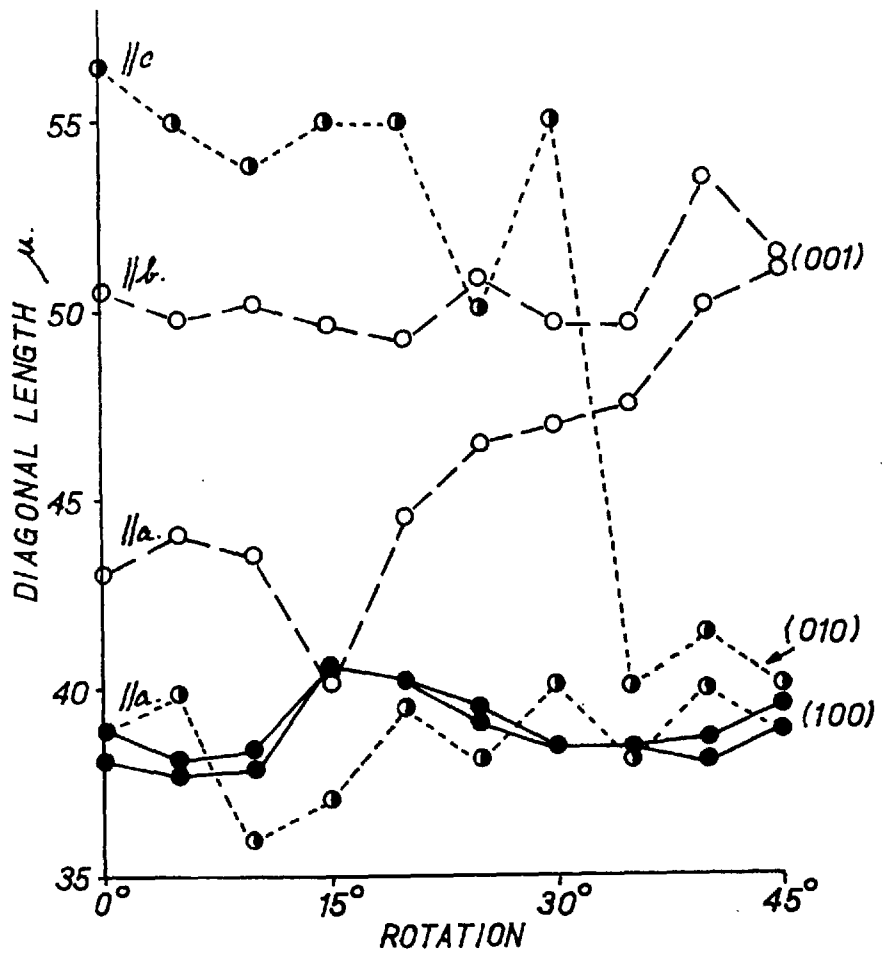


FIG. 53
STIBNITE



(b) Minerals whose orientations were not precisely known.

The following minerals showed considerable differences of the diagonal lengths of Vickers indentations, but no correlation could be made with glide and cleavage planes.

Altaite
Clausthalite
Emplectite
Jalpaite
Jamesonite
Sternbergite
Stibarsenic

Table XXXI shows the relationship of the elongation of indentation relative to the prominent glide or cleavage planes in a further 18 minerals.

In Volume II the "strength of anisotrovism" i.e. the amount of variation of the diagonal lengths of Vickers indentations is given for all the minerals studied.

(c) General Discussion

Of the 25 minerals studied, 24 show elongation of the indentations in positions where the long diagonals are perpendicular to the traces of the twin, glide or cleavage planes. Manganite, the exception, has more than two possible

planes of movement. Most of the 24 minerals show either strong cleavages or prominent glide planes.

Although no interferometric studies were carried out on the surface topography around indentations, it was possible, using oblique illumination, to observe the amount and type of "piling up" of material (Mott, 1956), or displacement relief around impressions. For example, it was observed that around indentations made in bismuth, considerable displacement of material occurred in areas where dislocation traces were prominent. When the diagonals were perpendicular or parallel to these dislocations, displacement relief occurred adjacent to the sides enclosing the long diagonal, Fig. 56. Where the diagonals were at 45° to the dislocation planes, the sides of the impression parallel to these glide planes showed convexity, Fig. 56 and photo 24. This is strong evidence for upwards displacement relief, (Mott 1956). Such induced relief was observed around indentations made in most of the 24 minerals.

Since deformation in these minerals occurs by movement along the cleavage or glide planes it follows that more movement over the surface will take place in a direction at right angles to the dislocation plane traces than in a direction parallel to the dislocation planes. Thus material is moved

into a position closer to the indenter and results in an indentation apparently elongated perpendicular to the dislocation planes. A characteristic of such indentations is the ragged nature of the sides, and this is borne out by photo 27, bismuthinite and photo 58, cinnabar.

No account has been given of the part played by elastic recovery which may also be anisotropic in effect. It is considered that the effect of anisotropism of elastic recovery on the dimensions of the indenter is probably small.

TABLE XXXI

The relationship of the elongation of indentations to movement planes

Mineral	Orientation	Relationship of elongation of indentation to movement planes
Antimony	Unknown	Elong. \perp to $(10\bar{1}4)$ translation twin plane traces.
Arsenic	Unknown	Elong. \perp to $(10\bar{1}4)$ translation twin plane traces.
Bismuth	Unknown	Elong. \perp to $(10\bar{1}4)$ and (0001) movement plane traces.
Cinnabar	$(10\bar{1}1)$	Elong. \perp to kite structure, photo 58.
Cosalite	Unknown	Elong. \perp to dislocation planes.
Covellite	$(10\bar{1}1)$	Elong. \perp to (0001) cleavage traces.
Cubanite	Unknown	Elong. \perp to disloc. planes. - also length of path.
Cylindrite	// length	Elong. \perp to length and cleavage.
Franckeite	(001)	Elong. \perp to (010) cleav.
Gypsum	(001)	Elong. \perp to (010) cleav.
Huebnerite-	(001)	Elong. \perp to (010) cleavage.
Ferberite	(010)	Elong. \perp to (100) cleavage.
	(100)	Elong. \perp to (010) cleavage.
Kyanite	(001)	Elong. \perp to (100) cleavage.
	(100)	Elong. \perp to (001) cleavage.

TABLE XXXI contd.

Mineral	Orientation	Relationship of elongation of indentation to movement planes.
Columbo-tantalite	(001)	Elong. $\underline{1}$ to (010) cleavage
Nagyagite	(001)	Elong. $\underline{1}$ to (010) cleavage
Stephanite	(100) (010)	Elong. $\underline{1}$ to (110)? twin planes. Elong $\underline{1}$ to (110)? twin planes
Teallite	(001)	Elong. $\underline{1}$ to (010) glide planes.
Tellurium	(10 $\bar{1}$ 0)	Elong. 1 to (10 $\bar{1}$ 0) cleavage.

CHAPTER V

THE SHAPE AND ASSOCIATED CHARACTERISTICS OF THE INDENTATIONS

A. General

A study of the shapes and deformation characteristics of the indentations was made for two reasons. Firstly, it seemed likely, from the results of a preliminary investigation that some of the characteristics of the indentations would be useful in the field of mineral identification, for further differentiating between minerals of similar hardness. Secondly, it was hoped that by studying the relationship between indentation characteristics and crystal orientation, some evidence would be brought forward to help explain the mode of deformation of the ore minerals during indentation.

During the preliminary investigations, it was found that Vickers indentations gave considerably more data than corresponding Knoop indentations. Hence, in Volume II, indentation characteristics have, in most cases, been given only for Vickers impressions. Typical indentations, and their associated deformation phenomena, for most of the ore minerals studied have been photographed, and these,

together with brief descriptions, are included in Appendix A.

In the following section, the various different types of shapes and characteristics are described and examples given. Frequent references will be made to the photographs in Appendix A.

Variation in shape of the indentations

Theoretically, the shape of a perfect Vickers indentation, made in a substance having perfect plasticity, is that of a square, i.e., the sides of the impression are straight. In the present study numerous deviations from the ideal shape were observed and in fact relatively few minerals exhibited indentations with straight sides.

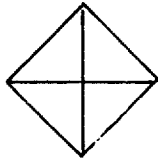
For convenience of description, the various shapes of indentations have been classified into 14 different types (Fig. 54).

The shapes of all these types are essentially composed of a combination of five fundamental curves. These are as follows:

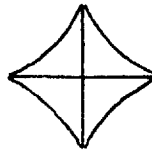
- (a) the "straight" edge, (str.)
- (b) the "concave" edge, (cc.), where the deviation is directed towards the centre of the impression.

FIG. 54 SHAPES OF INDENTATIONS

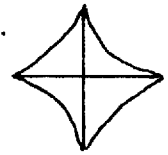
1.



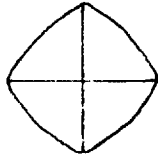
2(a).



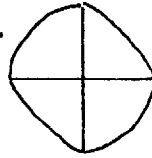
2(b).



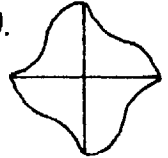
3(a).



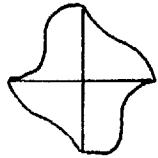
3(b).



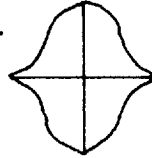
4(a).



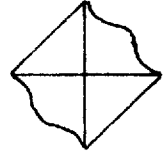
4(b).



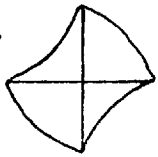
4(c).



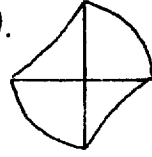
5.



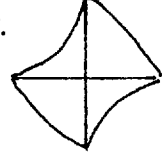
6(a).



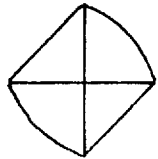
6(b).



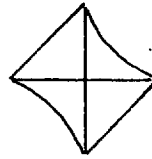
6(c).



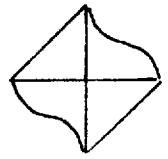
7.



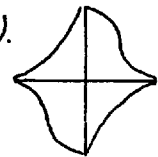
8.



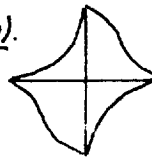
9.



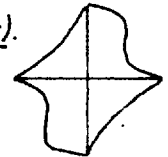
10(a).



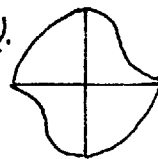
10(b).



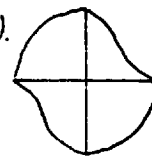
10(c).



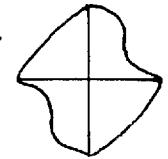
11(a).



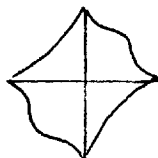
11(b).



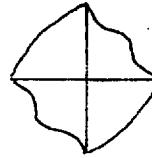
11(c).



12.



13.



14.

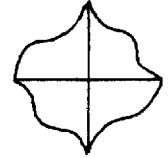


TABLE XXXII

Examples of Minerals Showing Different Indentation Types

Indentation type	Mineral	Photo No.
1	Rutile	202
2	Covellite	80
3	Cuprite	86
4	Silver	211
5	Galena	120
6	Niccolite	---
7	Sphalerite	217
8	Ferrite	108
9	Sphalerite	220
10	Bismuth	24
11	Copper	70
12	Wurtzite	---
13	Acanthite	---
14	Acanthite	---

TABLE XXXIII

Examples of Minerals Whose Indentations Show Different
Degrees of "Anisotropism"

Mineral	Anisotropism	Photo No.
Galena	zero	115
Altaite	v. weak	6
Copper	weak	71
Chalcocite	strong	53
Antimony	v. strong	12

- (c) the "convex" edge (c.v.) where the deviation is directed away from the centre of the impression.
- (d) the "sigmoidal" edge, (sig.), where concave and convex curves form an open S shaped figure
- (e) the "concavo-convex" edge, (cc-cv), where concave and convex curves form an open W shaped figure, the bottom of the W pointing towards the centre of the impression.

The amount of deviation of the curves may be termed the degree of "strength" of curvature of the edges. In this way it is possible to differentiate between two similarly shaped indentations having edges of different strengths of curvature. In Appendix A, such indentations are differentiated by using the terms "weak" and "strong". Thus in photo 115, the (100) face of galena exhibits an indentation of type 2(a) strong, whilst in photo 107, fergusonite exhibits an indentation of type 2(a) weak.

Examples of minerals showing the different types of indentations are given in Table XXXII together with references to photographs in Appendix A.

In general, the metals and alloys give the greatest variety of types of indentations and also the strongest curvature of the edges. Indentations made in the simple sulphides, the selenides and the tellurides show a lesser

degree of curvature and variety of types. The sulphosalts exhibit a considerable variety of shapes of indentations but the amount of curvature of the edges is relatively small. Apart from a few minerals, such as niccolite, breithauptite, zincite and löllingite, the complex sulphides, sulpharsenides and sulphantimonides, the oxides and the silicates all show very limited variations in the types and strength of curvature of indentations. The shape most commonly observed in all minerals was type 2(a) weak.

C. Variations in the dimensions of indentations

The variation between the lengths of the diagonals of indentations has been described and discussed in Chapter IV. It was decided to classify the variation in the diagonal lengths of indentations made in different minerals so that yet another physical property might be examined for utilisation in ore mineral identification. Thus the differences between the lengths of diagonals or the "anisotropism" of diagonal lengths of indentations may be divided into three main groups as follows:

- (a) the "equidimensional" or "isotropic" - i.e. no observable differences between the diagonal lengths,
- (b) the "weakly" anisotropic (weak) - i.e. the ratio of

the diagonal lengths (smaller/larger) is greater than 0.90, but less than 1.00.

- (c) the "strongly" anisotropic (strong) - i.e. the ratio of the diagonal lengths (smaller/larger) is less than 0.90.

Table XXXIII gives examples of minerals whose indentations show different strengths of anisotropism of diagonal lengths, with particular reference to the photographs in Appendix A.

A few minerals, for example, cylindrite, show another expression of physical anisotropism in their indentation characteristics. In this case, the indentations show diagonals which are not perpendicular to one another. Tertsch (1950) reported similar phenomena in indentations made on the $(11\bar{2}0)$ face of calcite. It is also of interest to note that the indentations in calcite on a $(10\bar{1}1)$ face, (Tertsch, 1950) show a remarkably low symmetry and bear some resemblances to those obtained by the present author on cinnabar (photographs 58, 59). No other minerals studied showed such remarkably unsymmetrical indentations.

D. Associated deformation characteristics

Deformation during the indentation of ore minerals takes place by elastic and plastic processes and/or by rupture of the structure and most frequently by a combination

of all three mechanisms. Elastic deformation is expressed by the recovery of the sides of the impression and is manifest in many of the more complex concave shaped indentations. These features have been described in the previous section. Plastic deformation is usually expressed by the movement of material around the impression without fracturing taking place. In many cases, the traces of slip and glide planes are evident around the impressions. Rupture of the mineral due to indentation takes place by cracking and fracturing of the surface of the polished section. In minerals where deformation during indentation occurs by a combination of these processes, the various characteristics are superimposed upon one another.

7. Features of plastic deformation

Evidence for plastic deformation falls into three main categories

- (a) the absence of fractures - photo 120
- (b) the presence of material around the indentation that has been distorted but is unfractured - photo 237
- (c) the presence of movement or "dislocation" traces - photo 179.

Movement usually takes place by translation or twin gliding, or by both mechanisms, along "flat" planes so that

their traces form straight lines. Sometimes, however, the dislocation traces are curved, usually convex towards the centre of the impression, as in osmiridium-iridium, braggite pearceite and platinum - photos 177, 179. The dislocations in such cases have been presumably distorted by subsequent lateral plastic movement. In addition, the intersection between the dislocation planes and the distorted surface immediately surrounding the indentation could also produce curved traces. Twin plane traces were distinguished from translation gliding plane traces by examination under polarised light or oblique illumination. Under such illumination the differences of orientation of the twin lamellae produce a "striped" structure, e.g. hessite, photo 138. Typical translation gliding is well shown by antimony in photo 12.

For oriented sections of some minerals, e.g. galena, it has been possible to relate the known glide planes with dislocation plane traces observed on the surface.

F. Fracturing phenomena

Practically all the minerals studied were found to fracture, to some extent, at 100 g. load, with the exception of most native metals and alloys, and some of the simple sulphides, selenides and tellurides. For convenience

of description the types of fracturing have been categorised as follows;

- (a) Radial fractures
- (b) Cleavage fractures
- (c) Parting fractures
- (d) Shell fractures.

The individual characteristics of these types of fractures are diagrammatically illustrated in Fig. 55.

(a) Radial fractures

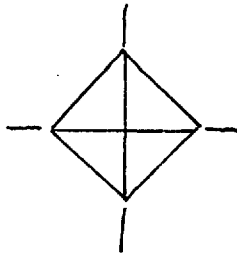
Radial fractures are slightly curved fractures, which as the name implies, radiate from the centre of the indentation. They may be conveniently subdivided into two main groups: "star-radial" fractures, where the cracks originate from the corners of the impression, and "side-radial", where the cracks originate from the sides of the indentation. Examples of these two types of radial fracture are shown by bournonite in photos 39 and 37. When the fractures are irregular in form and distribution, the term "irregular radial fractures" is used - for example in famatenite, - photo 106. "Star radial" fractures are by far the most common form of radial fracturing and this type is frequently interconnected by curving fractures from which "simple shell" fractures are developed.

FIG. 55

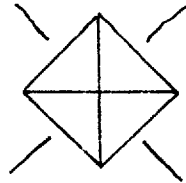
INDENTATION FRACTURE CHARACTERISTICS

RADIAL

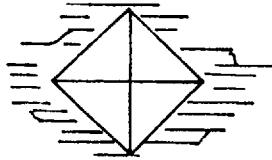
Star



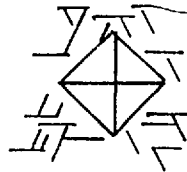
Side



CLEAVAGE

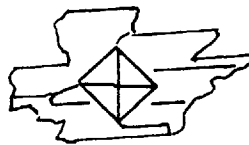


PARTING



SHELL

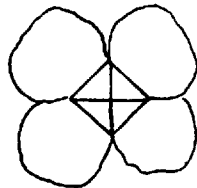
Cleavage



Concentric



Simple



(b) Cleavage fractures

Well-cleaved minerals, when indented, exhibit inter-connecting fractures around the indentation parallel to the cleavage traces. They are recognised by their parallelism and straightness. Good examples of such features are shown in covellite - photo 80. In some minerals different cleavages produce a network of cleavage fractures as for example in pentlandite, photo 180 and manganite, photos 159, 160, and 161. Cleavage fractures are distinguished from cleavage shell fractures by angularity and incompleteness of the fracture system. Photo 98 of enargite and 27 of bismuthinite illustrate the differences between cleavage shell fractures and cleavage fractures.

(c) Parting fractures

Parting fractures occur around impressions made in minerals in which the dominant planes of weakness are parting planes. These are similar to cleavage fractures in appearance, but whereas cleavage traces can usually be observed before indentation, parting planes can only be detected after indentation. Good examples of such fracture patterns are shown by bornite, photos 32 and 33, and chalcocite, photos 52 and 53.

(d) Shell fractures

Shell fractures originate from radial fractures and connect one fracture with another. They may be categorised as follows:

- (i) Simple shell fractures
- (ii) Cleavage shell fractures
- (iii) Concentric shell fractures.

(i) Simple shell fractures

These are by far the most common type of shell fracture. The shape described by a single shell fracture approximates to that of the outline of a sea-shell, the fractured area being as large or larger than the indentation itself. The thickness of the fractured flake is small in comparison to the diameter, being not usually greater than 1/5 of the diameter. Examples of minerals exhibiting such fracture patterns are as follows: ilvaite, photo 143; pyrrhotite, parallel to (0001), photo 195; wurtzite, parallel to (0001), photo 263.

(ii) Cleavage - shell fractures

Cleavage shell fractures are intermediate in character between cleavage fractures and simple shells. The fractured areas are elongated parallel to the cleavage

traces. Sometimes the elongation is terminated by curving fractures as in enargite, photos 98 and 102, and in others by irregular ragged lines, for example in stibnite, photo 232.

(iii) Concentric shell fractures

As the name suggests the fracture lines are roughly circular and sub-parallel to one another. This fracture pattern is almost entirely confined to indentations made on sections cut parallel to the dominant cleavage, in minerals exhibiting one perfect cleavage plane. Examples of such fracture patterns are shown by covellite, photo 79 and teallite, photo 240.

G. Variations of the shape and deformation characteristics with orientation

Several authors have described the variation of the characteristics of indentations made on different orientations of minerals. Tertsch (1950) showed that a considerable change occurred in the shape of Vickers indentations made on different orientations of calcite. Gottardi (1951) extended the work of Tertsch on calcite and concluded that the elastic and plastic constants showed maxima and minima in two directions at right angles to one another. Attinger (1952),

working on synthetic corundum, with a Knoop indenter found a variation in the incidence of fracture on the basal (0001) face, maxima being at 60° to one another. Henriques (1957) found considerable variations in the shape of Vickers indentations made on different orientations of sphalerite.

Detailed studies were carried out on the following minerals, all of which showed significant variations of shape and deformation characteristics with orientation.

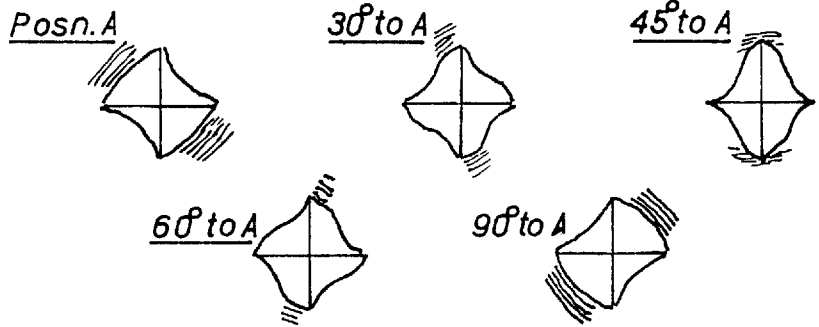
Bismuth	Gypsum
Bismuthinite	Halite
Bournonite	Molybdenite
Chalcocite	Nagyagite
Cinnabar	Pyrrhotite
Copper	Sphalerite
Covellite	Stephanite
Cubanite	Stibnite
Cuprite	Teallite
Fluorite	Tellurium
Galena	Wurtzite

The results are illustrated in diagrammatic form in Figs. 56 - 62.

FIG. 56
ORIENTED DEFORMATION CHARACTERISTICS

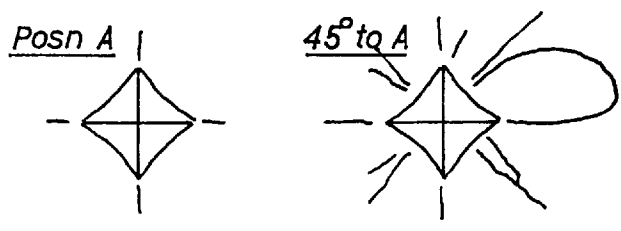
BISMUTH

Unknown Orientation



BOURNONITE

Unknown Orientation



CHALCOCITE

(110)

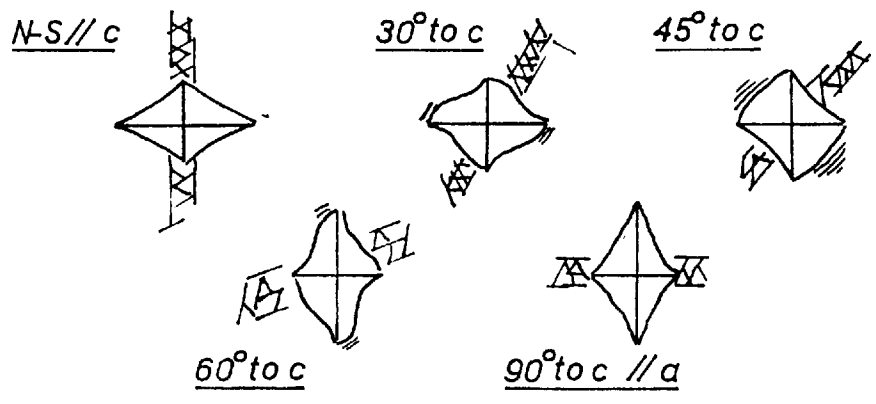


FIG. 57
ORIENTED DEFORMATION CHARACTERISTICS

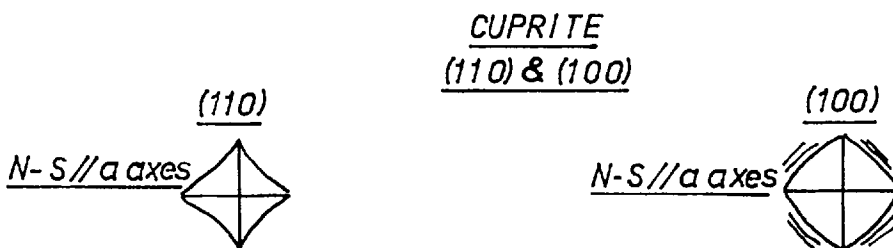
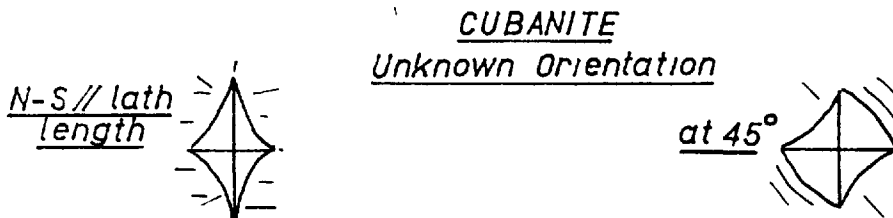
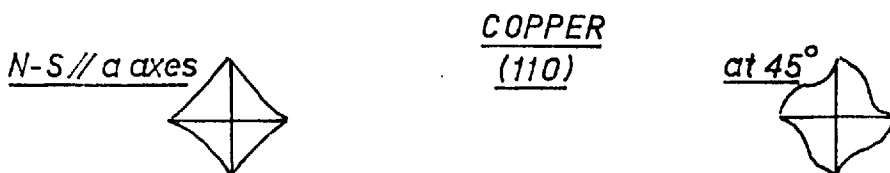
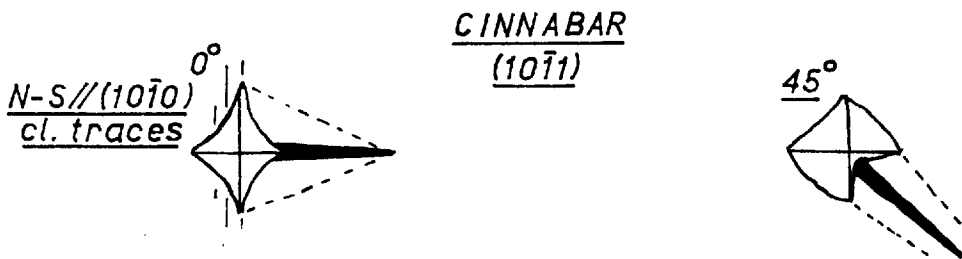
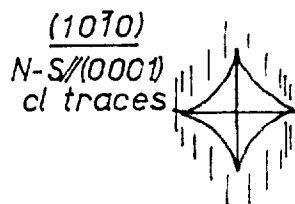
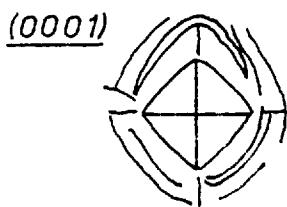


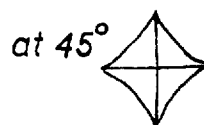
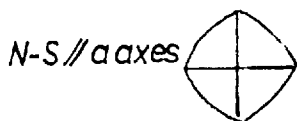
FIG. 58
ORIENTED DEFORMATION CHARACTERISTICS

COVELLITE



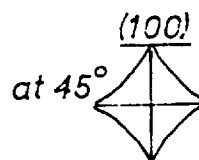
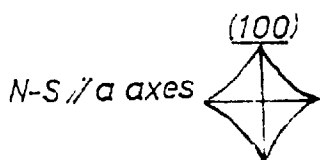
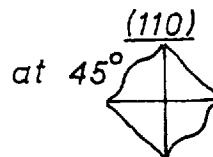
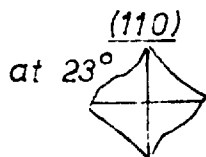
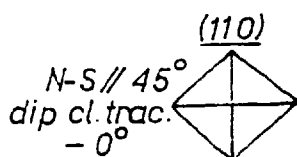
FLUORITE

(100)



GALENA

(100) & (110)



HALITE

(100)

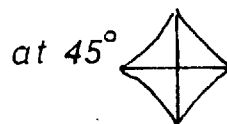
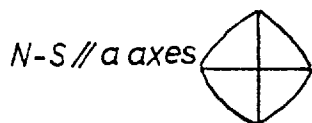
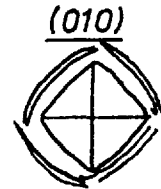
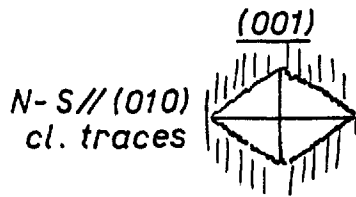
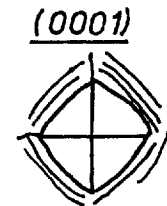
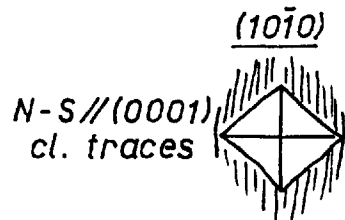


FIG. 59
ORIENTED DEFORMATION CHARACTERISTICS

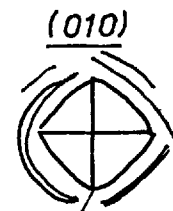
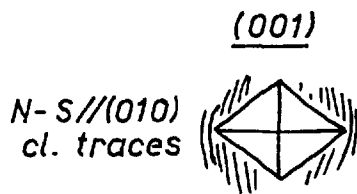
GYPSUM



MOLYBDENITE



NAGYAGITE



PYRRHOTITE

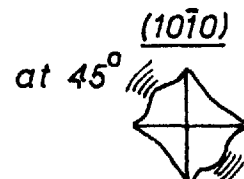
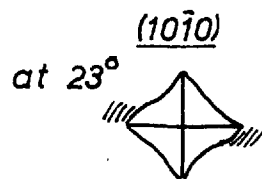
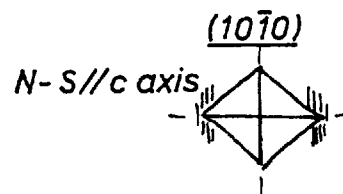
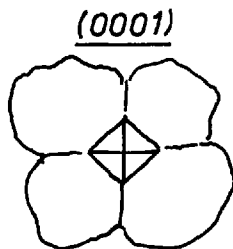


FIG. 60 INDENTATION SHAPES OBTAINED ON DIFFERENT ORIENTATIONS OF SPHALERITE.

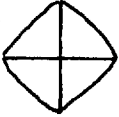




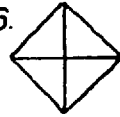
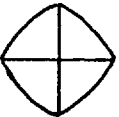





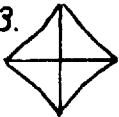

<u>HENRIQUES (1957)</u>		Ref No.	Surface (hkl)	Direction (hkl)	Angle of ind. diag. with (hkl) direction
1. 	2. 	1.	(100)	[001]	0°
		2.	(100)	[001]	15°
3. 	4. 	3.	(100)	[001]	30°
		4.	(100)	[001]	45°
5. 	6. 	5.	(111)	[112]	0°
		6.	(111)	[112]	60°
<u>YOUNG</u>					
7. 	8. 	7.	(100)	[001]	0°
		8.	(100)	[001]	15°
9. 	10. 	9.	(100)	[001]	30
		10.	(100)	[001]	45°
11. 	12. 	11.	(111)	[112]	0°
		12.	(111)	[112]	45°
13. 	14. 	13.	(110)	[100]	0°
		14.	(110)	[100]	45°

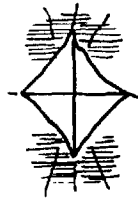
FIG. 61

ORIENTED DEFORMATION CHARACTERISTICS

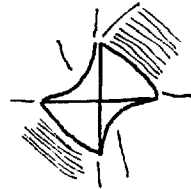
STEPHANITE

(110)

N-S//a&b axes



At 45° to axes

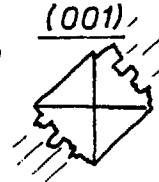


BISMUTHINITE

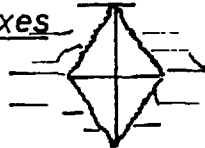
N-S//axes (001)



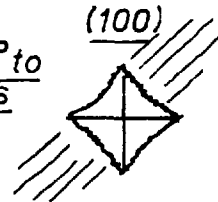
At 45° to axes (001)



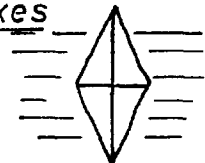
N-S//axes (100)



At 45° to axes (100)



N-S//axes (010)



At 45° to axes (010)

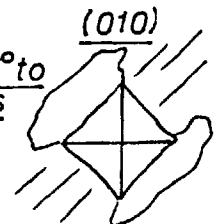
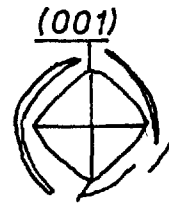
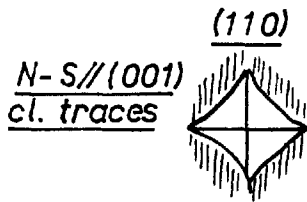


FIG. 62

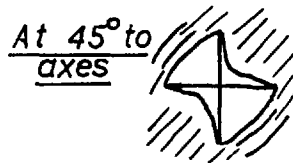
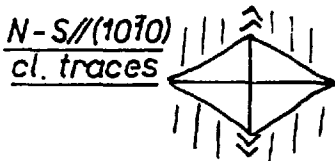
ORIENTED DEFORMATION CHARACTERISTICS

TEALLITE

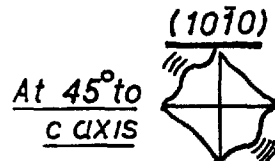
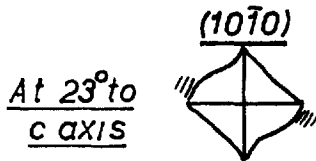
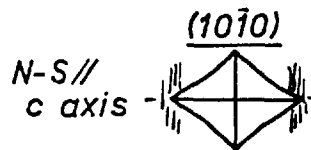
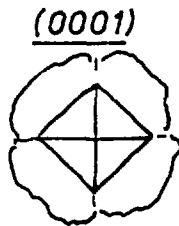


TELLURIUM

(1010)



WURTZITE



Discussion

In the light of the results obtained, the main theme for discussion is the relationship between the variation in the shape and fracture patterns with variations in the orientation of the movement planes of mineral to the indentation direction.

Mott (1956) discusses the causes of concave and convex sided indentation. During indentation material is moved in one of two ways; either the material is "piled up" around the indentation or "sinking-in" of material occurs. On the assumption that contact between indenter and material is maintained during loading, a convex side will result from the bulging associated with piling up, and a concave side with sinking in. Subsequent elastic recovery may alter the shape of the impression, as this will be a maximum at the centre of the faces. Thus elastic recovery will increase concavity due to sinking in and decrease convexity due to piling up. From this argument, it can therefore be appreciated that convexity is good evidence of piling up.

From Figs. 56-62 it can be seen that the sides of the indentations showing convexity are parallel with the traces of potential movement plane in the minerals. For example, on the (110) face of stephanite, convex faces occur when the

edges are parallel to the traces of the (110) twin planes. In most cases glide plane traces were observed running parallel to the convex faces and was further substantiated by the general studies on unoriented minerals such as osmiridium-iridium, photo 177. It is interesting to note that galena and halite show different shapes in the 0° and 45° positions, in spite of the fact that both minerals exhibit perfect (100) cleavage. This evidence, together with oriented hardness data, indicates that halite deforms in a different manner to galena, probably along either (110) or (111) planes.

The $(10\bar{1}0)$ faces of pyrrhotite and wurtzite, and the (110) face of galena show similar variations of shape of the indentations with rotation of the indenter. When the diagonals of the indenter are parallel to the crystallographic axes, concave sided indentations result. As the indenter is rotated, the indentation shapes change to a combination of sigmoidal and concave faces, and finally in the 45° position, it assumes concavo-convex and straight sides. The concavo-convex sides are parallel with the traces of the inclined $(10\bar{1}0)$ cleavage planes for pyrrhotite and wurtzite and the inclined (100) planes in galena. In nearly all of the minerals studied where convex sided indentations have been observed, the convexity is accompanied by minor slip-plane traces.

In minerals such as cuprite, fluorite and halite, the change from concave faces in one position to convex faces in another does not involve a transitional stage composed of sigmoidal face.

Translation data are known for bismuthinite, fluorite, galena, halite and sphalerite. In every case the convex faces of indentations made in these minerals are coincident with the traces of the known translation planes. Thus piling up of material around indentations made in these minerals occurs in directions normal to the glide plane traces. Hence, using this relationship, in conjunction with other observed features, we may deduce translation data for the other minerals studied, (Table XXXIV).

Fig. 60 shows a comparison of the results obtained by Henriques (1957) and the present author on oriented sections of sphalerite. The data for the (100) face are in complete agreement and only small differences occur for the (111) face. It is surprising to note that Henriques finds differences of shape in the 0° and 60° positions on the (111) face, since these two positions are identical from a symmetrical point of view. Henriques gives no data for the (110) faces, but some differences in shape with rotation of the indenter have been found in the present work. These results confirm the

conclusions in Chapter IV that sphalerite deforms by movement along (111) planes.

The variation of indentation characteristics for minerals exhibiting one good cleavage is well shown in figs. 57 and 59 for covellite, molybdenite, nagyagite etc. On faces parallel to the dominant cleavage, straight or convex sided indentations result, accompanied by concentric shell fractures. On faces perpendicular to the cleavage, concave sided indentations result, accompanied by strong cleavage fracturing. In the former orientation, lateral deformation movement can occur easily and the resultant piled up material produce convex sided indentations. In the latter orientation, no easy lateral movement can take place. In addition elastic recovery along the cleavage planes occurs easily, resulting in concave sided indentations. Similar characteristics were observed in unoriented sections of tetradymite.

Bournonite shows considerable variation in the type of radial fracture systems and in the strength of the concavity of the sides of the indentation with rotation of the indenter, Fig. 56 and photos 35 - 40. In most minerals the radial fractures originate from the corners of the indentation to form star radial fractures. The independence of the fractures from the orientation of the indenter indicate fixed

directions of fracturing in bournonite.

The fracture characteristics of the stibnite-bismuthinite series indicate that easiest movement takes place along (010) planes in a direction perpendicular to the (001) face. This is in accordance with the oriented microhardness results. Photos 25 - 30, and Fig. 61 illustrate that considerably more fracturing, and therefore less perfect gliding, occurs on the (100) and (010) faces, than on the (001) face.

The asymmetric "kite-tail" structure around indentations made on the $(10\bar{1}1)$ face of cinnabar defies interpretation and deserves closer and more detailed studies on different orientations of the mineral (Fig. 56, photos 58 and 59).

H. Variation of the shape and deformation characteristics of indentations with mineral species.

Deformation characteristics of minerals during indentation are dependent primarily upon two factors; the chemical composition and the structure. For analysis of the results, the minerals studied have been grouped according to chemical composition and the groups sub-divided according to atomic structure. The classification of the minerals

was based on the work of the following authors: the native metals - Evans (1939), the sulphides, selenides, tellurides and sulphosalts - Ross (1957), and the oxides, silicates and some of the sulphosalts etc. - Palache, Berman and Frondel (1944). It was found that each separate group of minerals possessed its own set of microhardness characteristics and these are described in detail below. Table XXXV outlines the broader variations of hardness characteristics with chemical composition.

. The Metals and Semi Metals

- (a) The metals studied may be grouped according to the type of packing of the atoms;
 - (i) The cubic close packed type
 - (ii) The B sub-group metal packing type.

(i) The cubic close packed type

Metals included in this group are as follows; copper, gold, lead, silver, iron, platinum, osmiridium-iridium and iridosmine. All these exhibit similar microhardness properties; medium anisotropy, indentation types 2(a) str., 3(a) str., 4(a) weak, no fractures, and weak glide plane traces.

(ii) The B sub-group metal packing types.

The following metals of this structure-type were studied; arsenic, antimony, bismuth and tellurium. Arsenic, antimony and bismuth being isostructural show similar characteristics, i.e. strong anisotropy, indentation types 2(a) str., 2(b) str., 4(a), 4(b) str., 6(a), 6(b), 6(c) str., 10(a) str., no fractures, no prominent glide planes. Tellurium, having a chain structure, has different properties i.e. v. str. anisotropism, indentation types 2(c) str., 6(c) str., medium cleavage fractures, and no dislocations.

(b) The Semimetals

The following minerals were studied; amalgam, electrum, domeykite, stibarsenic, dyscrasite and awaruite. Although these minerals have different structures, similar indentation characteristics were found; med. - str. anisotropism, indentation types 2(a), 3(a) weak, 4(a) weak - str., no fractures and weak glide planes.

Simple Sulphides, Selenides and Tellurides

This group contains such a wide variety of structural type that it was decided to sub-divide the mineral according

to indentation characteristics instead of structure. The three main groups are as follows:

- (a) Those showing "metallic" microhardness characteristics
- (b) Those showing slight indentation fractures
- (c) Those showing other deformation phenomena.

(a) Minerals Showing metallic microhardness characteristics

The following mineral sub-groups are included in this group: the galena group comprising galena, clausthalite and altaite; the cooperite group comprising cooperite and braggite; the sphalerite group comprising sphalerite, tiemannite and coloradoite; the antiferite group comprising acanthite, naumannite, hessite, digenite, jalpaite and uncairite, wurtzite and umangite. These minerals show similar characteristics to those of the metals i.e. strong anisotropism, similar shapes, no fracturing, except in the case of uncairite, and glide plane traces.

(b) Minerals showing slight indentation fractures

The following gold tellurides are included in this group; calaverite, knennerite, and sylvanite. Indentations are characterized by weak - medium anisotropism, indentation type 2(a) weak - strong, and slight star radial and shell fractures.

(c) Minerals showing other deformation phenomena

The following minerals have been included in this group; cinnabar, molybdenite, nagyagite, orpiment, realgar, and tetradymite. Large variations of the deformation phenomena in this group are due to the diversity of structures shown by the minerals.

Complex Sulphides of Cu, Fe, Ni, Ge and Sn

The minerals have been sub-divided, on a structural basis, into the following groups:

- (a) the "sphalerite - structure" minerals
- (b) the "wurtzite - structure" minerals
- (c) the "niccolite - structure" minerals.

(a) "Sphalerite-structure" minerals

The following minerals are included in this group; chalcopyrite, famatinite, stannite, germanite and renierite. Maucherite, although structurally dissimilar to sphalerite has been included because of its similar indentation characteristics. Indentations are characterized by zero to weak anisotropism, type 2(a) weak - strong shapes, and medium star and side radials with occasional shells.

(b) "Wurtzite-structure" minerals

The following minerals are included into this group; enargite, sternbergite, cubanite, emplectite and chalcocottibite. These minerals exhibit the following indentation characteristics; medium - strong anisotropism, indentation types 1, 2(a) strong, 5(a) weak, and strong radial and shell cleavage fractures.

(c) "Niccolite-structure" minerals

The following minerals are included into this group; niccolite, breithauptite, millerite, valleriite, pyrrhotite and bornite. Indentation characteristics are as follows; medium - strong anisotropism, indentation types 2(a) str., 3(a) weak, 4(a) weak, 6(a) weak, 10(a) strong and 12 slight star and side radials. Glide plane traces are frequently visible.

The Sulphosalt Minerals

A large number of sulphosalts were studied. However, the structures of the minerals have been established for only approximately half of them.

(a) Sulphosalt minerals of known structure

The minerals of known structure may be sub-divided as follows;

- (i) Minerals of the "sphalerite" structure
- (ii) Minerals of the "galena" structure
- (iii) Minerals having a "chain" structure.

(i) Minerals of the "sphalerite" structure

The following minerals were included in this group; tetrahedrite and tennantite. Pearceite and polybasite, although having different structures, are also included in this group as they have similar indentation characteristics; These minerals are characterised by zero anisotropism, indentation types 1, 2(a) weak, and star and side radial and occasional shell fractures.

(ii) Minerals of the "galena" structure

The following minerals of this group were studied; teallite, niagyrite and diaphorite. Minerals of this group have few characteristics common to one another, for example, teallite shows strong cleavage fractures whilst niagyrite exhibits only radial and shell fractures.

(iii) "Chain Structure" sulphosalt minerals

The following minerals of this type were studied; stibnite, bismuthinite, kermesite, aikinite, bournonite, berthierite, proustite, pyrargyrite, jamesonite, livingstonite, cosalite, and kobellite. These minerals show the following characteristics; medium-strong anisotropism, radial, simple shell and cleavage shell fractures, and indentation types 1, 2(a) weak-strong, 6(a) strong.

(b) Sulphosalt minerals of unknown structure

These minerals have been grouped according to chemical composition as follows;

- (i) Sulphosalts containing Pb, As, Sb.
- (ii) Sulphosalts containing Ag.
- (iii) Sulphosalts containing Cu.
- (iv) Other sulphosalts.

(i) Sulphosalts having the composition A_3BX_4 where $A = Pb$, $B = As, Sb$, and $X = S$.

The following minerals of this type were studied, gratonite, geocronite, jordanite and meneghinite. These minerals were characterised by the following features; weak anisotropism, indentation type 1, 2(a) weak, and irregular radial and shell fractures.

- (ii) Silver sulphosalts of the formula $A_m B_n X_p$ such that $\frac{m+n}{p} > \frac{4}{3}$ and where $A = Ag$, $B = As, Sb$, $X = S$

The two minerals of this group studied were argyrodite and stephanite, which showed the following characteristics common to both; strong anisotropism, indentation types 1, 2(a) str., 6(a) str., strong star and side radial fractures.

- (iii) Copper sulphosalts

Colusite and wittichenite, although having different structures, show similar indentation characteristics; very weak anisotropism, indentation type 1, and strong star and side radial fractures, and occasional shell fractures.

- (iv) Other sulphosalts

The remaining sulphosalts not yet considered i.e. boulangierite, cylindrite, franckeite, and zinkenite, show indentation characteristics common to one another.

Sulphides, Sulpharsenides and Sulphantimonides of Co,
Ni, Fe.

Minerals of this group may be sub-divided, structurally, into three main sub-divisions:

- (a) Minerals having a "pyrite" structure
- (b) Minerals having a "marcasite" structure
- (c) Minerals having a "spinel" type structure.

(a) Minerals of the "pyrite" structure

The following minerals of this group were studied; pyrite, hauerite, laurite, sperrylite, bravoite, cobaltite, gersdorffite, ullmannite and corynite. Their indentation characteristics are as follows; zero anisotropism, indentation types 1, 2(a) weak, strong star radials and shell fractures.

(b) Minerals of the "marcasite" structure

The following minerals of this group were studied; marcasite, loellingite, safflorite, rammelsbergite, pararammelsbergite, arsenopyrite, glaucodot and skutterudite. Their indentation characteristics are as follows; medium - strong anisotropism, indentation types 1, 2(a) weak, 6(a) weak, and strong star radial and shell fractures.

(c) Minerals of the "spinel" type structure

The following minerals of this group were studied; siegenite, linnaeite, violarite and pentlandite. Indentation characteristics of this group are as follows; zero anisotropism, indentation types 1, 2(a) weak, weak star radial and shell fractures.

Oxides

The oxides have been sub-divided into the following groups according to crystal structure and symmetry;

- (a) the hydrated oxides
- (b) oxides of the spinel and hausmannite structures
- (c) other isometric oxides
- (d) Hexagonal oxides of the hematite and zincite structures
- (e) oxides of the "rutile" structure
- (f) Metamict oxides of Cb, Ta, Ti, Tn and U.
- (g) oxides having unique structures.

(a) The hydrated oxides

The following minerals have been studied; manganite, lepidocrocite, merumite, psilomelane, cryptomelane, Chalconphanite, ilvaite, coronadite, goethite and schulzenite.

These minerals show a variety of indentation characteristics which may be summarised as follows: weak - strong anisotropism, indentation types 1, 2(a) weak, weak-strong star radial and shell fractures.

(b) Oxides of the spinel and hausmannite structures

The following minerals of this type were studied; spinel, gahnite, hercynite, chromite, magnetite, franklinite, jacobsite, trevorite, hausmannite and hetaerolite. Indentation characteristics of the group are as follows: very weak anisotropism, indentation types 1, 2(a) weak, occasional weak star radial fractures and occasional dislocations.

(c) Other isometric oxides

The following minerals are included in this group; cuprite, perovskite and bixbyite. Indentation characteristics of these minerals show the following common features; weak anisotropism, indentation types 1, 2(a) weak, 3(a) weak and occasional star radial fractures.

(d) Hexagonal oxides of the hematite and zincite structures

The following minerals are included in this group; hematite, titanohematite, ilmenite, corundum, eskolaite and zincite. Indentation characteristics of the group are as

follows; weak to strong anisotropism, depending upon orientation, indentation type 2(a) weak to strong, and occasional star radial fractures.

(e) Oxides of the "rutile" structure

The following minerals have been included in this group; ilmenorutile, rutile, pyrolusite, cassiterite and thorianite. In addition, anatase, brookite, columbite, tantalite, and struverite have been placed in this group on the basis of the similarity of their structures to rutile. Indentation characteristics of these minerals are as follows; weak anisotropism, indentation types 1, 2(a) weak, no indentation fracturing except for the columbite-tantalites.

(f) Metamict oxides of Cb, Ta, Ti, Th, U

The following minerals of this type were studied; aeschynite, allanite, brannerite, bröggerite, cleveite, davidite, euxenite, fergusonite, formanite and samarskite. Indentation characteristics of these minerals are as follows; zero - weak anisotropism, indentation type 2(a) weak - strong, weak star radial fractures.

(g) Oxides having unique structures

The following minerals were included into this group; tenorite, braunite and the huebnerite-ferberite series. These minerals have different indentation characteristics but the ranges may be summarised as follows; weak to medium anisotropism, indentation types 1, 2(a) weak, slight radial fracturing.

Silicates, phosphates, sulphates, carbonates and tungstates

In general the minerals of this group showed the following characteristics; zero - weak anisotropism, indentation type 2(a) weak, strong radial and shell fractures. Mineral species showing good cleavages exhibit good shell cleavage fractures.

I. The relationship of indentation characteristics to atomic structure

In the following paragraphs a review is given of the possible effects of variations in the structure and bonding of minerals on the deformation characteristics.

Indentation characteristics of minerals are primarily dependent upon the type of movement involved during and after indentation. In minerals that deform by elastic and plastic processes, movement takes place along glide planes, the

positions of which are dependent upon the configuration of the atoms in the structure. In a similar manner, brittle minerals deform by rupture of the structure whose characteristics are also controlled by the atomic configuration. The ease of deformation is controlled by the type and strength of bonding between the atoms in the weakest bond of the structure. Thus it is possible, having an accurate knowledge of their atomic structures, to predict the potential glide planes and glide directions of minerals, and the ease of movement along the planes. Similarly a knowledge of the bond types and bond strengths between atoms in minerals should enable predictions to be made concerning their mechanisms of deformation.

In metallic bonding, movement takes place easily due to a "loose" electronic configuration. The direction and ease of movement is controlled by factors such as atomic radii, coordination number, etc. The easy movement results in maximum anisotropism, complex sided indentations, and an absence of fractures. In ionic bonding, movement takes place by gliding along planes in directions which maintain the electronic stability. When gliding takes place in other directions, cleavage fractures are produced. In some cases where no gliding is possible, radial shell fractures are produced. The direction and ease of movement are controlled

by the following factors; the atomic structure, the ionic radii of the atoms, the valency of the atoms and the coordination number. In covalent bonding, where electrons are shared, deformation takes place by rupture of the bond which normally results in non planar fractures. Thus one may conclude that covalent compounds are both hard and brittle. Residual bonding - frequently the bonding across cleavage planes - is a very weak force and deformation takes place by rupture along these preferred planes.

The anisotropism of an indentation is a function of the orientation of the mineral grains tested. The range of anisotropism with orientation is dependent upon the number and attitude of the glide planes which are themselves an expression of the atomic structure and bonding.

The shape of an indentation is thus an expression of the anisotropism and strength of the elastic and plastic properties of a mineral.

Discussion of the results

The results obtained confirm the above suppositions. It is apparent that minerals of similar structure and bond type show similar indentation characteristics and that variations in the characteristics from one group to another

are dependent mainly upon the chemical composition and the type of bonding. A detailed comparison of indentation characteristics with microhardness will be made in Chapter VII.

Few minerals are completely metallic ionic or covalent. Rather they contain some proportion of all the different types, (Goldschmidt, 1954), and it is the dominant bond type which appears to control the indentation characteristics. Thus, the lack of fracturing in some of the simple sulphides, selenides and tellurides is due to the presence of metallic bonding in the structures. It is also of interest to compare the different characteristics of the "spinel" structured sulphides of Fe, Co, Ni e.g. linnaeite, violarite, etc., with those of the "spinel" structured oxides such as magnetite and chromite. Both groups of minerals show high hardness values but the sulphides show considerably more indentation fractures than the oxides. The difference may be attributed to the higher percentage of covalent bonding in the sulphides than in the oxides.

The gold tellurides, i.e. sylvanite, calaverite and krennerite show strong fracture characteristics in contrast to the more metallic characteristics of the tellurides of Pb, Hg, Ag, and Cn. This may be attributed to the presence of covalent bonding in their structures which would also explain

their comparatively hard hardness values. Sulphosalts having chain structures such as stibnite or bismuthinite have weak residual bonds linking the chain together. These minerals show strong cleavage fracture characteristics as compared with the weak and irregular fractures of other sulphides such as tetrahedrite and tennantite.

The sulphosalts and the multiple oxides are exceptions to the general rule that increasing hardness of minerals is accompanied by increasing brittleness.

The strength of anisotropism of the indentations is an expression of the symmetry of the structure and hence of the movement planes. Thus minerals such as copper, gold, galena and sphalerite show less anisotropism than arsenic, antimony, stibnite or bismuthinite. Anisotropism is more pronounced in metallic and ionic crystals, and those with residual bonds, as these bond types allow plastic and elastic movement to take place. In general, the amount of anisotropism of indentation in minerals decreases with increasing hardness. This is also indirectly due to the effect of the increasing effect of covalent bonding in the atomic structure with increasing hardness. Exceptions to this general rule do occur, e.g. marcasite and löllingite.

As the movement planes in minerals are a function of the atomic structure and bond type, and not to the density of

packing etc., the "apparently anomalous" anisotropism of optically isotropic minerals is in accordance with expectations. Conversely the complex covalent network structures of some of the silicates, phosphates, etc. result in indentations of negligible anisotropism.

The variation in the shapes of indentations is a function of the elastic and plastic properties of the minerals. In the softer minerals, where metallic bonding is important convex and concavo-convex sided impressions are relatively common showing that extensive plastic deformation takes place. In minerals of intermediate hardness, such as the sulphosalts, concave and convex sided impressions occur together with fracturing, indicating that elastic, plastic and rupture deformation all take place. These minerals have a complex mixture of bond types. In the harder minerals, concave sided impressions are common and are often associated with radial and shell cracks. These indentation characteristics indicate that elastic recovery is relatively more important than plastic deformation. Exceptions to these trends do occur e.g. niccolite and breithauptite.

Use of indentation characteristics in mineral identification

Bowie and Taylor (1958) showed how, in some instances, the nature of the indentations could be of diagnostic value

in mineral identification. They found that chalcopyrite and pentlandite, two minerals of similar hardness, could be distinguished on the basis of differences in shape; chalcopyrite showing straight sides and pentlandite showing concave sides. However, such techniques were considered as additional aids to a system of mineral identification based on microhardness and reflectivity values. As a result of joint work (Gray and Young, 1960), it was concluded that the system proposed by Bowie and Taylor for mineral identification was a useful one. Thus the additional data from the indentation characteristics need only be used as an aid to this system.

It has been shown in the previous section that the minerals can be grouped according to their particular indentation characteristics. In addition, it was noted that different mineral species of the same group have different diagnostic features by which they may be distinguished from one another. Such a system, incorporating all the new data, would assist in pin pointing the identity of an unknown mineral. However several drawbacks to this system exist:

- (a) Ranges of indentation characteristics occur with differing orientations.
- (b) Indentation characteristics, particularly fracture phenomena, are unreliable on very small grains.

(c) The fracture characteristics of minerals, like microhardness values, are dependent upon the load.

The differences of indentation characteristics with orientation are sometimes considerable, in a similar manner to the anisotropism of the reflectivity and microhardness values. If a number of indentations are made on grains of differing orientation, then a more complete range of characteristics will result. The fracturing that occurs around indentations made on small grains is a serious drawback, and this would imply that the minimum grain size for identification using fracture characteristics would have to be increased. As the fracture characteristics of minerals decrease in intensity with decrease of load, several standard loads would have to be used.

The results obtained so far indicate that the observations of the indentation characteristics would be useful in helping to identify unknown ore minerals, and in attributing possible "bond-type" structures to them. Such data could perhaps be best employed in a punched card system combining optical and reflectivity determinations with microhardness data.

TABLE XXXIV

Translation Data Deduced from the Present Studies

(a) Deduced translation data from the present studies compared with established translation data.

Mineral	Translation data deduced from present studies (T) ¹	Translation data established by other workers (T) ¹
Bismuthinite	(010)	(010) ^o
Chalcocite	(110)	(201)(131) ^o
Copper	(111)	(111) [≠]
Covellite	(0001)	(0001) [≠]
Cubanite	(110) and/or (1 $\bar{3}$ 0)	(001) [≠]
Galena	(100)	(100) [≠]
Gold	(111)	(111) [≠]
Halite	(110) and/or (111)	(110)(111) ^o
Hematite	(10 $\bar{1}$ 0) and (0001)	(0001) [≠]
Kyanite	(001)	(001) [≠]
Manganite	(010)	(010) ^o
Mangantantalite	(100)	(100) ^o
Molybdenite	(0001)	(0001) [≠]
Pyrrhotite	(10 $\bar{1}$ 0) or (11 $\bar{2}$ 0)	(0001) [≠]
Sphalerite	(111)	(111) [≠]

TABLE XXIV Contd.

Mineral	Translation data deduced from present studies (R)'	Translation data established by other workers (T)'
Stibnite	(010)	(010) ^o
Teallite	(010)	(010) ^o

' Translation plane

^o Taken from Palache et.al. (1944)

* Taken from Ramdohr (1951)

^ Taken from Winchell (1951)

TABLE XXXIV Contd

(b) Translation data deduced from present studies (no translation data previously recorded)

Mineral	Translation plane (T)'
Arsenopyrite	(101)
Cinnabar	(10 $\bar{1}$ 0)
Corundum	(0001) and/or (10 $\bar{1}$ 1)
Cuprite	(111)
Enargite	(110)
Eskolaite	(0001) and/or (10 $\bar{1}$ 1)
Fluorite	(111)
Franckeite	= (010)
Gypsum	(010)
Huebnerite	(010)
Nagyagite	(010)
Pyrargyrite	(10 $\bar{1}$ 4)
Pyrochlore	(111)
Pyrolusite	(110)
Spinel	(100)
Stephanite	(110)
Tellurium	(10 $\bar{1}$ 0)
Topaz	(001)
Wurtzite	(10 $\bar{1}$ 0) or (11 $\bar{2}$ 0)

TABLE XXXV

Deformation Characteristics of the Main Mineral Groups

Mineral Group	Microhardness deform ²		Characteristics Fracturing and gliding
	Anisotropism	Shape	
Metals and Semi-Metals	medium-strong	cc,cv, sig.	f. none. str. glide pl. trvs.
Simple Sulphides, selen- ides and tellurides	medium-strong	cc, cv, sig. cc.-cv.	slight f. sl. glide planes
Complex sulphides of Cu, Fe, Ni	weak-medium	cc-str. cc-cv sig.	slight f. some gl. pl. trs.
Sulphosalts	isotropic- strong	cc,cv, sig. str.	med-strong f. occ. gl. pl. trs.
Co, Ni, Fe, sulphides, sulpharsenides, sulph- antimonides	isotropic- strong	cc,cv, sig. str.	weak-strong f. occ. gl. pl. trs.
Oxides	isotropic- weak	cc, str.	weak-med f. occ. gl. pl. trs.
Hydrated oxides	weak-strong	cc, str.	med. strong f. no gl. pl. trs.

TABLE XXXV Contd.

Mineral Group	Microhardness deform ⁿ		Characteristics
	Anisotropism	Shape	Fracturing and gliding
Silicates, phosphates, sulphates, carbonates, tungstates	weak-medium	cc- str.	weak to strong f. no gl. pl. trs.

CHAPTER VI

Variation of Microhardness with Changes of Chemical Composition

A. Introduction

As described in Chapter I, variations in hardness for isostructural metallic and ionic bonded minerals can be correlated with valency and atomic radii. Hardness decreases with increasing atomic radii and increases with increase of valency. For minerals with covalent bonding, hardness decreases with increasing bond length. This early work by Goldschmidt (1926) and others, has recently been confirmed by Povarennykh (1959)

Several authors have investigated the variations of microhardness with variations in chemical compositions in isomorphous series. Henriques (1957) showed that increasing iron content in sphalerite could be related to increasing Vickers microhardness values. He suggested that the variation in microhardness was analogous to the hardening of iron caused by the addition of nickel and manganese. The resultant substitution causes a distortion of the crystal lattice resulting in increased hardness.

Microhardness variations in pentlandite and the cobaltiferous analogues of pentlandite have been reported by Kouvo, Hukna and Vuorelainen (1959), but no correlations

were made with variations in chemical composition.

The first investigation of the microhardness variations of a complete isomorphous mineral series was made by Mookherjee and Sahu (1960). In studying the plagioclase series, albite-anorthite, it was found that increasing microhardness was associated with increasing albite content, apart from the range, $An_{25} - An_{65}$. No theoretical explanation was given for the microhardness variations.

Variations in structure caused by the non-stoichiometry of minerals are potential sources of microhardness variations. The non-stoichiometry of synthetic PbS crystals are considered by Bloem and Kroeger (1955) to be the cause of microhardness differences, a minimum hardness being concordant with minimum non-stoichiometry.

It was decided to investigate the microhardness/chemical composition relationship for the following isomorphous series: sphalerite-christophite (varying iron content); hübnerite-ferberite (variation in Fe/Mn ratio); columbite-tantalite (variation in the Fe/Mn and Nb/Ta/Sn ratios). Variations of Vickers microhardness on the cube face of a particular galena crystal were investigated, there being indications that non-stoichiometry may be the cause of the variations. In addition, several end members of

isomorphous series - metals, sulphides, sulphosalts, and oxides - have also been investigated for microhardness variations. The results of this work may be found in Tables XXXIX - XLIV.

B. Microhardness Variations in Chemically Analysed Isomorphous Series.

(a) Sphalerite

Ten crystalline specimens of sphalerite, having different iron contents, were analysed for Fe, Mn and Cd. For details of the methods and results of the chemical analyses the reader is referred to Appendix B.

Cleavage fragments of the crystals were mounted in cold setting plastic so that the (110) cleavage faces were oriented parallel to the bases of the mounts. The crystals were then polished parallel to the (110) faces, the polishing technique being carefully controlled so that each section was given a similar amount of polish. Ten impressions were made on each polished section of sphalerite, each impression being made at an angle of 10° horizontal rotation to the previous one. Mean microhardness values are given in Table XXXVI, together with chemical analyses for iron and

TABLE XXXVI

Microhardness Mean Values for 10 Analysed Sphalerites

Ref. No.	Sphalerite No.	Chem. Analysis No.	V.M.H. Mean	K.M.H. Mean	%Fe	%Cd.
559	10	5594	181	170	10.70	0.3
587	7	5591	189	199	5.96	0.1
561	2	5586	192	185	4.08	0.3
535	3	5587	194	211	2.36	0.2
536	4	5588	199	197	1.20	0.2
598	8	5592	187	191	1.17	0.5
565	6	5590	182	160	0.61	0.1
601	9	5593	156	156	0.20	0.4
606	5	5589	152	151	0.10	0.1
549	1	5585	159	158	0.07	0.1

cadmium. Fig. 63 shows a graph of Vickers and Knoop microhardness mean values plotted against the iron content. Fig. 64 shows similar plots of Vickers microhardness against iron content obtained by Henriques (1957).

In general, the present results are in agreement with those of Henriques, i.e. increasing iron content results in increasing microhardness up to approximately 6%, by weight, of Fe. In both cases the increase of microhardness appears to be a function of the logarithm of the iron content. Above 6% Fe however, the present results suggest that the microhardness decreases with increasing iron content, microhardness being a maximum at between 2 and 3% Fe. The probable errors of the mean values do not exceed ± 4 microhardness units, except in the case of Sph. 3, whose microhardness mean values have probable errors of ± 7 microhardness units. It is therefore difficult to account for the large deviation of the graph from the straight line relationship above 6% Fe, on the grounds of inaccurate measurement. Henriques (1957), in discussing the causes of microhardness variations in sphalerite, points out that minor structural defects, such as sub-microscopic fractures may cause significant microhardness variations. It seems unlikely that such defects could cause differences of up to 40 microhardness units, between the values extrapolated by

FIG. 63

PLOT OF VICKERS AND KNOOP
MICROHARDNESS VALUES AGAINST
% Fe FOR 10 ANALYSED SPHALERITES
100g load ; (110) faces

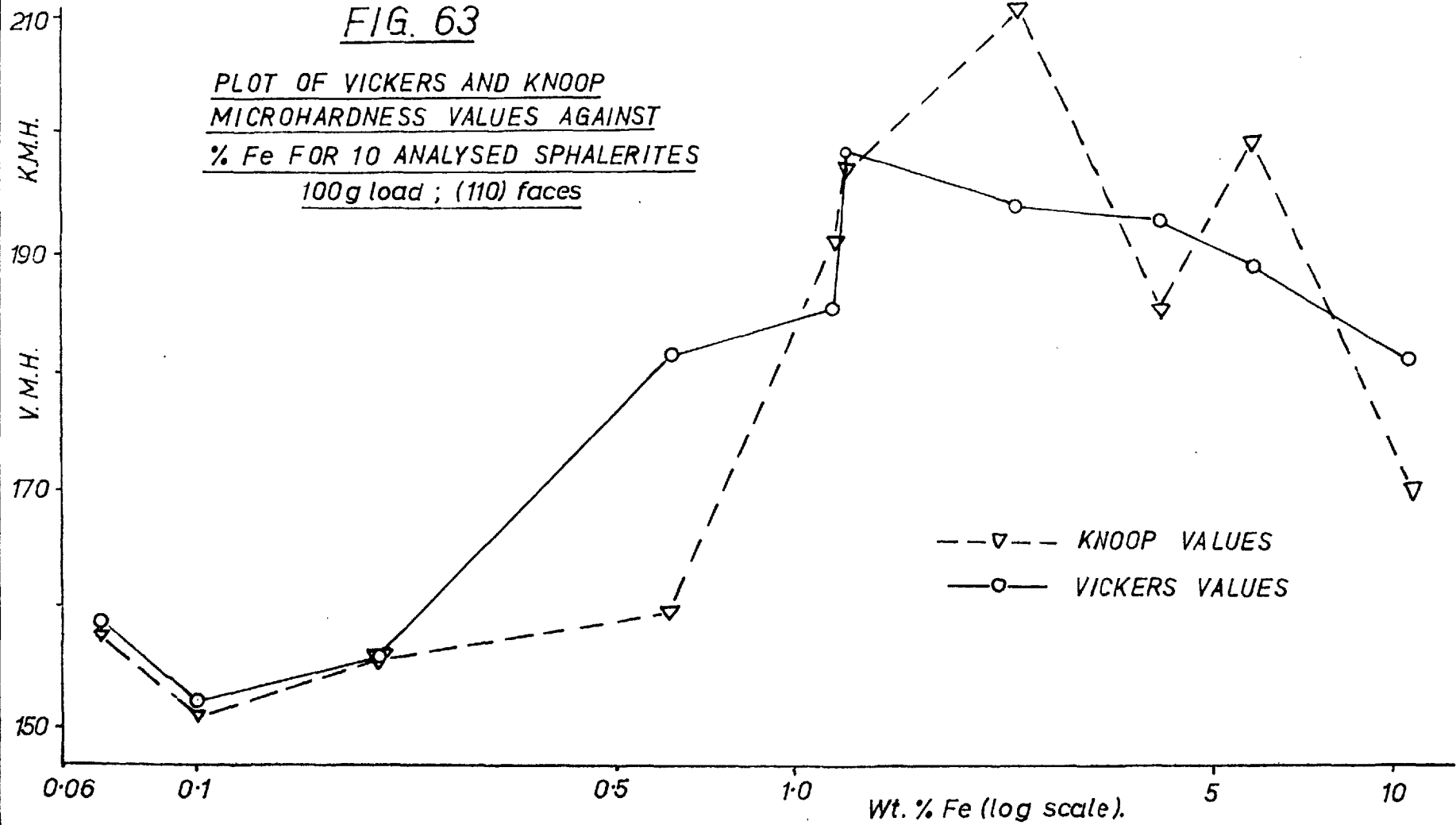
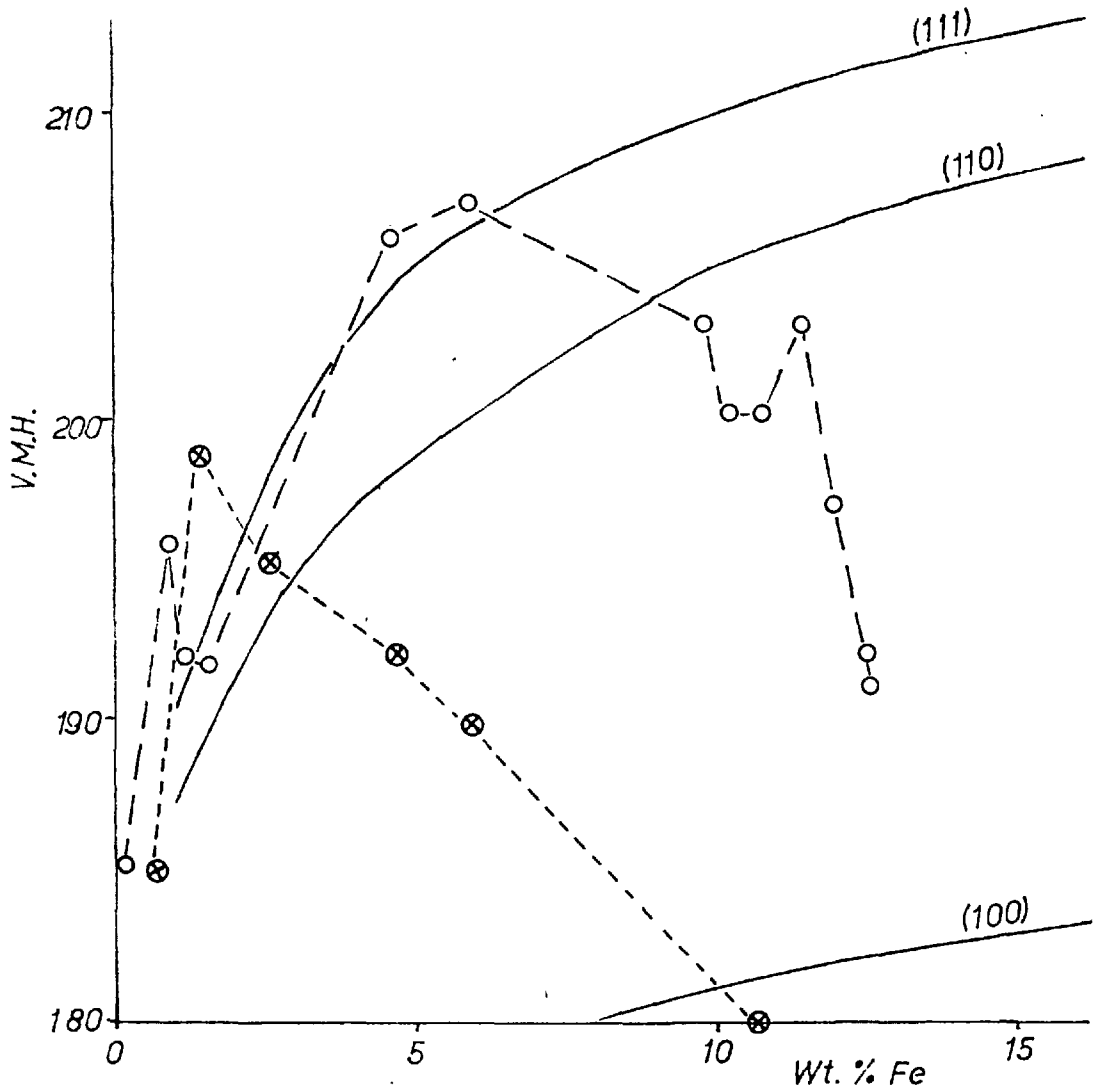


FIG. 64

PLOT OF VICKERS MICROHARDNESS
VALUES AND % Fe IN SPHALERITE



- Henriques "plots" for the (111), (110) and (100) faces
- - o - - Unoriented values obtained by Henriques
- - ⊗ - - Plots for (110) faces - (B.B.Y.)

Henriques and value obtained in the present investigation, for sphalerite containing approximately 10% Fe.

An alternative explanation of the present results is that at high iron concentrations in sphalerite, a more ordered structure occurs. It is well known, Edwards (1947), that when sphalerite contains excess iron in the lattice, the iron exsolves as pyrrhotite laths in the (111) planes of the sphalerite. One can visualize the state just prior to exsolution where the Fe and Zn atoms segregate themselves into a ordered structure i.e. along (111) planes. It has been shown by Buerger (1928), that deformation in sphalerite occurs by movement along (111) planes. The result has also been confirmed by orientation studies, described in Chapters IV, V. Slip during indentation will occur with greatest ease when the (111) movement planes are not distorted. Minimum distortion occurs when the iron content is zero and when the structure is ordered i.e. when the Zn and Fe atoms are segregated into separate planes. No exsolution pyrrhotite was observed in any of the sphalerite crystals examined.

A similar peak value of microhardness, at between 5-6% Fe is indicated by the results shown in Fig. 64. The mean microhardness values obtained by Henriques on unoriented aggregates of 15 sphalerite specimens having

iron contents ranging from 0.39% to 19.5% Fe, are plotted against iron content. Some of the spread in the results is undoubtedly due to orientation effects but in most cases the mean values were obtained from large ranges of readings.

The above explanation is based on the results obtained from a small number of analysed samples. Further work is required to substantiate this theory.

(b) The Huebnerite - Ferberite Series

Ten crystalline specimens of wolframite were analysed for their iron/manganese ratio. Details of the method and the results are given in Appendix B.

The crystals were cut and then ground such that sections were obtained parallel to the (100), (010) and (001) faces of each wolframite crystal. These crystals were mounted in cold setting plastic such that when polished, accurately oriented sections parallel to (100), (010) and (001) resulted. Ten Vickers indentations were made on each face, oriented such that the diagonals of the indentations were parallel to the crystallographic axes of the crystals. Mean microhardness values for each face are plotted against the percentage of MnO, by weight, in Fig. 65.

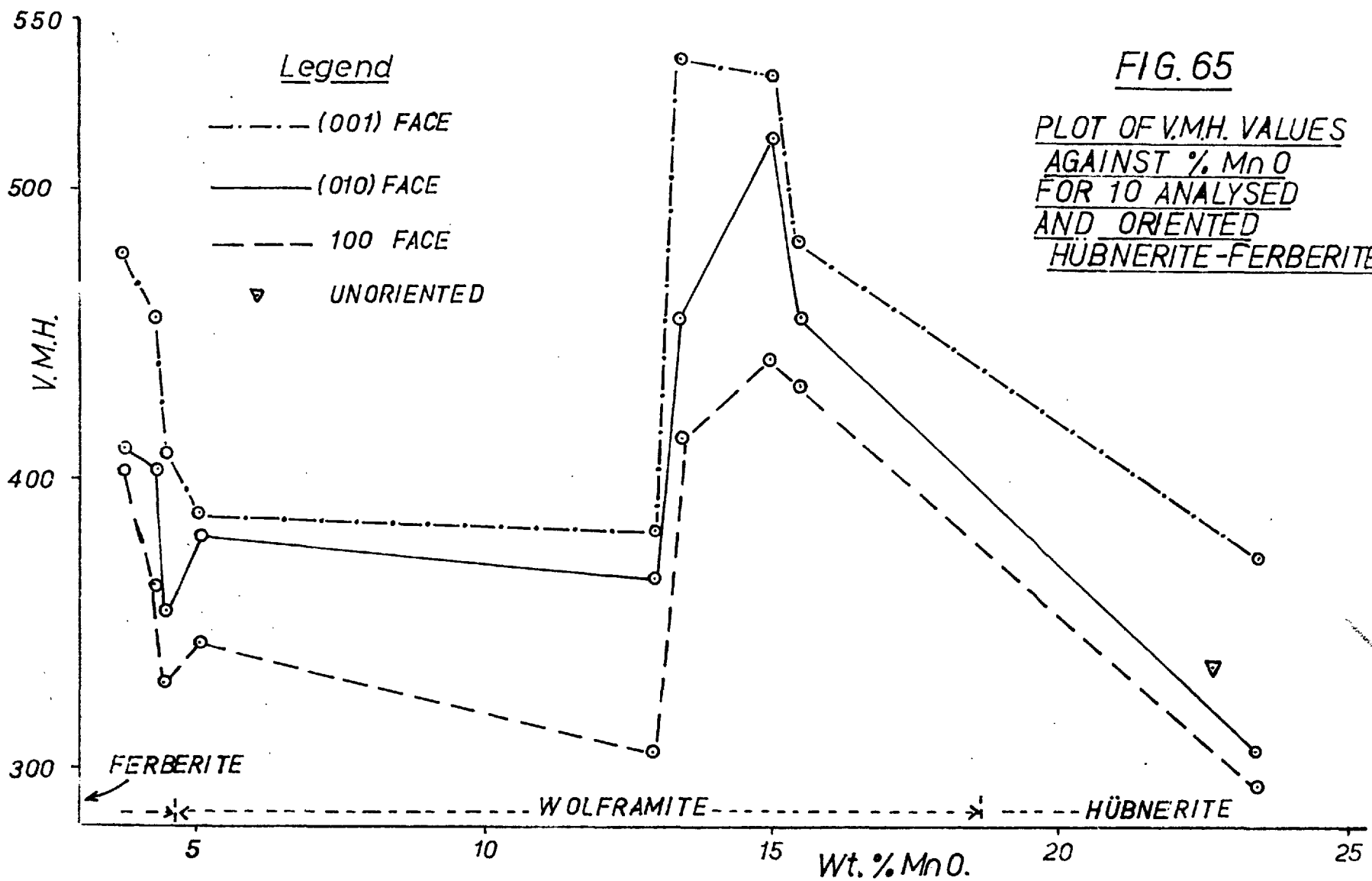
Palache, et. al. (1944), state that the scratch hardness in the wolframite series is greatest in the iron rich members.

FIG. 65

PLOT OF V.M.H. VALUES
AGAINST % MnO
FOR 10 ANALYSED
AND ORIENTED
HÜBNERITE-FERBERITES

Legend

- (001) FACE
- (010) FACE
- - - 100 FACE
- ▽ UNORIENTED



The results in Fig. 65 confirm that the ferberites are harder than the huebnerites. However, there appears to be no linear relationship, for the wolframites, between microhardness and iron content. In fact, anomalously high microhardness values were obtained on the wolframites containing approximately equal amounts of Mn and Fe.

According to analyses listed by Palache et. al. (1944), there is very little substitution of iron or manganese by other elements except for small amounts of Cb and Ta. Increased hardness in the series may be caused by such substitution. However, a more likely explanation of these high hardness values is that high hardness is caused by distortion of the crystal lattice. In a crystal structure where random distribution of unequally sized Fe and Mn ions occurs, ($\text{Fe}^{++} = 0.83$, $\text{Mn}^{++} = 0.91$), distortion should be a maximum where the ratio of Fe to Mn atoms is approximately equal to unity. Thus maximum hardness occurs in the wolframite group where the Fe/Mn ratio equals unity.

As only ten analysed wolframites have been tested no concrete conclusions may be drawn at this stage. Further work is needed to ascertain the structure of the anomalously hard wolframites.

TABLE XXXVII

Microhardness values obtained on 10 analysed huebnerite-ferberites

Ref. No.	Chem. Anal. No.	Wolf-feramite No.	V.M.H. MEAN VALUES			Calculated %FeO	Calculated %MnO	
			(100)	(010)	(001)			
1429	5600	6	403	411	478	19.9	3.8	
1426	5595	1	363	403	456	19.4	4.3	
1431	5604	10	330	354	409	19.2	4.5	
1425	5602	8	344	380	389	18.6	5.1	
1430	5603	9	305	366	383	10.7	13.0	
1424	5601	7	402	457	548	10.3	13.4	
1428	5599	5	442	519	540	8.7	15.0	
1427	5598	4	433	456	484	8.2	15.5	
1422	5597	3	UNORIENTED			336	1.7	22.7
1421	5596	2	294	307	375	0.3	23.5	

(c) The Columbite - Tantalite Series

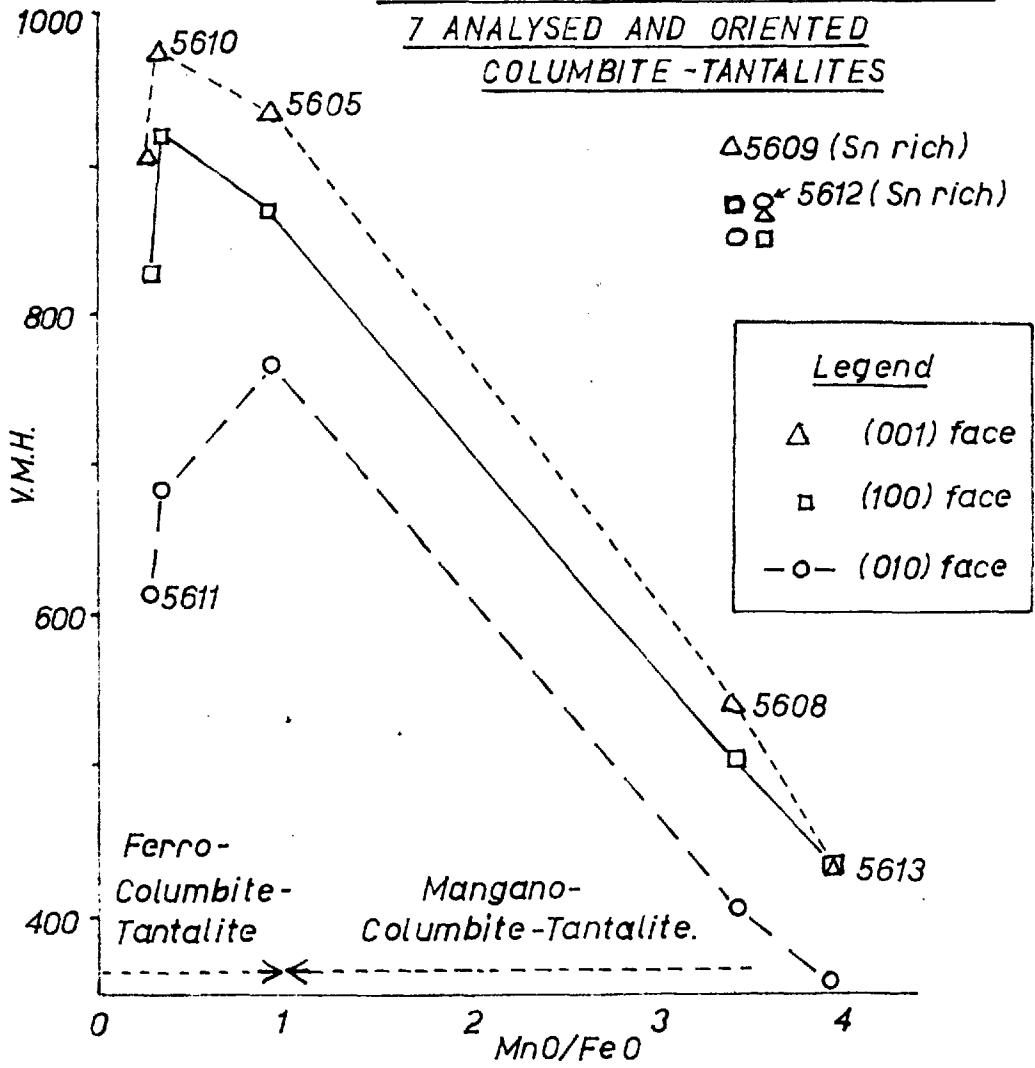
Seven columbite-tantalite crystals of different chemical compositions were analysed for their Fe/Mn and Nb/Ta ratios and for their amount of tin. Details of the methods and of the results of the chemical analyses are given in Appendix B.

Polished sections of the crystals were made parallel to the (100), (010) and (001) faces, in a manner similar to that described for the huebnerite-ferberite series. Ten Vickers indentations were made on each face oriented such that the diagonals of the indentations were made parallel to the crystallographic axes. The mean microhardness results, together with chemical analyses, are given in Table XXXVIII. Fig. 66 shows a plot of the mean microhardness values plotted against the MnO/FeO ratio.

Palache, et.al. (1944) note that tantalite ($H = 6 - 6\frac{1}{2}$) is slightly harder than columbite ($H = 6$). The results of the present work indicate that the microhardness of the series is controlled by the Fe/Mn ratio and/or the Nb/Ta ratio and also by the content of Sn. It is unfortunate that no crystals of ferro-tantalite or manganocolumbite were included for analysis. In the samples analysed high iron content was associated with high niobium content, and

FIG. 66

MICROHARDNESS: MnO/FeO PLOT FOR
7 ANALYSED AND ORIENTED
COLUMBITE-TANTALITES



Ferro-Columbite-Tantalite Mangano-Columbite-Tantalite.

FERRO-COLUMBITE

MANGANTANTALITE CONTAINING TIN

MANGANTANTALITE

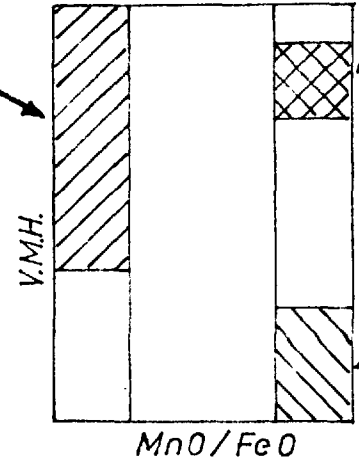


TABLE XXXVIII

Microhardness values for 7 analysed columbite-tantalites and 3 other minerals containing rare earth elements

Ref. No.	Chem. Analysis No.	Columbite Tantalite No	V.M.H. MEAN VALUES			MnO	FeO	Pb ₂ O ₅	Ta ₂ O ₅	SnO ₂
			(100)	(010)	(001)					
1393	5611	C.T.7	829	612	905	2.4	11.6	64.6	8.0	n.d.
1392	5610	C.T.6	920	680	967	2.2	7.09	35.1	25.8	n.d.
1390	5605	C.T.1	864	764	939	5.21	5.73	37.3	39.1	n.d.
1394	5612	C.T.8	856	877	871	6.56	1.75	31.1	32.1	0.4
1388	5613	C.T.9	431	362	430	7.00	1.8	14.4	50.4	n.d.
1387	5608	C.T.4	505	405	546	6.90	1.8	14.7	51.2	0.2
1391	5609	C.T.5	876	856	916	6.51	1.8	9.0	60.5	1.1
1381	5614	C.T.10	Unoriented, 947-ilmenorutile			1.4	6.40	22.9	10.0	2.64
1382	5615	C.T.11	Unoriented, 1081-strüverite			1.3	8.32	27.6	12.3	0.7
1383	5616	C.T.12	Thoreaulite - mean Value 637			0.8	1.8	4.0	57.0	22.0

manganese with high tantalum. It was therefore impossible to differentiate between the effect on the microhardness by the Fe/Mn ratio and the Nb/Ta ratio. By comparison, the effect of the presence of tin appears to be quite clear, i.e. to raise the microhardness of the mineral from the normal. Corresponding differences were observed in the reflection characteristics of the tin rich columbite-tantalites, e.g. loss of anisotropism and a lower reflectivity - (pers. comm. I.M. Gray). (An exception to this trend was found in sample 5608, which contains 0.2% Sn but show no great increase in microhardness.) The increase in the hardness of these columbo-tantalites containing tin is probably due to distortion produced by the introduction of Sn⁺⁺⁺⁺ ions.

From a theoretical point of view, the difference in hardness between ferrocolumbite and mangantantalite is more likely to be due to differences in the Fe/Mn ratio than the Nb/Ta ratio. The ionic radii of the elements concerned are given by Evans (1948), as follows:

Nb ⁵⁺	= 0.69
Ta ⁵⁺	= 0.68
Fe ²⁺	= 0.83
Mn ²⁺	= 0.91

The difference between the ionic radius of Nb⁵⁺ ions

and Ta^{5+} is small - 0.01, and from the Goldschmidt Rule (Goldschmidt, 1926) the presence of Ta^{5+} ions, having the smaller ionic radius, should increase the hardness of a mineral, relative to Nb^{5+} ions. The difference between the ionic radii for Mn^{2+} and Fe^{2+} ions is large - 0.08. Thus, Fe^{2+} ions should raise the hardness of a mineral more than Mn^{2+} ions. The huebnerite - ferberite series, by comparison, shows a definite variation in sympathy with the Goldschmidt Rule. From this argument it may be predicted that manganocolumbite will have the same hardness as manganotantalite, and ferrocolumbite the same hardness as ferrotantalite.

It is also of interest to note that a maximum micro-hardness occurs when the Fe/Mn ratio approaches unity, a manner similar to the anomalously hard wolframite crystals. However, the results so far underline the need for further work on this series in order that more definite conclusions may be drawn.

(d) Variations of Microhardness across the Cube Face of a Galena Crystal from Pfatterburg Mine, Harz, Germany

In the course of routine orientation studies, significant differences of Vickers microhardness were found across the cube face of a galena crystal from Pfatterburg Mine, Harz, Germany. The original cube face, before polishing, exhibited a "stepped-inlay" structure. A similar structure is shown in photograph A of an adjacent crystal. The difference in level between the two layers was approximately 1 m.m., and comparable to the difference shown in photograph A. The crystal was carefully polished by hand parallel to the original cube face such that the outer "zone" of the inlay structure was just removed. A series of microhardness indentation traverses were made across the polished face at different loads, the orientation of the diagonals of the indenter being kept constant i.e. i.e. parallel to the (100) cleavage traces. Plots of the mean diagonal lengths of the indentations obtained at 25 g. load across the face are given in Fig. 67. The crystal was then etched with a 3 : 1 mixture of concentrated nitric acid and ethyl alcohol for about ten seconds. Two well defined zones were brought out by this etching - photograph B. It was apparent that the shape of the zoning was identical with the shape of the original inlay structure.

Photograph A

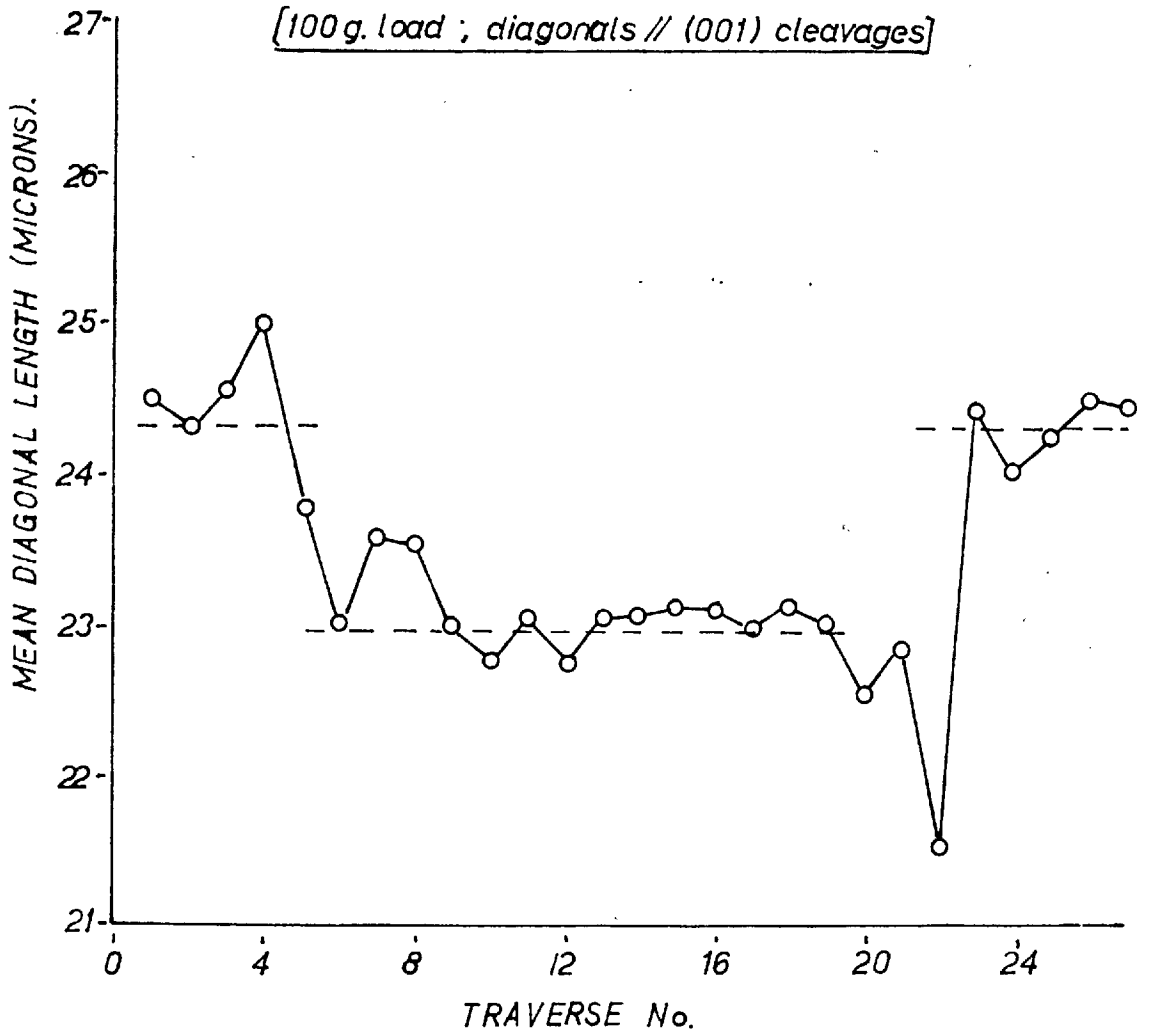


Photograph B



FIG. 67

PLOT OF MEAN INDENTATION DIAGONAL
LENGTHS FOR A TRAVERSE OF VICKERS
INDENTATIONS MADE ON THE (100) FACE
OF A GALENA CRYSTAL
FROM PFATTERBURG MINE, HARZ.
[100 g. load ; diagonals // (001) cleavages]



From Fig. 67 it can be seen that the "outer" etched zone exhibited a distinctly lower hardness than the "inner" zone. The boundary between the two etched zones is marked by a sharp change in microhardness values.

Small amounts of the galena were drilled from the inner and outer zones and spectrographically analysed for trace amounts of the following elements; Bi, Se, Te, Cd, Cu, Zn and Fe. No significant amounts of these elements were detected in either zones.

The crystal was then mounted in cold setting plastic, repolished, and etched as before with a 3 : 1 mixture of nitric acid and ethyl alcohol for ten seconds. Two very indistinct zones were produced, approximately similar in shape to the first etch zones.

The zone boundaries were then scanned using an X-ray microanalyser, manufactured by Cambridge Instruments Ltd., for variations in the content of Pb, Bi, S, Se and Te. No significant variations were recorded and the amount of Se and Te was estimated as being less than 1% (pers. comm. T. Kelly).

Check traverses of indentation were made across the etch boundaries, but no significant microhardness differences were recorded. Lack of time prevented control work to be done on another similarly featured crystal.

(e) Discussion

It seems clear from the results that the microhardness variations across the original polished face were, in some way, connected with a variation in the chemical composition. The possibility that the variations were due to orientation effects was eliminated by observations made on the (100) cleavage traces. Across the entire surface tested two sets of (100) cleavage traces were observed at right angles to one another. Spectrographic results indicate that the variations are not due to trace element variations. Results of X-ray microanalysis indicate that the second polished surface contained very low amounts of Se, Te and Bi, the amount of Se and Te being less than 1%.

An alternative explanation of the results is that non-stoichiometry of the galena crystal is a cause of the variations. Bloem and Kroeger (1955) showed that for artificially produced PbS crystals, a high concentration of vacancies of either Pb or S increases the microhardness. Minimum hardness occurs when the concentration of vacancies is a minimum.

If such non-stoichiometry did occur in the original polished surface then a significant difference in the Pb/S ratio would have been expected. From the weakness of the

etch reactions and the lack of microhardness variations on the second polished surface, it would appear that the thickness of the zoned part of the crystal removed by polishing is very small - about 2 - 3 mm.

The possible causes of the microhardness variations are as follows;

- (a) Variation due to orientation.
- (b) Variation due to trace element substitution.
- (c) Variation due to substitution of Te, Se and Bi.
- (d) Variation due to non-stoichiometry.

The first three potential causes of non-stoichiometry have been eliminated and it is therefore suggested that non-stoichiometry may have been the cause of the microhardness variations on the original surface.

C. Microhardness Differences Between End-Members of Isomorphous or Isostructural Series (not Chemically Analysed).

The microhardness values obtained for end-members of isomorphous series and for isostructural series are given in Tables XXXIX - XLIV. Tables XLV, XLVI give the atomic, ionic and covalent radii for the substituting elements.

(a) Discussion of the Results

The bulk of the results are in agreement with the first of Goldschmidt's rules (Goldschmidt 1926), in that the hardness of a mineral in any given isostructural series decreases with increase of interatomic distance. Several exceptions to this rule have been found, and these results are discussed more fully below. The microhardness results from the present work are compared with other hardness data, particularly those values obtained by Nakhla (1956), Bowie and Taylor (1958), Uytendogaardt (1951), Palache, Berman and Frondel (1944) and Povarennykh (1959). It is convenient to discuss the microhardness results in Tables XXXIX - XLIV under the following headings:

- (i) Native Metals
- (ii) Sulphides, selenides, tellurides
- (iii) Arsenides, etc.

- (iv) Sulphosalts
- (v) Oxides
- (vi) Carbonates, phosphates.

(i) The native metals

The microhardness of the native metals examined (Table XXXIX) are in total agreement with the Goldschmidt Rule and are in accordance with the Mohs' scale hardness values given by Palache et. al. (1944), the Talmage scratch values listed by Uyttenbogaardt (1951), and the microhardness values given by Nakhla (1959). No "alloy" metals, such as stibarsenic and arsenical copper, have been included in the table. Since no check chemical analyses were made, and only a limited number of specimens were tested, the microhardness values should be only tentatively accepted until further work has been carried out. The effect of the process of "alloying" on the hardness of synthetic metals is well known and this factor probably explains the discrepancies found by Bowie and Taylor (1958) in the arsenic antimony, bismuth group:

$H_{As} > H_{Sb} > H_{Bi}$ present work and others.

$H_{Sb} > H_{As} > H_{Bi}$ Bowie and Taylor.

(ii) The sulphides, selenides and tellurides.

The chalcocite, sphalerite and galena groups show microhardness values (Table XL) which are concordant with Mohs' and Talmage hardness values, and in agreement with the Goldschmidt Rule. Similarly, the microhardness values for the hessite, naumannite, eucairite group reflect the effect of the substitution of Cu and Te into the structure. Whilst these microhardness values are concordant with scratch hardness data, it is interesting to note that Bowie and Taylor obtained mean values of 148 and 33 for naumannite and hessite respectively. Thus we may conclude that the high value of 148 for naumannite is probably incorrect.

Although no differences in scratch hardness have been reported between stibnite and bismuthinite, the present results indicate differences in indentation microhardness. An explanation has already been given, Chapter IV, for this apparently anomalous hardness relationship. This may be summarised as follows: The stibnite-bismuthinite series has a chain structure comprising Sb or Bi atoms strongly bonded (covalent) to S atoms. Adjacent chains are weakly attached to one another by means of Van der Waal bonds. Whilst the substitution of Sb atoms (small atomic radii) for Bi atoms increases the strength of the individual chains, it weakens

the Van der Waal bond between chains. This results in easier deformation, (by gliding (010) planes), and consequently greater hardness in stibnite than in bismuthinite

The microhardness values for the siegenite group indicate that differences of chemical composition cause differences in hardness. The atomic radii of the transition elements in the sulphide and arsenide groups vary in relation to one another according to the type of bonding existing between themselves and the anionic elements. Thus, Evans (1948), Table XLV gives the ratio of the ionic and metallic radii as being $Fe > Co > Ni$; Goldschmidt (1954) gives the ratio of the semi-metallic radii as being $Fe > Ni > Co$; Pauling and Huggins (1934) gives the ratio of the covalent radii as being $Ni > Co > Fe$. As the type of bonding is not known for the siegenite group it is difficult to assess which elements cause the lower hardness of violarite. If a metallic, ionic or semi-metallic type of bonding is dominant then the decrease will be due to iron. Conversely, if covalent bonding is dominant, then the lowering of the hardness will be due to the presence of nickel. From the high reflectivity of the group, (Gray, 1961), it seems probably that the metallic type of bonding is dominant.

Table XLVII shows the microhardness values and chemical compositions of three naturally occurring cobalt-bearing

analogues of pentlandite, (Kuovo, Hukma and Vuoralainen, 1959). Hardness increases with increasing cobalt content, and decreasing iron and nickel content. Reflectivity measurements on pentlandite (Gray, 1961) indicate that the mineral group has a predominantly semi-metallic type of bonding. The microhardness values are in agreement with the Goldschmidt Rule, on the assumption that the bond type is semi-metallic.

The values for the pyrite group are in accordance with Goldschmidt, taking into consideration the octahedral covalent radii of Pauling and Huggins (1934), with the exception of laurite. No explanation can be given, on crystallochemical grounds, for the extremely high hardness of laurite.

(ii) The Arsenides

All the sub-groups within the arsenides, apart from niccolite and breithauptite, show microhardness values that are concordant with the Goldschmidt rule, assuming that the bonding in these minerals is dominantly "semi-metallic" in character. The cobaltite group exhibit microhardness values in accordance with Mohs' and Talmage hardness values, and to microhardness values given by Bowie and Taylor. For the diarsenide and arsenopyrite groups, Mohs' and Talmage

hardness values show inconsistencies with one another, but the microhardness values obtained by Bowie and Taylor show good agreement with the present results. There are no comparative values for the skutterudites.

The hardness values of niccolite and breithauptite are of considerable interest. The present results compare favourably with other published measured values but are discordant with the calculated values obtained by Povarennykh (1959), Table XLVIII. In all the different types of bonding in minerals, the atomic radius of arsenic is always smaller than that of antimony. Thus the actual hardness values are contrary to expectations based on atomic radii. Goldschmidt (1954) considers that niccolite has a mixed metallic-covalent type of bonding. Povarennykh considers that breithauptite has a higher percentage of covalent bonding than niccolite and this is substantiated by the fact that niccolite has a higher reflectivity than breithauptite (pers. comm. I.M. Gray). There is therefore some evidence to indicate that there is a greater degree of covalent bonding in niccolite than in breithauptite, and such a difference could well account for the apparent discrepancies in the hardness values.

(iv) The Sulphosalts

The microhardness variations within the sub-groups are in accordance with the Goldschmidt Rule, with the exception of bournonite and aikinite. For this group, the type of bonding is not significant since the covalent, metallic and ionic radii show the same values in relation to one another.

Thus,

$$\text{At. rad}_{\text{Bi}} > \text{At. rad}_{\text{Sb}} > \text{At. rad}_{\text{As}}$$

and similarly

$$\text{At. rad.}_{\text{Ag}} > \text{At. rad.}_{\text{Cu.}}$$

Although wittichenite is not isostructural with proustite-pyrargyrite, and meneghinite has a different structure from jordanite, both have been included for comparison purposes.

No microhardness data are available for the polybasite-pearceite series or for the meneghinite-jordanite group but Mohs and Talmage hardness values are concordant with present results. Microhardness values for chalcostibite and ~~en~~pletite correspond closely to other published values. According to Uytendogaardt, the Talmage values are identical. For the cosalite - kobellite series no microhardness data are available for comparison. Mohs and

Talmage values concur with the present results. In the tennantite-tetrahedrite series the present results are in agreement with those given by Bowie and Taylor, and Mohs scale values given by Winchell (1951) and Palache, et.al. Considerable variations for the microhardness of freibergite were found between values obtained by Nakhla, Bowie and Taylor and the present writer. These variations may be attributed to the variable amount of silver which can be accommodated in the crystal lattice. From the present result we may conclude that in the tennantite-tetrahedrite series, arsenic tends to raise the hardness and silver, to decrease the hardness. For the proustite-pyrargyrite series, the present results are concordant with Mohs and Talmage hardness values but Bowie and Taylor, however obtained a reverse relationship. The present microhardness results are contrary to the Goldschmidt Rule. Since however, no members of the series have been chemically analysed, and the differences in microhardness are small, no definite conclusions may be drawn. The bulk of the evidence indicate the present results show the true relationship.

Bournonite and aikinite show a microhardness relationship contrary to expectations. Mohs scale hardness values (Palache et.al. 1944) indicate a relationship concordant with expectations whilst Talmage values give values which indicate

a trend similar to the present microhardness results. Bowie and Taylor give a microhardness value for bournonite very close to that obtained for aikinite in the present studies. In view of the conflicting evidence, no significance can be placed on the present results for these minerals until further work has been carried out on further specimens of the same minerals.

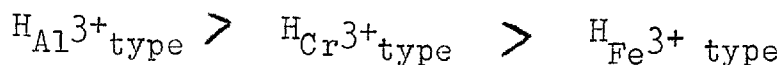
(v) The Oxides and Hydroxides

Agreement with the Goldschmidt Rule in the oxide and hydroxide groups is not so perfect as, for example, in the sulphosalts. It has been assumed that the oxides have dominantly ionic structures.

In the hematite group, the present microhardness values are concordant with Mohs and Telmage hardness values for hematite, ilmenite and corundum. Microhardness values obtained by Kouvo and Vuorelainen (1958) for eskolaite are in reasonable agreement with the present values for this mineral. Apart from eskolaite, the values are in accordance with expectations. The anomalously high hardness of eskolaite from Outukumpu may be due to a distortion of the crystal lattice caused by the presence of small amounts of vanadium. In pure stoichiometric Cr_2O_3 having an undistorted lattice, the hardness should be less than that of corundum.

Hausmannite and hetaeralite show hardness values concordant with the Goldschmidt Rule. This relationship is substantiated by Mohs and Talmage hardness values.

The spinels show good agreement with theoretical expectations. Hardness appears to be mainly controlled by the ionic radii of the trivalent elements in the structure,



Agreement within the individual spinel groups is less well defined. In the aluminium spinels, the magnesium-rich members are harder than the ferrous or zinc-rich members. This relationship is concordant with Mohs scale hardness values and the Goldschmidt Rule. In the ferric spinels, the microhardness values show a reverse relationship to the Goldschmidt Rule based on ionic radii. These relationships are substantiated by microhardness values obtained by Bowie and Taylor for magnetite and jacobsite and Mohs scale hardness values given by Winchell (1951). Whilst it is possible to account for the lower hardness of trevorite by assuming that the divalent element is bound by covalent bonds, a similar argument cannot explain the high value obtained on jacobsite. Such anomalies **emphasise** the need for detailed chemical analyses before definite

crystallochemical conclusions can be drawn.

Hardness values for lepidocrocite and manganite are contrary to those values listed by Bowie and Taylor, Palache et.al., and Uylenbogaardt and also to theoretical expectations. However, it is well known that hydrated oxides vary considerably in hardness depending upon their degree of hydration and oxidation. Pyrolusite when fresh and crystalline has a Mohs scale hardness of 6, but when oxidised it can have a value as low as 2. Such variations have been noted in uraninite, i.e. oxidation giving rise to a much lower hardness value. This "softening" effect explains the apparently anomalous relationship between uraninite and thorianite.

In the rutile structural oxides, the present microhardness values show a relationship contrary to the Goldschmidt Rule. The microhardness values of Bowie and Taylor indicate that rutile is harder than cassiterite, but Mohs and Talmage hardness values together with the present results indicate that cassiterite is harder than rutile. Nakhla gives a value of over 1400 for cassiterite. Povarennykh (1959) showed that theoretically rutile should be harder than cassiterite, but the present results together with the bulk of the evidence from the literature indicate that the reverse occurs in nature. It is tentatively suggested that

the greater hardness of cassiterite may be due to a greater percentage of covalent bonding, or a lower percentage of metallic bonding in the structure of the mineral, compared with rutile. Supporting evidence for this suggestion is as follows. Rutile exhibits a higher reflectivity and a less pronounced tendency to fracture on indentation. The brittleness of cassiterite is evidence of covalent bonding.

(vi) Carbonates, Phosphates.

In the carbonates and phosphates examined, the main character of the bonding is assumed to be ionic. The present results are concordant with Mohs scale hardness values, and apart from smithsonite, they are concordant with the Goldschmidt Rule. There appears to be no theoretical reason for the high hardness of smithsonite. A similar anomalously high hardness value is attributed to smithsonite by Palache et.al., in Mohs scale hardness values.

D. Variation of Microhardness with Chemical Composition
Between Different Mineral Species

It is evident from the discussion of the results earlier in the chapter that one of the fundamental factors controlling the hardness of a mineral is the position of the elements in the mineral in the Periodic Table. The position of an element in the table governs the atomic radii, the valency and its polarisability. Nakhla (1956) found that there was a definite relationship between the atomic radius of an element and the hardness of minerals containing that element. With increasing atomic radius, the hardness of the minerals decreased. Povarennykh (1959) has derived a formula for calculating the hardness of a mineral from crystallochemical data. This subject will be discussed more fully in Chapter VIII.

Another factor controlling the hardness of a mineral is the relative abundance of the elements in the minerals. This relationship is well illustrated by the copper-iron sulphide group (Table XLIX). As the percentage of copper in the minerals decreases so the microhardness values increase, irrespective of crystal structure.

Similarly, in the lead sulphosalt group, (Table L), it can be seen that the microhardness is

- (a) independent of the structure
- (b) dependent on the percentage of Pb in the mineral
- (c) dependent upon the atomic radii of the B sub-group metals.

Table LI illustrates how the strength of a mineral is governed primarily by chemical composition and not structure. Thus although sphalerite and wurtzite have very different structures, they have similar microhardness values.

TABLE XXXIX

Native Elements

Mineral	Chemical Compn.	V.M.H. Mean
Lead	Pb	4.5
Silver	Ag	58
Gold	Au	67
Copper	Cu	85
Ferrite	Fe	260
Platinum	Pt	304
Bismuth	Bi	12
Antimony	Sb	67
Arsenic	As	124

TABLE XL

Sulphides, Selenides, Tellurides

Mineral	Chemical Compn.	V.M.H. Mean
Altaite	PbTe	36
Clausthalite	PbSe	68
Galena	PbS	75
Alabandite	MnS	161
Messite	Ag ₂ Te	30
Naumannite	Ag ₂ Se	34
Encairite	CuAgSe	76
Acanthite	Ag ₂ S	24
Jalpaite	(Ag,Cu) ₂ S	31
Chalcocite	Cu ₂ S	75
Coloradrite	HgTe	22
Tiemannite	HgSe	28
Sphalerite	(Zn,Fe)S	170

TABLE XL Contd.

Mineral	Chemical Compn.	V.M.H. Mean
Violarite	Ni_2FeS_4	307
Linnaeite	Co_3S_4	532
Siegerite	$(\text{Co},\text{Ni})_3\text{S}_4$	525
Bismuthinite	Bi_2S_3	140
Stibnite	Sb_2S_3	90
Pyrite	FeS_2	1600
Bravoite	$(\text{Fe},\text{Ni})\text{S}_2$	1224
Laurite	RuS_2	1886
Sperrylite	PtAs_2	1100
Hauerite	MnS_2	503

TABLE XLI

Arsenides, Antimonides, Sulpharsenides, Sulphantimonides

Mineral	Chemical Compn.	V.M.H. Mean
Breithauptite	NiSb	520
Niccolite	NiAs	420
Ullmannite	NiSbS	530
Gersdorffite	NiAsS	780
Cobaltite	CoAsS	1150
Lollingite	FeAs ₂	620
Safflorite	(Co,Fe)As ₂	940
Rammelsbergite	NiAs ₂	710
Pararammelsbergite	NiAs ₂	720
Arsenopyrite	FeAsS	900
Glaucodot	(Co,Fe)AsS	1000
Fe-skutterudite	(Fe,Co,Ni)As ₃	
Skutterndite	(Fe,Co,Ni)As ₃	672

TABLE XLII

Sulphosalts

Mineral	Chemical Compn.	V.M.H. Mean
Polybasite	$(\text{Ag}, \text{Cu})_{16}\text{Sb}_2\text{S}_{11}$	136
Pearceite	$(\text{Ag}, \text{Cu})_{16}\text{As}_2\text{S}_{11}$	146
Proustite	Ag_3SbS_3	96
Pyrrargyrite	Ag_3AsS_3	112
Witichenite	Cu_3BiS_3	185
Tetrahedrite	$(\text{Cu}, \text{Fe})_{12}\text{Sb}_4\text{S}_{13}$	347
Tennantite	$(\text{Cu}, \text{Fe})_{12}\text{As}_4\text{S}_{13}$	375
Freibergite	$(\text{Cu}, \text{Ag})_{12}\text{FeSb}_4\text{S}_{13}$	305
Bournonite	PbCuSbS_3	173
Aikinite	PbCuBiS_3	198
Chalcostibite	CuSbS_2	230
Emplectite	CuBiS_2	198
Cosalite	$\text{Pb}_2\text{Bi}_2\text{S}_5$	113
Kobellite	$\text{Pb}_2(\text{Bi}, \text{Sb})_2\text{S}_5$	129
Jordanite	$\text{Pb}_{14}\text{As}_7\text{S}_{24}$	188
Meneghinite	$\text{Pb}_{13}\text{Sb}_7\text{S}_{23}$	110

TABLE XLIIIOxides, Hydroxides

Mineral	Chemical Compn.	V.M.H. Mean
Hematite	Fe_2O_3	950
Eskolaite	$(\text{Cr},\text{V})_2\text{O}_3$	2670
Corundum	Al_2O_3	2390
Ilmenite	FeTiO_3	700
Rutile	TiO_2	1000
Pyrolusite	MnO_2	229
Cassiterite	SnO_2	1310
Pitchblende	UO_2	398
Thorianite	ThO_2	1066
Lepidocrocite	$\text{FeO}(\text{OH})$	274
Manganite	$\text{MnO}(\text{OH})$	736
Hausmannite	MnMn_2O_4	556
Hetaerolite	ZnMn_2O_4	711
Spinel	MgAl_2O_4	1580
Hercynite	FeAl_2O_4	1450
Gahnite	ZnAl_2O_4	1520

TABLE XLIII Contd.

Mineral	Chemical Compn.	V.M.H. Mean
Magnetite	FeFe_2O_4	625
Franklinite	ZnFe_2O_4	772
Jacobsite	MnFe_2O_4	855
Trevorite	NiFe_2O_4	584
Chromite	FeCr_2O_4	1290

TABLE XLIV

Carbonates, Phosphates

Mineral	Chemical Compn.	V.M.H. Mean
Calcite	CaCO_3	110
Dolomite	$\text{CaCO}_3 \cdot \text{MgCO}_3$	400
Ankerite	$\text{CaCO}_3 (\text{Mg}, \text{Fe})\text{CO}_3$	421
Magnesite	MgCO_3	442
Siderite	FeCO_3	350
Rhodochrosite	MnCO_3	238
Smithsonite	ZnCO_3	451
Pyromorphite	$\text{Pb}_5(\text{PO}_4)_3\text{Cl}, \text{F}$	224
Apatite	$\text{Ca}_5(\text{PO}_4)_3\text{Cl}, \text{F}$	530

TABLE XLV

IONIC AND ATOMIC RADII

The ionic radii are those for 6-fold co-ordination. The atomic radii are one-half the distance of closest approach in the element

	1	2	3	4	5	6	7	8	0	
1							H ⁻ 1.54 H 0.46		He	
2	Li 1.52 Li ⁺ 0.78	Be 1.12 Be ²⁺ 0.34	B 0.97	C 0.77 C ⁴⁺ < 0.2	N 0.71 N ³⁺ 0.1-0.2	O ²⁻ 1.32 O 0.60	F ⁻ 1.33		Ne 1.60	
3	Na 1.86 Na ⁺ 0.98	Mg 1.60 Mg ²⁺ 0.78	Al 1.43 Al ³⁺ 0.57	Si ⁴⁻ 1.98 Si 1.17 Si ⁴⁺ 0.39	P P ³⁺ 0.3-0.4	S ²⁻ 1.74 S 1.04 S ⁴⁺ 0.34	Cl ⁻ 1.81 Cl 1.07		A 1.91	
4	K 2.31 K ⁺ 1.33 (NH ₄ ⁺ 1.43)	Ca 1.96 Ca ²⁺ 1.06	Sc 1.51 Sc ³⁺ 0.83	Ti 1.46 Ti ²⁺ 0.69 Ti ⁴⁺ 0.64	V 1.30 V ²⁺ 0.65 V ³⁺ 0.81 V ⁵⁺ ca. 0.4	Cr 1.25 Cr ²⁺ 0.64 Cr ³⁺ 0.3-0.4	Mn 1.18 Mn ²⁺ 0.91 Mn ³⁺ 0.70 Mn ⁴⁺ 0.52	Fe 1.24 Fe ²⁺ 0.83 Fe ³⁺ 0.67	Co 1.25 Co ²⁺ 0.82	Ni 1.24 Ni ²⁺ 0.78
	Cu 1.28 Cu ⁺ 0.96	Zn 1.33 Zn ²⁺ 0.83	Ga 1.22 Ga ³⁺ 0.62	Ge 1.22 Ge ⁴⁺ 0.44	As 1.25 As ³⁺ 0.69 As ⁵⁺ ca. 0.4	Se ²⁻ 1.91 Se 1.16 Se ⁴⁺ 0.3-0.4	Br ⁻ 1.96 Br 1.19		Kr 2.01	
5	Rb 2.43 Rb ⁺ 1.49	Sr 2.15 Sr ²⁺ 1.27	Y 1.81 Y ³⁺ 1.06	Zr 1.56 Zr ²⁺ 0.87	Nb 1.43 Nb ²⁺ 0.69 Nb ³⁺ 0.69	Mo 1.36 Mo ⁴⁺ 0.68	Ma	Ru 1.33 Ru ²⁺ 0.65	Rh 1.34 Rh ²⁺ 0.68	Pd 1.37
	Ag 1.44 Ag ⁺ 1.13	Cd 1.49 Cd ²⁺ 1.03	In 1.62 In ³⁺ 0.92	Sn ⁴⁻ 2.15 Sn 1.40 Sn ²⁺ 0.74	Sb 1.45 Sb ²⁺ 0.90	Te ²⁻ 2.11 Te 1.43 Te ⁴⁺ 0.89	I ⁻ 2.20 I 1.38 I ⁺ 0.94		Xe 2.20	
6	Cs 2.62 Cs ⁺ 1.65	Ba 2.17 Ba ²⁺ 1.43	La 1.86 La ³⁺ 1.22	Ce 1.82 Ce ²⁺ 1.18 Ce ³⁺ 1.02	Pr 1.81 Pr ²⁺ 1.16 Pr ³⁺ 1.00	Nd 1.80 Nd ²⁺ 1.15	II			
	Sm ²⁺ 1.13	Eu ²⁺ 1.13	Gd ²⁺ 1.11	Tb ²⁺ 1.09 Tb ³⁺ 0.89	Dy ²⁺ 1.07	Ho ²⁺ 1.05	Er 1.86 Er ²⁺ 1.04			
	Tm ²⁺ 1.04	Yb ²⁺ 1.00	Lu ²⁺ 0.99	Hf 1.68 Hf ²⁺ 0.84	Ta 1.43 Ta ²⁺ 0.68	W 1.36 W ²⁺ 0.68	Re	Os 1.35 Os ²⁺ 0.67	Ir 1.35 Ir ²⁺ 0.68	Pt 1.38
	Au 1.44 Au ⁺ 1.37	Hg 1.50 Hg ²⁺ 1.12	Tl 1.70 Tl ⁺ 1.49 Tl ²⁺ 1.06	Pb ⁴⁻ 2.15 Pb 1.75 Pb ²⁺ 1.32 Pb ⁴⁺ 0.84	Bi 1.55	Po	85			Rn
7	87	Ra	Ac	Th 1.80 Th ²⁺ 1.10	Pa	U 1.38 U ²⁺ 1.06				

After Evans (1939)

TABLE XLVI

'TETRAHEDRAL' ATOMIC RADII
(After Pauling and Huggins, 1934)

	1	2	3	4	5	6	7
2		Be 1.07	B 0.80	C 0.77	N 0.70	O 0.66	F 0.64
3		Mg 1.40	Al 1.26	Si 1.17	P 1.10	S 1.04	Cl 0.99
4	Cu 1.35	Zn 1.31	Ga 1.26	Ge 1.22	As 1.18	Se 1.14	Br 1.11
5	Ag 1.53	Cd 1.48	In 1.44	Sn 1.40	Sb 1.36	Te 1.32	I 1.28
6	Au 1.50	Hg 1.48	Tl 1.47	Pb 1.46	Bi 1.46		

TABLE XLVII.

Variation in microhardness with chemical composition in some cobalt-bearing analogues of pentlandite

V.M.H. Mean.	%Ni	%Co	%Fe
245	26.98	18.84	21.10
280	21.10	30.94	15.62
310	9.06	49.33	10.32

After Kuovo, Hukma, and Vuorelainen (1959)

TABLE XLVIII

Comparison of calculated and actual hardness values for niccolite and breithauptite (After Povarennykh, 1959)

Mineral	Inter-atomic dist.	Degree of Covalency	Coord. No.	Hardness	
				Calc.	Actual
NiAs	2.43	97	6	7.68	5.5
NiSb	2.60	100	6	6.82	5.0

TABLE XLIX

The Variation of Microhardness with Chemical Composition in
Some Copper-Iron Sulphides

Mineral	Chemical Compn.	Crystal System	%Cu.	V.M.H. Mean Value (100g.)
Chalcocite	Cu_2S	Ortho.	79.9	71
Digenite	$Cu_{2-x}S$	Isom.	78.8	71
Covellite	CuS	Hex.	66.0	99
Bornite	Cu_5FeS_4	Isom.	63.3	92
Chalcopyrite	$CuFeS_2$	Tetra.	34.6	188
Cubanite	$CuFe_2S_3$	Ortho.	23.4	207
Pyrrhotite	$Fe_{1-x}S$	Hex.	trace	298

TABLE L

The Variation of Microhardness with Chemical Composition in
some Lead Sulphosalt Minerals

Mineral	Chemical Compn.	Crystal System	%Pb.	V.M.H. Mean Value (100g.)
Jordanite	$Pb_{14}As_7S_{24}$	Mono.	69.2	189
Gratonite	$Pb_9As_4S_{15}$	Hex.	70.5	174
Boulangerite	$Pb_5Sb_4S_{11}$	Mono.	50.0	163
Meneghenite	$Pb_{13}Sb_7S_{23}$	Ortho.	62.9	134

TABLE LI

The Relationship between Crystal System and Microhardness in Minerals having the Compositions ZnS and FeS₂

Mineral	Chemical Compn.	Crystal System	V.M.H. Min. Value (100g)
Wurtzite	ZnS	Hex.	205
Sphalerite	ZnS	Isom.	180
Marcasite	FeS ₂	Ortho.	1064
Pyrite	FeS ₂	Isom.	1600

CHAPTER VII

SYSTEMATIC MICROHARDNESS DATA

Ranges and mean values of Vickers and Knoop microhardness for all the mineral species studied are given in Table XVIII in Chapter IV and Vickers values are also presented diagrammatically, in Fig. 68, (enclosed in the folder at the end of the thesis). The minerals are arranged in order of increasing hardness.

A. Accuracy and Reproducibility of the Results

Microhardness values have been obtained using two different types of indenters, the Knoop, and the Vickers. The Knoop indenter has been mainly used in orientation studies, whilst the Vickers indenter has been utilised primarily in the determination of the ranges and mean values of microhardness of the ore minerals.

(a) Vickers microhardness results

Values of Vickers microhardness have been obtained for all the mineral species studied at 100 g. load. It has been conclusively shown in Chapter III that microhardness values

obtained at varying loads on the same mineral are considerably different from one another. It is therefore incorrect to compare values obtained, for example, at 50 g. or 25 g. with the present results. Only Nakhla (1956), and Bowie and Taylor (1958) have obtained comparable microhardness values for the opaque minerals.

The results of Nakhla (1956) show inconsistent variations of microhardness with load. In addition, no mention was made of the number of measurements taken. For the above reasons, these results have not been used for comparison purposes. The results of Bowie and Taylor (1958) are more comprehensive but their mineral specimens were mounted in bakelite, instead of cold setting plastic. The disadvantages of bakelite, as a mounting media, have been pointed out in Chapter II. It was shown that the hardness of a galena crystal was increased by 40% from its normal value. Thus, one might expect the results of Bowie and Taylor, for the soft minerals, to be higher than corresponding values obtained from polished sections mounted in cold setting plastic.

A comparison of the present results, and those of Bowie and Taylor's indicates such a trend. Of the minerals that have been jointly studied, and have microhardness values about 200, approximately 30% give results which agree to within $\pm 5\%$ of each other. The remaining 70% show microhardness

differences greater than $\pm 5\%$. Of these results, one half show that Bowie and Taylor's values are higher than the present, and the other half show the reverse relationship. However, of the minerals with microhardness values less than 200, excluding the native metals, 20% give results which agree to within $\pm 5\%$ of one another, 65% show Bowie and Taylor's microhardness values higher than the present, and 15% show the reverse relationship. The divergence between Bowie and Taylor's results and the present ones increases with decreasing microhardness. This is further evidence of the "work hardening" effect on minerals due to the high temperatures and pressures that occur in bakelite mounting processes.

Bowie and Taylor found that approximately 20% of the minerals studied exhibited cracking around indentations. The present studies, however, indicate that over 75% of the opaque minerals fracture to some extent around the indentations, but the present survey has included many more sulphosalts, and some silicate, and this discrepancy may therefore not be serious. Only the least fractured impressions were measured in the present studies, and it therefore seems unlikely that the difference in microhardness values for the softer minerals could be due to inaccurate measurement of the indentations.

In general, the results are in agreement with those of Bowie and Taylor. The survey of both sets of results suggests

that if standard conditions are applied, i.e. standard load, mounting media and measuring technique, then a microhardness reproducibility of approximately $\pm 5\%$ may be expected. This value depends mainly upon the hardness of the mineral species and its ability to change in chemical composition. Thus the reproducibility of the simple sulphides, selenides, tellurides and some of the sulphosalts is about 3% whilst those of the harder oxides and sulphides approach 8 - 10%. Large variations occur in the native metals, due to the variability of chemical composition.

Several notable discrepancies occur between the results of Bowie and Taylor and the present studies. There are large differences in the microhardness values for the oxides and hydroxides of iron and manganese. This is attributed to variations in the state of hydration and oxidation that may occur in these minerals. Bowie and Taylor's value for naumannite contradicts the Goldschmidt Rule and is not concordant with listed Mohs or Talmage values. Differences in the values obtained for sylvanite are probably due to variations in chemical composition.

(b) Knoop microhardness results

Knoop microhardness values have been determined at different loads, i.e. softer minerals were tested at 15 g.

load and hard minerals at 100 g. load. It is therefore incorrect to compare directly the Knoop results with the Vickers microhardness values obtained at 100 g. load. However, taking into account the effect of the load on the microhardness values, the Knoop results compare favourably with the Vickers results. Where identical loads have been used with both indenters on the same minerals, the Knoop microhardness mean values are usually slightly lower than corresponding Vickers values. The differences are of the order of 5% but this value varies according to the hardness and anisotropism of the mineral. Due to the lower symmetry of the Knoop indenter, Knoop microhardness ranges are considerably greater than corresponding Vickers values (Table XVIII).

Robertson and Van Meter (1951) determined the ranges of Knoop microhardness values for 48 ore minerals, using loads ranging from 2 g. to 300 g. Many of the minerals were determined at 15 g., 25 g. and 100 g. load. Where the microhardness ranges, obtained in the present studies and by Robertson and Van Meter, have been determined at the same loads, they show excellent agreement with one another, less than $\pm 5\%$. It is interesting to note that Robertson and Van Meter also found much less Knoop microhardness anisotropism on the isometric minerals, eg. chromite,

compared with the anisotropic minerals such as arsenopyrite, enargite and molybdenite.

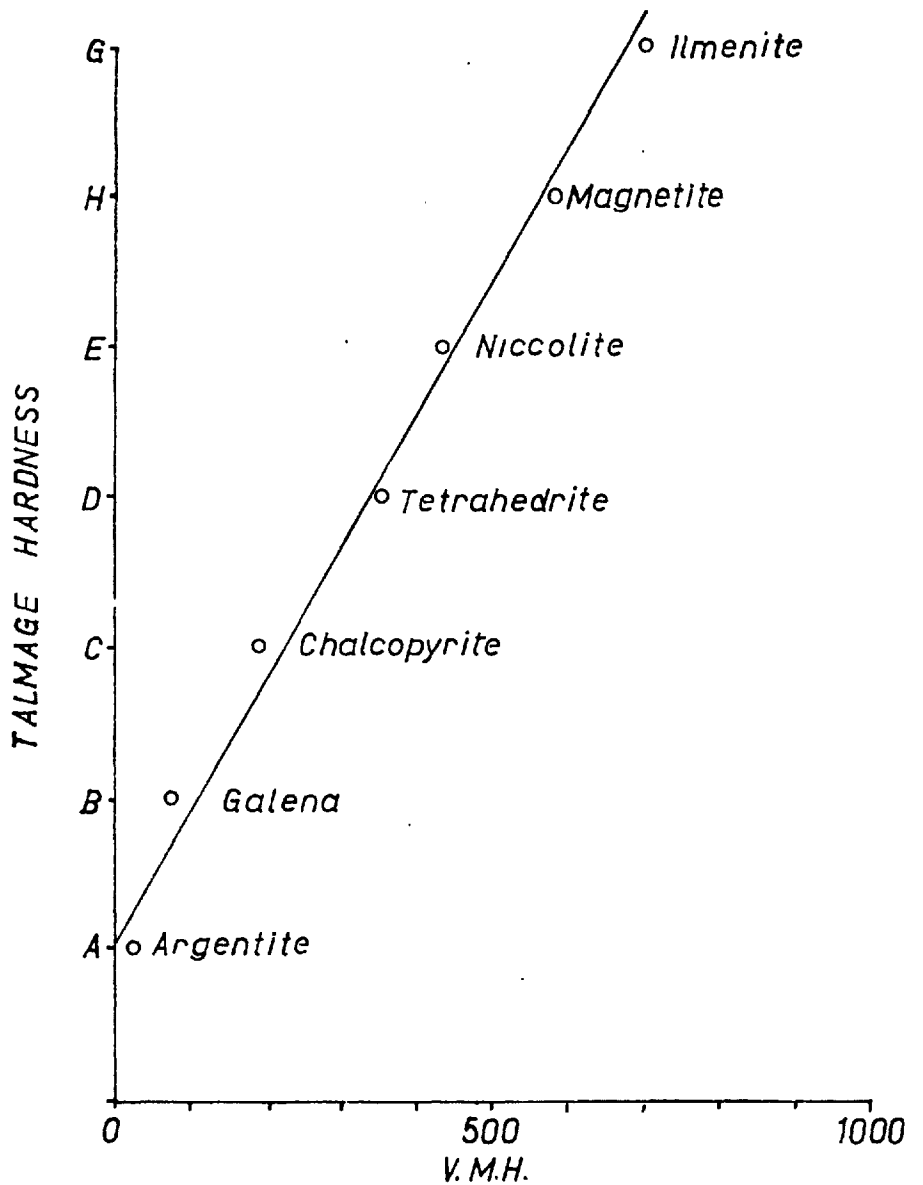
B. Comparison of the Microhardness Values with Established Mohs and Talmage Hardness Values

A comparison has been made of the microhardness results with Mohs scale of mineral hardness listed by Palache et.al. (1944), and with Talmage hardness values listed by Uytendogaadt (1951). The comparisons have been used to assess approximately the microhardness of some of the rarer minerals, samples of which were not available for the direct determination of their microhardness.

(a) Comparison with Talmage hardness values

Fig. 69 shows that a reasonably linear relationship exists between the Talmage hardness values of the standard minerals, i.e. argentite, galena, chalcopyrite, tetrahedrite, niccolite, magnetite and ilmenite, and their microhardness values. A comparison of the Talmage hardness and microhardness values of most of the ore minerals shows that many discrepancies occur. For example, minerals in the "B" group show microhardness values ranging from 26 to 175. However, within certain limits, the Talmage and microhardness values for these minerals do show a roughly linear relationship.

FIG. 69
PLOT OF TALMAGE AND MICRO-
HARDNESS VALUES FOR THE
STANDARD MINERALS



It is interesting to note that the microhardness of ilmenite (Talmage rating G.) is only 700. Thus all the minerals above 700 microhardness units should, according to the linear relationship, logically have a higher rating than G. Rutile, chromite, pyrite and laurite, having microhardness mean values of 1000, 1300, 1600, 1850 respectively should have Talmage ratings of J⁻, L⁺, O, and R⁻. Summarising, we may conclude that for the soft and medium-hard minerals i.e. up to 700, the Talmage and the microhardness values show a general concordance with one another. For the minerals of microhardness greater than 700, the microhardness and Talmage hardness values do not show a linear relationship i.e. the Talmage ratings are consistently too low relative to the microhardness values. It is obvious that by limiting the Talmage ratings from A to G, both Talmage (1925), and Short (1940) introduced large inconsistencies into their hardness ratings for the harder minerals.

(b) Comparison with Mohs scale values

As a further check on the accuracy of the results, Vickers and Knoop microhardness values were determined for the standard minerals in the Mohs scale of hardness. These results are given in Table LII. Table LIII compares the

TABLE LI I

Vickers and Knoop Microhardness Values for the Standard Mohs Scale Minerals

Mineral Species	V.M.H. Values		K.M.H. Values	
	Range	Mean	Range	Mean
Talc	7.0-18.5 ⁴	10.5	3.8-7.4 ⁴	11.8
Gypsum(001)	30.5-47.5 ¹	39.2	38.0-156 ⁴	65.5
(010)	34.8-48.2 ¹	42.2	38.0-69.3 ⁴	50.2
Calcite(10 $\bar{1}$ 1)	105-116 ¹	112	123-174 ²	155
Fluorite(100)	174-181 ¹	179	166-188 ²	181
(111)	174-203 ¹	191	182-220 ²	205
Apatite(0001)	454-606 ¹	544	498-638 ²	552
(10 $\bar{1}$ 0)	476-596 ¹	538	423-634 ²	536
Orthoclase(001)	642-933 ¹	727	531-665 ²	608
(110)	681-882 ¹	770	463-717 ²	590
(010)	642-913 ¹	770	423-717 ²	608
Quartz(0001)	1266-1465 ¹	1349	1039-1307 ¹	1145
(10 $\bar{1}$ 0)	1378-1561	1457	890-1231 ¹	1066
Topaz(001)	1666-2021 ¹	1726	1389-1739 ¹	1526
(010)	1478-1747 ¹	1620	1380-1635 ¹	1480
(100)	1620-1818 ¹	1734	1238-1815 ¹	1487
Corundum(0001)	2097-2598 ¹	2264	1751-2186 ¹	1902
(10 $\bar{1}$ 0)	2341-2758 ¹	2519	2186-2470 ¹	2270

- 1 - Obtained at 100 g. load.
 2 - Obtained at 50 g. load
 4 - Obtained at 15 g. load.

TABLE LIIIA Comparison of Vickers Mean Microhardness Data.

Mohs' Scale	Mineral Species	V.M.H(mean values) E.W.Taylor (1949)	V.M.H(mean values) S.H.U.Bowie (B&T, 1958)	V.M.H(mean values) R.Taylor (B&T, 1958)	V.M.H(mean values) (B.B. Young)
1	Talc	47	43	43	10
2	Gypsum(010)	60	52	50	41
3	Calcite(10 $\bar{1}$ 1)	136	126	118	112
4	Fluorite	200	193	191	185
5	Apatite	659	552	560	541
6	Orthoclase	714	768	764	755
7	Quartz(001)	1103	1135	1132	1349
7	Quartz(10 $\bar{1}$ 0)	1206	1187	1180	1457
8	Topaz	1648	1699	1640	1693
9	Corundum	2085	2121	2108	2391

microhardness mean values obtained by Taylor (1949) and Bowie and Taylor (1958), with the present results. All the values were obtained at 100 g. load. Agreement between the values obtained by Bowie and Taylor, and E.W. Taylor is very good, with the exception of apatite. For the softer minerals i.e. From Talc to Apatite, Bowie and Taylor's values are consistently lower than those of Taylor's, whilst the values for the harder minerals are in much closer agreement. The present values in general agree with the measurements of the other authors. It is noticeable, however, that the values for the softer minerals, i.e. from talc to orthoclase are lower than corresponding values obtained by Bowie and Taylor, and E.W. Taylor. Present values for quartz and corundum seem rather high by comparison, whilst values obtained on topaz are in close agreement with those obtained by the other authors.

Although the differences between the various sets of microhardness values are small, the manner of their variation is significant when attempting to deduce a relationship between Mohs scale hardness values and the microhardness values. Whilst the values of Taylor, and to a lesser extent, Bowie and Taylor, approach a logarithm/linear relationship, the present values indicate a logarithm/logarithm relationship between the hardness scales (Fig. 71).

FIG. 70
COMPARISON OF V.M.H. AND MOHS' SCALE
HARDNESS VALUES OF THE STANDARD
MINERALS WITH THE CUBIC PARABOLA

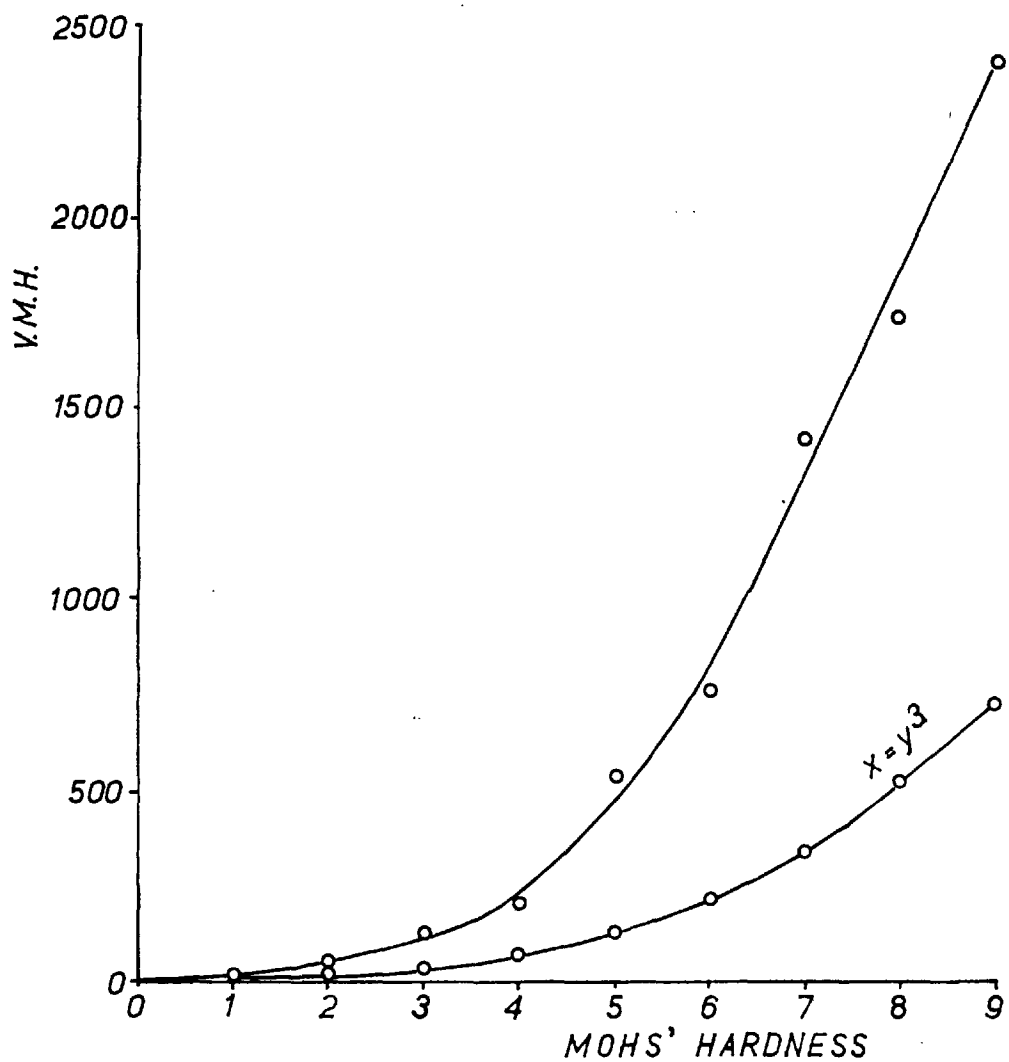
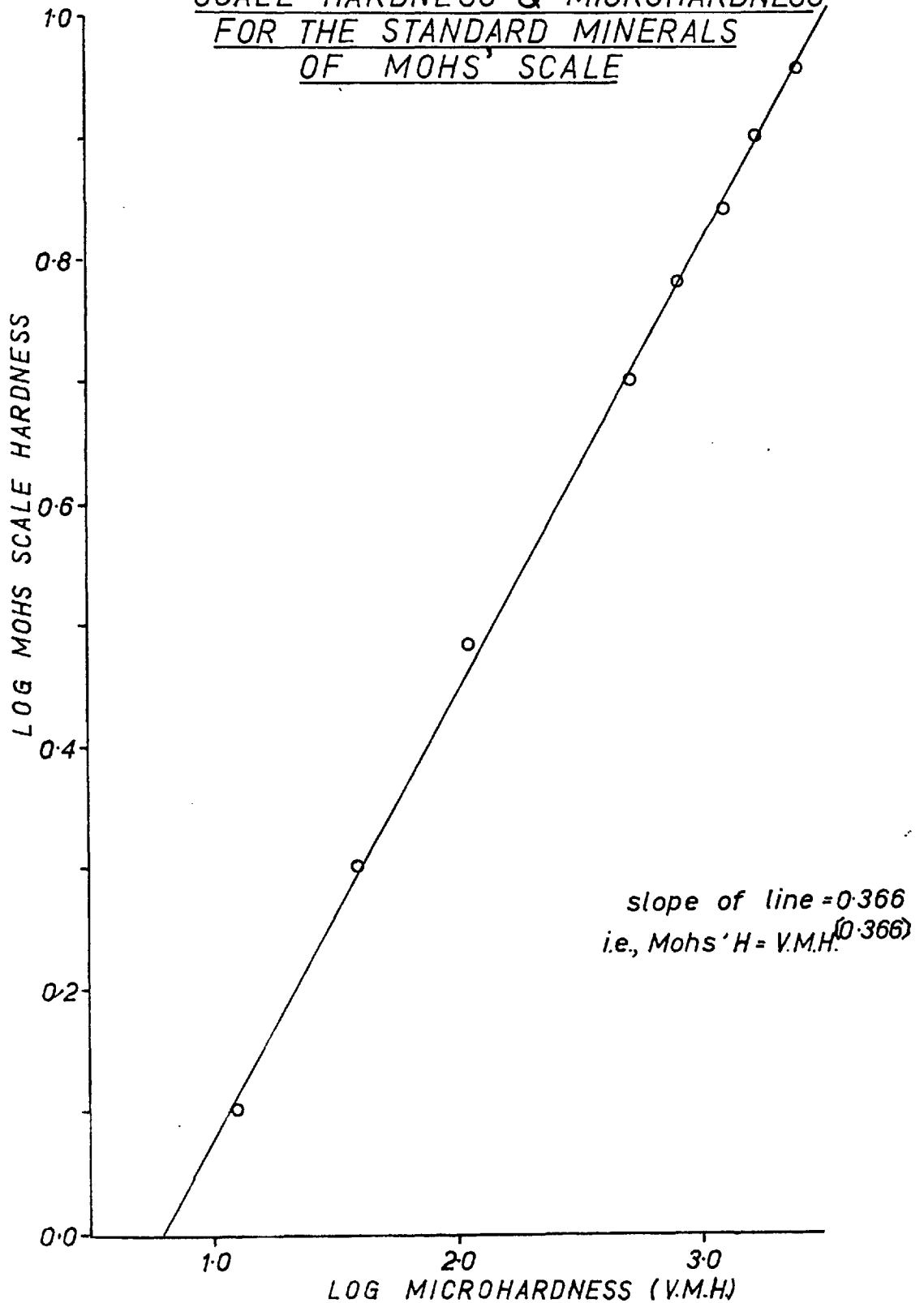


FIG. 71
THE RELATIONSHIP BETWEEN MOHS'
SCALE HARDNESS & MICROHARDNESS
FOR THE STANDARD MINERALS
OF MOHS' SCALE



Kruschov (1950), investigated the relationship between the Mohs scale hardness values and the microhardness values and found that a logarithm/logarithm relationship between the scales existed. He deduced the following relationship;

$$H_0 = 0.675 \sqrt{H}$$

where H_0 = Hardness number on the Mohs scale

H = indentation hardness number, using a triangular pyramid.

Tabor (1954), used the results of Winchell (1945) and E.W. Taylor (1949), to show that, contrary to the results of Kruschov (1950), the relationship between the scales was a logarithm/linear one. He expressed the relationship in the following formula;

$$\text{Log } H = 1.6 M$$

where M = Mohs scale number,

and H = microhardness number.

Povarenrykh (1959), investigated in detail the relationship between the scales. Using the microhardness values obtained by several authors (Table LIV) he found that a plot of the values formed a curve very close to that of the cubic parabola, $y = x^3$.

The present results are in very close agreement with those of Povarenrykh, the curve approximate in shape to the $y = x^3$ parabolic form, (Fig. 70). When logarithms of the

TABLE LIV

Microhardness Values Obtained on the Standard Mohs Scale Minerals.

Относительные числа твердости эталонных минералов шкалы Мооса, полученные методами склерометров и вдавливания*

Шкала Мооса	Склерометрич. твердость			Твердость по методам вдавливания			
	По Пфаффу	По Ходжун-Мак-Кею	По Бирбауму	По Хрущову	По Кнупу	По Тейлору	По Аурбаху
1		0,2	2	1,2	—	22	4
2	12	2	5	18	17	29	12
3	15	24	20	53	70	62	80
4	37	27	23	92	84	90	96
5	54	98	215	260	219	316	206
6	191	184	380	386	289	343	220
7	254	510	500	543	386	568	268
8	459	645	600	692	642	792	457
9	1000	1000	1000	1000	1000	1000	1000
10	—	—	—	~4900	4225	—	2170

* Все числа твердости пересчитаны, причем число твердости корунда принято за 1000.

Values recalculated assuming that corundum has a V.M.H. No. 1000.

microhardness and Mohs scale hardness values are plotted against one another (Fig. 71) a straight relationship results i.e.

$$\begin{aligned} \text{Log } M &= 0.366 \log H \\ \text{or} \quad M &= H^{(0.366)} \end{aligned}$$

where M = Mohs scale number

H = Vickers microhardness number (100 g.)

0.366 = slope of the line.

Povarenrykh, using the microhardness value of 10,000, for diamond, obtained by Kruschov, (1950), arrived at a figure of 15.0 on the Mohs scale hardness. Using the present results, the same data gives a Mohs scale hardness value for diamond of 14.96. As the present results show such close agreement with those of Povarenrykh, it seems probable that the microhardness values for the softer minerals obtained by Bowie and Taylor, and E.W. Taylor are too high. There are two possible explanations for these discrepancies. Firstly, it is possible that some of the softer minerals may have been determined at loads lower than 100 g. load, and secondly, the "work-hardening" effect that appears to occur in bakelite mounting may have produced increased hardness in the minerals.

FIGURE 71

100

A considerable spread of the values occurs particularly for the softer minerals. For example, in the groups of minerals listed as having a hardness of 2.5 on the Mohs scale, corresponding microhardness values range from 12 to 200. The spread is less pronounced in the harder minerals. By comparison, the Mohs scale values appear to be slightly more reliable than corresponding Talmage values.

(c) Assessment of the microhardness of rare minerals from their Mohs, Talmage and polishing hardness values

Although microhardness values have been obtained for over 200 mineral species, many of the softer sulphides and sulphosalts were not examined. Talmage and Mohs scale hardness values are given for most minerals in the mineralogical textbooks of Uytendogaardt (1951) and Palache et.al (1944). Table LV lists the approximate microhardness values extrapolated from the curves in Figs. 69, 71 for a further 65 minerals. A final extrapolated values of the microhardness for each mineral has also been given. This value is the mean value of the extrapolated Talmage and Mohs values. The accuracy of these hardness values is dependent upon the accuracy of the original determinations. It should therefore be appreciated that these results are only

TABLE LV

Microhardness Values Extrapolated from Mohs and/or Talmage Values (for 100 g. load)

Mineral	Microhardness from Talmage Value	Microhardness from Mohs' Value	Mean Micro- hardness Value.
Aguilarite	25 - 75	60	55
Alaskaite	200	40 - 150	150
Aramovoite	200	60	130
Baumhauerite	200	100	150
Berzelianite	75	40	60
Canfieldite	200	60	130
Dufrenoy'site	200	100	150
Empressite	200	125	160
Fülöppite	---	60	60
Freislebenite	200	50	125
Frohbergite	230	---	230
Galenobismutite	75	100	90
Greenockite	---	120	120
Gruenlingite	75	40	60
Guanajualite	100	100	100
Gudmundite	600	700	650

TABLE LV Contd.

Mineral	Microhardness from Talmage Values	Microhardness from Mohs' Values	Mean Micro- hardness Values
Hauecornite	400	---	400
Heazlewoodite	230	---	230
Hedleyite	25 - 75	---	50
Högbomite	---	1000	1000
Hutchinsonite	---	30	30
Joseite	25 - 75	40	45
Klockmannite	200	100	150
Lautite	---	120	120
Lengenbachite	75	---	75
Liveingite	---	100	100
Lorandite	75	50	60
Maghemite	---	500	500
Melonite	15	75	45
Metacinnabar	75	100	85
Metastibnite	---	60	60
Montbrayite	200	---	200
Niggliite	300 - 400	100	225
Owyheelite	75	60	70
Palladium	---	475	475

TABLE LV Contd.

Mineral	Microhardness from Talmage Values	Microhardness from Mohs' Values	Mean Micro- hardness Values
Paramelaconite	---	400	400
Parkeriite	100	70	85
Penroseite	---	80	80
Plagionite	200	60	130
Plattnerite	---	650	650
Polydymite	550	500	525
Potarite	230	150	190
Pseudobrookite	---	800	860
Pyrostilpnite	---	40	40
Rathite	200	100	150
Rezbanyite	200	75	140
Rickardite	75 - 200	150	145
Samsonite	200	60	130
Sartorite	---	100	100
Schaphbachite	60 - 200	---	130
Schirmerite	200	40	120
Schreibersite	----	1200	1200
Selenium	----	40	40
Seligmannite	200	100	150

TABLE IV Contd.

Mineral	Microhardness from Talmage Values	Microhardness from Mohs' Values	Mean Micro- hardness Values
Stibiopalladinite	---	400	400
Stromeyerite	75	80	80
Sulvanite	200	150	175
Tellurbismuth	25 - 70	30	60
Tungstenite	25	75	50
Vrbaite	200	150	175
Wehrlite	75	40	55
Weissite	75	100	90
Xanthaconite	---	60	60

TABLE LVI

Microhardness Values Extrapolated from "Polishing Hardness"
Data (at 100 g. load)

Mineral	Polishing Hardness data	Microhardness Values (extrapolated)
Allopalladium	> cpy. < pyrr.	> 200 < 300
Coulsonite	~ mag.	~ 600
Csiklovaite	~ tetradymite	~ 40
Eskebornite	~ claus. < cpy.	80 - 150
Fülöppite	< gal.	< 70
Freiseite	sl. > sternberg.	> 40
Frohbergite	> cpy. < tetrah.	250
Greenockite	> cpy. < py.	> 200
Hauchecornite	sl. > millerite	sl. > 280
Heazlewoodite	< pent.	< 220
Herzenbergite	gal. < cpy.	100 - 200
Högbomite	> spinel	> 1450
Hutchinsonite	< gal.	< 70
Lautite	< arsenic	< 130
Leneghenbachite	~ gal.	70
Liveingite	~ gal.	70

TABLE LVI. Contd.

Mineral	Polishing Hardness data	Microhardness Values (extrapolated)
Maghemite	sl. > mag.	sl. > 600
Metastibnite	< gal.	< 70
Palladium	< Pt.	< 300
Paramelaconite	> cpy. < py.	> 200 < 1200
Penroseite	> cpy. < py.	> 200 < 1200
Plattnerite	> cpy. < py.	> 200 < 1200
Pseudobrookite	> cpy. < py.	> 200 < 1200
Pyrostilpnite	< gal.	< 70
Sartorite	~ gal.	70
Schapbachite	sl. > gal.	> 70
Schreibersite	> cohenite	> 1150
Selenium	< gal.	< 70
Stibiopalladinite	~ Pt.	~ 300
Villiamannite	> linnaeite	> 530
-Vredenburgite	< bixby.	< 930
Xanthconite	< gal.	< 70

approximate and should be used with the greatest caution. Where large differences between the values occur, the values derived from the Mohs scale values are probably more correct.

For some minerals no Mohs and/or Talmage values are available. Table LVI gives a series of approximate microhardness values for such minerals. These values have been extrapolated from the "polishing hardness" data listed by Uytendogaardt (1951).

C. Comparison of Vickers Microhardness and Reflectivity Values

Fig. 72 shows a plot of the Vickers microhardness and reflectivity (white light) mean values for all the opaque minerals studied. The positions of the minerals on the chart are broadly similar to those obtained by Bowie and Taylor (1958). Bowie and Taylor showed that the minerals sub-divided themselves into separate groups, depending basically upon their chemical composition and structure. The following groups were established;

(i) The native metals

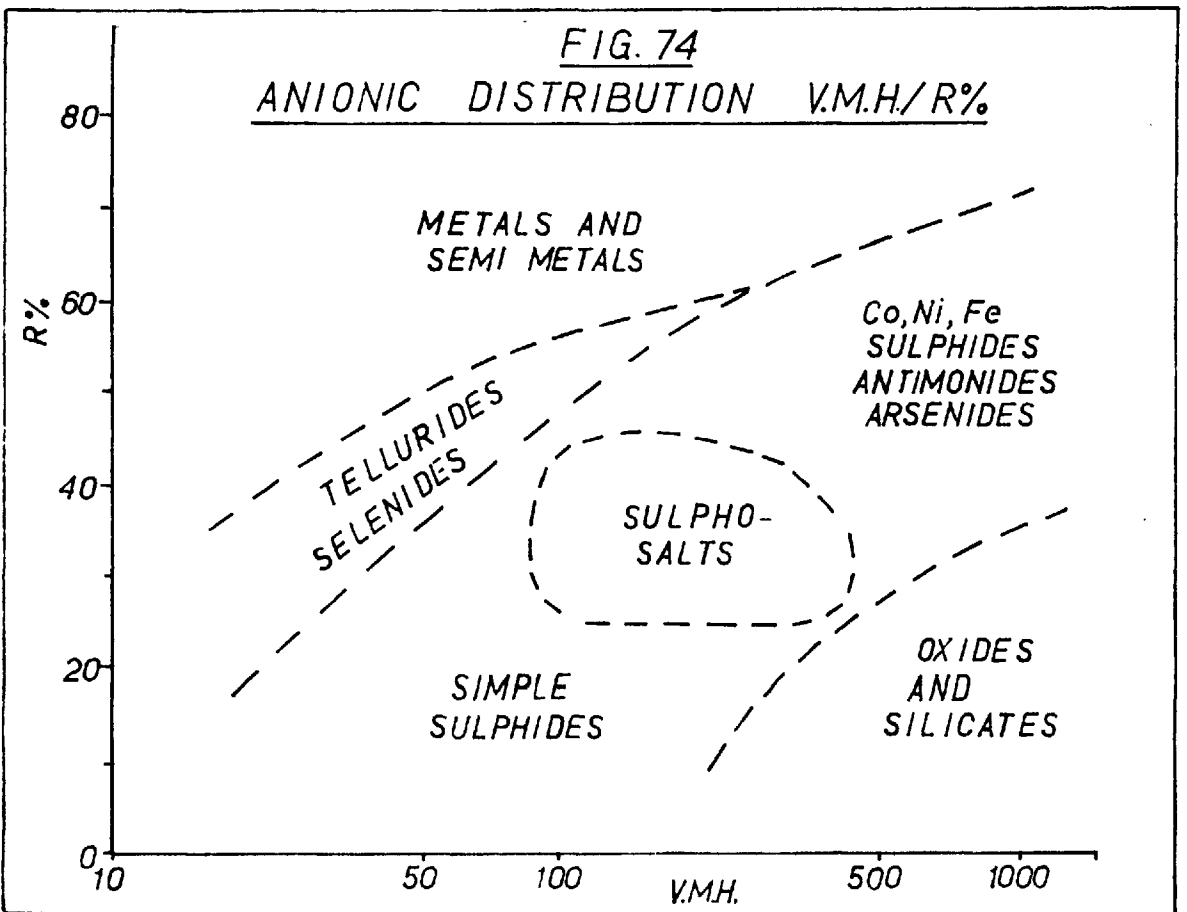
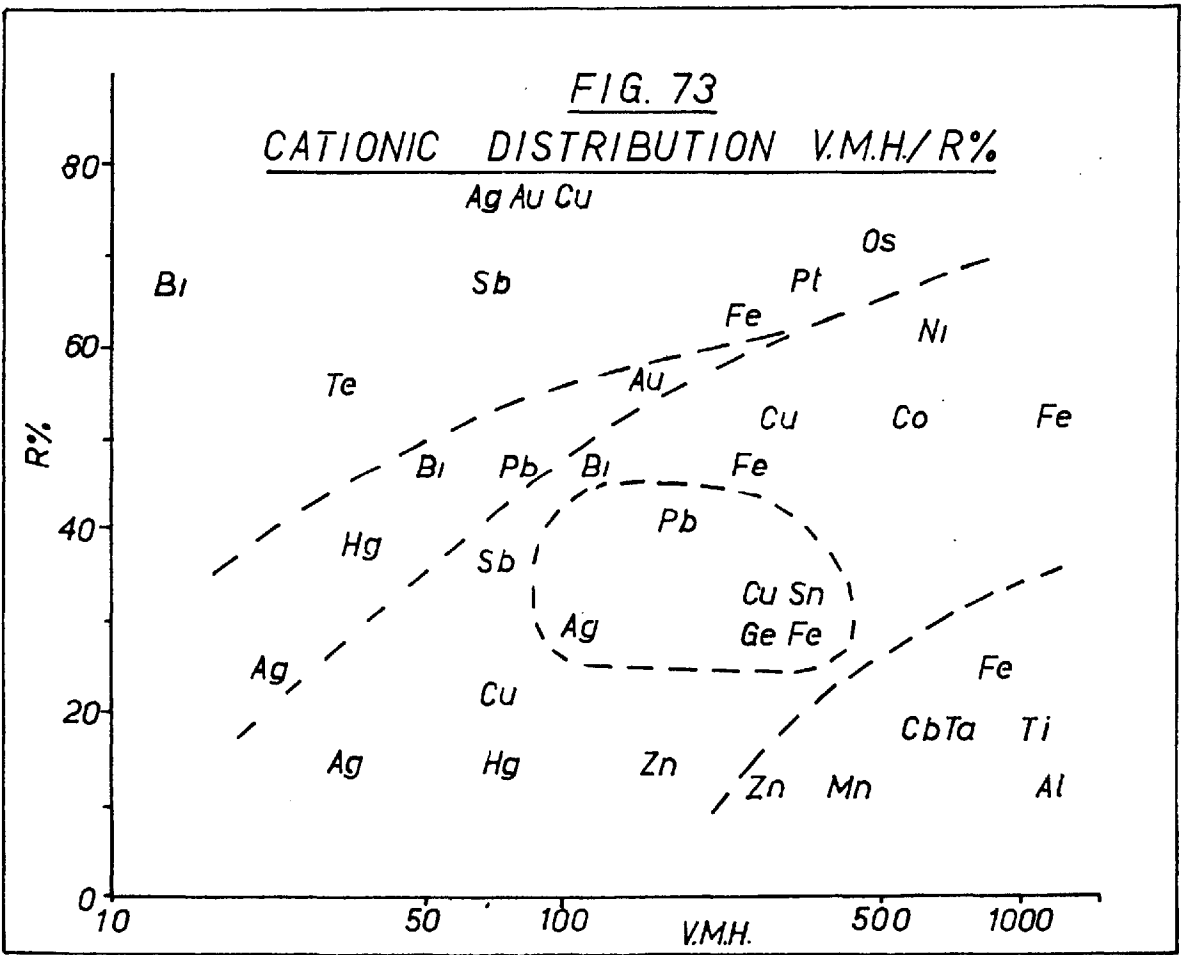
(ii) The cobalt, nickel and iron sulphides and arsenides

- (iii) The sulphosalts
- (iv) The simple sulphides
- (v) The oxides.

The present studies have enabled further sub-division of the minerals to be made. In addition the position of several other mineral groups such as the tellurides and the selenides have been established. A considerable number of sulphosalt and transition element sulphides and arsenides have been studied, and this has enabled further sub-division of these groups to be made. Fig. 73 shows the distribution of the cationic elements in the main groups.

(a) The distribution of the main mineral groups with respect to microhardness and reflectivity values.

It is evident, from Fig. 74, that the microhardness-reflectivity values, and the position of a group on the chart, are determined primarily by chemical composition, atomic structure and bonding. Thus the metals and semi-metals, which have high conductivities, and metallic bonding, are relatively soft and highly reflecting. On the other hand, the oxides and silicates which are essentially non-conducting and have ionic or covalent bonding, are hard and poorly reflecting. The simple sulphides, being dominantly ionic, and poor conductors, are poorly reflecting and show variable



hardness. The more complex cobalt, nickel and iron sulphides and arsenides, having metallic-covalent bonding and medium to high conductivity, are highly reflecting and hard. Intermediate to the sulphides and the metals are the sulphosalts, the selenides and the tellurides. The mineral groups show every gradation from metallic or semi-metallic to ionic or covalent bonding and consequently show intermediate microhardness and reflectivity values. Fig. 74 illustrates the distribution of the mineral groups.

(b) The distribution of the mineral species within the mineral groups

(i) The metals and semi-metals

The mineral species show considerable differences in microhardness values. The hardness of the metals are dependent upon the atomic radii of the elements and upon their structure and valency, as shown in Chapter VI. Whilst the hardness in a particular structural series increases with decreasing atomic radius, reflectivity appears to decrease. For example, copper, gold and silver are softer and more highly reflecting than ferrite or platinum.

(ii) The tellurides and selenides

The tellurides and selenides occupy a position between the metals and the sulphides, having a bond type of a metallic-ionic character. Increasing atomic radii of the cationic element produces a decrease in reflectivity and a decrease in microhardness. For example, coloradoite (Hg Te) and tiemannite (Hg Se) have lower reflectivity values and are softer than altaite (Pb Te) and clausthalite (Pb Se). The tellurides, due to their larger anionic radii, are more metallic in behaviour than the selenides. The high hardness values of the gold-silver tellurides are attributed to the presence of strong metallic-covalent bonds. This bonding structure puts calaverite in a position intermediate between the transition element metals and their corresponding arsenides. It seems very probable that the bond type and microhardness-reflectivity values when determined, will also lie intermediate between the native elements metals and their arsenides.

(iii) The simple sulphides

Bonding in the simple sulphides is dominantly ionic, particularly for the highly coloured minerals such as cinnabar, orpiment and realgar. In other, some degree of metallic bonding exists as for example in acanthite, chalcocite, and galena. The position of a sulphide with the group is

determined by the degree of metallic bonding and also by the atomic radii of the cationic elements. With increasing ionic radii of the cationic element, the hardness of a sulphide decreases. However, the reflectivity values of the sulphides show a considerable dependence upon the amount of metallic bonding. Thus alabandite, (MnS), a dominantly ionic mineral, has a low reflectivity but a high hardness. By contrast, galena, although isostructural with alabandite, has a strongly metallic character. This gives the mineral a fairly high reflectivity but a low hardness. In general, the greater the percentage of ionic bonding the higher the hardness and the lower the reflectivity.

(iv) The complex cobalt nickel iron sulphides and arsenides.

Included in this group are also the following copper bearing sulphides: chalcocite, vallereite and cubanite.

The position of a mineral species in this group appears to be controlled by the nature of the cationic and anionic constituents. The group may be sub-divided according to the type of cationic elements in the mineral structures as follows: the sulphides, the arsenides and antimonides, and the sulpharsenides and sulphantimonides.

Within these sub-groups, the positions of a mineral species is determined by the degree of metallic bonding and

the nature of the cationic elements(s). The metallic character of a mineral is dependent upon proportion of metallic bonding relative to the covalent bonding. The greater the covalency, the harder the mineral, also the greater the covalency, the less the strength of the metallic bonding and the lower the reflectivity. A third factor influencing the microhardness-reflectivity values is the degree of covalency of the ionic sulphides. Hauerite, (MnS_2) is non-metallic, and non covalent, and consequently has a low reflectivity and a low hardness compared with other members of the pyrite group.

The cations in these groups usually comprise the element Co, Ni, Fe and Cu, and have valency states which vary from two to four. The positions of mineral sub-groups within the sulphides, sulpharsenides, and antimonides etc. are dependent upon the valency and atomic radii of the cations. Thus the sulphide sub-group may be divided into sub-sub-groups, i.e. the divalent metal sulphides, the ditrivalent metal sulphides and the quadrivalent metal sulphides. The grouping of these minerals agrees with Goldschmidt Rule, i.e. that increasing valency increases the microhardness.

The main mineral-sub-groups in this group, and their characteristics may be summarised as follows:

1. The divalent copper iron sulphides:- soft, due to the low valency state of the cations and also the large ionic radii, and only medium reflectivity due to limited metallic bonding.
2. The hexagonal divalent nickel-iron sulphides:- low hardness is due to the low valency state of the cations and their large ionic radii; medium-high reflectivity due to considerable metallic bonding.
3. The "siegenite" di-trivalent sulphides:- medium hardness is due to di and trivalent cationic state; low to medium reflectivity is due to weak metallic bonding and strong ionic bonding.
4. The arsenide group:- medium to high hardness is due to the higher valency state of the ions, the hardness of the individuals increasing with valency; the high reflectivity is due to strong metallic bonding.
5. The quadrivalent sulphides:- high hardness values are due to the high valency state of the cations and also to the strong covalent bonding; low reflectivity is due to the weak metallic bonding, as a result of the strong covalent bonds.

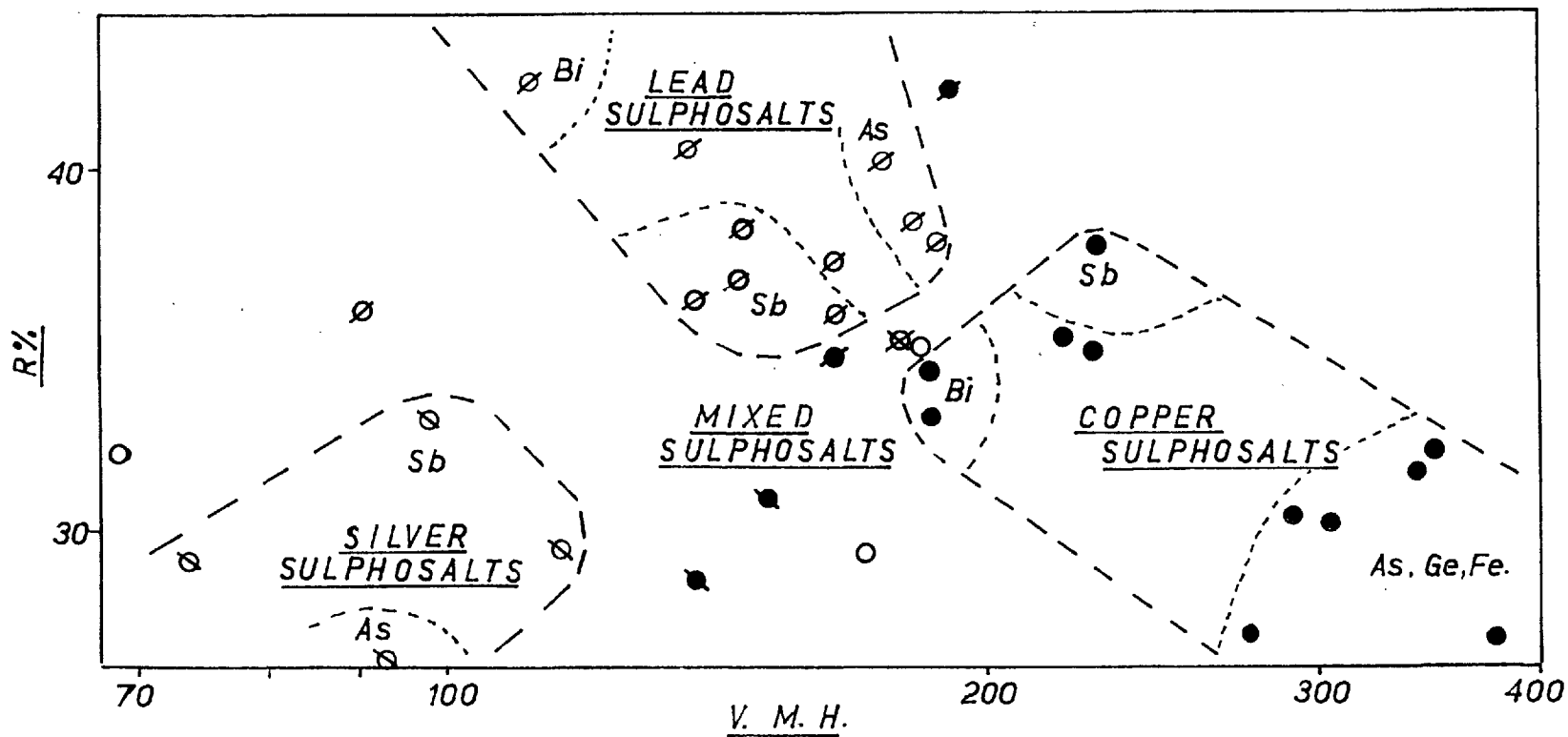
6. The sulphantimonides and sulpharsenides:- the high hardness values are due to the strong covalent bonds and high valency states; medium reflectivity values are due to a weak type of metallic bonding.

(v) The sulphosalts

The bonding in the sulphosalts is a mixture of metallic, ionic and covalent types, the ratio of the proportions of these bond types determining the individual properties of the sulphosalts. In the more metallic, the reflectivity values are higher and the hardness values low. In the more ionic, the reflectivity values are low and the hardness values also low. The more covalent show higher hardness values and low reflectivity values.

The sulphosalts sub-divide themselves (Fig. 75) into three distinct groups according to their main metallic constituent, either lead, silver or copper. The lead group minerals have higher reflectivity values than the copper or silver groups and have hardness values comparable with the silver group. The silver group is lower in reflectivity and is presumably more ionic in character. The copper group, which includes minerals containing iron, germanium and tin, have low reflectivity values but high hardness values indicative of ionic-covalent bonding.

FIG. 75
GROUPING OF THE SULPHOSALTS
ACCORDING TO MICROHARDNESS AND REFLECTIVITY



Within the individual groups reflectivity values of minerals do not appear to be controlled by atomic radii or by the proportion of elements present. Microhardness values show a definite variation in accordance with atomic radii, bismuth bearing sulphosalts being softer than antimony, and antimony softer than arsenic.

(vi) The oxides and silicates

Reflectivity values of the silicate minerals were not determined but they are presumed to be very low - less than 5%. The position of the silicates is mainly dependent upon the degree of covalency in the structures, the hardness increasing with increasing covalency. In a similar manner the oxides are dependent upon the covalency of the structures and also upon the valency and atomic radii of the elements. The more highly reflecting oxides are those containing iron, a transition element. High reflectivity for these oxides is due to the presence of some metallic bonding. The minerals increase in hardness with decreasing atomic radii. Thus cuprite, tenorite and zincite, having large atomic radii are anomalously soft compared with the other oxides.

. Correlation of the Microhardness-Reflectivity Values of the Minerals with their Structure and Bond Types

Fig. 76 represents diagrammatically the position of the main mineral groups with respect to their bond types. It can be seen that the hardness-reflectivity plot corresponds, in a distorted manner, (Fig. 77), to this relationship. The microhardness-reflectivity results show how all types of bonding may be present in a mineral. It is interesting to note the comparison between hardness values, type of bonding, valency and atomic radii. In the metallic bonded minerals which are soft, the atomic radii are large and the valency state low. As the metallic bonding is replaced by ionic the hardness increases due to higher valency states and small atomic radii. Finally as the covalent bonded state is approached, high hardness occurs due to high valency states and small atomic radii. Within each mineral group examined, part of this trend can be observed.

Reflectivity values appear to be controlled almost exclusively by the amount of metallic bonding occurring in the minerals.

FIG. 76
RELATION OF BONDING TO MINERAL COMPOSITION

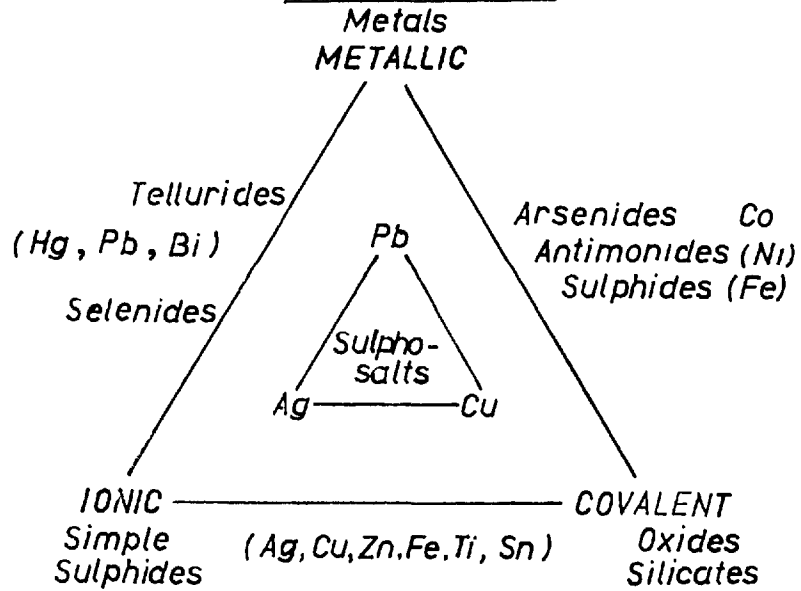
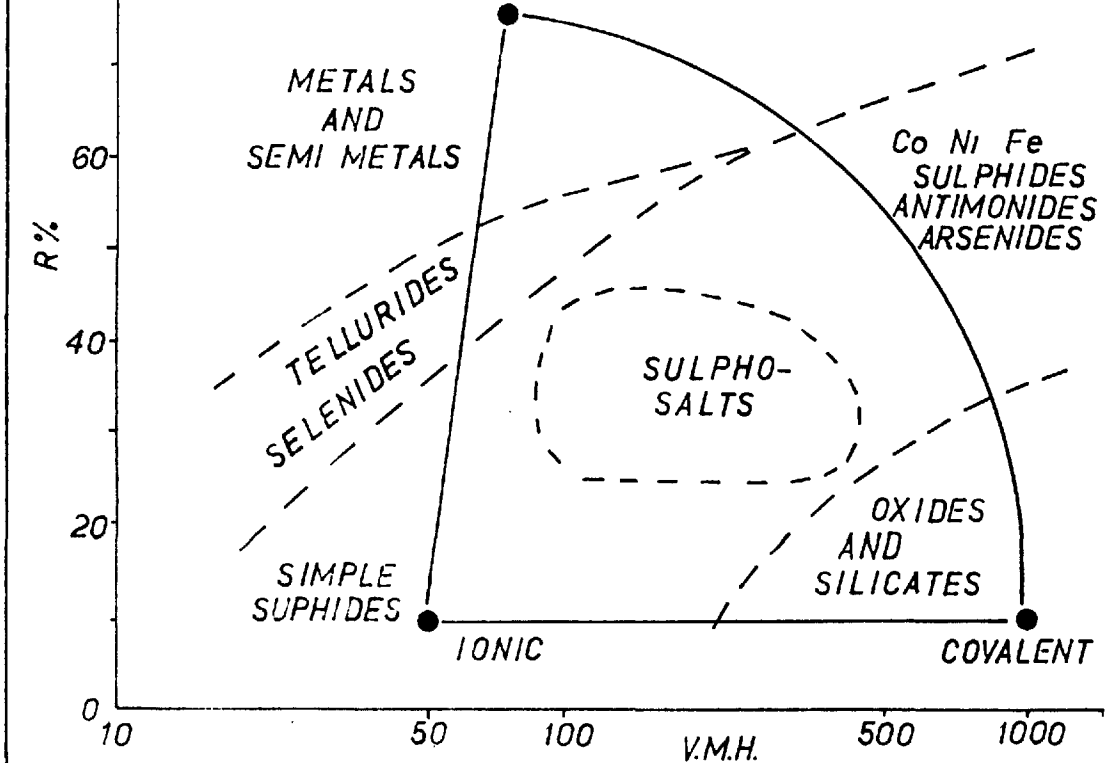


FIG. 77
BONDING IN RELATION TO MICROHARDNESS AND REFLECTIVITY



D. Comparison of other Physical Properties of Minerals with Microhardness Values

Graphical comparisons of microhardness values with other physical properties are given in Figs. 78, 79, 80, 81, 82. The values of the properties have been collected from various sources. Resistivity values have been obtained from the work of Harvey (1928). Refractive and absorption indices (for yellow light) have been obtained from the following publications; Winchell (1951), Larsen and Berman (1934) and the International Critical Tables (1928). Values of specific gravity have been taken from Palache et.al. (1944).

The conductivity/microhardness relationship

Specific resistivity values have been plotted on regular scale against microhardness (log. scale) in Fig. 78. It can be seen that the relationship between conductivity and microhardness is practically identical to that between reflectivity and microhardness and indicates a linear relationship between conductivity and reflectivity.

The refractive and absorption indices/microhardness relationships

The relationships between these physical properties

are broadly similar to the reflectivity/microhardness relationship. Figs. 79, 80 and 81 indicate a log/linear relationship between absorption index and reflectivity and a broadly linear relationship, with some exceptions between reflectivity and refractive index.

The specific gravity/microhardness relationship

The specific gravity of the minerals have been plotted logarithmically against microhardness values. The plot, Fig. 83, shows a general concordance with the microhardness/reflectivity plot in Fig. 72. We may conclude from the results that an approximately log/linear relationship occurs between specific gravity and reflectivity.

The indentation characteristics/microhardness relationship

Perfect plastic deformation occurs in both metallic and ionic crystals, but deformation in covalent minerals usually takes place by fracturing of the structure. Thus the mode of deformation of minerals is a reflection of the nature of the bonding in minerals. A comparison of the indentation characteristics with the microhardness-reflectivity values shows how the indentation characteristics reveal the different structures of the mineral groups. For example, niccolite and breithauptite deform plastically indicating some degree

FIG. 78

THE MICROHARDNESS/RESISTIVITY
RELATIONSHIP

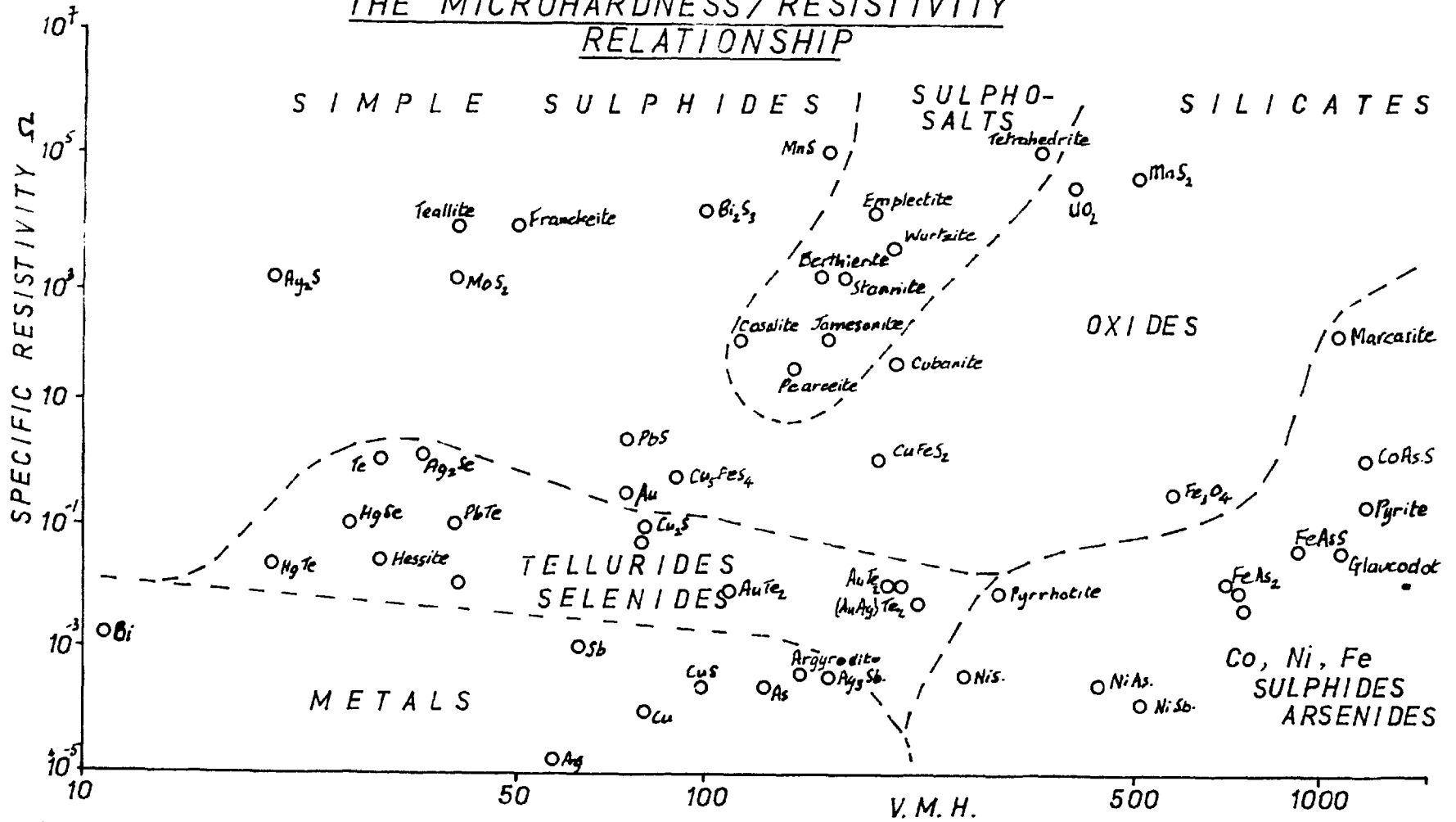


FIG. 79
THE MICROHARDNESS/
REFRACTIVE INDEX
RELATIONSHIP

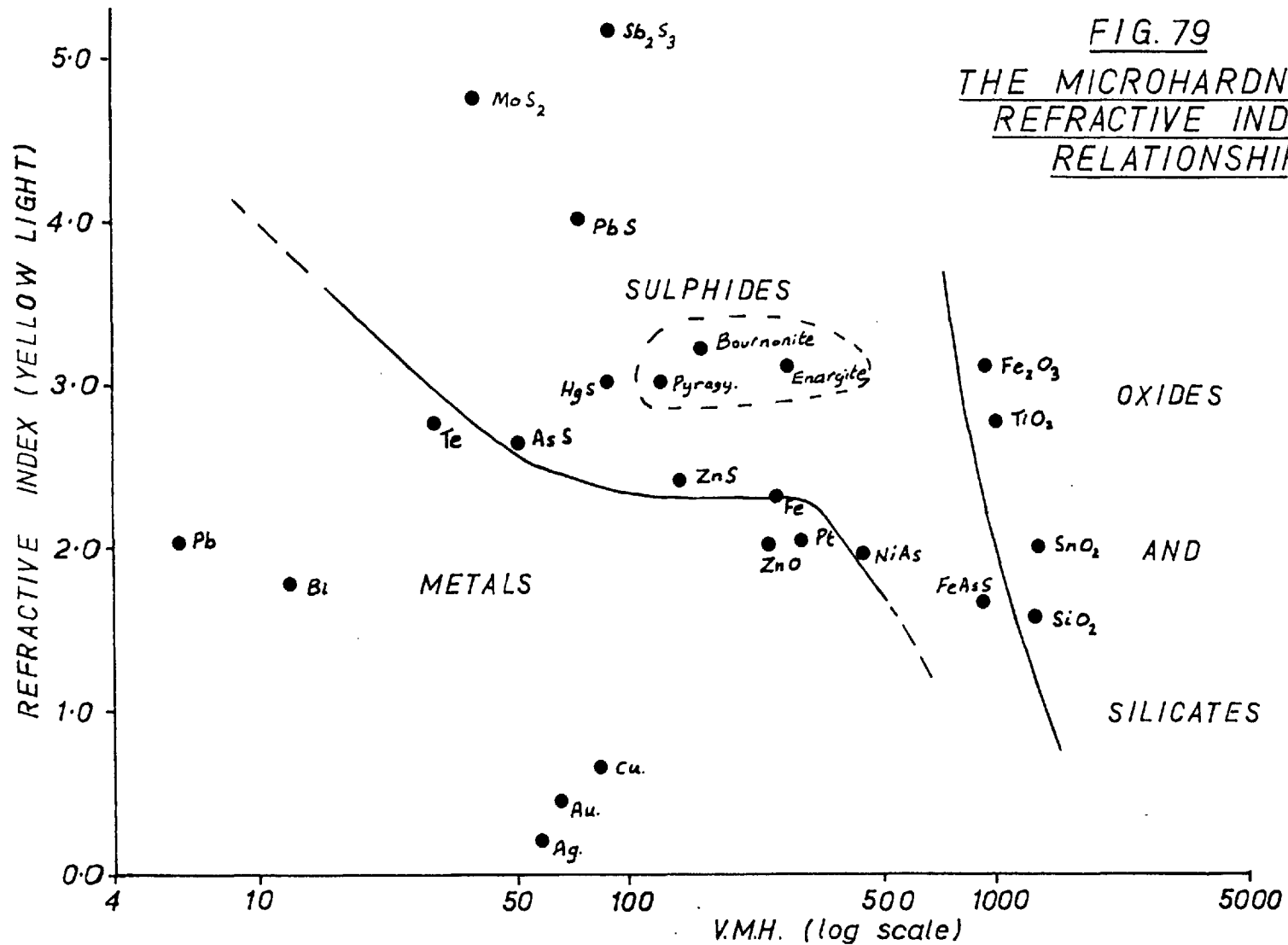


FIG. 80
THE MICROHARDNESS/ABSORPTION INDEX RELATIONSHIP.

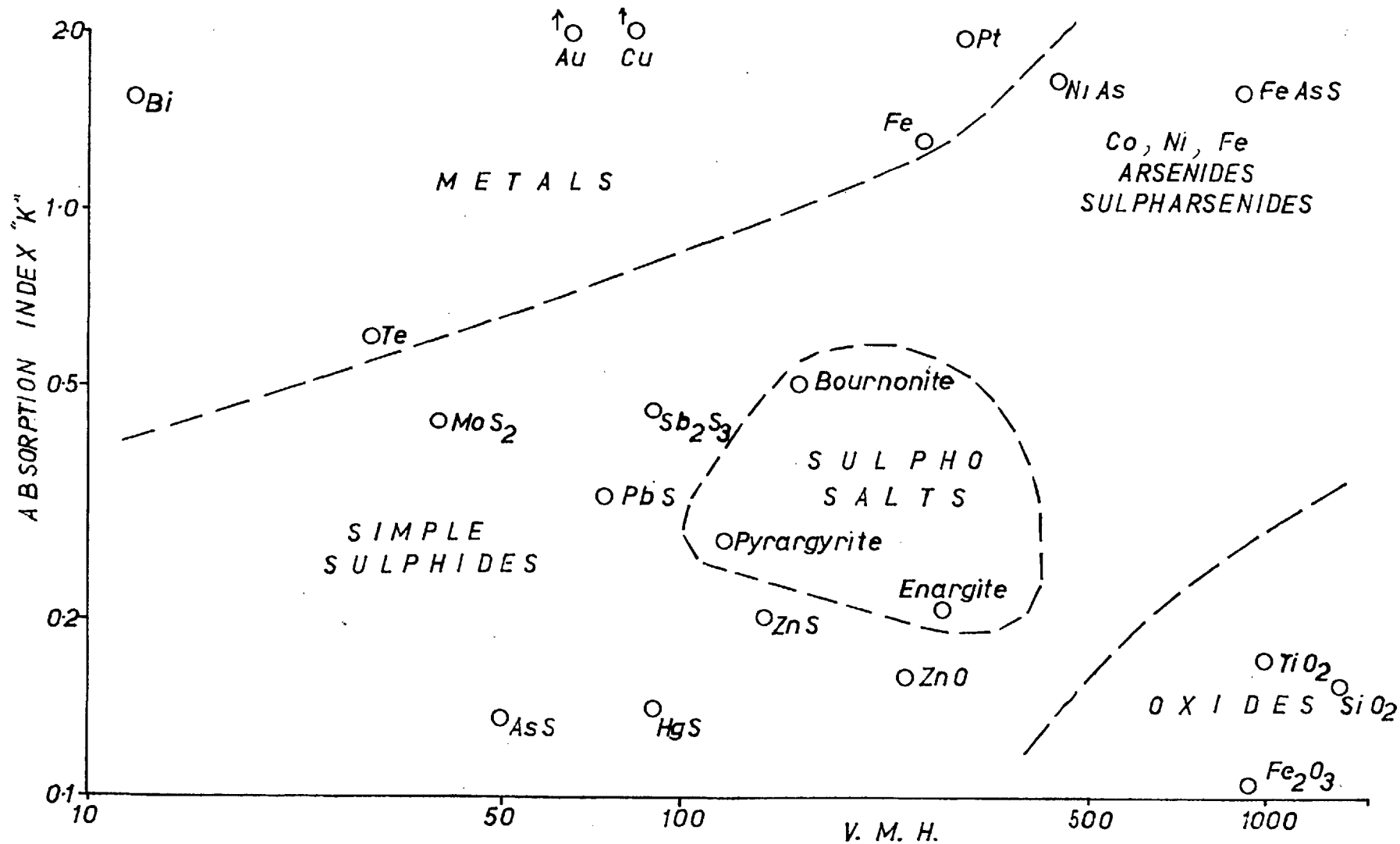


FIG. 81

THE MICROHARDNESS/SPECIFIC GRAVITY
RELATIONSHIP FOR THE HIGHLY
REFLECTING MINERALS

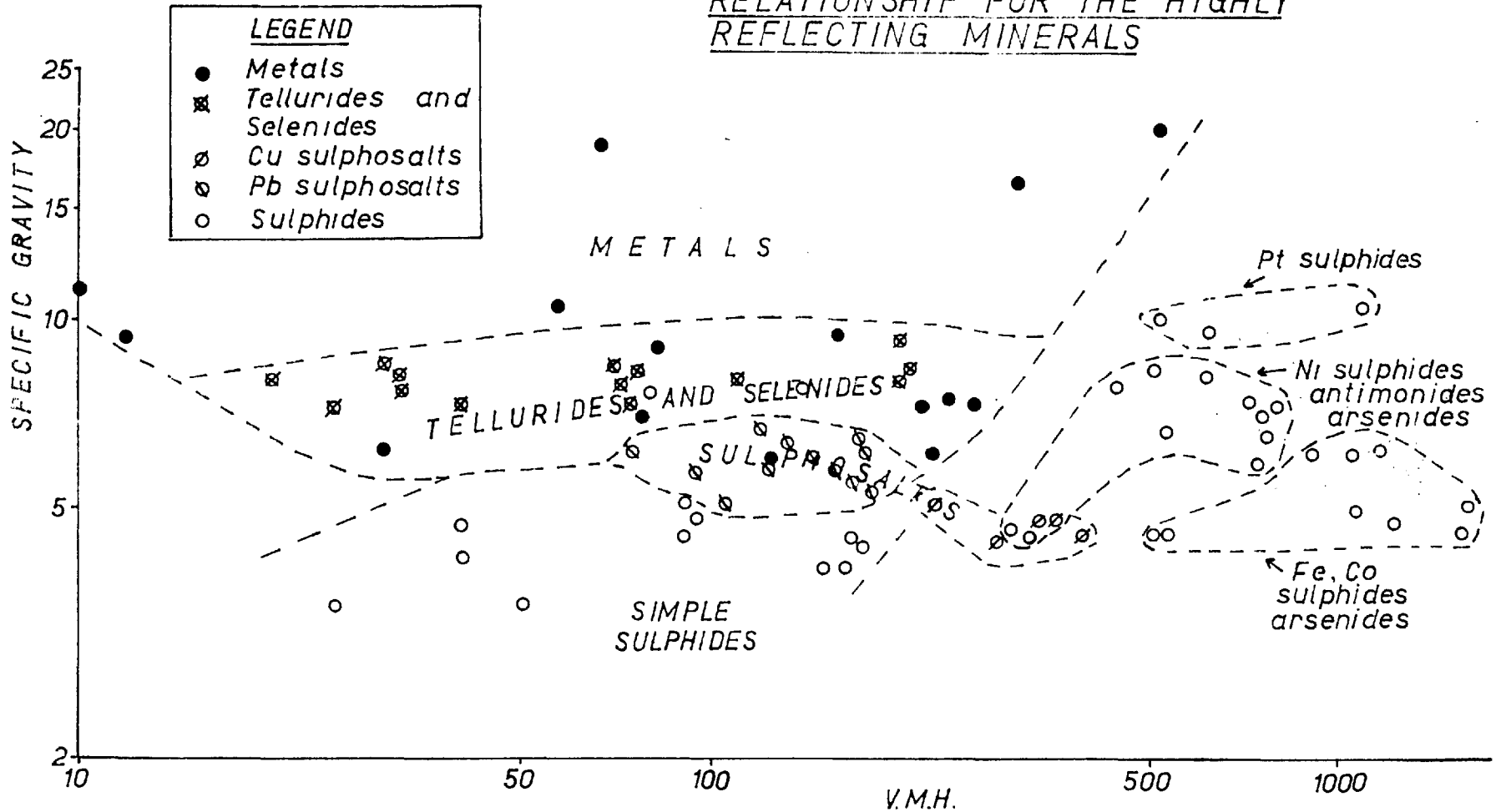
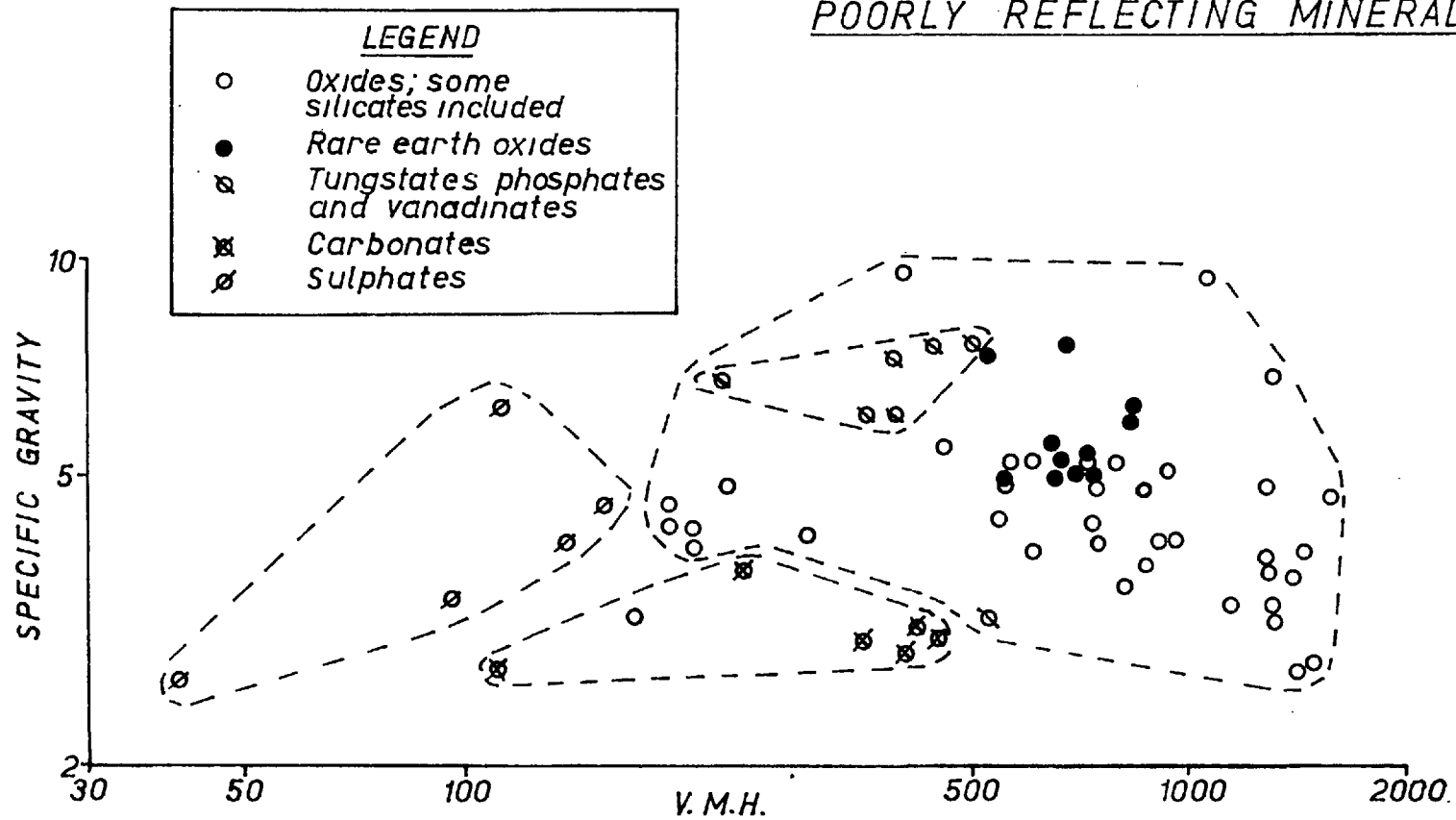


FIG. 82

THE MICROHARDNESS / SPECIFIC GRAVITY RELATIONSHIP FOR THE POORLY REFLECTING MINERALS



of metallic bonding in the minerals, whilst pentlandite and cubanite, although softer, deform by fracture. The metals, most of the tellurides and selenides, and some of the simple sulphides deform plastically. The gold tellurides are an exception, and by their strong fracturing reveal their dominantly metallic-covalent bonding. The sulphosalts and the cobalt nickel iron arsenides and sulphides are brittle minerals and contradict theories that postulate increasing brittleness accompanied by increasing hardness. Many of the oxides, particularly the spinels, show little indentation fracturing and indicate the presence of ionic bonding.

General conclusions

There appear to be definite relationships between the reflectivity, the conductivity, the refractive and absorption indices, and the specific gravity of the opaque minerals. These properties, like microhardness and indentation characteristics, are an expression of the fundamental atomic structure and bonding of the minerals. The properties of the different bond types are summarized in Table LVII.

TABLE LVII

The Relationship between bonding and the physical properties of minerals.

Physical Property	Bond Types		
	Metallic	Ionic	Covalent
Microhardness	Low-med.	med.-high	high
Reflectivity	high	low	low
Conductivity	high	low	low
Refractive Index	low	med.	low
Absorption Index	high	low	low
Specific Gravity	high	low	low
Indent. Charact.	Perfect	Perf.sl.fract.	Strong fracts.

E. The Relationship between Microhardness, Paragenetic Sequence and Temperature of Formation

(a) The microhardness/paragenetic sequence relationship

The relationship between hardness and paragenetic sequence was first described by Gilbert (1924). He found that the first formed minerals were generally harder (and more insoluble) than later formed minerals. Correlation between paragenesis and other fundamental properties is discussed by Edwards (1954). Edwards shows that the normal sequence of deposition corresponds with a progressive decrease in heats of formation and solubilities of minerals and an increase in the atomic number of the electronegative elements. These relationships reflect a fundamental correlation between paragenesis and crystal structure. Many anomalies have been found. These exceptions to the general trend emphasize the fact that other factors also control the paragenetic sequence, such as the availability of elements in the ore solutions, etc. The anomalous position of the iron sulphides in the paragenetic sequence may be explained in such a manner.

Edwards shows that the normal sequence of deposition in sulphide ore deposits is controlled by the structure type of the mineral groups. The sequence given is as follows:

- (i) pyrite and marcasite structured minerals
- (ii) nickel arsenide type structured minerals
- (iii) zinc blende type structured minerals
- (iv) Rock salt type structured minerals.

Ross (1957) has classified the sulphides according to their atomic structure and geochemistry. Using this system of classification, in conjunction with the paragenetic relationships between minerals, as observed by Uytendogaardt (1951), it has been possible to extend the paragenesis of the structure type of the minerals, (Table LVIII).

Table LVIII shows the relationship between the paragenetic sequence of the structure type, the bond type, the hardness and the cationic valencies. It has been established earlier in the text that the hardness of the ore minerals are dependent upon the bond type as follows;

$$H_{\text{(covalent)}} > H_{\text{(ionic)}} > H_{\text{(metallic)}}$$

From Table LVIII it follows that the paragenetic sequence is controlled by the relative amounts of covalent, ionic and metallic bonding existing in the minerals. More fundamentally, the paragenesis of a mineral is determined by the strength of the chemical affinities of the electro-negative and electropositive elements towards one another.

TABLE LVIII

The Relationship between Structure, Bonding, Valency, Microhardness and Paragenetic Sequence of the Sulphides.

Structure Type	Para-genetic Sequence	Bond Type	Mean Microhardness value for each group	Valent Type of Cation
Pyrite	1	Covalent	1100	4
Marcasite	2	Covalent	1000	4
NiAs.	3	Met.-Covalent	450	3
Spinel	4	Ionic-Covalent	450	2-3
Sphalerite)	5	Met.-Ionic-	200	2-3
Wurtzite)		Covalent	200	2-3
Chain struc-)	6	Met.-Ionic	130	2-3
tured sulpho-)		Covalent	130	2-3
salts and)				
sulphides)				
Galena	7	Met.-Ionic	70	2
Antifluorite	8	Metallic	40	1-2

Extending the field to include the oxides, silicates, metals and semi-metallic compounds, we see that the same relationship holds good. Thus the oxides, hard and dominantly ionic-covalent bonded, appear early in the paragenetic sequence. Whilst the metals and semi-metals, soft and metallic in bond type, occur usually late in the paragenetic table.

A few exceptions do occur, particularly the layer lattice minerals such as molybdenite and graphite. These minerals, although soft, appear early in the paragenetic sequence. The low hardness is due to perfect translation between adjacent layers, but the lattice strength of the individual layers is high, being covalently bonded.

(b) The microhardness/temperature of formation relationship

Edwards (1954) lists a number of both ore and gangue minerals characteristics of high, medium and low temperature ore deposits. Table LIX illustrates the relationship between the hardness of the minerals of these groups and their deposition temperatures. Thus, increasing temperature of formation is accompanied by increased hardness of the minerals. As discussed above the paragenesis is controlled by the bonding with the minerals. Table LIX illustrates that high temperature of formation is associated with

TABLE LIX

Relationship between Temperature of Formation of Minerals and
their Hardness Values

Ore Minerals	Mean V.M.H. Value	Gangue Minerals	Mean V.M.H. Values
<u>(High Temperature Minerals (deposited above 500° C)</u>			
Cassiterite		Tourmaline	
Wolframite		Topaz	
Molybdenite [Ⓜ]	720	Rhodonite	1300
Magnetite		Garnet	
Hematite		- quartz	
Pyrrhotite			
Lollingite			
<u>(Intermediate Temperature Minerals (deposited below 500°C)</u>			
Galena		- quartz	
Tetrahedrite		Fluorite	
Jamesonite	160		700
Stannite			
Bornite			

TABLE LIX Contd.

Ore Minerals	Mean V.M.H. Value	Gangue Minerals	Mean V.M.H. Values
<u>Low Temperature Minerals (deposited below 250°C)</u>			
Stibnite		Rhodochrosite	
Realgar		Siderite	
Cinnabar	70		300
Tellurides			
Argentite			
Chalcocite			
Pyrrargyrite			
Marcasite*			

*Excluded from mean.

minerals having covalent bonding and low temperature minerals with ionic or metallic bonding.

F. Crystallochemical Factors Controlling Microhardness

Early investigators, Kenngott (1952), Rydberg (1900), Kip (1907), Pöschl (1909), and others tried to calculate the hardness of minerals by using properties such as specific gravity, atomic weight and atomic volume. Later workers, Reis and Zimmerman (1922), and Frederich (1934), showed that valency was important in the calculation of hardness but did not succeed in evolving a formula that gave values close to the actual results. Further efforts were made by Goldschmidt (1926, 1933) and Fersman (1937) to find the factors that controlled the hardness of minerals. These two workers found that hardness was dependent upon the interatomic distances, the valencies and the coordination number. More recently, Povarennykh (1959) showed that the hardness of minerals is dependent upon the following additional factors; the degree of covalent bonding, the strength of the repulsion between atoms and the amount of metallic bonding. He proposed the following formula for the calculation of the hardness of binary isodesmic minerals;

$$H = \alpha K \frac{W_k \cdot W_a}{d^2} \beta \gamma$$

where H = Mohs scale hardness number

α' = Coefficient taking into account the forces of repulsion between atoms of different valent types

K = Coefficient taking into account the degree of covalent bonding in the mineral

W_k & W_a = Valencies of the cation and anion

d = Interatomic distance

β = Special coefficient, mainly for transition elements to compensate for the effect of metallic bonding

χ = Coefficient taking into account the volumetric influence of coordination number.

Petty (1961) has shown that for the intermetallic compounds Mg_2Si , Mg_2Sn and Mg_2Pb , the Vickers microhardness values are in close agreement with the formula proposed by Goldschmidt i.t.

$$H = S \frac{l_A \cdot l_B}{r^m}$$

where,

S and m are constants

l_A and l_B = Valency of the atoms

r = Interatomic distance

m = Slope of the graph.

The present studies indicate that the microhardness

mean values of the minerals are dependent upon the atomic radii of the elements involved and also upon the valency of the elements. Microhardness values have been plotted, Figs. 83, 84 and 85, against the interatomic distances for four isostructural series. The results show very close relationships to the Goldschmidt formula.

In the calculation of the hardness of minerals of the transition elements, or divalent lead, Povarennykh found that the calculated values were considerably higher than the actual hardness values. He, therefore, introduced a special coefficient, f_c , (0.75, ± 0.05 for covalent minerals, -0.05 for ionic minerals), to reduce the calculated hardness values to the actual values.

It has been noted earlier, in Chapter VI that some anomalies occur when the theoretical hardness values are compared with the actual values. For example, breithauptite (Ni Sb) and cassiterite (SnO_2) are respectively harder than niccolite (NiAs) and rutile (TiO_2), but calculations based on the formula of Povarennykh indicate the reverse relationships. It has been deduced that these reversals are caused by differences in the amounts of metallic bonding.

Although the present results are in agreement with the Goldschmidt formula i.e. that a log/log relationship exists between microhardness and interatomic distance, the formula

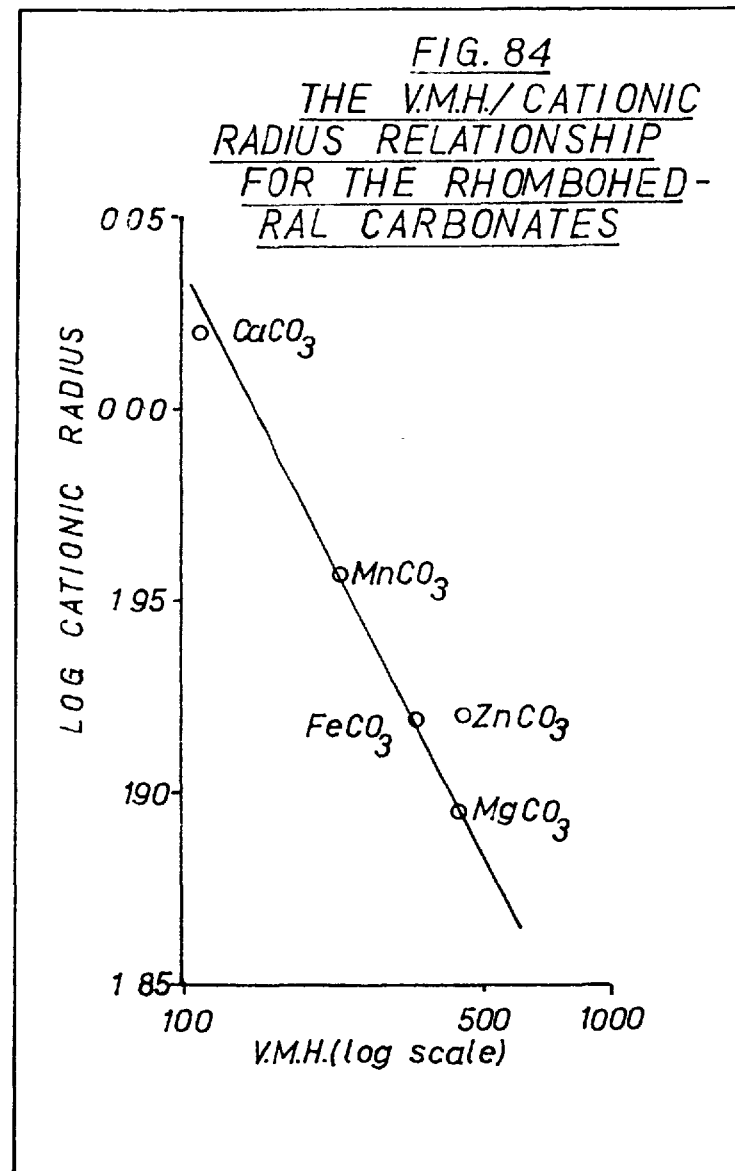
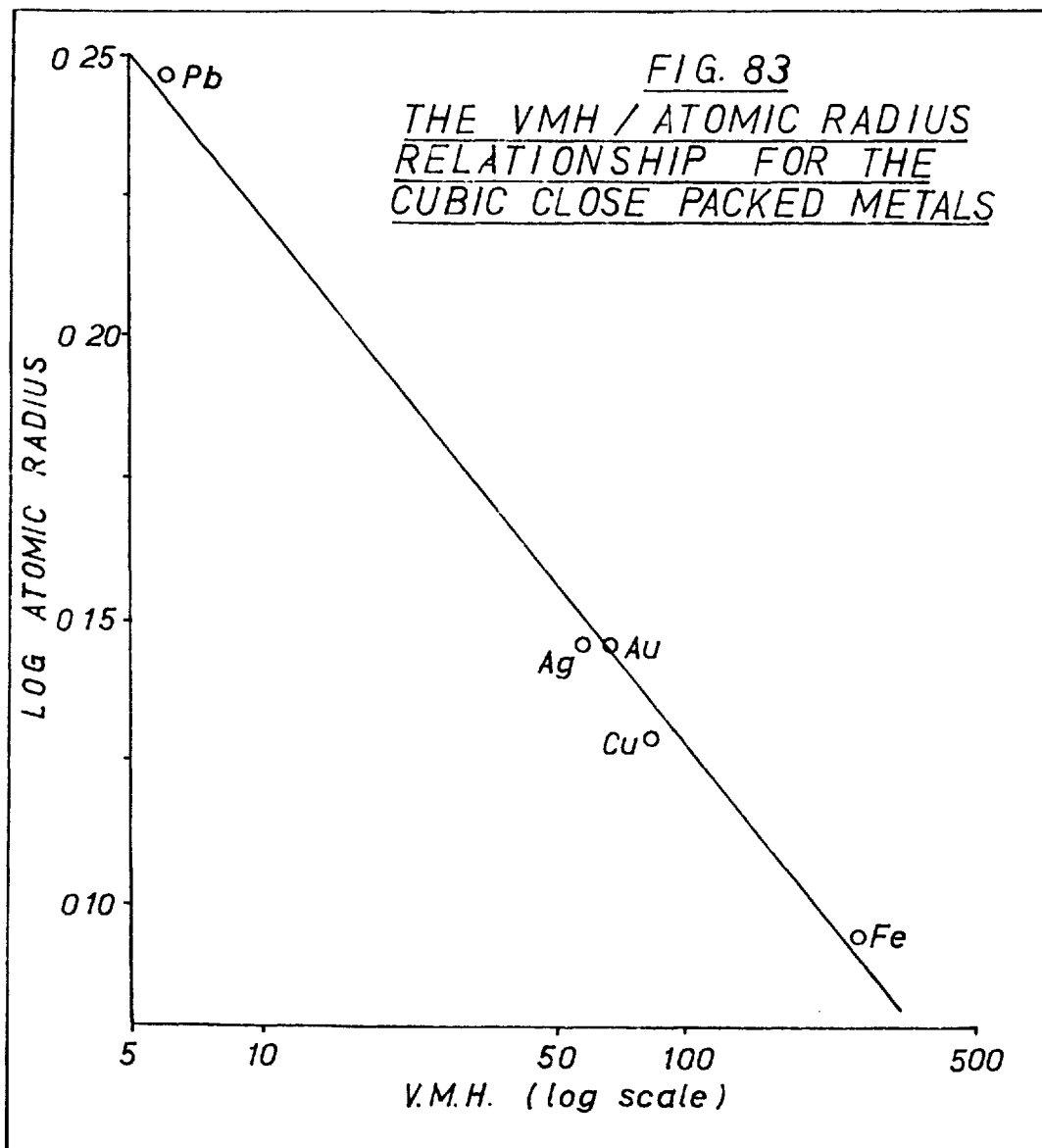
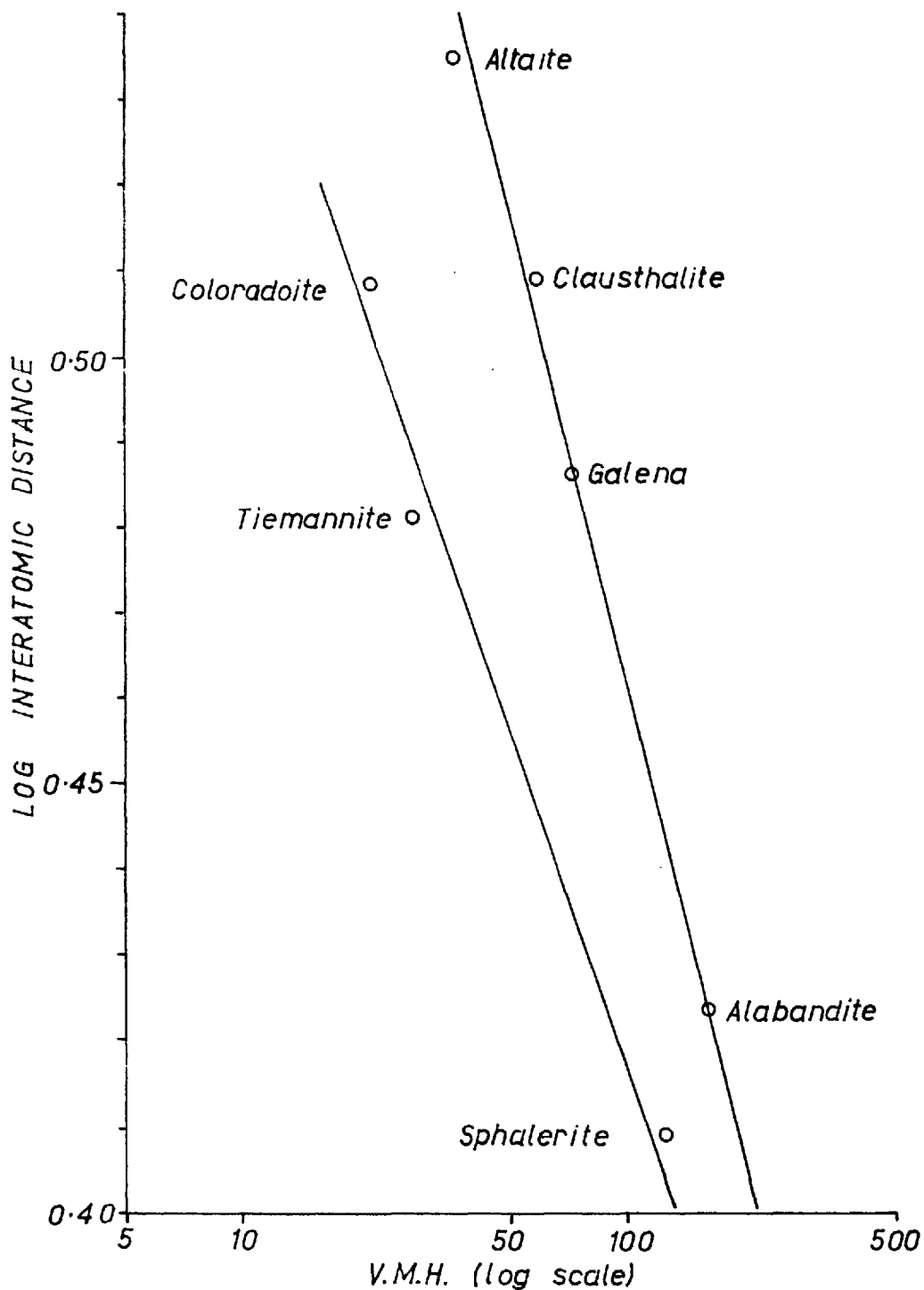


FIG. 85

RELATIONSHIP BETWEEN MICROHARDNESS
AND INTERATOMIC DISTANCE FOR MINERALS
OF THE GALENA AND SPHALERITE STRUCTURE
TYPES



is not in convenient form to calculate the hardness of other minerals. The formula of Povarenykh enables a direct calculation to be made without the knowledge of any factors. However, instead of applying a constant coefficient, used only for the transition element and divalent lead, it would seem more logical to insert a coefficient which would take into account the effect of variations of the amount of metallic bonding.

If metallic radii are substituted for ionic radii in partially metallic bonded minerals a closer approximation to the true value results. For example, if the metallic radius of lead is substituted for that of divalent lead, in galena, in the formula of Povarenykh, the calculated hardness is reduced from 3.4 to 2.5. As the actual value for galena is 2.5, and galena is only partly metallic, it seems incorrect to substitute the atomic radius in this manner. Such a method would also not account for the anomalous values for breithauptite etc. It is therefore suggested that a coefficient be used similar to that of β in Povarenykh's formula, i.e. 0.75 ± 0.05 + ve for weakly metallic minerals and -ve for strongly metallic minerals. The "degree" of metallicness may be judged from other physical properties such as reflectivity, refractive index etc.

The final formula for the determination of the

microhardness of binary isodesmic minerals is as follows:

$$0.366 \log mH = \log \left(\alpha K \frac{W_k \cdot W_a}{d^2} M \gamma \right)$$

where mH = Mean microhardness value

α = Coefficient taking into account the forces of repulsion between atoms in different valent types of compounds that form, for the valent types 1/1 - 15.0; 2/1 - 7.95; 2/2 - 4.8; 3/2 - 3.92; 4/2 - 2.26; 3/3 - 2.56; 4/4 - 1.71.

K = Coefficient showing part of the exchanged bond with a covalent link, changing from 1 (for 0%) to 2 (for 100%) covalency.

W_k & W_a = Valencies of the cation and anion.

d = Distance between atoms

M = Coefficient taking into account the degree of metallic bonding, used mainly for transition elements, and equal to 0.75 ± 0.05 , +ve for weak metallic bonding and -ve for strong metallic bonding.

γ = Coefficient taking into account the effect of the coordination number; For C.N. 4, 6, and 8 the coefficients are respectively 0.65, 1.0 and 1.3.

TABLE LX

Mineral	Chem. Comp.	% Covalent bonding	Inter-atomic distance	Value for M	Calc. hardness	Measured hardness
Fluorite	CaF ₂	8	2.39 [#]	1.0	210	190
Zincite	ZnO	37	1.97 ^o	1.0	310	241
Sphalerite	AnS	74	2.35 ^o	1.0	195	150
Galena	PbS	63	3.06 [#]	0.7	65	72
Altaite	PbTe	80	3.43 [#]	0.7	50	36
Alabandite	MnS	63	2.65 [#]	1.0	275	161
Tenorite	CuO	43	2.18 [#]	1.0	190	228
Millerite	NiS	76	2.52 [#]	0.7	125	269
Corundum	Al ₂ O ₃	40	1.89 [#]	1.0	2500	2427
Eskolaite	Cr ₂ O ₃	46	1.96 [#]	1.0	2350	2600
Hematite	Fe ₂ O ₃	45	1.99 [#]	0.8	1250	950
Quartz	SiO ₂	52	1.71 [#]	1.0	925	1414
Cassiterite	SnO ₂	43	2.06 [#]	1.0	950	1310
Rutile	TiO ₂	49	1.96 [#]	0.8	680	1000
Thorianite	ThO ₂	27	2.42 [#]	1.0	470	1066
Niccolite	NiAs	97	2.49 ^x	0.7	500	440
Breithauptite	NiSb	100	2.69 ^x	0.75	425	509

[#]Ionic radii obtained from Table XLV

^oAtomic radii obtained from Table XLV

^xTetrahedral radii obtained from Table XLVI

Table LX gives a series of microhardness values obtained for seventeen minerals using the above formula. Values for the coordination numbers and "degree of covalency" of the bonding were taken from the work of Povarennykh (1959), and interatomic distances obtained from atomic radii established by Evans (1948) and Pauling and Huggins (1934). Eleven of the seventeen minerals give calculated microhardness values which approximate to the measured microhardness values. Closest agreement occurs in minerals where the interatomic distances are known precisely, as for example in essentially ionic compounds such as fluorite and corundum. In other minerals the calculated microhardness values deviate considerably from the measured values, particularly in the group, quartz, cassiterite, rutile and thorianite where the calculated values are consistently lower than the measured. For this group it seems likely that the interatomic distance, obtained from the individual ionic radii of the elements, are too large. Although most of the minerals examined are known to be partly covalent, ionic radii have been used in the calculations, no precise interatomic distances being available. With the quadrivalent elements, Si, Sn, Ti and Th, strong polarisation due to the high valency changes will cause reduction in the interatomic distances in the minerals quartz, cassiterite, rutile and thorianite. If a reduction

of 0.1 units is made in the interatomic distances, close agreement occurs between calculated and measured values. Polarisation effects probably also account for the low calculated value for millerite. Calculations for alabandite give a higher hardness than the value obtained in the present study. However, it compares favourably with a value of 261 obtained by Bowie and Taylor (1958).

Taking into account the accuracy of the data for interatomic distances and percentage covalent bonding in minerals, the proposed formula gives microhardness values which agree to within $\pm 25\%$ of the measured values. With more accurate crystallochemical data, the calculated hardness values may be expected to show a closer agreement with measured values.

CHAPTER VIII

Mineralogical Applications of Microhardness Testing Techniques

The applications of microhardness testing in the mineralogical field are three fold. Firstly it may be used as a reliable aid in mineral identification; secondly, on a broader front, it may be used in studies of the atomic structure, bonding and deformation of the opaque minerals; and thirdly it has a potential application in the field of ore fabric analysis.

(a) The application of microhardness testing in mineral identification

(i) The identification of individual mineral species

The use of microhardness testing as an aid to mineral identification has been demonstrated by many authors. Bowie and Taylor (1958) showed that the combination of microhardness and reflectivity values provided a rapid and reliable means of mineral identification. This system has been employed by I.M. Gray and the present author (Gray and Young, 1960) for over 160 fully identified opaque minerals and has proved to be a highly satisfactory technique. Only the oxides and hydroxides of iron and manganese gave

unreliable results. In the foreseeable future, ultimate positive identification of minerals in polished sections will be achieved by means of X-ray scanning microanalysis technique. However, as this is primarily an expensive research tool, routine identification based on the ore microscope must at present remain pre-eminent. By incorporating all the indentation, microhardness, and reflection characteristics into a punched card system, the Bowie and Taylor system of mineral identification could be further improved. The following information should be used in such a system;

1. Vickers microhardness ranges and mean values
2. Knoop microhardness ranges and mean values
3. The characteristics of the shape of the indentations
4. The elongation of Vickers indentations
5. The absence or presence of glide planes and their characteristics
6. The absence or presence of fractures and their characteristics.

(ii) The positioning of an intermediate member in an isomorphous series

The present results indicate that end members of isomorphous series can be distinguished from one another on

microhardness values alone. Similar changes in reflectivity have been found (Gray, 1961) and ideally both properties should be used in conjunction with one another. Work carried out on the three isomorphous series studied, sphalerite-cristophite, huebnerite-ferberite, and columbite-tantalite indicate non-linear hardness relationships between end members. Extrapolation from such relationships should be treated with caution until further work backed by detailed chemical analysis has been carried out.

(b) The application of microhardness testing to problems of bonding and deformation in minerals

(i) The application of microhardness testing to problems of mineral deformation

In the past mineral deformation has been studied by subjecting mineral crystals to very high pressures, e.g. (Buerger, 1928). Results in Chapters IV and V show that the same translation data can be deduced from a study of the microhardness values and indentation characteristics obtained on oriented sections of the minerals. Observations of the following characteristics provide useful information in this field.

1. The directions of minimum Knoop microhardness
2. The shape of Vickers indentations

3. The elongation of Vickers indentations
4. The presence and orientation of glide plane traces, cleavage fractures, or twin planes.

(ii) The application of microhardness testing to problems of mineral structure and bond type

As shown earlier in Chapters V and VII, a study of the deformation characteristics of minerals enables deductions to be made concerning their bond types. Thus, niccolite and breithauptite are considered to have considerable amounts of metallic bonding in their structures on the basis of their lack of indentation fractures, and the presence of glide planes and concave and convex sided impressions.

By comparing measured microhardness values with calculated microhardness values it is possible to predict more precisely, the percentage of covalent and metallic bonding in minerals. In addition such hardness values provide approximate checks on the interatomic distances in minerals. For example, the microhardness values for niccolite and breithauptite, and rutile and cassiterite indicate that the former minerals, niccolite and rutile have a greater percentage of metallic bonding than the latter minerals. Also the calculated microhardness values for the quadrivalent oxides, rutile, quartz, cassiterite and

thorianite indicate that their interatomic distances are lower than the sum of the ionic radii of their component elements.

(c) The application of microhardness testing to ore-fabric analysis

Considerable variations of microhardness have been found with orientation, for many of the opaque minerals and similar reflectivity variations have also been found, (Gray, 1961). A potential application of these variations is in the field of ore fabric analysis. Many of these anisotropic minerals show corresponding variations in their indentation characteristics. Microhardness characteristics would have a particular application in the determination of the orientation of isotropic minerals, such as galena and sphalerite, for which reflectivity values show no variations. An immediate application of this technique is in the determination of whether an isotropic mineral grain occurs as an exsolution product or as an unreplaced remnant. Microhardness determinations, analogous to "optical-continuity" tests, would help to solve this problem. The genesis of some of the deformed galena-sphalerite ore bodies might well be established by such petrofabric techniques. Present results justify further work in this field.

CHAPTER IX

GENERAL CONCLUSIONS

1. The hardness values of minerals have been shown to be dependent upon the nature and relative amounts of the elements in their atomic structures. These values, together with the indentation characteristics of the minerals, confirm the concept that mineral properties are determined primarily by the position of the elements in the Periodic Table. Elements possessing high valency states, small atomic radii, and hence high potential polarisabilities i.e. the group III, IV and V elements of low atomic number, produce mineral compounds of great hardness. Elements having large atomic radii and low valency states combined with a tendency towards metallic bonding, i.e. the group I, II, VI and VII elements with high atomic numbers, produce compounds of low hardness. The present results show that the microhardness value of a mineral is directly related to the valency state of the atoms and inversely related to a function of their interatomic distance.
2. High hardness values in certain isomorphous mineral series have been attributed to "inhibited translation" produced by

distortion of their crystal structures. This distortion occurs in three different ways: firstly by non-stoichiometry of the atoms; secondly by the presence of small amounts of foreign atoms; and thirdly, by "disordered" differences in the atomic radii of the cations. Non-linear microhardness relationships were found in the following isomorphous series; sphalerite-christophite, huebnerite-ferberite and columbite-tantalite. Increased microhardness values occurred particularly in the intermediate members of the columbite-tantalites and huebnerite-ferberite series where the ratio of the iron and manganese atoms approximated to unity. These high hardness values are probably results from disorder of the crystal structure caused by differences in the dimensions of the ionic radii of the iron and manganese ions. Such disorder would be a maximum when approximately equal amounts of the ions exist in the crystal lattice. The presence of very small amounts of tin and iron has been found to cause considerable increases in the hardness values of mangan-tantalite and sphalerite respectively. Non-stoichiometry has been deduced to be the cause of anomalously high hardness values obtained on a particular galena crystal.

3. The results indicate that covalent bonding is stronger than ionic bonding, and that ionic bonding is, in turn,

stronger than metallic bonding. A formula, proposed by Povarennykh, for the calculation of the hardness of binary isodesmic minerals from crystallochemical data, has been examined and found to produce hardness values inconsistent with the present microhardness data. A modification of this formula has been evolved incorporating a coefficient dependent upon the degree of metallic bonding and this has been found to give microhardness values which agree more closely with measured values, the agreement being of the order of $\pm 25\%$. The order of accuracy is expected to be improved when more accurate data is available concerning interatomic distances and degree of covalent and metallic bonding in minerals.

4. The present microhardness results show an approximately linear relationship with published Talmage scratch hardness ratings and an approximately log./log. relationship with published Mohs scale hardness values. By comparison, microhardness values are much more accurate and reliable than Mohs or Talmage values. A comparison of the Vickers indentation and Mohs hardness values of the standard minerals of the Mohs scale, excepting diamond, reveals that their relationship closely follows that of the cubic parabola $y = x^3$. According to microhardness determinations, the

hardness of diamond, on the Mohs scale is equal to 15.

5. Comparison of the microhardness values of the minerals with other physical properties, such as reflectivity, refractive and absorption indices, conductivity and specific gravity reveals that the minerals sub-divide themselves into broad chemical groupings. Direct relations between the physical properties of minerals and their fundamental crystal chemistry have been deduced. Examination of these relationships illustrates the inter-dependence of chemical composition, interatomic distance, bonding and valency in minerals. Metallicly bonded minerals, for example, the metals, tellurides, and the selenides, show high reflectivities and relatively low microhardness values, whilst covalently bonded minerals such as the oxides and silicates show low reflectivities and high hardness values. Ionically bonded minerals, such as the simple sulphides, have low reflectivities and low to medium microhardness values. Intermediate to these groups are sulphosalts which have ionic, covalent and metallic bonding. The transition-element sulphides have high reflectivity and microhardness values due to their metallic-covalent bonding. Sub-division of these anionic groupings of minerals can be made on the basis of the electronic configurations of the cationic elements in the minerals.

6. The paragenetic sequence of the ore minerals has been shown to be related to microhardness by reason of their bonding characteristics rather than their atomic structures. Early formed minerals have been shown to be dominantly covalent and/or ionic in character, and later formed minerals dominantly metallic. A corresponding decrease in the cationic valency has also been found. At high temperatures only the elements with strong chemical affinities link together to form compounds. The strength of this affinity is expressed by the linking or sharing of bonds which give rise to high microhardness values. At low temperatures, the chemical affinities are weaker and more loosely bonded structures are formed. In this manner softer minerals appear later in the paragenetic sequence.

7. The indentation characteristics of the opaque minerals have been shown to be an expression of the type of bonding existing in their structures. Perfect deformation without rupture, occurs only in metallic, or in a few cases, ionic bonded structures. The fracture characteristics have been classified into four main types; radial, cleavage, parting and shell fractures. Shell and radial fracturing have been found to be an indication of covalent bonding in a mineral, and cleavage fracturing an indication of the presence of weak Van der Waal bonds.

Indentation characteristics have been found to vary with

orientation, and have been correlated with glide plane directions as well as with Knoop and Vickers microhardness determinations. On particular crystal faces showing marked Knoop microhardness anisotropy, the direction of minimum hardness, or glide plane trace, has been found to be parallel to those edges of a Vickers indentation showing convex sides. This direction is perpendicular to the position of maximum elongation of Vickers indentations. It has been deduced that sigmoidal faces indicate that the diagonals of an indentation are neither parallel nor perpendicular to the glide plane. Study of both Knoop and Vickers indentation characteristics, together with corresponding microhardness values, enables predictions to be made as the probable glide plane directions in minerals. More indentation fracturing occurs at higher loads than at lower loads; slip planes are also more easily discerned at higher loads. Microhardness and brittleness have been shown to be independent of one another, brittleness being related more to the presence of covalent bonds.

8. At identical loads, Knoop microhardness values are about 5% lower than corresponding Vickers values. For most minerals Vickers microhardness values show a smaller range of anisotropism compared with similar Knoop values.

9. When the indentation direction is not perpendicular to the plane of the polished section, asymmetric indentations are produced. Whilst the microhardness values of Vickers indentations are not appreciably affected by such "tilting", Knoop indentations give considerably lower hardness values if the tilt exceeds 1° .

10. The high temperatures and pressures involved in the thermoplastic mounting of polished sections have been found to affect the microhardness values of minerals appreciably, particularly the softer ones. In most cases the hardness is increased - in one particular case up to 40%. In addition, the minerals are made more brittle.

11. The microhardness values of the opaque minerals studied have been found to vary with the load applied during indentation. For over 98% of the minerals examined, a decrease in load results in an increase in the microhardness values. A significant exception to this rule was found on the (111) face of a crystal of native gold. The normal variation, for the softer minerals at least, is not due to optical errors involved in the measurement of the indentation diagonals. Detailed orientation studies, on a number of minerals of different hardness, reveal that the amount of

increase of microhardness with decreasing load, increases with increasing hardness of the mineral. In other words, the hard minerals have high logarithmic indices and the softer minerals low logarithmic indices. The logarithmic indices of certain minerals have been found to vary with orientation, the differences being attributed to differences in the mechanisms of deformation with orientation. The load/microhardness variations are attributed to the increased importance of elastic recovery, relative to plastic deformation, at low loads, and in addition, to the independence of the elastic recovery upon the size of the indentation. At high loads it is suggested that plastic deformation is superceded by rupture of the atomic structure. Consequently, little elastic recovery can take place and low hardness values result.

12. Most minerals have been found to exhibit some degree of microhardness anisotropism. Although many exceptions to the rule occur, isometric minerals tend to be more isotropic in microhardness than anisometric minerals. The fact that reflectivity and hardness anisotropy are not directly related to one another suggests that these properties, while both fundamentally related to the basic structure, are dependent upon different "aspects" of the atomic structures of minerals.

Variations of microhardness have been correlated with variations of the orientation of the movement planes to indentation directions. Maximum slip, resulting in minimum hardness, occurs when the movement planes are oriented at 45° to the indentation direction. Maximum hardness is shown when the movement planes are parallel or perpendicular to the indentation direction. From a knowledge of the microhardness anisotropism of a mineral, it is possible to deduce its planes of translation gliding. Conversely a detailed knowledge of the atomic structure and bonding of a mineral can enable its microhardness anisotropism to be deduced. The strength of the hardness anisotropy has been shown to be dependent upon the strength of the weakest bond. For example, molybdenite MoS_2 , with a layer lattice structure is much more anisotropic than quartz with a network structure.

13. The Knoop microhardness of a particular crystal face is a minimum when the long diagonal is parallel to the traces of the movement planes, and a maximum at right angles to this position. Where more than one movement plane occurs, maximum hardness obtains in an intermediate direction between the glide plane trace positions. For the minerals galena, halite and Kyanite, scratch and Knoop microhardness maxima

and minima are in antipathetic positions to one another. These differences indicate a difference in the mode of deformation during testing. For over 70% of the oriented minerals studied, where reflectivity values were available, Knoop microhardness maxima and minima occupied antipathetic positions to the white light reflectivity maxima and minima. This relationship appears to be directly connected with the anisotropy of the bonds strength of the atomic structures high reflectivity and low microhardness being coincident with planes of loosely packed atoms, and low reflectivity and high hardness with planes of *tightly packed atoms*.

14. Vickers indentations made on sections of anisotropic minerals show elongations perpendicular to the traces of the movement planes, when the shorter diagonal is parallel to the movement plane traces. This is attributed to the preferential "piling up" of material during deformation in the areas around the elongated diagonal.

15. The present results indicate that the microhardness values, used in conjunction with other physical properties, particularly reflectivity, provide a rapid and reliable means of identifying unknown opaque minerals in polished sections. The indentation characteristics would be useful as ancilliary

data used in conjunction with reflection properties on a punched card system of mineral identification. Fourteen different types of indentation shapes have been found, and the degree of elongation of Vickers indentations has been shown to be useful in mineral identification. The characteristics of dislocation and fracture planes have also been found to be diagnostic for certain mineral species.

16. It has been proved that **significant errors** are introduced into a system of mineral identification if the same hardness values, determined at high loads, are applied to tests made at low loads. By using lower loads, down to 15 g., together with suitably modified microhardness values the minimum grain size for the softer minerals has been considerably reduced. The microhardness values established in the present studies have been found to be reliable in the identification of small mineral grains. Tests have shown that the indentation size for small grains should not exceed one third of the grain size in order to obtain reliable microhardness results. The minimum optimum grain size should be of the order of 40μ for hard minerals and up to 400μ for the softest minerals.

17. The microhardness testing of isomorphous series, to determine the position of an intermediate member, should be used with great caution as the present studies indicate that non-linear relationships between end members may occur.

Unoriented determinations, made on end members of isomorphous series which were not chemically analysed, indicate that the technique may be used with greater confidence to differentiate between the end-members. Indentation characteristics and microhardness values have been shown to be of value in helping to determine the nature of the structure of minerals. By correlating these characteristics with other physical data it is now possible to predict, at least semi-quantitatively, the degree of metallic and covalent bonding in minerals.

18. A knowledge of the deformation characteristics and microhardness values, obtained on oriented sections of opaque minerals, enables deductions to be made as to their mode of deformation under stress, and also to an understanding of particular features of their atomic structures. Such knowledge can be usefully employed, together with reflection characteristics, in problems of ore fabric. Microhardness testing has a particular application in this field in the case of the isometric minerals where reflection characteristics

show no anisotropy. Further work in this field on galena and sphalerite in particular, is recommended. Such studies would find immediate applications in the genetic problems associated with deformed galena-sphalerite ore bodies.

19. The present microhardness values are probably more precise than any other known published data. However, it is realised that the conclusions have been drawn from a limited number of results. These conclusions should be regarded as tentative until further work has been carried out to confirm or refute the findings. In general terms the ranges and means are probably reproducible to within $\pm 5\%$ of the stated values.

REFERENCES

- Ashby, N.A. 1951. The factor of hardness in metals. New Zealand Engineering, 6,1,33.
- Attinger, C. 1952. Orientation and Hardness of synthetic corundum. Ind. Dia. Rev. 12, 136-137.
- Barringer, A.R. 1953. The preparation of polished sections of ore and mill products using diamond abrasives and their quantitative study by point counting methods Trans. I.M.M. 63, 21-41.
- Beilby, G. 1921. Aggregation and Flow of Solids. London, 1921.
- Berkovich, E.S. 1950. Triangular diamond pyramid for studying micro-indentation hardness. Zavodsk. Lab. Moscow. 16, 345-347.
- Bierbaum, C.H. 1930. The microcharacter. Trans. Amer. Soc. Steel. Treat. 18, 1009-1023.
- Bloem, J and Kroeger, F.A. 1955. A relation between hardness and stoichiometry in lead sulphide single crystals. Nature, 175, 861.
- Bloss, F.D., Shekarchi E. and Shell, M.R. 1959. Hardness of Synthetic and Natural Micras. Am. Min. 44, 33 - 48.
- Boiaskaia, Yu. S. 1957. Investigation of the anisotropy of hardness of single crystals of PbS by scratching Sov. Phys. Cryst. 2,(5), 702-705.

- Bowie S.H.U. & Taylor K. 1957. Ore mineral indentification simplified. Nature 179, 628-629.
- Bowie S.H.U. & Taylor K. 1958. A system of ore mineral indentification. Mining. Mag. 99, 265-277, 337-345.
- Broschke, H. 1952. A hardness tester for small loads. Microtecnic 6,1.
- Brown, A.F. 1952. Advances in Physics. 1, 427.
- Buckle, H. 1954. Characteristics and limits of diamond pyramid micro-hardness. Rev. Metals 51, 1 - 12.
- Buerger, M.J. 1928. The plastic deformation of the ore minerals. Am. Min. 13, 1 - 17, 35 - 51.
- Buerger, M.J. 1930. Translation of gliding of the NaCl structural type. Am.Min. 15, 180-187, 226-238.
- Buerger, N.W. and M.J. 1934. Crystallographic relations between cubanite segregation plates, chalcopyrite matrix, and secondary chalcopyrite twins. Am. Min, 19, 289.
- Bulian, W. & Fahrenhorst E. 1944. Metallography of Magnesium and its alloys, London.
- Butkovich, T.R. 1958. Hardness of single ice crystals. Am. Min. 43, 48-57.
- Cotter, P.G. 1958. Microhardness of aluminium boride monocrystals. Am. Min. 43, 781 - 784.
- Edwards, A.B. 1947. Textures of the ore minerals and their significance. Aust. I.M.M. Melbourne.

- Ephraim, F. 1931. ^Uber die Ursachen der Eigenschaften chemischer Stoffe. *Ergebn. Physiol.* 32, 1.
- Evans, R.C. 1939. *An introduction to crystal chemistry.* Cambridge.
- Fersmann, A.E. 1937. *Geochemistry.* Moscow-Leningrad.
- Fitzer, E. 1952. H^ochsttemperaturbest^ondige Werkstoffe durch Silizieren von Wolfram und Molybd^oan. *Plansee Proc.* 1, 244. .
- Friederick, E. 1926. ^Uber die H^orte anorganischer Verbindungen und die der Elemente *Fortschr. Chem. Phys.* 18, 12, 1 - 44.
- Gilbert, G. 1924. The relation of hardness to the sequence of the ore minerals.
- Gogoberdize, D.B. and Kopatski, N.A. 1950. Problems of the mechanism of polishing and grinding. *Zhurn. Techn. Fiz.* 20, 910 - 915.
- Goldschmidt, V.M. 1926. Geochemische Verteilungsgesetze der Elemente VII, Die Gesetze der Kristallochemie *Skrift. Det. Norske Acad. Oslo.* 1, 2.
- Goldschmidt, V.M. 1928. Der Kristallbau und die Arten der chemischen Bindung. 34, 453.
- Goldschmidt, V.M. 1933. *Essential concepts of Geochemistry - collected works.* Oslo.
- Goldschmidt, V.M. 1954. *Geochemistry,* Oxford.
- Gottardi, F. 1951. *Mem. Soc. Tosc. Sci. Nat.* 58(A), 161.
- Gray, I.M. 1961. Reflection characteristics of opaque minerals - unpublished Ph.D. Thesis, University of London.

- Gray, I.M. & Young, B.B. 1960. Research in Ore Mineral Identification. Jour. Roy. Sch. Mines, 9, 22 - 28.
- Grodzinski, P. 1952. Microindentation hardness - its dependence on load and a suggested new definition. Ind. Dia. Rev. 12, 209-218, 235-238.
- Harvey, R.D. 1928. Electrical conductivity and polished mineral surfaces. Econ. Geol. 23, 778-783.
- Henriques, A. 1957. Vickers Hardness of Zincblende Ark. Min. 2, 283-297.
- Internationsl Critical Tables 1928.
- Kenngott, A. 1852. ^{II}Über ein bestimmtes Verhältniss zwischen dem atomigewichte der Härte und dem specifischen Gewichte isomorpher Minerale. Jahrl. Keiserl. Kön. Geol. 3, 104 - 116.
- Kip. H. 1907. A new method for determination of ~~the~~ hardness of minerals Amer. Journ. Sci. 27, 96 - 98.
- Kohn, J.A., Cotter, P.G. & Potter, R.A. 1955. Directional hardness in tungsten carbide (WC) monocrystals. Am. Min. 40, 522 - 526.
- Kuovo, O. & Vuorelainen, Y. 1958. Eskolaite, a new chromium mineral. Am. Min. 43, 1098-1106.
- Kouvo, O., Hukma, M., & Vuorelainen, Y. 1959. A natural cobalt analogue of pentlandite. Am. Min. 44, 897-900.
- Kruschov, M.M. 1950. C.R. Acad. Sci. U.S.S.R. 72, 779.

- Larsen, E.S. & Berman H. 1934. The microscopic determination of the non opaque minerals. U.S. Geol. Surv. Bull. 848.
- Martens, A. 1890. Untersuchung drier Härteprüfer Mitt. techn. Versuchs. Berlin, 8, 215-237.
- Meyer, E. 1908. Untersuchungen über Härte prufung und Härte. Physik. Zeitschrift, 9, 66 - 74.
- Mitsche, R. & Onitsch E.M. 1948. Über die Mikrohaerte die Mineralien. Mikroskopie 3, 257-309.
- Mitsche, R. & Onitsch E.M. 1951. Mikrohaerte und Bindungsart Mikrochem/Mickrochim Acta. 36, 841-862.
- Mohs, F. 1824. Grundriss der Mineralogie English translation by W. Haidinger.
- Mookherjee A. & Sahu, K.C. 1960. Microhardness of the plagioclase series. Am. Min., 45, 742-744.
- Mott, B.W. 1956. Micro-indentation Hardness Testing. London.
- Mügge, O. 1898. Neu. Jahrb. Min. 1, 77, 147.
- Mügge, O. 1920. Neu. Jahrb. Min. 24, 39.
- Nakhla, F.M. 1956. The hardness of metallic minerals in polished sections. Econ. Geol. 51, 811-827.
- Onitsch, E.M. 1948. The microhardness of metals and minerals. Berg. Huettenmaenn. Monatsch. Loeben. 93, 7 - 12.

- Onitsch, E.M. 1950. Present state of the hardness testing of minerals. Berg. Huettenmaenn Monatsch. Loeben. 95, 12 - 14.
- Onitsch, E.M. 1953. Theory and practice of microhardness testing. Schweiz Arch. 19, 330 - 343.
- Palache, C., Berman, H., and Frondel, C. 1944. Dana's system of Mineralogy. New York. 1, 2.
- Pauling, L. & Huggins, M.L. 1934. Covalent radii of atoms and interatomic distances in crystals containing electron-pair bonds. Zeits. Krist. 87, 205.
- Petty, E.R. 1961. Microhardness and other properties of Magnesium compounds with the calcium fluorite structure. Nature, 189, 132.
- Pöschl, V. 1909. Die Härte der festen Körper und ihre physikalisch-chemische Bedeutung. Dresden.
- Povarennykh, A.S. 1957. Hardness of minerals as dependent on the state of the chemical bond. Dokl. Acad. Sci. U.S.S.R. 112, 1098-1100.
- Povarennykh, A.S. 1959. Calculation of the hardness of minerals on the Mohs scale by crystalchemical data. Min. Geol. Soc. Lvov. 13, 84-106.
- Ramdohr, P. 1955. Die Erzminerale. Berlin.
- Reis, A. & Zimmerman, L. 1922. Untersuchungen über die Härte fester Stoffe und ihre Beziehungen zur chemischen Konstitution. Zeits. phys. chem. 102, 298-311.

- Robertson, F. &
Van Meter, W.J. 1951. The Kentron microhardness tester, a quantitative tool in opaque mineral identification. Econ. Geol. 46, 541-550.
- Ross, V. 1957. Geochemistry, crystal structure and mineralogy of the sulphides. Econ. Geol. 52, 755-773.
- Rydberg, J.R. 1900. Die härte der ein fachen Körper. Zeits. Phys. Chem. 33, 3 - 4, 353-359.
- Samuels, L.E. 1952. The use of diamond abrasives for a universal system of metallographic polishing. Journ. Inst. Metals. 81, 471.
- Samuels, L.E. 1954. The practical applications of a system of metallographic polishing using diamond abrasives. Metallurgia, 50, 302.
- Schulze, R. 1954. Relation between Vickers microhardness and macrohardness. Microtecnic. 8, 13-26.
- Shazly, E.M.El. and Saleeb, G.S. 1959. Contributions to the mineralogy of Egyptian Manganese deposits. Econ. Geol. 54, 873.
- Short, M.N. 1940. Microscopic determination of the ore minerals. Bull. U.S. Geol. Survey.No. 914.
- Siebel, J. 1943. On the applicability of microhardness testing as a diagnostic aid in the microscopic investigation of ores. Metall. Erz. 40, 169-174.
- Stanton, R.L. 1957. Studies of polished surfaces of pyrite and some implications. Canad. Min. 6, 1, 87 - 118

- Tabor, D. 1954. The hardness of solids. Endeavour 13, 27-32.
- Talmage, S.B. 1925. Quantitative standards for the hardness of the ore minerals. Econ. Geol. 20, 535-543.
- Taylor, E.W. 1949. Correlation of the Mohs' scale of hardness with the Vickers hardness number. Min. Mag. 28, 718-721.
- Tertsch, H. 1930. Einfache kohasionversinche III, die (110) - Spaltung am steinsalz. Zeits. Crystal. 81, 264.
- Tertsch, H. 1950(a) Beobachtungen über Vickers mikrohaerte am Kalkspat. Mikroskopie. 5, 172-183.
- Tertsch, H. 1950(b) Anisotropie-Erscheinungen bei der mikrohaerte-prufung nach der Vickers methode. Radex. Runds. 4, 194-201.
- Thilbault, N.W. and Nyquist, H.L. 1947. The measured Knoop hardness number of hard factors and factors affecting its determination. Trans. Am. Soc. Metals 38, 271,- 323.
- Uytenbogaardt, W. 1951. Tables for Microscopic Identification of the Ore Minerals. Princeton University Press.
- Van der Veen, R.W. 1925. Mineragraphy and ore deposition. 1, The Hague.
- Winchell, A.N. 1951. Elements of Optical Mineral 2. New York.
- Winchell, H. 1945. The Knoop microhardness tester as a Mineralogical Tool. Am. Min. 30, 583 - 595.

Winkler, H.G.F.

1950. Struktur und eigenschaften der kristalle eine einführung in die physikalische und chemische krystalkunde. Berlin.

Winton.

1956. Priv. commn. to B.W. Mott from A.E.I. Research Labs. Aldermaston - see B.W.Mott(1956)

APPENDIX A

PHOTOGRAPHS OF INDENTATION CHARACTERISTICS

Photo No.	Mineral	Ref. No.	Photo No.	Mineral	Ref. No.
1	Aeschynite	1401	22	Berthierite	1196
2	Aikinite	1193	23	Beryl	1373
3	Alabandite	1021	24	Bismuth	290
4	Algodonite	265	25	Bismuthinite	1005
5	Allanite	1376	26	Bismuthinite	1005
6	Altaite	684	27	Bismuthinite	1005
7	Amalgam	216	28	Bismuthinite	1005
8	Anatase	1266	29	Bismuthinite	1005
9	Andorite	1194	30	Bismuthinite	1005
10	Anglesite	1416	31	Bixbyite	1310
11	Ankerite	1358	32	Bornite	402
12	Antimony	271	33	Bornite	402
13	Apatite	1412	34	Boulangerite	1174
14	Acanthite	504	35	Bournonite	1189
15	Argyrodite	1216	36	Bournonite	1189
16	Arsenic	242	37	Bournonite	1189
17	Arsenopyrite	1075	38	Bournonite	1189
18	Arsenopyrite	1075	39	Bournonite	1189
19	Awaruite	323	40	Bournonite	1189
20	Axinite	1379	41	Braunite	1363
21	Barite	1415	42	Bravoite	1140

Photo No.	Mineral	Ref. No	Photo. No.	Mineral	Ref. No.
43	Breithauptite	1129	65	Coloradoite	671
44	Bröggerite	1303	66	Columbite	1389
45	Brookite	1267	67	Columbite	1389
46	Colaverite	518	68	Columbite	1389
47	Calcite	1352	69	Colusite	1224
48	Cassiterite	1284	70	Copper	19
49	Cerussite	1355	71	Copper	15
50	Chalcocite	368	72	Copper	15
51	Chalcocite	368	73	Copper	15
52	Chalcocite	371	74	Coronadite	1289
53	Chalcocite	371	75	Corundum	1255
54	Chalcophanite	1252	76	Corynite	1134
55	Chalcopyrite	464	77	Corynite	1134
56	Chalcostibite	1153	78	Cosalite	----
57	Chromite	1294	79	Covellite	397B
58	Cinnabar	652	80	Covellite	397B
59	Cinnabar	652	81	Cryptomelane	----
60	Clausthalite	681	82	Cubanite	487
61	Clausthalite	679	83	Cuprite	1228
62	Cleveite	1298	84	Cuprite	1228
63	Coballite	1105	85	Cuprite	1228
64	Cohenite	322	86	Cuprite	1228

Photo No	Mineral	Ref. No.	Photo No.	Mineral	Ref. No.
87	Cuprite	1228	109	Fluorite	1350
88	Cylindrite	1207	110	Formanite	1399
89	Cylindrite	1207	111	Franc	1209
90	Davidite	1301	112	Franklinite	1253
91	Descloizite	1413	113	Freiburgite	1167
92	Diaphorite	1195	114	Gahnite	1251
93	Digenite	376	115	Galena	1245
94	Dolomite	1353	116	Galena	1245
95	Domcykite	267	117	Galena	1245
96	Dyscrasite	288	118	Galena	1245
97	Emplectite	1154	119	Galena	1245
98	Enargite	1222	120	Galena	1245
99	Enargite	1222	121	Geocronite	1183
100	Enargite	1222	122	Gersdorffite	1127
101	Enargite	1222	123	Germanoite	1212
102	Enargite	1222	124	Glaucodot	1112
103	Enargite	1222	125	Goethite	1343
104	Eucairite	509	126	Gold	187
105	Euxenite	1403	127	Graphite	222
106	Famatinite	1223	128	Gratonite	1172
107	Fergusonite	1398	129	Grossularite	1374
108	Ferrite	322	130	Gypsum	1414

Photo. No.	Mineral	Ref. No.	Photo No.	Mineral	Ref. No.
131	Gypsum	1414	153	Linnaeite	1091
132	Halite	1349	154	Livingstonite	1170
133	Hauerite	1023	155	Loellingite	1068
134	Hausmannite	1304	156	Magnesite	1351
135	Hematite	1333	157	Magnetite	1318
136	Hercynite	1346	158	Magnetite	1318
137	Hessite	505	159	Manganite	1307
138	Hessite	505	160	Manganite	1307
139	Hetaerolite	1252	161	Manganite	1307
140	Idaite	417	162	Marcasite	1058
141	Ilmenite	1269	163	Maucherite	1115
142	Ilvaite	1366	164	Meneghenite	1185
143	Ilvaite	1366	165	Merumite	1290
144	Iridosmine	325	166	Miargyrite	1165
145	Jamesonite	249	167	Millerite	1113
146	Jordanite	1172	168	Millerite	1113
147	Kermesite	1144	169	Molybdenite	1015
148	Kobellite	1199	170	Monazite	1410
149	Krennerite	525	171	Nagyagite	1168
150	Kyanite	1368	172	Naumannite	----
151	Lead	239	173	Niccolite	1118
152	Lepidocrocite	1345	174	Nigerite	1287

Photo No.	Mineral	Ref. No.	Photo No.	Mineral	Ref. No.
175	Orpiment	1002	196	Pyrrhotite	1025
176	Orthoclase	1371	197	Quartz	1256
177	Osmiridium-Iridium	326	198	Rammelsbergite	1099
178	Pararammelsbergite	1123	199	Realgar	1001
179	Pearceite	----	200	Renierite	1214
180	Pentlandite	1389	201	Rhodonite	1362
181	Perovskite	1268	202	Rutile	1259
182	Pitchblende	1296	203	Safflorite	1093
183	Platinum	331	204	Samarskite	1406
184	Pleonaste	1238	205	Scheelite	1418
185	Polybasite	1244	206	Schulzenite	1347
186	Psilomelane	----	207	Semsevite	1173
187	Pyrargyrite	1159	208	Siderite	1357
188	Pyrargyrite	1159	209	Siegenite	1142
189	Pyrite	1044	210	Silver	81
190	Pyrite	1044	211	Silver	81
191	Pyrochlore	1579	212	Fe-skutterudite	1103
192	Pyrolusite	1306	213	Fe-skutterudite	1103
193	Pyrolusite	1306	214	Smithsonite	1354
194	Pyrolusite	1413	215	Sperryllite	1143
195	Pyrrhotite	1025	216	Sperryllite	1143

Photo No	Mineral	Ref. No.	Photo No.	Mineral	Ref. No.
217	Sphalerite	549	239	Sylvanite	527
218	Sphalerite	549	240	Teallite	1206
219	Sphalerite	549	241	Teallite	1206
220	Sphalterite	549	242	Tellurium	319
221	Sphalerite	549	243	Tennantite	1146
222	Sphalerite	549	244	Tenorite	1236
223	Sphene	1360	245	Tetradymite	1008B
224	Stannite	1200	246	Tetradymite	1008B
225	Stephanite	1166	247	Tetrahedrite	1150
226	Stephanite	1166	248	Thorianite	1281
227	Stephanite	1166	249	Tiemannite	670
228	Stibarsenic	510	250	Titanohematite	1279
229	Stibnite	1003	251	Topaz	1378
230	Stibnite	1003	252	Tourmaline	1380
231	Stibnite	1003	253	Trevorite	1348
232	Stibnite	1003	254	Ullmannite	1131
233	Stibnite	1003	255	Umangite	392
234	Stibnite	1003	256	Vallereite	493
235	Stibnite	1003	257	Violarite	1135
236	Jalpaite	507	258	Wittichenite	1155
237	Jalpaite	507	259	Wolframite	1426
238	Sulphur	310	260	Wolframite	1426

Photo No.	Mineral	Ref. No.	Photo No.	Mineral	Ref. No.
261	Wolframite	1426	265	Zincite	1241
262	Wurtzite	644	266	Zinkerite	1171
263	Wurtzite	644	267	Zircon	1361
264	Zincite	1241			

DESCRIPTION OF INDENTATION CHARACTERISTICS

1. AESCHYRITE, ^x18.2.18 A₁. - str. sides - slight star radials. - square.
2. AIKINITE, 5.7.13 A₁. - str. sides - strong irregular radials - square.
3. ALABANDITE, 3.8.6 B₁. - str. sides - slight star radial - square.
4. ALGODONITE, 1.30 A₁. - sl. cc. sides - strong star radials - elongate.
5. ALLANITE, 16.13.10 B₁. - cc. sides - no fractures - slightly elongate.
6. ALTAITE, 3.6.7 A₂. - str., sig. and sl. cv. faces no fractures - faint glide plane traces - sl. elongate.
7. AMALGAM, 1.10 A₁. - str., cc., and cv. faces - no fractures or glide pl. traces - elongate.
8. ANATASE, 7.9.2 A (OH) - str., sl. cc. faces - irregular fracturing - square.
9. ANDORITE, 5.7.15 A₁. - str. sides - strong star rad. fractures - square.
10. ANGLESITE, 25.7.1 A₁. - irregular an' cleav. fractures + small cl. shells at edges - square - (indistinct).
11. ANKERITE, 11.13.6 A₁, (10 $\bar{1}$ 1) - cleavage and shell fract. - elongate - indistinct due to internal reflections.
12. ANTIMONY, 1.35 A₁. - cc. and sig. faces - no fract. but strong glide pl. traces - strongly elongate.
13. APATITE, 22.1.7 A₁, (0 $\bar{1}$ 01). - star radial and shell fractures - square - indistinct due to internal reflections.
14. ACANTHITE, 3.2.2. A₂. - sl. cc. faces - no fractures - square.
15. ARGYRODITE, 6.2.2. A₁. - str. sides - irregular rad and shell fractures - elongate.

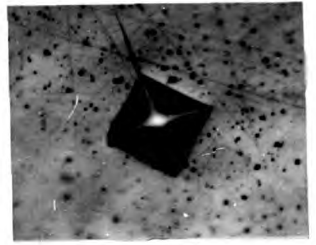
^xACANTHITE - see No. 14



1



2



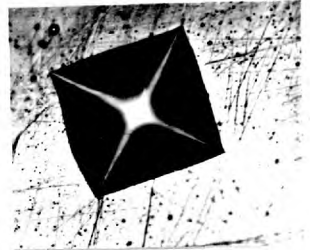
3



4



5



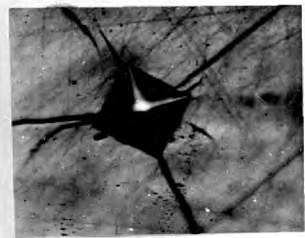
6



7



8



9



10



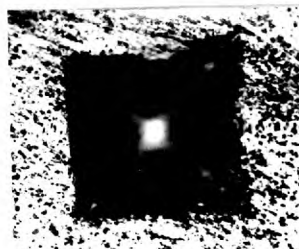
11



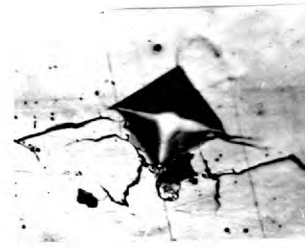
12



13



14



15

16. ARSENIC, 1.2⁴ A₁. - sl. cc. sides - sl. shells good glide planes in two direction - elongate.
17. ARSENOPYRITE, 3.9.12, C₂, (100). - sl. cc. faces - strong star rads. and shells - sl. elongate.
18. ARSENOPYRITE, 3.9.12, C₃ (010). - sl. cc. faces - sl. rads. - elongate.
19. AWARUITE, 1.63 A₁. - cc. and sig. faces - no fractures - elongate.
20. AXINITE, 17.5.8 A₁, (1 $\bar{1}$ 1). - cc. faces - star rads. and shells - square.
21. BARITE, 25.4.14 A₁, (001). - star rads. and shells - indistinct due to strong internal reflections.
22. BERTHIERITE, 5.8.3 A₁. - str. sides - sl. radial fractures - slightly elongate.
23. BERYL, 16.6.1 A₁, (10 $\bar{1}$ 0). - cc. faces - sl. star radials. - slightly elongate.
24. BISMUTH, 1.44 B₃. - cc. and cv. faces - no fractures - strongly elongate.
25. BISMUTHINITE, 3.7.11 C₁, (001). - diag. cl. tr. - cc. faces. - sl. (010) cl. fract. - square.
26. BISMUTHINITE, 3.7.11 C₁, (001). - diags. at 45° to cl. trs. - sl. cc. faces - sl. cl. fract. - square.
27. BISMUTHINITE, 3.7.11 C₂, (100). diag. (010) cl. tr. - cc. faces. - cl. fract. and shells. - strongly elongate.
28. BISMUTHINITE, 3.7.11 C₂, (100). diags. at 45° to (010) cl. trs. - cc. faces - cl. and shell fract. - sl. elongate - diags. not at 90° to one another.
29. BISMUTHINITE, 3.7.11 C₃, (010). - diags. to (001) parting traces. - str. but ragged sides. - strong (001) parting, cl., and shell fract. - v. strongly elongate.
30. BISMUTHINITE, 3.7.11 C₃, (010). - diags. at 45° to (001) part. traces. - irregular faces. - strong (001) cleav. and shell fract. - square.



16



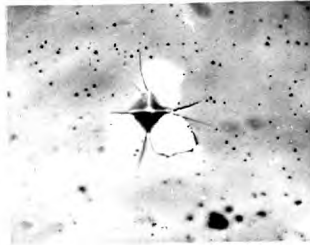
17



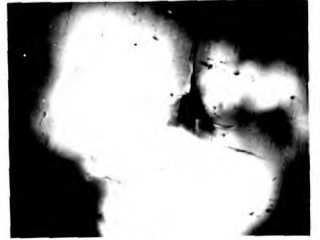
18



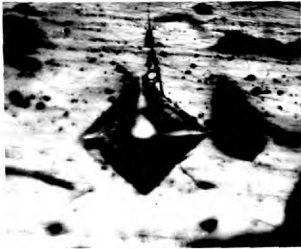
19



20



21



22



23



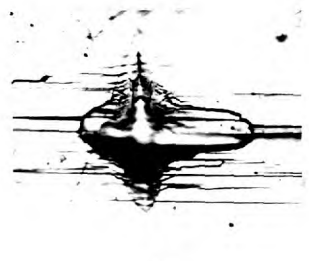
24



25



26



27



28

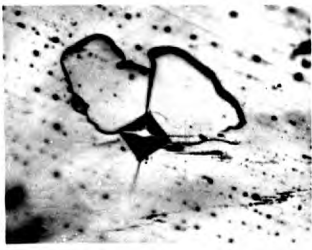


29

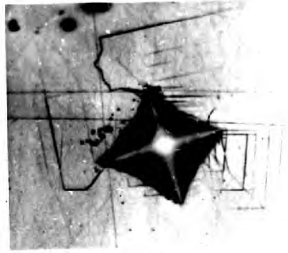


30

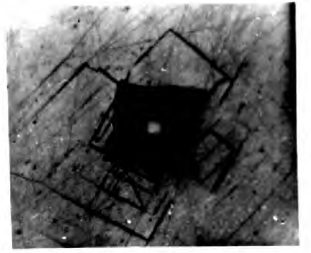
31. BIXBYITE, 7.19.3 A_1 . - str. sides - strong star rad. and shell frags. - square.
32. BORNITE, 3.1.11 B_1 . - cc. faces - (111) cleav. fract. system - square.
33. BORNITE, 3.1.11 B_1 . - sigmoid faces - similar to photo 31.
34. BOULANGERITE, 5.6.19 A_1 . - str. and cc. faces. - cleav. and irregular rad. frags. - sl. elongate.
35. BOURNITE, 5.7.5. C_1 , (001). - sl. cc. faces - star rads. and shells - square.
36. BOURNONITE, 5.7.5 C_1 , (100). - str. and sl. cc. faces - star and side rad. frags. - square.
37. BOURNONITE, 5.7.5. C_1 , (010). - cc. faces - strong side rads. - slightly elongate.
38. BOURNONITE, 5.7.5. E_1 . - sl. cc. faces - strong star rads. and shells - square.
39. BOURNONITE, 5.7.5. E_1 . - sl. cc. faces - star rads. - square.
40. BOURNONITE, 5.7.5. E_1 . - str. sides - star and side rad. and shells fract. - square.
41. BRAUNITE, 14.17.4 A_1 . - str. sides - sl. star rads. and shells - square.
42. BRAVOITE, 3.11.30 A_1 . - sl. cc. faces - irregular rad and shell frags. - square.
43. BREITHAUPTITE, 3.11.15 B_1 . - cc. and sig. faces. - sl. rad. frags. - square.
44. BRÖGGERITE, 7.16.12 A_1 . - str. sides - irregular side and star. rads. - square.
45. BROOKITE, 7.9.3 A_1 , (120). - str. sides - no frags. - square.



31



32



33



34



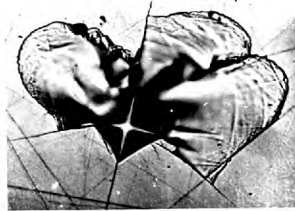
35



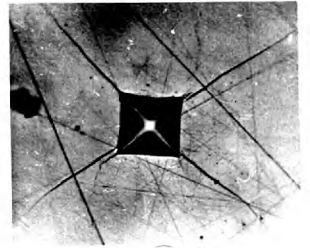
36



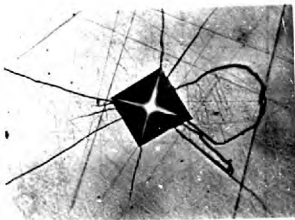
37



38



39



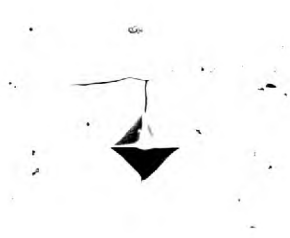
40



41



42



43

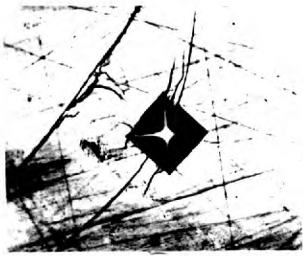


44



45

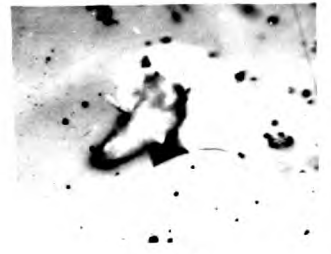
46. CALAVERITE, 3.3.1 B₁. - str. sides - side rad. frags. - square.
47. CALCITE, 11.4.1. A₁, (10 $\bar{1}$ 1). - indistinct due to internal reflections - (10 $\bar{1}$ 1) cleav. frags. and shells - square.
48. CASSITERITE, 7.11.1 C₁, (111). - sl. cc. faces - star rads. and shells. - sl. elongate.
49. CERUSSITE, 11.9.1 A₁. - str. sides - star and side rads and shells - indistinct due to internal reflections.
50. CHALCOCITE, 3.1.1 D₁. - str. sides - shells and microgranular frags. - square.
51. CHALCOCITE, 3.1.1 D₁. - sl. cc. faces - microgranular frags. - sl. elongate.
52. CHALCOCITE, 3.1.1 C₁, (001). - str. sides - tetrahedral parting (111) frags. - square.
53. CHALCOCITE, 3.1.1 C₂, (110). - N-S diag. a axes. - str. and sig. faces² - tetrahedral (111) parting frags. elongate.
54. CHALCOPHANITE, 7.5.7 A₁. - cc. sides - strong cleav. frags. and cleav. shells. - square.
55. CHALCOPYRITE, 3.1.12 C₁ (112). - sl. cc. faces. - no frags. - square.
56. CHALCOSTIBITE, 5.1.3 A₁. - str. sides - irregular rads. and shells. - square.
57. CHROMITE, 7.14.5 C₃, (111). - sl. cc. faces - star and side rads. - square.
58. CINNABAR, 3.5.2 B₁, (10 $\bar{1}$ 1). - diags. principal directions cc. faces - rad. and cleav. frags. - "kite-tail". - depression - elongate.
59. CINNABAR, 3.5.2 B₁, (10 $\bar{1}$ 1). - diags. skew to principal directions - str., c.v., and one strongly cc. face - asymmetric "kite-tail" depression. - equidimensional.
60. CLAUSTHALITE, 3.6.5. B₁. - str. sides - no frags - square.



46



47



48



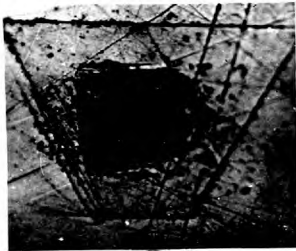
49



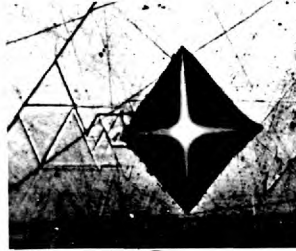
50



51



52



53



54



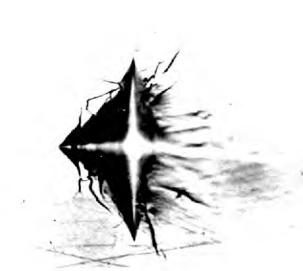
55



56



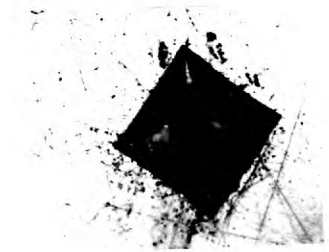
57



58

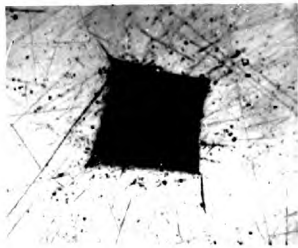


59



60

61. CLAUSTHALITE, 3.6.5 A_1 . - cc. sides - no fractures - square.
62. CLEVEITE, 7.16.7 A_1 . - cc. sides - sl. star rad. frags. - square.
63. COBALTITE, 3.10.9 A_1 . - str. sides - star and rad. frags and sl. shells. - square.
64. COHENITE, 2.7 A_1 . - cc. faces - no frags. - elongate.
65. COLORADOITE, 3.5.6. A_1 . - cc. faces - no frags. - square.
66. COLUMBITE, 18.1.18 A_1 , (010). - str. sides - star. rads. and shells. - square.
67. COLUMBITE, 18.1.18 A_2 , (001). - sl. cc. sides - side rads. and shells - sl. elongate.
68. COLUMBITE, 18.1.18 A_3 , (100). - str. sides - irregular rads. and shells. - elongate - darker zone in centre of indentation.
69. COLUSITE, 6.4.2 A_1 . - str. sides - star rads. and shells - square.
70. COPPER, 1.1 B_1 . - cv., and sig. faces - no frags. - glide pl. traces - strongly elongate.
71. COPPER, 1.1 A_1 , (001). - str. and sig. faces - no frags. - square.
72. COPPER, 1.1 A_2 , (111). - str. and cv. faces - no frags. - square.
73. COPPER, 1.1 A_3 , (110). - sl. cc. faces - no frags - sl. elongate.
74. CORONADITE, 7.11.11 A_1 . - str. and cc. faces - irregular rad. frags. - elongate.
75. CORUNDUM, 7.6.1 B_1 , (10 $\bar{1}$ 0). - cc. faces - sl. star rads. - elongate.



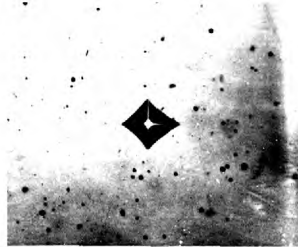
61



62



63



64



65



66



67



68



69



70



71



72



73



74

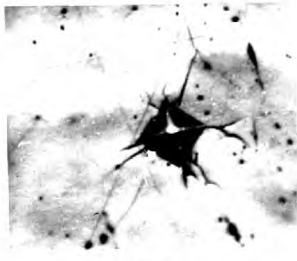


75

76. CORYNITE, 3.11.8 A₂. - str. sides - star and side rads - square.
77. CORYNITE, 3.11.8 A₂. - str. sides. - "forking" star rad. fract. - sl. Side rads and shells. - square.
78. COSALITE, 5.7.11 A₁. - str. sides - sl. cleav fract. - elongate.
79. COVELLITE, 3.1.4 B₁, (0001). - irregular str - cc. sides - concentric shells and irregular rads. - sl. elongate.
80. COVELLITE, 3.1.4 B₂, (10 $\bar{1}$ 0). - cc. faces - (0001) cleav. fract. - elongate.
81. CRYPTOMELANE, 7.4.11 A₁. - str. sides - no fract. - square.
82. CUBANITE, 3.1.14 A₁. - elong. lath. - fract. parallel to lath (001)? and disloc. fract. \perp to lath (110)(?), also irregular rad. and shells. - elongate.
83. CUPRITE, 7.3.1 B₁, - (111). strong cc. faces - no fract. - square.
84. CUPRITE, 7.3.1 B₁, (111). - cc. faces. - star rads. fract. square.
85. CUPRITE, 7.3.1 B₁, (100). - str. faces - (111) disloc. pl. traces sides. - square.
86. CUPRITE, 7.3.1 B₁, (100). - str. and sl. cv. faces - (111) disloc. pl. traces sides. - square.
87. CUPRITE, 7.3.1 B₃, (110). - cc. faces - no fract. - square.
88. CYLINDRITE, 6.1.4 A₁. - length. - str. and cc. faces - strong cylindrical cleav. fract. - elongate.
89. CYLINDRITE, 6.1.4 A₂. - \perp length. - str. and sl. cc. faces. curved. cylindrical cleav. fract. - elongate.
90. DAVIDITE, 7.16.9 (a) A₁. - cc. faces. - v. sl. star rad. fract. - elongate.



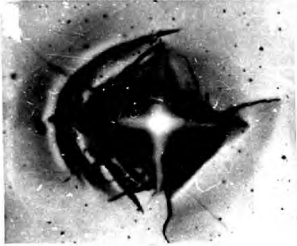
76



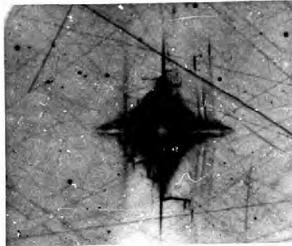
77



78



79



80



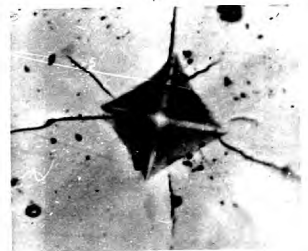
81



82



83



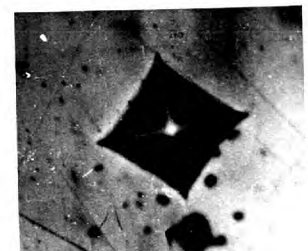
84



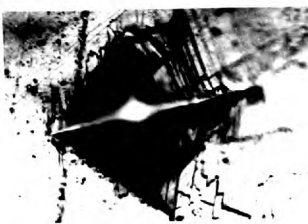
85



86



87



88



89

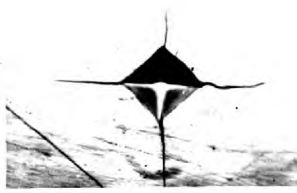


90

91. DESCLOIZITE, 21.3.5 A_1 , (001). - str. sides - irregular rad. frags. and shells. - sl. elongate.
92. DIAPHORITE, 5.7.20 A_1 . - str. and sl.cv. faces. - star rad. frags. - square.
93. DIGENITE, 3.1.3 A_1 . - str. - cl. cv. sides. - no frags.- square.
94. DOLOMITE, 11.4.13 A_1 , ($10\bar{1}1$). - indistinct due to strong internal reflections. - shells and cl. frags.
95. DOMEYKITE, 1.27 A_1 . - sl. cc. and str. sides - rad frags.- sl. glide pl. traces. - square.
96. DYSCRASITE, 1.42 A_2 . - str. sides. - no frags. 2 prom. sets of glide plane or part. traces - elongate.
97. EMPLECTITE, 5.1.6 A_1 . - str. sides - side rad. frags. - square.
98. ENARGITE, 6.3.1 F_1 , (100) - diag. cl. trace - indistinct sides. - strong (110) cleav. and cleav. shell frags - square.
99. ENARGITE, 6.3.1 F_1 , (100) - diags. at 45° to cl. traces - cc. faces - strong (110) cleav. shell frags. - square.
100. ENARGITE, 6.3.1 F_2 , (001). - diags a & b axes. - sl. cc. faces. - "side" rad. frags. (110) cleavs. not touching sides. - square.
101. ENARGITE, 6.3.1 F_2 (001). - diags. at 45° to a & b axes. - str. sides. - star rad. frags. and sl. shells. - square.
102. ENARGITE, 6.3.1 F_3 , (010). - diag. cl. traces. - indistinct sides - (110) cleav. shell frags. - elongate.
103. ENARGITE, 6.3.1 F_3 , (010). - diags at 45° to cl. traces - str. and cc. sides - (110) cleav. shell frags. - square.
104. EUCAIRITE, 3.2.12 A_1 . - str. sides. - irregular rad. frags. - square.
105. EUKENITE, 18.4.4 A_1 . - sl. cc. faces - star rad. frags. sl. elongate.



91



92



93



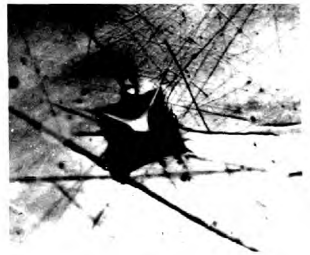
94



95



96



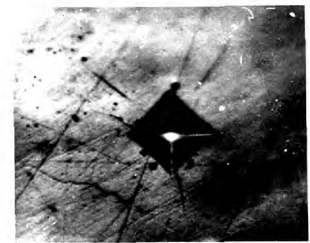
97



98



99



100



101

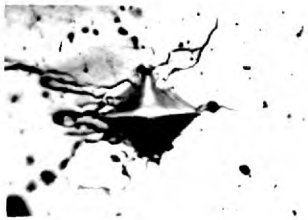


102



105

106. FAMATINITE, 6.3.3 A_1 . - sl. cc. faces. - irregular rads. and shells. -¹elongate.
107. FERGUSONITE, 18.2.1 A_1 - v.sl. cc. faces - no fract. - square.
108. FERRITE, 1.57 A_1 . - sl. cc. faces - no fract. - sl. elongate.
109. FLUORITE, 8.4.15 A_1 , (100). - all sl.cv. faces v. sl. star rads. - square.
110. FORMANITE, 18.2.2 A_1 . - cc. faces - star rads. - square.
111. FRANCKEITE, 6.1.6 C_1 . - irregular faces. - prom. cleav. fract. - square.
112. FRANKLINITE, 7.5.10 A_2 , (111). - sl. cc. faces - star rads. - sl. elongate.
113. FREIBERGITE, 5.2.20 A_1 . - sl. cc. faces. - star rads. and shells. - square.
114. GAHNITE, 7.5.2. A_1 . - cc. faces. - star rads. - elongate.
115. GALENA, 3.6.3. L_1 , (100) - diags. cl. traces. - strongly cc. faces - no fract. - square.
116. GALENA, 3.6.3 L_1 , (100) - diags. at 45° to cl. traces - cc faces - no fract. - square.
117. GALENA, 3.6.3 L_2 , (111) - N-S diag. cl. traces. sl. cc., c.v., and str. faces. - no fract. - sl. elongate.
118. GALENA, 3.6.3. L_2 , (111). - N-S diag. at 15° to cl. traces sl. cc., c.v., and str. faces - no fract. - sl. elongate.
119. GALENA, 3.6.3. L_3 , (110). N-S diag. 45° dipping cleav. trs. - v. sl. cc., faces - no fract. - elongate.
120. GALENA, 3.6.3. L_3 , (110) - diags at 45° to cl. traces str. and sl. cv. faces - no fract. - square.



106



107



108



109



110



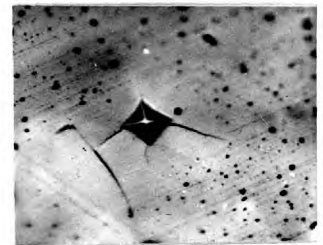
111



112



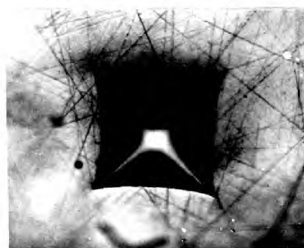
113



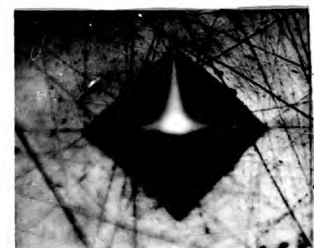
114



115



116



117



118



119



120

121. GEOCRONITE, 5.6.25 A_1 . - sl. cc. faces - sl. irregular rad. frags. - sl. elongate.
122. GERSDORFFITE, 3.11.14 C_1 . - str. sides - star rad. frags. - square.
123. GERMANITE, 6.2.1 A_2 . - sl. cc. faces - star and irreg. rad. frags. - sl. elongate.
124. GLAUCODOT, 3.10.19 A_1 . - sl. cc. faces - star rad. frags. - sl. elongate.
125. GOETHITE, 7.20.7 B_1 . - sl. cc. faces - star and side rads. and shells.
126. GOLD, 1.49, - cc., sig., and str. faces. - sl. glide plane traces - no frags. - elongate.
127. GRAPHITE, 1.18 A_1 - cc. faces - cleav. frags. - square.
128. GRATONITE, 5.6.9 A_1 . - str. and sl. cc. faces - star rads. - square.
129. GROSSULARITE, 16.9.6 A_1 , (110). - indistinct due to internal reflections - star rads. - circular.stressed zone around indentation - square.
130. GYPSUM., 25.4.3 A_1 , (001) - indistinct cc. sides - strong (010) cleav. frags. - strongly elongate.
131. GYPSUM, 25.4.3. A_2 , (010). - indistinct due to internal reflections - strong shells.
132. HALITE, 8.1.2 A_1 , (100). - all cv. faces. - no frags. - square.
133. HAUERITE, 3.8.7 A_1 , (111). - sl. cc. faces. - star rad. frags. - square.
134. HAUSMANNITE, 7.18.4 A_1 . - sl. cc. faces. - sl. irregular rads. - glide plane traces in two directions - square.
135. HEMATITE, 7.20.5 C_2 , (10 $\bar{1}$ 0). - cc. faces - star rad. frags. - sl. elongate.



121



122



123



124



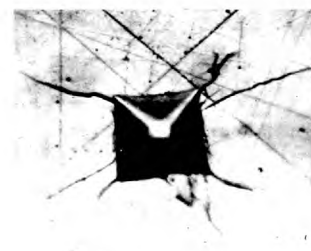
125



126



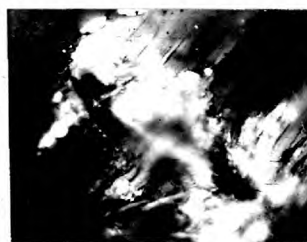
127



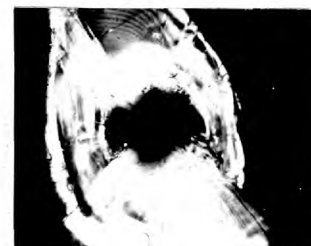
128



129



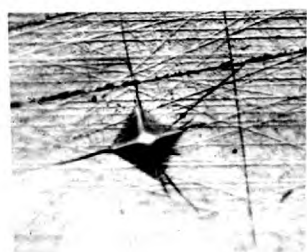
130



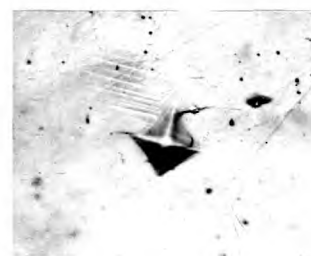
131



132



133



134



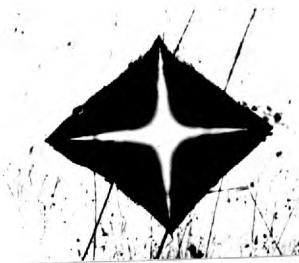
135

136. HERCYNITE, 7.20.18 A_1 , (100). - str. sides - sl. star rads. and shells. - square.
137. HESSITE, 3.2.6 A_1 . - cc. faces. - no fract. - elongate.
138. HESSITE, 3.2.6 A_1 . - as for 137. but oblique illum. used. - strong glide planes shown - elongate.
139. HETAEROLITE, 7.5.5. A_1 - str. sides - star rads. and shells. - square.
140. IDAITE, 3.1. ? - sl. cc. faces. - no fract. - square.
141. ILMENITE, 7.9.14 C_1 . - v. sl. cv. and cc. sides. - no fract. - square.
142. ILVAITE, 14.22.6 A_1 , (001). - str. sides. star and side rads. and shells. - square.
143. ILVAITE, 14.22.6 A_1 , (100). - str. sides. - star rads and shells. - square.
144. IRIDOSMINE, 1.71 A_1 . - sl. cc. faces. - no fract. - sl. elongate.
145. JAMESONITE, 5.8.7 B_1^* - str. and cv. sides - irregular rads. and shells - strongly curved disloc. planes - square.
146. JORDANITE, 5.6.8 A_1 . - cc. and cv. faces - irregular rads. and shells - square.
147. KERMESITE, 4.2 A_1 - irregular cc. faces - strong cleav. fract. - square.
148. KOBELLITE, 5.8.7 (b) A_2 - str. sides - star and side rads and shells - square.
149. KRENNERITE, 3.3.2 A_1 . - cc. faces - star rads. - sl. elongate.
150. KYANITE, 15.2 A_1 , (100). - indistinct due to strong internal reflections - cleav. shell fract. - elongate.

* Jalpaite - see Nos. 236, 237



136



137



138



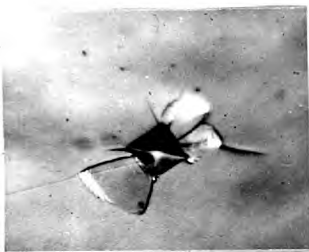
139



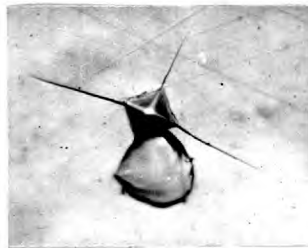
140



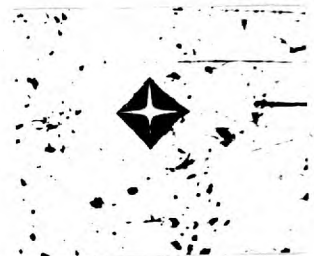
141



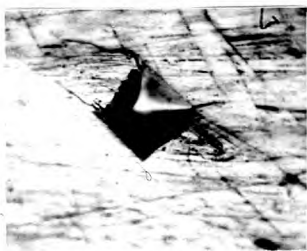
142



143



144



145



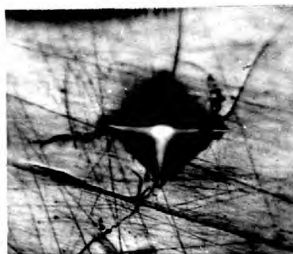
146



147



148

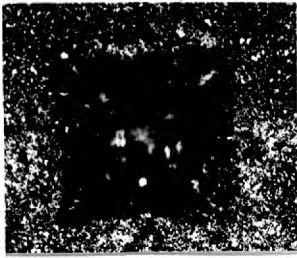


149



150

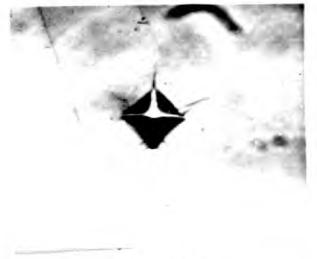
151. LEAD, 1.21 A_1 . - cc. faces - no fract. - square.
152. LEPIDOCROCITE, 7.20.8 A_1 . - sl. cc. faces - sl. side
rads. - elongate.
153. LINNAEITE, 3.10.2 A_1 . - str. sides - star rad. fract. -
square.
154. LIVINGSTONITE, 5.4.4 A_1 . - irregular sides - ragged side
rads. - square.
155. LÖLLINGITE, 3.9.10 A_1 . - str. sides. - sl. star and side
rads. - elongate.
156. MAGNESITE, 11.3.1 A_1 , (10 $\bar{1}$ 1). - cc. sides - (10 $\bar{1}$ 1) cleav.
fract. - elong. - indistinct due to internal reflections.
157. MAGNETITE, 7.20.3 H_1 , (111). - v. sl. cc. faces - sl.
star rads. - square.
158. MAGNETITE, 7.20.3 H_1 , (111). - str. and sl. cc. faces -
no fract. - square.
159. MANGANITE, 7.18.8 A_1 , (010). - str. sides - (110) and
(001) cleav. shells and rad. fract. - square.
160. MANGANITE, 7.18.8 A_2 , (100). - str. sides. - (110) and
(010) cleav. shells and rad. fract. - sl. elongate.
161. MANGANITE, 7.18.8 A_3 , (001). - sl. cc. sides - (110) and
(010) cleav. fract. - sl. elongate.
162. MARCASITE, 3.9.7 B_1 , (001). - str. sides - strong rad.
and shell fract. - square.
163. MAUCHERITE, 3.11.8 A_1 . - str. sides - star and side rads. -
sl. elongate.
164. MENECHMINITE, 5.7.4 A_1 . - sl. cc. faces - sl. irregular
rad. - sl. elongate.
165. MERUMITE, 7.14.1 (a) A_1 - sl. cc. faces. - star rads.
square.



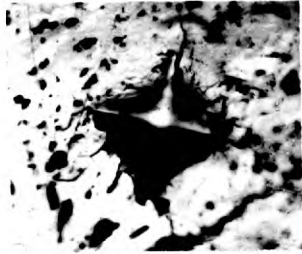
151



152



153



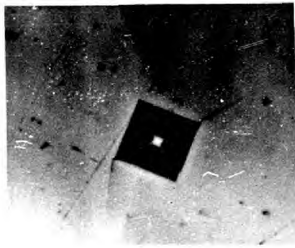
154



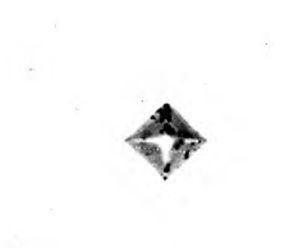
155



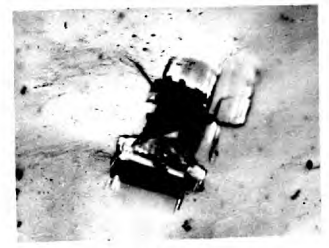
156



157



158



159



160



161



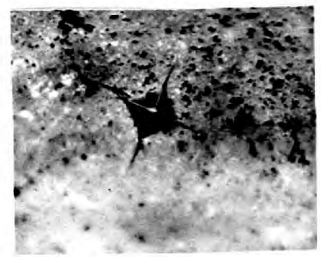
162



163



164



165

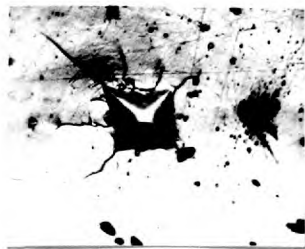
166. MIARGYRITE, 5.2.8 A_1 . - sl. cc. faces - side rads. - elongate.
167. MILLERITE, 3.11.1 A_1 - sl. cc. sides - star and side rads. - elongate.
168. MILLERITE, 3.11.1 A_2 . - sl. cc. sides - star and side rads. - elongate.
169. MOLYBDENITE, 3.8.3 A_1 . - cc. sides - (0001) cleav. fract. - square.
170. MONAZITE, 19.9.2 A_1 , (010). - str. sides - star and cleav. fract. - elongate.
171. NAGYAGITE, 5.3.2 A_1 . - irregular sides - cleav. (010) fract. - elongate.
172. NAUMANNITE, 3.2.4. A_1 - cc. and cv. faces. no fract. - v. sl. disloc. - strongly elongate.
173. NICCOLITE, 3.11.9 B_1 . - sl. cc. faces - no fract. - square.
174. NIGERITE, 7.11.2 A_1 . - str. sides - sl. star rads and shells - square.
175. ORPIMENT, 3.7.3. A_1 . - irregular cc. sides - strong cleav. fract. - square.
176. ORTHOCLASE, 16.3.5 A_1 , (010). - indistinct due to internal reflections - star rads.
177. OSMIRIDIUM-IRIDIUM, 1.7⁴ A_1 . - cv. faces - no fract. - curving disloc. pl. traces sides - square.
178. PARARAMMELSBERGITE, 3.11.10 B_1 . - sl. cc. sides - star and side rads - sl. elongate.¹
179. PEARCEITE, 5.2.6. A_1 . - str. and cv. sides - star and side rads. - curved disloc. pl. traces sides - square.
180. PENTLANDITE, 3.11.2⁴ A_3 . - str. and sig. sides - side rads and cleav. fract. - elongate.



166



167



168



169



170



171



172



173



174



175



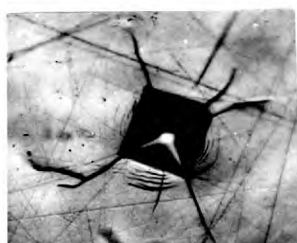
176



177



178



179



180

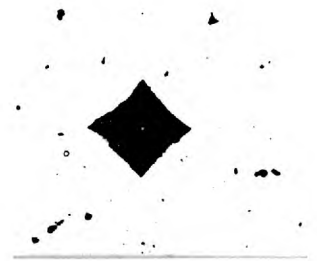
181. PEROVSKITE, 7.9.8 A₁. - str. sides - star rads. and shells - square.¹
182. PITCHBLENDE, 7.11.1 A₁. - cc. sides - star rads - square.
183. PLATINUM, 1.78 A₂. - cc. sides - no fract. - sl. elongate.
184. PLEONASTE, 7.4.5 B₁. - str. sides - v. sl. shells. - square.
185. POLYBASITE, 5.2.12 A₁. - str. sides - star and side rads. - square.
186. PSILOMELANE, 7.4.11 A₁. - sl. cc. faces - sl. star rad. fract. - square.
187. PYRRARGYRITE, 5.2.4/5.2.9 A₁. - str. sides - side and star rads - square.
188. PYRRARGYRITE, 5.2.4/5.2.9 A₁. - sl. cc. sides - side and star rads - sl. elongate.¹
189. PYRITE, 3.9.6 E₁, (111). - indistinct - strong rads and shells - square.
190. PYRITE, 3.9.6. E₂, (100). - indistinct - strong rads. and shells - square
191. PYROCHLORE, 18.2.9 A₁, (111). - indistinct due to internal reflections - star rads and shells.
192. PYROLUSITE, 7.18.6 B₁, (100). - "faint" indentation - cc. sides - no fract. - square.
193. PYROLUSITE, 7.18.6 B₂, (001). - str. sides - no fract. - sl. elongate.
194. PYROMORPHITE, 7.11.6 B₁, (0001). - sl. cc. sides - strong star rads. and shells - square.
195. PYRRHOTITE, 3.9.1 C₁, (0001). - sl. cc. sides - star rads and shells. - square.



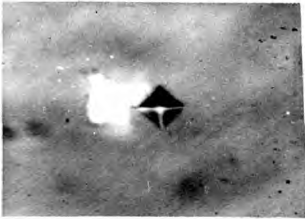
181



182



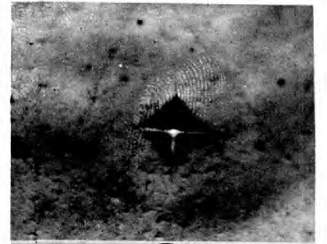
183



184



185



186



187



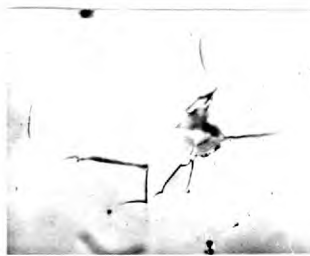
188



189



190



191



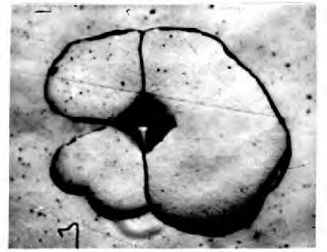
192



193



194



195

196. PYRRHOTITE, 3.9.1 C₂, (10 $\bar{1}$ 0). - sl. cc. sides - sl. star rads. - elongate.
197. QUARTZ, 7.8.1 A₁, (10 $\bar{1}$ 0). - cc. sides - sl. rads - square.
198. RAMMELSBERGITE, 3.11.11 A₁. - sl. cc. sides - star rads and sl. shells - sl. elongate
199. REALGAR, 3.7.2. A₁. - sl. cc. sides - shell fract. - square.
200. RENIERITE, 6.2.1.(a) A₁. - sl. cc. sides - star and side rads. - square.
201. RHODCNITE, 14.17.1 A₁. - str. sides - star and irregular rads. - sl. shells - square.
202. RUTILE, 7.9.1 B₁, (001). - str. sides star rad. fract. - faint disloc. pl. traces sides. - square.
203. SAFFLORITE, 3.10.6 B₁. - sl. cc. faces - sl. star. rads. - square.
204. SAMARSKITE, 18.4.14 A₁. - sl. cc. faces - sl. star rads. - square.
205. SCHEELITE, 27.3.4 B₁, (111). - indistinct due to internal reflections - star rads. and shells.
206. SCHULZENITE, 7.21.5 A₁. - str. sides - v. sl. side rads. - square.
207. SEMSEYITE, 5.6.18 A₁. - str. sides - irregular rads. - square.
208. SIDERITE, 11.13.1 A₁, (10 $\bar{1}$ 1). - cc. sides - (10 $\bar{1}$ 1) cleav. fract. - shells - elongate - indistinct due to internal reflections.
209. SIEGENITE, 3.11.3⁴ A₁. - sl. cc. faces. - side rads. shells. - square.
210. SILVER, 1.3 A₁. - sig. faces - no fract. disloc pl. traces - elongate.



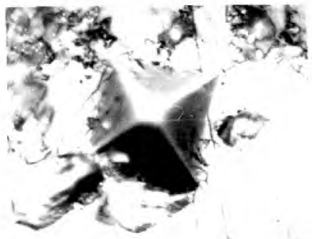
196



197



198



199



200



201



202



203



204



205



206



207



208

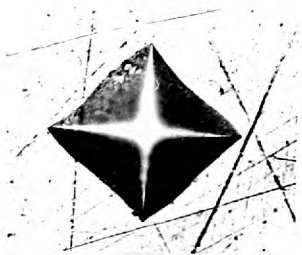


209



210

211. SILVER, 1.3 A_1 . - all sig. faces. - no cracks - sl. dislocs pl. traces - elongate.
212. FE-SKUTTERNDITE, 3.10.8 C_1 , (111). - str. sides - star rads. - square.
213. FE-SKUTTERNDITE, 3.10.8 C_2 , (100). - sl. cc. sides - star and side rads and shells. - square.
214. SMITHSONITE, 11.6.1 A_1 , (10 $\bar{1}1$). - str. sides - cleav. fract. and shells. - square.
215. SPERRYLITE, 3.12.5 A_1 , (100). - str. sides - star rads and shells. - square.
216. SPERRYLITE, 3.12.5 A_2 , (111). - str. sides - star rads and shells - square.
217. SPHALERITE, 3.4.2. A_a , (100). - diags. at 45° to cl. traces - str. and cv. faces - no fract. - square.
218. SPHALERITE, 3.4.2 A_a , (100). - E-W diag. cl. traces all cc. faces. - no fract. - square.
219. SPHALERITE, 3.4.2. A_{a2} , (111). - E-W diag. cleav. traces sl. cc. faces. - no fract. - square.
220. SPHALERITE, 3.4.2 A_{a2} , (111). - diags. at 45° to cl. traces - sl. cc. faces - no fract. - square.
221. SPHALERITE, 3.4.2 A_{a3} , (110). - E-W diag. cl. traces - cc. faces - no fract. - square.
222. SPHALERITE, 3.4.2. A_{a3} , (110). E-W diag. at 45° to cl. traces - cc. and sig. faces - no fract. - square.
223. SPHENE, 14.9.2 A_1 , (011). - indistinct due to internal reflections - star rad. fract.
224. STANNITE, 6.1.1 A_1 . - cc. faces - star and side rads. - sl. elongate.
225. STEPHANITE, 5.2.11 A_1 , (001). - str. sides. - star rads. - square.



211



212



213



214



215



216



217



218



219



220



221



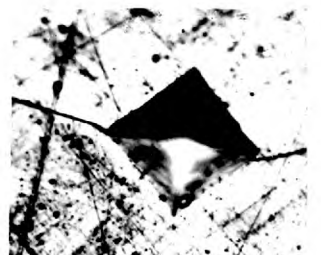
222



223



224



225

226. STEPHANITE, 5.2.11 A₂, (110). - cc. faces - side rads. and shells. - strong (110) disloc. pl. traces. - elongate.
227. STEPHANITE, 5.2.11 A₃, (010). - cc. faces star rads. - strong (110) disloc pl. traces - elongate.
228. STERNBERGITE, 3.2.14 A₁. - irregular faces - cleav. fract. - sl. elongate.
229. STIBARSENIC, 1.38 A₁ - sl. cc. faces - no fract. - square.
230. STIBNITE, 3.7.9 A₂, (010). - E-W diag. (001) parting pl. traces - side and (001) part. shell fract. - elongate
231. STIBNITE, 3.7.9 A₄, (001). - E-W diag. (010) cleav. pl. traces - (010) cleav. fract. and shells. - elongate
232. STIBNITE, 3.7.9 A₄, (001). - diags. at 45° to cleav. traces - (010) cleav. fract. and shells. - diags not at 90° to one another. - square.
233. STIBNITE, 3.7.9 A₃, (100). - E-W diag (010) cl. pl. trs. - (010) cleav. fract. - square.
234. STIBNITE, 3.7.9 A₃, (100). - diags. at 45° to (010) cl. pl. traces - (010) cleav. fract. and shells - square.
235. STIBNITE, 3.7.9 A₂, (010). diags. at 45° to (001) cl. pl. traces - sl. rads - (001) cleav. fract. and shells - square.
236. JALPAITE, 3.2.10 A₁, - cc. and cv. faces - no fract. strong disloc. plane traces - elongate.
237. JALPAITE, 3.2.10 A₁. - sig., str. and cc. faces - no fract. - prom. disloc. plane traces - elongate.
238. SULPHUR, 1.47 A₁. - indistinct cc. faces - irregular shell fract. - square.
239. SYLVANITE, 3.3.7 B₁. - sl. cc. faces - sl. star rads. and shells - square.
240. TEALLITE, 6.1.3 A₁, (001) - cv. faces - concentric shell fract. - square.



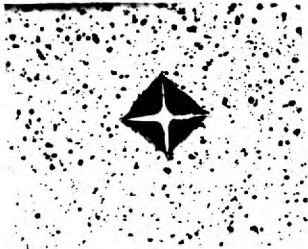
226



227



228



229



230



231



232



233



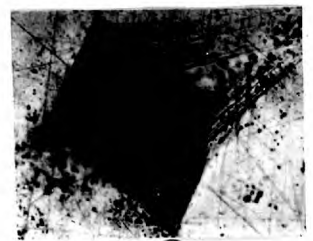
234



235



236



237



238



239



240

241. TEALLITE, 6.1.3 A_1 , (110). - str. and irregular sides--
(001) cleav. fract's. - square.
242. TELLURIUM, 1.53 A_1 , (10 $\bar{1}$ 0). - N-S diag (10 $\bar{1}$ 0)
cleav. traces - cc. faces - (10 $\bar{1}$ 0) cleav. fract's -
elongate.
243. TENNANTITE, 5.1.1 B_1 . - str. sides - star rads. -
square.
244. TERONITE, 7.3.3 A_1 . - str. sides - sl. star rads. -
square.
245. TETRADYMITTE, 3.7.15 A_2 , (0001). - cc. and cv. sides -
concentric shell fract's. - square.
246. TETRADYMITTE, 3.7.15 A_2 . - cc. faces. - strong (0001)
cl. fract's and glide pl. traces - square.
247. TETRAHEDRITE, 5.1.2 D_1 . - str. sides - star rads. and
shells - square.
248. THORIANITE, 7.10.6 A_1 , (100). - str. sides - sl. star
rads. - square.
249. TIEMANNITE, 3.5.4 A_1 . - sig. faces - no fract's. -
square.
250. TITANOHEMATITE, 7.9.19 A_1 . - str. sides - sl. star
rads and shells - square.
251. TOPAZ, 17.2.1 A_1 , (001) - indistinct due to internal
reflection - star rads and shells.
252. TOURMALINE, 17.5.21 A_1 , (10 $\bar{1}$ 0). - indistinct due to
internal reflections¹ - str. sides and star rads.
253. TREVORITE, 7.22.5 A_1 . - str. sides - v. sl. star rads -
square.
254. ULLMANNITE, 3.11.16 A_1 . - str. sides - star and side
rads. - sl. shells - square.
255. UMANGITE, 3.1.6 B_1 . - str. and cv. sides - sl. side
rads. - square.



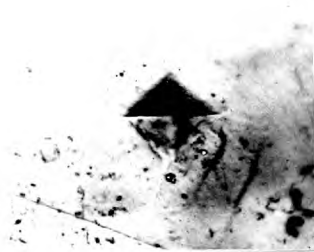
241



242



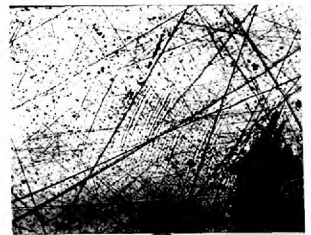
243



244



245



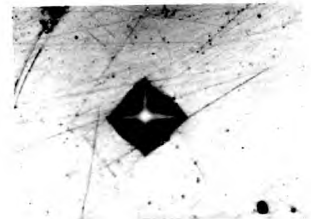
246



247



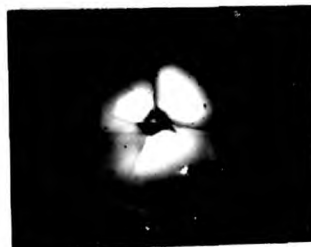
248



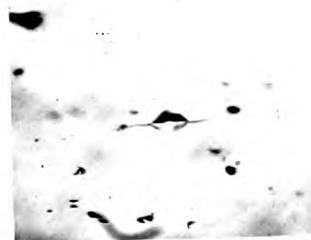
249



250



251



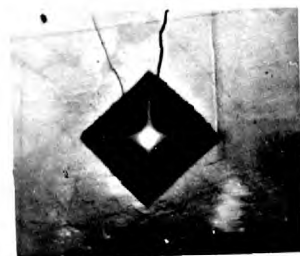
252



253

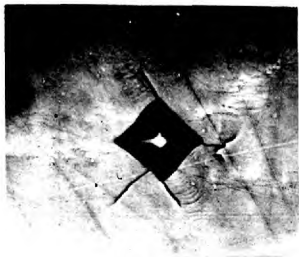


254

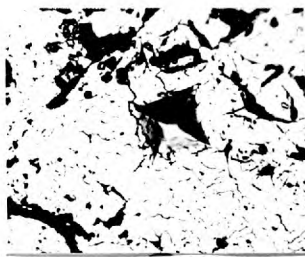


255

- 256. VALLEREITE, 3.1.15 A_1 . - sl. cc. and sig. faces - star and side rads. - disloc. plane traces - square.
- 257. VIOLARITE, 3.11.23 A_1 - sl. cc. faces - irregular rads. - shells.
- 258. WITTICHENITE, 5.1.8 A_1 . - str. sides - irregular rads. and shells - square.
- 259. WOLFRAMITE, 27.3.13 C_1 , (010). - sl. cc. faces - v. sl. side rads. - square.
- 260. WOLFRAMITE, 27.3.13 C_2 , (001). - sl. cc. faces - no fract. - square.
- 261. WOLFRAMITE, 27.3.13 C_3 , (100). - cc. faces - irregular and (010) cleav. fract. - sl. elongate.
- 262. WURTZITE, 3.4.3 B_1 , (10 $\bar{1}$ 0). - E-W diag. a axes - cc. faces - sl (0001) cleav. fract. - (110)(?) disloc. pl. traces. - elongate.
- 263. WURTZITE, 3.4.3 B_2 , (0001). - str. sides - shell fract. - square.
- 264. ZINCITE, 7.5.11 A_2 . - indistinct due to heavy shell fract.
- 265. ZINCITE, 7.5.11 A_1 . - cc. faces - side rads - elongate.
- 266. ZINKENITE, 5.6.14² A_1 . - cc. and str. sides - star and side rads. - square.
- 267. ZIRCON, 14.10.1 A_1 . - str. sides - rad. fract. and shells. - square.



256



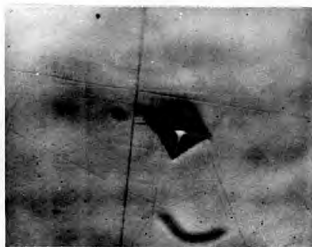
257



258



259



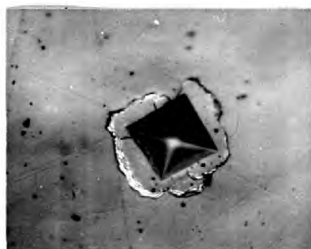
260



261



262



263



264



265



266



267

APPENDIX B

The following are the results of the analyses carried out by the Pure Geochemistry Department of the Royal School of Mines on the three mineral series, previously described in Part 4 chapter 1.

A) The Sphalerite Series

(i) Iron Wt.% : The samples were taken into solution with a mixture of concentrated HNO_3 and HCl . An aliquot of the resulting solution was coloured by ammonium thyoglycollic and an estimation of Fe. Wt% made with the aid of a 'Unicam' spectrophotometer at 520 m .

(ii) Manganese Wt%: As above only the aliquot was oxidised by potassium periodate to the permanganate. Again, an attempt was made to estimate the Mn wt% with the spectrophotometer, but this was found impossible owing to the very low manganese contents - 0.01% - this being the sensitivity of the method.

(iii) Cadmium: The relative proportions of cadmium were obtained with the aid of the X-ray fluorescent Spectrometer. These were converted into approximate wt% by reference to a previous trace element content analysis of specimen 598 (Shazly, 1951) which contained 5000 p.p.m. Cd.

Geochem. Ref. No.	Min. Geol. Ref.	Fe wt. %	Cd. signal Strength	Cd	wt. approx. %Cd.
5585	549	0.077	49	16	0.1
5586	561	4.08	63	30	0.26
5587	535	2.36	56	23	0.2
5588	536	1.20	58	25	0.2
5589	606	0.10	48	15	0.1
5590	565	0.61	54	19	0.15
5591	587	5.96	46	13	0.06
5592	598	1.17	114	80	0.5
5593	601	0.20	87	54	0.4
5594	559	10.7	65	32	0.3

3) The Columbite-Tantalite Series

The members of this series were analysed with the aid of an X-ray Fluorescent Spectrometer using the following internal standards:

1. Ni (K_{α_1, α_2}) for Fe. Mn
2. Zr (K_{α_1, α_2}) for Nb
3. Yb (L_{β_2}) for Ta

and four chemically prepared reference standards X 104 to 108. The following relative amounts of FeO, MnO, Nb₂O₅ and Ta₂O₅ were obtained by comparing the line intensities against those of the internal standards and integrating over the series of standard reference curves. Although the totals range between 72% and 87%, the FeO: MnO and Nb₂O₅: Ta₂O₅ ratios are believed to hold good (Dr. J. Butler, personal communication).

Geochem. Ref.	Min. Geol. Ref.	MnO	FeO	Nb ₂ O ₅	Ta ₂ O ₅
5616	1383	0.8±0.2	<1.8	<4.0	57.0
5605	1390	5.21	5.73	37.3	39.1
5613	1388	7.00	<1.8	14.4	50.4
5610	1392	2.2±1.0	7.09	35.1	25.8
5615	1382	1.3±0.1	8.32	27.6	12.3
5614	1381	1.4±0.2	6.40	22.9	<10.0
5608	1387	6.90	<1.8	14.7	51.2
5612	1394	6.56	1.75	31.1	32.1
5609	1391	6.51	<1.8	<9.0	60.5
5611	1393	2.4	11.6	64.6	<8.0

In addition, the relative % SnO₂, where n% is that of 5616 (thoreaulite, SnTa₂O₇) are as follows:

5615	0.03%
5614	0.12
5608	0.01
5612	0.02
5609	0.05

c) The Wolframite Series

Members of this series were similarly analysed with the aid of the X-ray Fluorescent Spectrometer, integrating the K lines of Fe and Mn with reference to the standards X 104 to X 108.

Geochem. Ref.	Min. Geol. Ref.	FeO/MnO Signal	FeO:MnO	Calculated	
				FeO	MnO
X104		0.15			
105		7.47			
106		2.87			
107		1.04			
108		0.41			
5595	1426	9.05	4.55	19.4	4.3
5596	1421	0.038	0.01	0.3	24.5
5597	1422	0.218	0.075	1.70	22.7
5598	1427	1.30	0.534	8.2	15.5
5599	1428	1.42	0.585	8.7	15.0
5600	1429	10.2	5.22	19.9	3.8
5601	1424	1.78	0.77	10.3	13.4
5602	1425	7.6	3.70	18.6	5.05
5603	1430	1.02	0.83	10.7	13.0
5604	1431	8.5	4.27	19.2	4.5